Chemoproteomic Strategies for Drug Discovery and Natural Product Target Identification

By

Bridget Phelan Belcher

A dissertation submitted in partial satisfaction of the

requirements for the degree of

Doctor of Philosophy

in

Chemistry

in the

Graduate Division

of the

University of California, Berkeley

Committee in charge:

Professor Daniel K. Nomura, Chair
Professor Evan W. Miller
Professor James A. Olzmann

Spring 2023

ABSTRACT

Chemoproteomic Strategies for Drug Discovery and Natural Product Target Identification

By

Bridget Phelan Belcher

Doctor of Philosophy in Chemistry
University of California, Berkeley

Professor Daniel K. Nomura, Chair

Targeted protein therapeutics have garnered significant interest in modern drug discovery, in part due to their ability to target classically “undruggable” proteins. “Undruggable” proteins, which make up the majority of disease-related proteins, are those that cannot be targeted by a therapeutic that targets a well-defined binding pocket. Chemoproteomic strategies can expand the “druggable” proteome by mapping and profiling reactive, nucleophilic amino acids in the proteome that may interact with covalent small molecules. The work discussed in this dissertation highlights the utility of chemoproteomic strategies in drug discovery and drug development spaces.

These strategies are first described in the context of targeted protein degradation, a powerful modality for eliminating disease-related proteins from cells. Targeted protein degradation therapeutics utilize proteolysis targeting chimeras (PROTACs) and molecular glue degraders to accomplish this. PROTACs and molecular glue degraders employ heterobifunctional or monovalent small molecules, respectively, to chemically induce the proximity of target proteins with E3 ubiquitin ligases to ubiquitinate and degrade target proteins via the proteasome. I review the E3 ligases that have been successfully exploited for targeted protein degradation, and discuss chemoproteomics-enabled covalent screening strategies for the discovery of new E3 ligase recruiters. Additionally, I provide a database of reactive cysteines across 97% of known E3 ligases, identified using mass-spectrometry based chemoproteomics.

In one example highlighting the utility of chemoproteomic strategies, I employed chemoproteomic profiling to identify the targets of the electrophilic anti-cancer natural product dankastatin B, from the fungus *Gymnascella dankaliensis*. I discovered that dankastatin B covalently reacts with a cysteine on the voltage-dependent anion channel protein 3 (VDAC3) using activity-based chemoproteomic profiling. I demonstrate that the covalent modification of VDAC3 by dankastatin B leads to the initiation of intrinsic apoptosis in triple-negative breast cancer cells. Dankastatin B also covalently reacts with voltage-dependent anion channel 2 (VDAC2) and E3 ligase RNF114, which also contribute to the natural product’s anti-cancer activity, validated by knockdown studies.

In another example, I present a robust strategy for the synthesis of photoaffinity labeling probes for covalent capture. Photoaffinity labeling probes are powerful tools for the identification of small molecule—protein interactions that work by inducing a covalent interaction between the drug-like molecule and proteins that it interacts with. I

demonstrate that photoaffinity labeling probes containing an acyl silane moiety rather than the traditional diazirine moiety can be utilized in chemoproteomic activity-based profiling to identify potential off-targets of (+)-JQ1. I show that (+)-JQ1 linked to a photoreactive acyl silane alkyne probe binds to BRD4 and, through mass-spectrometry based chemoproteomic profiling, identify potential off-targets of (+)-JQ1 in leukemia cells. The data discussed provides evidence that acyl silanes may be a more tunable scaffold for photoaffinity labeling and covalent capture.

DEDICATION

To my grandparents,
who have supported and believed
in me endlessly.

TABLE OF CONTENTS

ACKNOWLEDGEMENTS

In writing this dissertation, I have had many opportunities to reflect on how grateful I am for the support of my mentors, family, and friends.

I'd first like to thank my family, who begrudgingly supported me moving 3,000 miles away to pursue cool science. Mom – thank you for always picking up my calls, even when I forget about the time difference. Dad – thank you for encouraging me to follow my passions and do what's best for me. Ian – thank you for keeping me humble and reminding me that it's not *that* important. Grampa – thank you for supporting me moving across the country and encouraging me to keep going, no matter what. The four of you have always supported me in everything I do, and I hope that I will make you all proud. To my extended family – thank you for always supporting me and making time to see me every time I reappear on the East coast. I love you all!

To all of my friends from Berkeley, Stonehill, and beyond, thank you for keeping me grounded and making sure I had a life outside of lab. Claire, Michaela, Jess, Anna, and Meg – thank you for making time for me when I visit the East coast and visiting to explore the West coast with me. I'll always appreciate our Zoom calls that got us through the pandemic. You are all such amazing friends, and I couldn't ask for a stronger or smarter group of women. Immy – thank you for being the most amazing long-distance best friend anyone could ask for. I'm so happy that Berkeley brought me the best travel buddy, shopping buddy, and so much more. Pooja and Kyle – you've stuck with me since 2011, and I'm so glad we all got to experience life as Bay Area transplants together. I'll always cherish the memories we've made in our excursions out of the city. I will never stop inviting you to very specifically-themed parties. Morgan – thank you for encouraging me to adopt my three post-qual kittens. Salem, Smudge, and Onyx have given me something besides my experiments to worry about, and I'll always appreciate that you fell just as in love with them as I did. Scott – thank you for always being such a supportive partner and dealing with my quarter life crises as I wrap up my PhD. Whether we're co-working, watching TV, or going wine tasting at way-too-fancy-for-us wineries, I can always count on you to help me relax. Lauren, Margot, Ellie, Ethan, James, and Vienna – thank you for keeping me sane in lab and outside of lab. I definitely wouldn't have survived grad school without any of you. Thank you for always being down to go to baseball games, concerts, musicals, ballets, and anything else that pops up! Brian, Helen, and Emily – thank you for being the best undergrads I could imagine. I'm so insanely proud of all three of you, and I will always appreciate our times spent gossiping in the corner in lab. To the rest of the Nomura lab – I have learned so much from all of you, and you have always made working in lab such a fun experience. There's so much more to life in grad school than just the science, and I'm so glad that we all get to experience the fun side together.

To my mentors, thank you for instilling confidence in me and encouraging my growth no matter which direction it takes me. Dan, thank you for convincing me to come to Berkeley and supporting me throughout grad school. Your enthusiasm for the field truly has kept me motivated at the bench. I will always appreciate you encouraging my decision to take a less-traditional career path after grad school. Prof. Harris, Prof. Rogers, Prof.

Hinkle, Prof. Lombardi, Prof. Tilley, Prof. Liotta, Prof. Del Sesto, and Prof. Hall – I can't thank you all enough for the support you've given me. You instilled the confidence I needed to pursue a PhD, and you are all the best science and life mentors. I can't imagine how I could've been nearly as successful without all of you. Ms. Ritchie – I will forever remember you as the person who launched my career in chemistry. Without your encouragement, I would have never taken AP chemistry or AP biology, nor would I have realized that there were so many careers for women in STEM that I was interested in. Thank you so much for believing in me even when I was 15. All of you have permanently impacted me, and one day I hope that I can make as positive of a difference in someone's career that each of you have for me.

LIST OF FIGURES

LIST OF ABBREVIATIONS

ABPP	Activity-based protein profiling
Apaf1	Apoptotic peptidase activating factor 1
APC	Anaphase-Promoting Complex
AR	Androgen receptor
ATP	Adenosine Triphosphate
ATRA	All-trans retinoic acid
AUTAC	Autophagy Targeting Chimera
BAX	BCL2 associated X, apoptosis regulator
BCA	Bicinchoninic acid assay
BCR-ABL	Breakpoint cluster region protein – tyrosine kinase ABL1 fusion gene
BD1	Bromodomain 1
BSA	Bovine serum albumin
BET	Bromo- and extra-terminal
BRD4	Bromodomain containing protein 4
BTZ	Bortezomib
β-TrCP	Beta-transducin repeat containing E3 ubiquitin protein ligase
C65	Cysteine at position 65
C76	Cysteine at position 76
C8	Cysteine at position 8
C95	Cysteine at position 95
CCDHI	Cyclosome
CDDO-Me	Bardoxolone methyl
CFTR	Cystic fibrosis transmembrane conductance regulator
cIAP	Cellular inhibitor of apoptosis protein
CRABP-II	Cellular retinoic acid binding protein II
CRBN	Cereblon
CRL	Cullin-RING ligase
CuAAC	Copper(I) Azide-Alkyne Cycloaddition
CUL2	Cullin 2
DA	Diazirine
DCAF16	DDB1 and CUL4 associated factor 16
DDB1	Damage specific DNA binding protein 1
DMEM	Dulbecco's modified Eagle medium
DMSO	Dimethyl sulfoxide
DTT	Dithiothreitol
DUBTAC	Deubiquitinase Targeting Chimera
D46	Aspartic acid at position 46
EC_{50}	50% effective concentration
ERα	Estrogen Receptor-$\boldsymbol{\alpha}$
ERLIN2	ER lipid raft associated 2
FA	Formic acid
FBS	Fetal bovine serum
FDR	False discovery rate

FEM1B	Fem-1 homolog B
FKBP12	FK506 Binding Protein
FLAG Tag	DYKDDDDK polypeptide protein tag
FNIP1	Folliculin interacting protein 1
G12C	Glycine to cysteine mutant at position 12
GSK	GlaxoSmithKline
HECT	Homologous to the E6-AP Carboxyl Terminus
HIF-1α	Hypoxia-inducible factor-1
IA	Iodoacetamide
IKBIP	IKBKB interacting protein
IP	Immunoprecipitation
isoTOP-ABPP	Isotopic tandem orthogonal proteolysis-enabled activity-based protein profiling
IKZF1	Ikaros family zinc finger 1
IKZF3	Ikaros family zinc finger 3 (Aiolos)
IMiD	Immunomodulatory drug
KEAP1	Kelch like ECH associated protein 1
KRAS	Kirsten rat sarcoma viral oncogene homologue
LC-MS	Liquid chromatography-mass spectrometry
LGMN	Legumain
LYTAC	Lysosomal Targeting Chimera
L15	Leibovitz's 15 medium
MAPK	Mitogen-activated protein kinase
MDM2	Mouse double minute 2 homologue
MeBS	Methyl bestatin
MetAP2	Methionine aminopeptidase 2
MS1	First MS for detection of initial ionization in MS/MS
MS2	Second MS for detection of fragment ionization in MS/MS
MS/MS	Tandem mass spectrometry
mTOR	Mammalian target of rapamycin
MT-ATP6	Mitochondrially encoded ATP synthase membrane subunit 6
NRF2	Nuclear factor erythroid 2-related factor 2
OTUB1	OTU deubiquitinase, ubiquitin aldehyde binding 1
RBM39 (CAPERα)	RNA-binding protein 39
RIBOTAC	Ribonuclease Targeting Chimera
RIPK2	Receptor interacting serine/threonine kinase 2
PAGE	Polyacrylamide gel electrophoresis
PAL	Photoaffinity labeling
PBS	Phosphate-buffered saline
PDB	Protein Data Bank
PEG	Polyethylene glycol
PHIC	Phosphorylation-Inducing Chimera
PHORC	Phosphatase-Recruiting Chimera
PP6R1	Protein phosphatase 6 regulatory subunit 1
PROTAC	Proteolysis Targeting Chimera

p21 (CDKN1A)	Cyclin-dependent kinase inhibitor 1A
p53	Cellular tumor antigen p53
RBR	RING-between-RING
RBX1	Ring-box 1
RING	Really Interesting New Gene
RIPA	Radio-immunoprecipitation assay buffer
RNA	Ribonucleic acid
RNF114	Ring finger protein 114
RNF4	Ring finger protein 4
RPL27A	Ribosomal protein L27A
RPMI	Roswell Park Memorial Institute Medium
SALL4	Spalt like transcription factor 4
SARM	Selective androgen receptor modulator
SDS	Sodium dodecyl sulfate
shRNA	Short hairpin RNA
SNIPER	Specific and nongenetic inhibitor-of-apoptosis protein-dependent protein eraser
SUMO	Small ubiquitin like modifier
TACC3	Spindle regulatory protein transforming acidic coiled-coil-3
TEV	Tobacco etch virus
TFA	Trifluoroacetic acid
TF-PROTAC	Transcription Factor PROTAC
TMT	Tandem mass tag
TNBC	Triple-negative breast cancer
TPD	Targeted Protein Degradation
TRAFTAC	Transcription Factor Targeting Chimera
TUB1A	Tubulin alpha 1A
Ub	Ubiquitin
VDAC3	Voltage-dependent anion channel 3
VHL	Von-Hippel Lindau
XIAP	X-linked inhibitor of apoptosis protein

CHAPTER 1

Ligandability of E3 Ligases for Targeted Protein Degradation

This chapter is based on the *Biochemistry* publication “Ligandability of E3 Ligases for Targeted Protein Degradation Applications”[1] and has been adapted with permission from all co-authors.

1.1 Introduction

Targeted protein degradation (TPD) has arisen as a powerful chemical biology platform for inducing the degradation of specific proteins in, on, or outside of cells and has made a tremendous impact on drug discovery in both academic and industrial settings.[2–4] TPD uses heterobifunctional or monovalent small molecules or biologics to induce the proximity of a component of the cellular degradation machinery with a neo-substrate protein, inducing the degradation of that specific protein. Heterobifunctional degraders, or proteolysis-targeting chimeras (PROTACs), consist of a protein-targeting ligand linked to an E3 ubiquitin ligase recruiter to induce the proximity of an E3 ligase with a neo-substrate protein, causing the ubiquitination and elimination of that protein through proteasomal degradation (Figure 1.1).[2–4] Molecular glue degraders also bring together an E3 ligase with a neo-substrate protein, but employ monovalent small molecules rather than heterobifunctional small molecules.[5] Whereas the genesis of TPD as a potential therapeutic paradigm arose from heterobifunctional or monovalent small molecules that induce the proximity of an E3 ubiquitin ligase with a neo-substrate protein to ubiquitinate and degrade the target protein via the proteasome, next-generation TPD strategies have arisen that exploit (1) the targeted degradation of the cell surface and extracellular proteins through the lysosome with lysosome-targeting chimeras (LYTACs), (2) the targeted degradation of larger intracellular proteins and cell compartments through autophagy with autophagy-targeting chimeras (AUTACs), (3) the targeted degradation of transcription factors with transcription-factor-targeting chimeras (TRAFTACs) and transcription factor PROTACs (TF-PROTACs), (4) the targeted degradation of bacterial proteins through the recruitment of bacterial proteases with BacPROTACs, and even (5) the targeted degradation of RNA with ribonuclease-targeting chimeras (RIBOTACs).[6–10] Induced proximity paradigms are even being extended beyond degradation to include the targeted manipulation of other protein post-translational modifications beyond ubiquitination, including (1) targeted phosphorylation with phosphorylation-inducing chimeras (PHICs), (2) targeted dephosphorylation with phosphatase-recruiting chimeras (PHORCs), and (3) targeted deubiquitination with deubiquitinase-targeting chimeras (DUBTACs).[11–13] These induced proximity paradigms have garnered significant interest within pharmaceutical companies because of the potential of TPD and next-generation induced proximity paradigms to tackle the “undruggable” proteome, representing most of the proteome that still cannot be therapeutically exploited using classical drug discovery approaches. All of these potential therapeutic paradigms are enabled by the discovery of small-molecule, peptide, or biologic recruitment handles that, either by themselves or through linkage to protein-targeting ligands, enable the induced proximity of a protein modulator with a neo-substrate protein of interest.

Despite the emergence of many PROTAC and molecular glue degrader drug candidates in the clinic, in clinical development, or entering clinical trials and the development of new induced proximity paradigms beyond TPD, a major bottleneck in using classical PROTACs and molecular glue degraders for TPD is still the paucity of pharmacological tools that exist for the ubiquitin-proteasome system, in particular for E3 ubiquitin ligases. E3 ubiquitin ligases are of particular interest because they are responsible for substrate recognition and specificity in the ubiquitin-proteasome system. E3 ligases are also the most diverse component of the ubiquitin-proteasome system, with

over 600 estimated members.[14,15] Yet only a handful of E3 ligase recruiters currently exist, with most attention placed on two E3 ligases — cereblon (CRBN) and von Hippel−Lindau (VHL).[16–18] These two E3 ligase recruiters are likely insufficient to degrade any and every protein target of interest with the desired selectivity. Evidence of this includes the lack of degradation observed against KRAS G12C with CRBN-based recruiters but successful degradation achieved with VHL recruiters.[19,20] In a recent beautiful study by Donovan, Ferguson, Sim, Gray, and Fischer et al., where they developed >90 CRBN- and VHL-based kinase PROTACs with various linkers and protein-targeting ligands, the authors impressively showed the degradation of >200 kinases, but there was still a significant number of kinases that were not degraded out of the >500 kinases that were detected.[21]

The discovery of new E3 ligase ligands will undoubtedly help in expanding the scope of TPD and the targets that can be degraded by PROTACs and molecular glue degraders. Furthermore, the development of tissue-type-, cell-type-, or cell-compartment-restricted E3 ligase recruiters may enable the development of degraders that achieve the location-specific degradation of targets. Here we review current E3 ligase recruiters, ligands, and molecular glues that have been successfully used in TPD and discuss chemoproteomic and covalent ligand screening approaches that have been used to discover new E3 ligase recruiters. We also present an aggregated chemoproteomic atlas of reactive cysteines that can potentially be targeted by cysteine-reactive covalent ligands across a large swath of the human E3 ligase family.

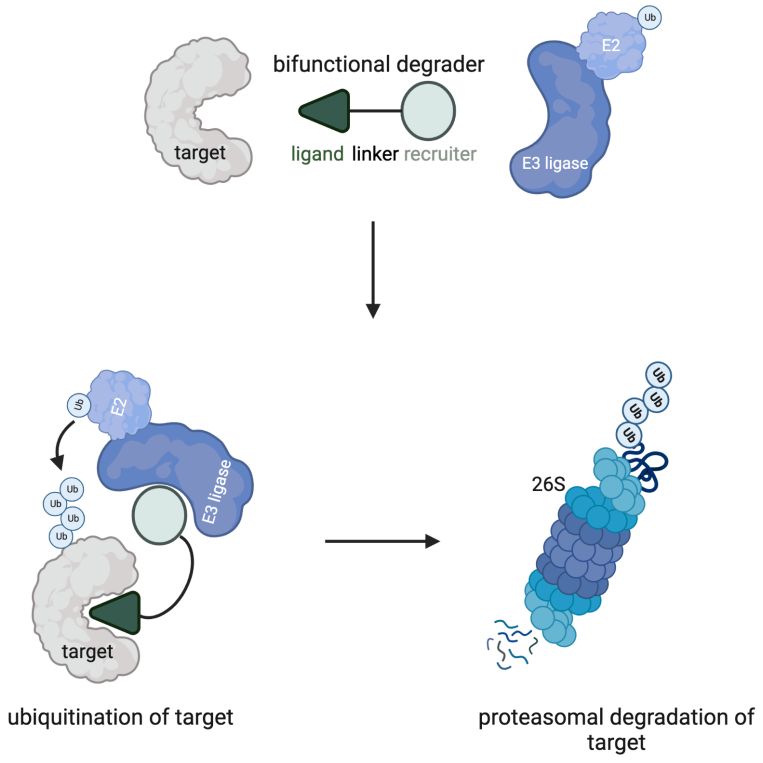

Figure 1.1 Targeted Protein Degradation with heterobifunctional PROTACs. PROTACs consist of a protein-targeting ligand linked to an E3 ubiquitin ligase recruiter via a linker to induce the proximity of an E3 ligase with a neo-substrate target protein to induce ubiquitination and proteasome-mediated degradation of the target protein.

1.2 Ubiquitin-Proteasome System and E3 Ligases

The ubiquitin-proteasome system is a major regulator of protein homeostasis and is responsible for the degradation of a wide range of cellular proteins. Degradation occurs through an enzyme cascade that results in ubiquitination, a covalent posttranslational modification. Hershko, Ciechanover, and Rose discovered this cascade in the 1970s while studying the degradation of denatured globin. They showed that degradation was ATP-dependent and proteins were marked for degradation by the covalent addition of multiple molecules of a small protein later identified as ubiquitin.[22,23] Ubiquitin is activated via the consumption of ATP by an E1 ubiquitin-activating enzyme. The activated ubiquitin is transferred from the E1 enzyme to the E2 ubiquitin conjugation enzyme via a transthiolation reaction. Ubiquitin is then transferred to the substrate by an E3 ubiquitin ligase. The transfer is accomplished via an isopeptide bond between the C-terminal glycine of ubiquitin and a lysine side chain on the substrate. The cycle is repeated to polyubiquitinate the substrate, marking it for proteasomal degradation (**Fig. 1.1**).[24] The system, although complex and regulated, is generally applicable to the diverse proteome.

E3 ligases are classified based on their mechanisms of action. There are two main classes: RING E3 ligases, which recruit E2 ubiquitin conjugates via the RING domain and catalyze the transfer of ubiquitin directly to the substrate, and HECT (Homologous to the E6-AP Carboxyl Terminus) E3 ligases, which transfer ubiquitin to a substrate only after forming a thioester bond with ubiquitin. Within RING E3 ligases, there are three subcategories. Cullin-Really Interesting New Gene (RING) ligases (CRLs) are multisubunit complexes where a Cullin protein links an E2-binding subunit and a target-binding subunit.[25] Anaphase-promoting complex (APC) ligases are also multisubunit complexes that bring E2 proteins and the target protein together without a linker protein. RING-between-RING (RBR) ligases are considered RING E3 ligases because they bind to E2 proteins via their RING domain, but they form a thioester bond with ubiquitin before transferring it to the target protein.

1.3 E3 Ligase Recruiters

In 2001, the first example of artificial E3 ligase recruitment was shown with the E3 ligase ß-TrCP. A PROTAC linked a ß-TrCP peptide ligand to a covalent methionine aminopeptidase 2 (MetAP2) ligand, resulting in the degradation of MetAP2.[26] A peptide ligand was also used as the recognition sequence for the VHL E3 ligase in the first cell-permeable PROTAC in 2004.[27] As interest in E3 ligase recruitment grew, the field shifted away from peptide ligands and toward reversible small-molecule E3 ligase recruiters, with the recruitment of the MDM2 E3 ligase by the ligand nutlin in 2008.[28] Reversible small-molecule ligands continued to gain recognition with the recruitment of the E3 ligase cIAP in 2010.[29] Thalidomide, an immunomodulatory drug (IMiD), was shown to bind to the E3 ligase CRBN in 2010 by Ito, Ando, and Handa.[30] In recent years, more covalent small-molecule E3 ligase recruiters have been identified.

1.3.1 Von Hippel−Lindau

The VHL complex E3 ligase consists of VHL, elognins B and C, cullin 2, and RING box protein 1. VHL was one of the first E3 ligases targeted artificially by mimicking the recognition sequence of hypoxia-inducible factor-1 (HIF-1α), the primary target of VHL. In the early 2000s, the central hydroxyproline residue in the ALAPYIP recognition sequence of HIF-1α was determined to be essential for the formation of the HIF-1α/VHL complex via hydrogen bonding between the hydroxyproline of HIF-1α and a hydroxyproline pocket on VHL.[31,32] In 2004, Schneekloth and Crews et al. used the ALAPYIP recognition sequence as a VHL recruiter for the first cell-permeable PROTAC, targeting and degrading FK506 binding protein (FKBP12).[27] This set the stage for interfering with proteins on a post-translational level, presenting the opportunity to create chemical knockdowns to study protein function without genetic modification. In 2005, a PROTAC targeting estrogen receptor-α (ERα) was developed that used a shorter peptide recognition sequence to recruit VHL. The shorter, pentapeptide sequence used for VHL recruitment improved the cell permeability of the PROTAC. This E2-penta PROTAC successfully degraded ERα, and angiogenesis was inhibited as a result of ERα degradation.[33] VHL continued to be recruited with peptide recognition sequences resembling the HIF-1α sequence, but as more proteins were targeted, issues with cell permeability and drug-like properties became more apparent.[34]

Following the discovery of small-molecule recruiters for mouse double minute 2 homologue (MDM2) and cellular inhibitor of apoptosis protein (cIAP), discussed later in this dissertation, a more drug-like small-molecule ligand for VHL was identified. In 2012, Buckley, Crews, and Ciulli et al. identified a small-molecule ligand that interrupted the interaction between HIF-1α and VHL. By analyzing the crystal structure of the HIF-1α/VHL complex, they were able to identify the key residues for binding and design small-molecule analogues to the key binding motif.[35] Between 2012 and 2015, the original small-molecule VHL recruiter was optimized to yield a VHL ligand with nanomolar potency.[36,37] In 2015, Bondeson and Crews et al. used this optimized VHL recruiter in several PROTACs to specifically degrade ERα and receptor interacting serine/threonine kinase 2 (RIPK2) in cells and in vivo in mice (**Fig. 1.2**).[37] Also in 2015, Zengerle, Chan, and Ciulli et al. designed a PROTAC linking JQ1, a bromo- and extra-terminal (BET) protein inhibitor, to the small-molecule VHL ligand. JQ1 is a nonselective BET inhibitor, but they observed selectivity of the PROTAC for BRD4. At the time, chemical knockdown had only been achieved for all BET family members, but none selectively. A different downstream pharmacological response was observed for BRD4 degradation than for nonspecific BET inhibition. The PROTAC was successful at low concentrations, and the endogenous expression of HIF-1α was not impacted.[38] The VHL recruiter has since been used in many PROTACs to degrade a wide range of targets.[3,21,39,40]

More recently, Bond, Chu, and Crews et al. targeted the oncogenic G12C mutant form of Kirsten rat sarcoma viral oncogene homologue (KRAS) with a small-molecule PROTAC-recruiting VHL. The Crews lab designed a PROTAC linking MRTX849, a covalent KRAS G12C ligand, to a VHL ligand. The degradation of KRAS G12C was observed along with the downstream suppression of MAPK signaling. This was the first successful PROTAC to target KRAS G12C in cancer cells.[19] This work follows the unsuccessful degradation of KRAS G12C by the Gray lab using CRBN recruiters.[20]

1.3.2 Cereblon

CRBN is one of the substrate receptors for the Cullin-RING E3 ubiquitin ligase 4 (CRL4) containing DDB1, CUL4, and RBX1. Whereas the endogenous substrates of CRBN are still under investigation, CRBN recognizes neo-substrates upon binding to thalidomide and other IMiD analogs by engaging in ternary complexes, subsequently leading to the ubiquitination and proteasome-mediated degradation of these neo-substrates. Thalidomide, a drug originally developed for morning sickness in pregnant women in the 1950s, was found to exert profound birth defects called phocomelia, hallmarked by short limbs.[41] CRBN was identified as the primary target of thalidomide responsible for these birth defects by Ito and Handa et al. in 2010.[30] The neo-substrate protein responsible for the birth defects associated with thalidomide, Sal-like protein 4 (SALL4), was not uncovered until more recently through concurrent discoveries by Matyskiela and Chamberlain et al. and Donovan and Fischer et al. in 2018.[42,43] Once CRBN was identified as the target of thalidomide responsible for its immunomodulatory effects, less toxic IMiDs such as lenalidomide and pomalidomide were developed as cancer drugs to target CRBN as treatments for multiple myeloma.[44] A series of studies in 2014 and 2015 provided both structural and biological insights, showing that different thalidomide analogs altered the E3 ligase neo-substrate specificity of CRBN and that the anticancer effects of lenalidomide and pomalidomide were through the CRBN-mediated degradation of neo-substrate transcription factors Ikaros (IKZF1) and Aiolos (IKZF3).[45–49] Subsequent studies have continued to showcase the diversity of neo-substrate degradation with an expanding scope of IMiD analogs.[46,50–53]

In 2015, Winter and Bradner et al. demonstrated that IMiD CRBN recruiters could be linked to protein-targeting ligands to selectively degrade specific proteins in cells (**Fig. 1.2).** They then showed selective degradation of the transcriptional coactivator BRD4 and FKBP12 by linking IMiDs to their previously developed BET family protein ligand JQ1 and FKBP12 ligand SLF, respectively, in a CRBN-dependent manner.[54] Alongside this paper in 2015, Lu and Crews et al. also published on IMiD-based PROTACs for BRD4.[55] These results opened up the possibility for a fully synthetic drug-like heterobifunctional degraders that could be used to specifically degrade target proteins in cells and spurred the development of many IMiD-based PROTACs that have now been exploited against countless protein targets and PROTACs that have entered clinical development.[3,21,39,40]

1.3.3 MDM2

In 2008, the Crews lab demonstrated that nutlin, a known MDM2 E3 ligase ligand that displaces the interaction between MDM2 and the tumor suppressor p53, could be used in a PROTAC to recruit MDM2 to degrade the androgen receptor (AR) (**Fig. 1.2**). AR was targeted by a selective androgen receptor modulator (SARM) linked to nutlin by a polyethylene glycol (PEG) linker.[28] Using a small-molecule E3 ligase ligand instead of the peptidic E3 ligase ligands that existed at the time helped to increase both the cell permeability and stability of PROTACs while decreasing the molecular weight. The Crews lab found success in recruiting MDM2 with nutlin again in 2019 with the successful degradation of BRD4. Because nutlin inhibits the interactions between MDM2 and p53, MDM2-based PROTACs have the potential to both degrade their target and stabilize p53.

The Crews lab demonstrated that their MDM2 PROTAC worked synergistically to exert anticancer activity by both degrading BRD4 and stabilizing p53.[56]

1.3.4 cIAP1

Cellular inhibitor of apoptosis protein 1 (cIAP1) degrades caspase proteins and is overexpressed in many cancer cells. In 2008, the Naito lab demonstrated that methyl bestatin (MeBS) bound to cIAP1 and promoted autoubiquitylation, facilitating its proteasomal degradation (**Fig. 1.2**).[57] This study indicated that cIAP1's intrinsic ubiquitin ligase activity had the potential to be manipulated for the degradation of other proteins. In 2010, Itoh and Hashimoto designed specific and nongenetic inhibitor-of-apoptosis protein-dependent protein erasers (SNIPERs) that utilized MeBS to recruit cIAP. The original SNIPER contained an ester, which was readily hydrolyzed in the cell and caused off-target degradation.[29] Amide-linked SNIPERs were designed with an all-trans retinoic acid (ATRA) ligand to bind the cellular retinoic acid binding protein II (CRABP-II). The selectivity of the SNIPER was improved, and degradation of CRABP-II was observed.[58] In 2011, the group demonstrated that the SNIPER technology could be applied to different protein targets by degrading a variety of nuclear receptors (retinoic acid receptor, ERα, and AR).[59]

Following the facile expansion of SNIPER technology, the Naito lab designed a SNIPER(TACC3) in 2014 to target the spindle regulatory protein transforming acidic coiled-coil-3 (TACC3). Although degradation of TACC3 was observed, it was determined that cIAP1 was not the E3 ligase responsible for the degradation. Through mechanistic studies, it was determined that the E3 ligase anaphase-promoting complex/cyclosome (APC/CCDHI) was responsible for mediating TACC3 degradation.[60]

In more recent years, cIAP ligands have been improved over the original compounds, as demonstrated by GlaxoSmithKline (GSK) in 2020 with the PROTAC-mediated degradation of receptor-interacting serine/threonine protein kinase 2 (RIPK2) (**Figure 1.2**).[61] This study demonstrated that RIPK2 could be selectively degraded in vivo at nanomolar potency. It is important to note that the RIPK2 PROTAC is more potent than the RIPK2 inhibitor alone due to the catalytic pharmacological benefits offered by PROTACs.[61] These findings demonstrate that PROTACs recruiting a variety of E3 ligases have therapeutic potential.

In 2021, Genentech demonstrated that E3 ubiquitin ligases could degrade themselves in a proteasome-dependent manner using modified X-linked inhibitor of apoptosis protein (XIAP) recruitment ligands.[62] This novel degradation modality is composed of an XIAP recruitment ligand linked to a nucleophilic primary amine. The degradation depends on the isopeptide bond formation between the nucleophilic amine and the C-terminus of ubiquitin, leading to the XIAP-promoted ubiquitination of the small-molecule recruitment ligand. This complex is then recruited to the proteasome, leading to the degradation of XIAP. Interestingly, the ubiquitylation state of XIAP is not changed, and the degradation depends only on the binding to and E3 ubiquitin ligase function of XIAP. This K-tag approach demonstrates not only the successful recruitment of XIAP, but also the expansion of the field of TPD to include the self-degradation of E3 ubiquitin ligases.[62]

1.3.5 RNF4

In 2019, Ward and Nomura discovered a small-molecule cysteine-reactive covalent RING finger protein 4 (RNF4) recruiter using activity-based protein profiling (ABPP)-based covalent ligand screens, to be described in more depth later. RNF4 is an E3 ligase that ubiquitinates SUMOylated proteins for proteasomal degradation.[63] Cysteine-reactive covalent ligands were screened against the fluorescent cysteine-reactive iodoacetamide probe (IA-rhodamine) labeling of pure human RNF4 in a gel-based ABPP screen, described later in this Dissertation. The initial covalent ligand hit TRH 1-23 was found to react with the zinc-coordinating cysteines C132 and C135 within RNF4 without inhibiting the RNF4 ubiquitination activity.[63] Upon hit optimization, CCW 16 was identified as the most potent compound against RNF4 and was subsequently linked to JQ1 to demonstrate the RNF4dependent degradation of BRD4 (**Fig. 1.2**).[63] This study demonstrated the utility of target-based covalent ligand screening to discover new E3 ligase recruiters.

1.3.6 RNF114

Concurrent with the discovery of covalent RNF4 recruiters, the neem tree-derived anticancer natural product nimbolide was discovered as a covalent RNF114 recruiter.[64] In 2019, Spradlin, Maimone, and Nomura et al. discovered that nimbolide reacts preferentially with the intrinsically disordered N-terminal cysteine 8, involved in the substrate recognition of the E3 ubiquitin ligase RNF114 using the ABPP-based chemoproteomic approaches discussed later in this Dissertation.[64] The authors showed that nimbolide exerts its anticancer effects by inhibiting RNF114 substrate interactions with tumor suppressors p21 and p57, leading to their accumulation and eventual cell death. More importantly, the authors demonstrated that nimbolide could be used as a covalent RNF114 recruiter for PROTACs in TPD, where they linked nimbolide to JQ1 to show both the selective degradation of BRD4 and the stabilization of endogenous RNF114 tumor suppressor substrates (**Fig. 1.2**).[64] Subsequent studies showed that nimbolide could also be used to degrade the fusion oncogene BCR-ABL in leukemia cancer cells. In this study, the authors demonstrated that RNF114-based degraders showed the preferential degradation of BCR-ABL over c-ABL compared with CRBN or VHL-based degraders that showed the preferential degradation of c-ABL.[65]

To develop a more synthetically tractable RNF114 recruiter, Luo, Spradlin, and Nomura et al. performed a target-based covalent ligand screen using gel-based ABPP approaches against RNF114 to identify a fully synthetic recruiter, EN219, that mimicked the action of nimbolide in preferentially targeting C8 of RNF114 in cells.[66] The authors subsequently linked EN219 to JQ1 to demonstrate the RNF114-dependent degradation of BRD4 in cancer cells (**Fig. 1.2**).[66] Whereas nimbolide was discovered as an RNF114 recruiter through target identification studies using ABPP-based chemoproteomic approaches, this later study showcased how target-based covalent ligand screening can be used to discover new E3 ligase recruiters against specific E3 ligases of interest.[64,66]

1.3.7 DCAF16

Also concurrent with the discovery of covalent RNF4 and RNF114 recruiters, Zhang and Cravatt et al. discovered a novel covalent DDB1 and CUL4 associated factor 16 (DCAF16) E3 ligase recruiter that could be deployed in TPD applications in 2019 using a cellular covalent PROTAC screening strategy coupled to downstream chemoproteomic target identification.[67] The authors linked covalent and promiscuous scout ligands to the FKBP12 ligand SLF and screened for the selective degradation of nuclear FKBP12 that possessed a C-terminal nuclear localization signal. Through this effort, they identified the covalent scout ligand KB02 as a recruiter for TPD applications (**Fig. 1.2**). To identify the E3 ligase target of KB02, they performed FKBP12 pulldown proteomic studies to identify ubiquitin-proteasome system proteins that were specifically enriched upon the treatment of cells with their KB02-based PROTAC. Through this effort, they identified and subsequently validated DCAF16, a substrate recognition component of the CUL4-DDB1 E3 ligase complex, as the E3 ligase target of KB02 responsible for the degradation activity of their PROTAC. The authors demonstrated that the KB02-based PROTAC was able to degrade its target proteins with the low fractional engagement of DCAF16. With a KB02-based PROTAC linked to JQ1, they also demonstrated the degradation of BRD4.[67]

1.3.8 DCAF15

Since the mid-2000s, sulfonamides have been utilized in the clinic for cancer treatment due to their antitumor activity.[68–70] However, the mechanisms of action of sulfonamide derivatives indisulam, E7820, and chloroquinoxaline sulfonamide were uncharacterized. In 2017, Uehara et al. and Han et al. independently reported that the sulfonamide derivatives form a complex between the coactivator of activating protein-1 and estrogen receptors like RNA-binding protein 39 (RBM39) (also known as CAPERα) and the DCAF15-DDB1CUL4 complex. The formation of the complex led to the induced ubiquitination and proteasomal degradation of RBM39.[71,72] In 2019, three crystal structures of the RBM39-sulfonamide-DCAF15-DDB1-CUL4 complex were reported.[73,74] In 2020, Li and Chen et al. reported the first DCAF15-targeting PROTAC based on E7820 (**Fig. 1.2**).[75]

1.3.9 KEAP1

In 2020, Tong, Luo, Maimone, and Nomura et al. demonstrated that the targeted degradation of BRD4 could be enabled by exploiting the triterpene derivative bardoxolone methyl (CDDO-Me), a ligand reported to activate the antioxidant NRF2 pathway by targeting the E3 ligase Kelchlike ECH-associated protein 1 (KEAP1).[76] Whereas DCAF16, RNF4, and RNF114 recruiters acted irreversibly toward their respective E3 ligases, bardoxolone was unique as an E3 ligase recruiter due to its presumed covalent reversible interactions with cysteines on KEAP1. Bardoxolone may also interact with targets beyond KEAP1, and it will be of future interest to better understand the mechanisms through which bardoxolone may act as a recruiter for TPD applications.

1.3.10 DCAF11

In 2021, Zhang and Cravatt et al. discovered another covalent E3 ligase recruiter against the Cullin-RING E3 ligase substrate receptor DCAF11 using a similar approach to their strategy for discovering their DCAF16 recruiter.[77] In this study, the authors screened a library of PROTACs consisting of the FKBP12 ligand SLF linked to a wider panel of electrophilic ligands to identify compounds that degraded luciferase-conjugated FKBP12 in a luciferase reporter assay. Through this effort, they identified 21-SLF as a covalent PROTAC that degraded luciferase-FKBP12 in 22Rv1 prostate cancer cells but not in other cancer cell lines tested (**Fig. 1.2**). Upon pulldown proteomic studies to identify E3 ligase components that were enriched with FKBP12 and PROTAC treatment, they identified and validated DCAF11 as the E3 ligase responsible for the degradation of 21-SLF. Interestingly, the authors showed that whereas this PROTAC caused degradation through targeting C460 on DCAF11, in the absence of this cysteine, C443 and C485 also serve as additional engagement sites that support 21SLF-induced target degradation. Using this DCAF11 recruiter, the authors also demonstrated the degradation of the AR in 22Rv1 cells.[77]

1.3.11 FEM1B

Also in 2021, Henning, Manford, Rape, and Nomura et al. discovered a cysteine-reactive covalent E3 ligase recruiter against the CUL2 E3 ligase FEM1B through a targeted functional screen.[78] FEM1B was recently discovered as a critical regulator of the cellular reductive stress response, a cellular environment where there is a persistent depletion of reaction oxygen stress.[79] Manford and Rape et al. discovered that FEM1B, under reductive stress, recognizes its substrate FNIP1, leading to the FEM1B-dependent ubiquitination and proteasome-mediated degradation of FNIP1 and the restoration of mitochondrial activity and redox homeostasis.[79] In this study, the authors identified a key cysteine residue, C186, that was critical for substrate recognition. To target this substrate recognition cysteine in FEM1B as a possible FEM1B recruitment site, Henning, Manford, Rape, and Nomura et al. performed a fluorescence polarization screen with a cysteine reactive covalent ligand library to identify compounds that would disrupt FEM1B interactions with a fluorescently tagged FNIP1 degron peptide sequence. Through this screen, the authors identified a covalent ligand EN106 that bound to C186 of FEM1B to displace FEM1B−FNIP1 degron interactions (**Fig. 1.2**). They subsequently linked this EN106 recruiter to JQ1 to demonstrate selective FEM1B-dependent BRD4 degradation in cells.[78] This study highlighted the utility of covalent ligand libraries coupled to functional E3 ligase substrate degron displacement screens to discover new recruiters against specific E3 ligases of interest.

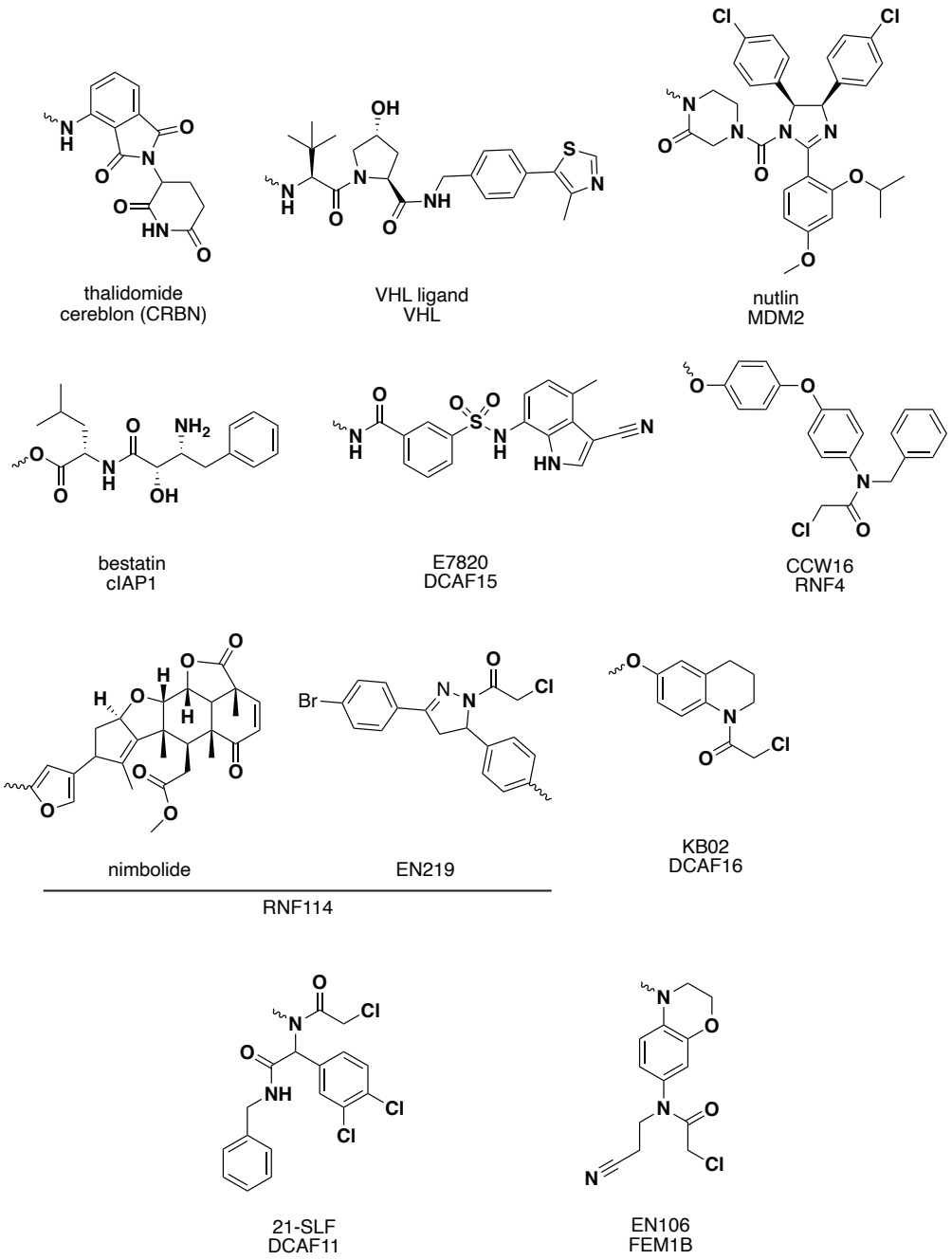

Figure 1.2 Existing E3 ligase recruiters for targeted protein degradation applications.

1.4 Discovery Strategies for New E3 Ligase Recruiters

Despite the significant advances made in recent years, only a handful of E3 ligase recruiters exist for the >600 E3 ligases that can potentially be exploited for targeted protein degradation or other induced proximity paradigms. As has already been described in the above examples, chemoproteomic platforms and covalent ligand discovery approaches have arisen as powerful strategies for discovering new E3 ligase recruiters and more broadly for discovering covalent ligands and ligandable sites across the wider proteome. One particularly useful chemoproteomic strategy has been the ABPP approach. ABPP uses activity-based or reactivity-based chemical probes to profile proteome-wide reactive, functional, and ligandable sites directly in complex biological systems.[80–83]

Weerapana and Cravatt et al. demonstrated in 2010 that broadly promiscuous cysteine-reactive probes could be used in complex proteomes using a quantitative proteomic platform, termed isotopic tandem orthogonal proteolysis-ABPP (isoTOP-ABPP), to identify solvent-accessible cysteines and hyperreactive cysteines that were enriched in functional sites or binding pockets due to the local protein microenvironment.[84] Since this discovery over 10 years ago, quantitative mass spectrometry-based ABPP platforms have been coupled to covalent ligand screening paradigm targeting to radically expand the scope of proteome-wide ligandability. Starting with discoveries from Wang and Cravatt et al. showing that isoTOP-ABPP could be used in a competitive format with competing lipid electrophiles to enable target identification[85] and Backus and Cravatt et al. demonstrating that this platform could be used to identify more drug-like covalent ligands against a broad swatch of ligandable cysteines in the proteome[86], there have been an increasing number of studies using chemoproteomics-enabled covalent ligand discovery approaches against cysteines, lysines, and other amino acids to enable ligand discovery against the proteome.[64,87–95]

As previously described in this Dissertation, chemoproteomics-enabled covalent ligand discovery platforms, whether through target-based or target discovery approaches, have greatly enabled the expansion of E3 ligase recruiters for targeted protein degradation and PROTAC applications, including covalent recruiters against RNF4, DCAF16, RNF114, DCAF11, and FEM1B.[63,64,67,77,78] Recently, Henning and Nomura et al. extended this approach to develop a deubiquitinase recruiter against OTUB1 and showed proof-of-concept for deubiquitinase-targeting chimeras (DUBTACs) for targeted protein stabilization by stabilizing cystic fibrosis transmembrane conductance regulator (CFTR).[13] As such, isoTOP-ABPP and other chemoproteomics-enabled covalent ligand discovery platforms are powerful approaches for uncovering unique ligandable sites and corresponding ligands to enable TPD, PROTACs, and other induced proximity-based therapeutic modalities.

Our lab, like many others in the TPD field, has been performing many ABPP-based chemoproteomic experiments using reactivity-based chemical probes for various target identification, target engagement, and selectivity profiling studies of covalently acting small molecules, accumulating large data sets that include a large amount of probe-modified peptide data from human proteomes. To better enable the mining of potential reactive cysteines that may exist across the human E3 ligase family of proteins, we have aggregated all of our chemoproteomic data from 455 distinct experiments using the

alkyne-functionalized iodoacetamide probe and the isoTOP-ABPP method first reported by Weerapana and Cravatt et al.[84] across various human cell line proteomes. We have quantified the total number of spectral counts for each tryptic peptide identified within each E3 ligase family member across all experiments (**Fig. 1.3A**; Dataset S1). These include data from our research group's published papers and our currently unpublished studies.[13,63,64,66,92,93,95–104] We show reactive cysteines identified across a representative set of E3 ligases in Table 1.1.

Across 675 E3 ubiquitin ligases, substrate receptors, and related components mined, we identified probe-modified cysteines across 653 of these proteins. These sites of probe labeling represent potential solvent-accessible reactive cysteines that exist across 97% of E3 ligases (**Fig. 1.3B**). We have included **Dataset S1** that includes all probe-modified sites within these 653 proteins identified from our aggregate chemoproteomic data with the individual peptides and sites of modification identified for each E3 ligase, the aggregate spectral counts identified for each site, and the number of experiments in which the particular probe-modified tryptic peptide has been observed. There are several caveats to this list of probe-modified sites within human E3 ligases that we point out here before the further interpretation of these data below. First, these 675 proteins mined do not represent the total list of all human E3 ligases. There are likely many more E3 ligases that we failed to mine here. Second, whereas we believe that within these data there exist many potential ligandable cysteines within E3 ligases, there is also likely a large fraction of these sites that do not represent true ligandable sites and may just represent surface cysteines that are not part of binding pockets. Third, there are very likely many reactive and ligandable cysteines within E3 ligases that are not represented in this list. This may be for many reasons, including E3 ligases that may (1) be of low abundance, (2) not be expressed in the cell lines profiled to date, (3) show poor ionization of tryptic peptides, (4) show poor reactivity with the iodoacetamide probe, or (5) show destabilization, unfolding, or aggregation upon cell lysis. Fourth, this list includes only probe-modified cysteines and does not include other amino acids that can potentially be interrogated by other reactivity-based probes. These data merely represent an aggregate list of probe-modified cysteines wherein we have quantified the number of times each particular probe-modified tryptic peptide has appeared across our group's internal chemoproteomic data sets.

To identify potentially interesting cysteines that could be targeted by covalent ligands, we postulated that probe-modified cysteines within E3 ligases that showed higher aggregate spectral counts for a particular cysteine compared with other sites within the same E3 ligase may represent more reactive and potentially more ligandable cysteines. Caveats to this premise include cysteines located in regions within a protein sequence that do not yield suitable tryptic peptides with respect to the ionization and compatibility with mass spectrometry-based sequencing and the labeling of surface-exposed cysteines that may not be part of binding pockets. However, we conjectured that the aggregate chemoproteomic data would still yield potential ligandable sites within E3 ligases that may be of interest to the TPD community.

Consistent with this premise, if we assess RNF114, a RING E3 ligase for which we have previously identified nimbolide and EN219 as covalent recruiters that can be used in PROTAC applications[64,66], we observe nine probe-modified cysteines – C8, C49, C32/C52, C64/C67, C110, C173, and C176. However, among these nine sites, C8 collectively shows 1641 aggregate spectral counts over the next most recognized site

C110 with 40 spectral counts (**Dataset S1**). Both nimbolide and EN219 react specifically with C8 on RNF114. However, this does not always correlate. For example, in DCAF16, we observe three probe-modified cysteines, C119, C173, and C179, where C119 shows the highest number of aggregate spectral counts. However, Zhang and Cravatt et al. found that their KB02 likely engages with C177 or C179 and not C119.[67] However, C119 may represent another additional site that could be liganded for DCAF16 recruitment. FEM1B and DCAF11 either have not yet appeared in our chemoproteomic profiling experiments or were captured with low aggregate spectral counts.

Nonetheless, we still believe that this data set likely has many potential entry points into ligand discovery against E3 ligases. For example, in assessing CRBN, an E3 ligase for which IMiDs exist as recruiters but for which a covalent recruiter has not yet been disclosed, we observe four probe-modified cysteines – C188, C287, C326, and C441 – in which C188 and C287 show the highest aggregate spectral counts with 422 and 100, respectively, compared with the other sites (**Dataset S1**). Interestingly, C188 sits at the interface between CRBN and DDB1, indicating that targeting this site might either disrupt or stabilize CRBN/DDB1 interactions (**Fig. 1.3C**). In contrast, C287 appears to be in an allosteric site within CRBN that sits at the bottom of defined pocket (**Fig. 1.3C**). C287 may be a potential ligandable cysteine that can be targeted within CRBN. VHL also possesses a probe-modified cysteine C77 that also appears to be part of a potential binding pocket (**Fig. 1.3D**).

An important consideration for using this database of potential ligandable cysteines within E3 ligases to prioritize the development of covalent E3 ligase recruiters is the location of the cysteine in the protein. Many E3 ligase recruiters that have been discovered thus far, including those for CRBN, VHL, RNF114, DCAF15, cIAP, and FEM1B, target substrate recognition domains within the E3 ligases. Whether an E3 ligase-targeting ligand needs to bind to a substrate recognition site to be successfully recruited for TPD remains unclear. Targeting allosteric sites within the E3 ligase that are not directly involved in substrate recognition may still yield successful recruitment. However, if the cysteine rests within a known interaction domain between the E3 ligase and an important functional adapter protein necessary for the function of the E3 ligase complex, then these sites would likely not be ideal for recruiter development.

Other important considerations for prioritizing E3 ligases within the database include the cell type, tissue, or cell compartment expression of the E3 ligase in relation to the target of interest if one aims to achieve the location-specific degradation of a protein. Another critical consideration is the functional role of the individual E3 ligases. Many E3 ligases remain poorly characterized as to their endogenous biochemical, cellular, and physiological functions, and the E3 ligases listed in our **Dataset S1** may cause toxicity upon recruitment, may not be involved in ubiquitin conjugation, and may not confer specific ubiquitin linkages that destine a protein for degradation versus the many other roles of ubiquitin or ubiquitin-like proteins.[105] Some classes of E3 ligases, such as the RBR proteins, are highly regulated and autoinhibited and may not be ideal or more complicated for recruitment and TPD.[106] The ligandability and the ability to develop potent and selective chemical matter for a particular E3 ligase must be balanced with these aforementioned aspects associated with the biology of each E3 ligase.

Hundreds of additional probe-modified cysteines exist across the >600 human E3 ligases mined here against our lab's aggregate chemoproteomic data. Many of these sites

may represent unique ligandable sites that can be accessed with covalent ligand discovery approaches, and we encourage the ubiquitin proteasome and targeted protein degradation fields to mine this database and deploy covalent ligand screening platforms to expand the arsenal of E3 ligase recruiters that can be exploited in PROTACs and molecular glue degraders.

A

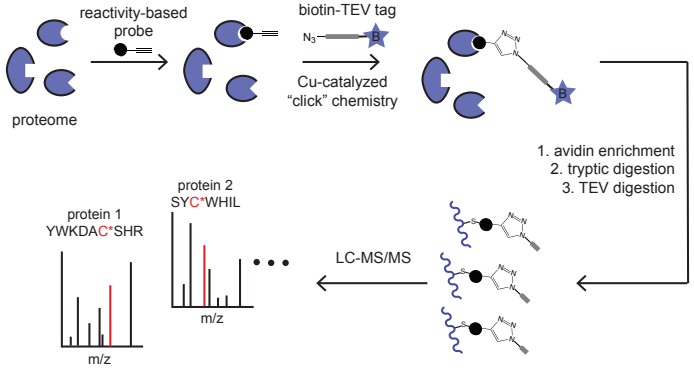

B

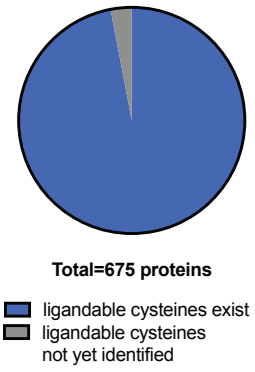

C

CRBN

C188

K.VQILPEC*VLPSTMSAVQLESLNK.C

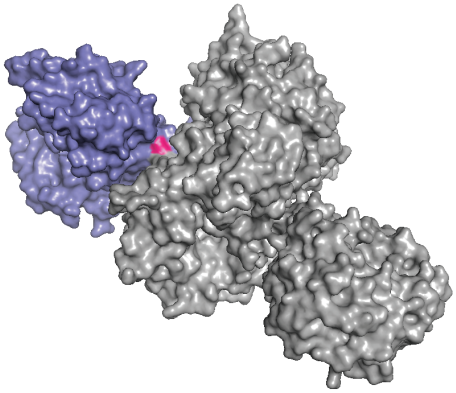

C287

R.VAAC*LPIDDVLR.I

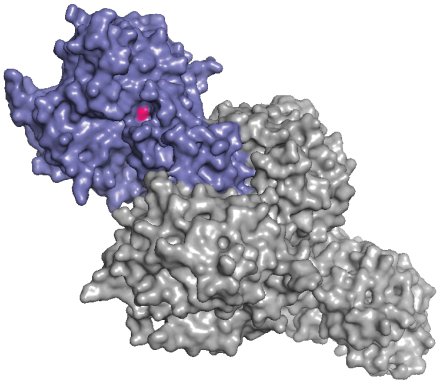

D

VHL

C77

R.EPSQVIFC*NR.S

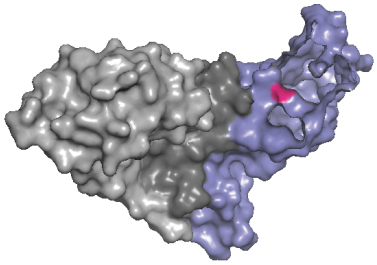

Figure 1.3 Using chemoproteomic platforms to identify potential reactive and ligandable cysteines across the human E3 ligase family. (**A**) ABPP-based chemoproteomic approaches using reactivity-based probes. Reactivity-based alkyne-functionalized probes can be used to label reactive cysteines in complex proteomes, after which a TEV protease-cleavable biotin-azide tag can be appended to probe-labeled proteins using copper-catalyzed azide-alkyne cycloaddition (CuAAC). Probe-modified proteins can be avidin-enriched and digested with trypsin, and probe-modified tryptic peptides can be eluted by TEV protease for quantitative proteomic analysis. (**B**) Aggregating our lab's chemoproteomic data sets of all probe-modified cysteines from ABPP experiments, we have identified probe-modified cysteines across 97% of human E3 ligases. Data can be found in **Table S1**. (**C**) Probe-modified tryptic peptides and structure of the reactive cysteines C188 and C287 in CRBN. The structure of CRBN-DDB1 is shown with CRBN in blue, DDB1 in gray, and C188/C287 in magenta (PDB 4TZ4). (**D**) Probe-modified tryptic peptides and structure of the reactive cysteine C77 in VHL. The structure of VHL-elongin B/C is shown with VHL in blue, elongin B/C in gray, and C77 in magenta (PDB 1VCB).

E3 ligase	UniProt ID	reactive cysteine(s)
RNF114	Q9Y4L5	C8,[b] C110
RNF4	P78317	C132/C135[b]
DCAF16	Q9NXF7	C177 or C179[b]
DCAF11	Q8TEB1	C460[b]
FEM1B	Q9UK73	C186[b]
CRBN	Q96SW2	C188,[c] C287
VHL	P40337	C77[c]
RNF2	C99496	C72[c]
RNF14	Q9UBS8	C262[c], C417
RNF20	Q5VTR2	C383, C905, C924
RNF25	Q96BH1	C316[c]
RNF31	Q96EP0	C504,[c] C551
RNF111	Q6ZNA4	C968[c]
RNF113A	O15541	C15[c]
RNF123	Q5XPI4	C461[c]
RNF126	Q9BV68	C32
RNF128	Q8TEB7	C15[c]
RNF130	Q86XS8	C320[c]
RNF149	Q8NC42	C295[c]
RNF167	Q9H6Y7	C271[c]
RNF180	Q86T96	C28[c]
RNF213	Q63HN8	C614[c]
UBR1	Q8IWV7	C180, C1603[c]
UBR2	Q8IWV8	C1360, C1619,[c] C576
UBR4	Q5T4S7	C1358, C2554,[c] C4049, C2222, C1274
ZNF598	Q86UK7	C456[c]
KCTD21	Q4G0X4	C166[c]
KBTBD7	Q8WVZ9	C527/C529[c]
KLHL20	Q9Y2M5	C356[c]
KLHL24	Q6TFL4	C359[c]
KEAP1	Q14145	C23, C288, C196, C319
FBXL18	Q96ME1	C468[c]
FBXL7	Q9UJT9	C386/C401[c]
FBXW8	Q8N3Y1	C579[c]
FBXO10	Q9UK96	C430[c]
FBXO22	Q8NEZ5	C228[c]
FBXO30	Q8TB52	C592,[c] C433, C723/C725
FBXO9	Q9UK97	C68[c]
SKP1	P63208	C120, C160
SKP2	Q13309	C113,[c] C240, C205, C345
ASB6	Q9NWX5	C153[c]
ASB9	Q96DX5	C216[c]
RAB40C	Q96S21	C159[c]
NOSIP	Q9Y314	C8[c]
PRPF19	Q9UMS4	C298,[c] C230, C351
STUB1	Q9UNE7	C199,[c] C48
UBE4A	Q14139	C79,[c] C989, C1002
DCAF5	Q96JK2	C503[c]
DCAF7	P61962	C61,[c] C120
DCAF8	Q5TAQ9	C297, C272
DCAF13	Q9NV06	C190, C215, C120

Table 1.1 Representative List of Reactive Cysteines within E3 Ligases.[a]

[a] Reactive cysteines annotated are derived from the aggregate chemoproteomic data in Dataset S1. Listed cysteines show at least seven aggregate spectral counts for the particular site.

[b] From experimental data from Zhang, Cravatt et al. 2019; Spradlin, Nomura et al. 2019; Ward, Nomura et al. 2019; Zhang, Cravatt et al. 2021; or Henning, Nomura et al. 2021.[63,64,67,77,78]

[c] Represents the dominant probe-modified site over the other sites identified in the same E3 ligase from the aggregate chemoproteomic data in Dataset S1.

CHAPTER 2

Chemoproteomic Profiling of Anti-Cancer Natural Product Dankastatin B

This chapter is based on the *Chemical Science* publication “Chemical investigations into the biosynthesis of the gymnastatin and dankastatin alkaloids”[107] and the *ChemBioChem* publication “Chemoproteomic Profiling Reveals that Anti-Cancer Natural Product Dankastatin B Covalently Targets Mitochondrial VDAC3”[108] and has been adapted with permission from all co-authors.

2.1 Introduction

Natural products have served as a rich source of medicinal agents for various diseases, including cancer. They have also served as inspiration for numerous clinical candidates and FDA-approved drugs.[109,110] Among these natural products are those that possess electrophilic functional groups that can covalently act with nucleophilic amino acids within proteins to exert their biological activity. These covalently-acting natural products can selectively engage with unique ligandable sites within proteins and provide sustained target engagement, expanding the druggable proteome.[111] Members displaying this reactivity include β-lactam antibiotics such as penicillin that covalently target transpeptidases, epoxomicin that irreversibly inhibits the proteasome, fumagillins that target methionine aminopeptidase 2, Wortmannin that targets kinases including phosphoinositide 3-kinase, and acetylsalicylic acid that acetylates a serine within cyclooxygenases.[111,112] Despite the identification of numerous natural products possessing both protein-reactive functional groups and therapeutically relevant biological activities, the biological targets and mechanism(s) of action of most covalently-acting natural products are unknown.

Among these natural products, we became interested in chlorinated gymnastatin and dankastatin alkaloids derived from the fungus *Gymnascella dankaliensis* isolated from the sponge *Halichondria japonica*, first reported in 1997 (**Fig. 2.1**).[113–116] Presumably produced through the merger of tyrosine and a 14-carbon polyketide fragment (**Fig. 2.1**) to first generate gymnastatin N (**2**), electrophilic halogenation and various oxidative cyclization reactions create a small library of architecturally complex natural products from a common and simple precursor. Many of these tyrosine-derived alkaloids have been reported to possess significant anti-cancer activity, but their mechanisms of action remain unknown.[113–116] These gymnastatin and dankastatin alkaloids possess many distinct electrophilic functional groups, including chloroenone, α-chloroketone, epoxyketone, lactol, acetal, and $\alpha,\beta,\gamma,\delta$-unsaturated amide moieties that can potentially react with nucleophilic amino acids such as cysteines (**Fig. 2.1**).

With over 20 members isolated possessing varying degrees of oxygenation, halogenation, and cyclization, it is not unreasonable to suspect that gymnastatin A (**3**) plays a central role in the biosynthesis of other tyrosine-derived alkaloids (**4–14**), possibly through chemistry which can be replicated without enzymes (**Fig. 2.2**). Indeed, biosynthetic logic has guided synthetic routes to various gymnastatin members and related alkaloids.[117–121] Despite this, detailed chemical insight regarding the formation, stereochemistry, and interconversion of various members is lacking. Given our interest in bicyclo[3.3.1]nonane-containing natural products and covalently binding natural products, especially those containing similar lipophilic amide side chains,[100] we sought to develop a unified synthetic platform to these alkaloids as a gateway into studying their biological targets.[122–125]

In this chapter, we report simple synthetic solutions to multiple chlorinated gymnastatin and dankastatin metabolites, uncovering very subtle factors which favor the formation of a given skeletal type. We also provide an unappreciated link between this natural product family and the well-known fungal natural product aranorosin (**15**) which has also been isolated from a terrestrial variant of *G. dankaliensis*.[126] Finally, we provide

the first proteomic profiling, target identification, and mechanistic elucidation for a member of this class of cytotoxic natural products, dankastatin B.

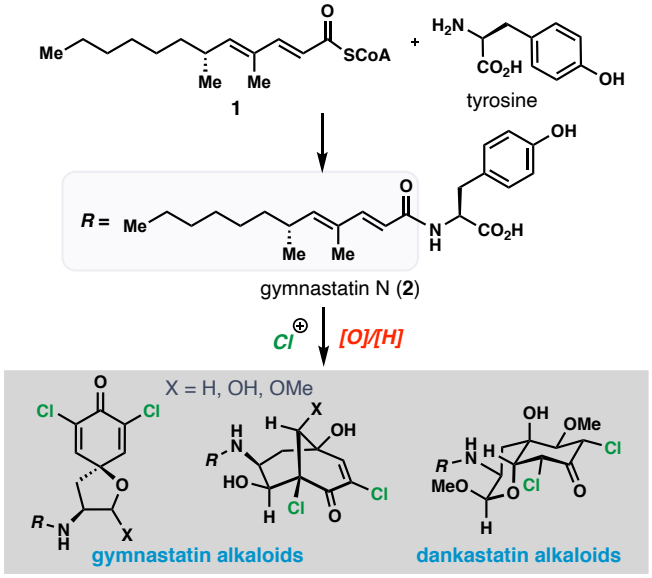

Figure 2.1 Tyrosine-derived alkaloids from *Gymnascella* sp. fungi.

2.2 Synthesis of Gymnastatin and Dankastatin Family Members

Bicyclo[3.3.1]nonane-containing gymnastatins and the oxodecalin-containing dankastatins are proposed to arise from **3** via aldol (**16**) and oxa-Michael (**17**) pathways respectively (**Fig. 2.3A**).[113,115,116,127–129] The presence of a C-9 methyl ether in gymnastatins F (**9**) and Q (**10**) relative to a secondary hydroxyl group in gymnastatin G (**11**) raises questions regarding the identity of the "OR" group that can trigger this process (*i.e.* H_2O vs. MeOH), in addition to stereochemical concerns arising from inter- vs. intramolecular delivery of the oxygen nucleophile. Additionally, dankastatins exists as two different sets of oxo-cis-decalin diastereomers (compare **12** vs. **13/14**); how (or if) nature controls the formation of a given isomer is an intriguing question.

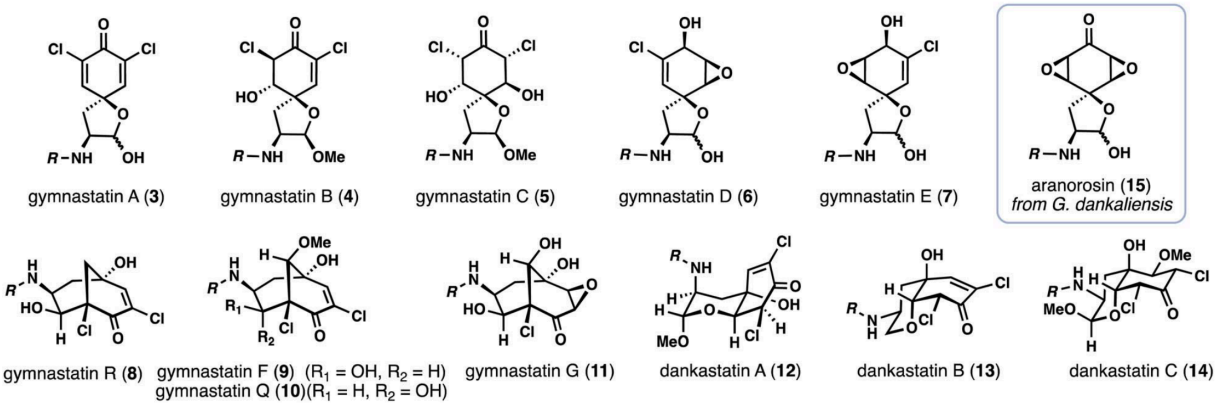

Figure 2.2 Selected chlorinated gymnastatin and dankastatin members and related natural product aranorosin.

2.2.1 Gymnastatin Family Members

We initially targeted gymnastatin G (**11**) owing to its potent reported activity against the P388 lymphocytic leukemia cell line and reactive epoxyketone functionality.[113] Inspired by the work of Nishiyama on ether-containing gymnastatins F/Q, we had hoped that simply substituting methanol with water would forge the bicyclo[3.3.1]nonane core of **11** in a biomimetic cascade (**Fig. 2.3B**).[120] Known compound **18**, derived from (L)-tyrosine, **6** was treated with aqueous KOH in MeCN yielding two bicyclo[3.3.1]nonane-containing products, **19 and 20** in a 1.2:1 ratio. Surprisingly, however, the C-9 stereocenter was incorrectly set during this process, confirmed by x-ray crystallography. Isomer **20** could be converted to **19** by treatment with catalytic amounts of base, suggesting that diastereomers at C-1 are formed in a reversible aldol reaction step, and that the oxa-Michael addition step, albeit producing an undesired outcome, was stereoselective. Presumably this outcome arises from fast intramolecular oxa-Michael addition, wherein a hydrated aldehyde intermediate (**17**, R = H) serves to deliver the oxygen nucleophile internally forming the cis-6,6-fused (dankastatin-type) bicyclic lactol. Subsequent lactol ring-opening then generates an aldehyde which participates in the aldol process. This observed reactivity questions the strategy nature employs in setting the correct C-9 stereocenter if water is used as a nucleophile. In principle, the epoxide motif found in gymnastatin G could arise from the chloroenone found in gymnastatins F/Q via conjugate addition of water and halide displacement. In our hands, this reaction did not occur using **19/20**. Additionally, chemoselective hydrodechlorination of the vinyl chloride in the presence of the tertiary chloride was not possible.

Given these results, we examined alternative alcohol-based nucleophiles in order to prevent the proposed reaction pathway that leads to undesired C-9 stereochemistry; the resulting alkyl ethers formed could in principle be deprotected and ultimately processed to **11** which we desired for biological testing (**Fig. 2.3C**). Dienone **18** was reacted with various quantities of either allyl or benzyl alcohol using a variety of bases and subsequently quenched at various temperatures. Employing sub stoichiometric quantities of Li-, Mg-, and Na-based bases was ineffective at low temperatures (entries 1–3), but potassium bases employed in excess afforded substantial amounts of the desired bicyclo [3.3.1]nonane **21** and isomeric counterpart **22** (entries 4–7). The gymnastatin-type scaffold was favored under these conditions, and optimal ratios of **21** were obtained using two equivalents of base (entries 6 and 7). A somewhat significant (up to 20%) side reaction in many of these reactions was the cleavage reaction. A related process in proteins involving tyrosine has been observed during thyroid hormone synthesis.[130] Of note, in entry 5, wherein the reaction was kept colder, we observed formation of small amounts of the dankastatin scaffold (**23**) in addition to **21/22**. Finally, maintaining a -78°C reaction temperature (entries 8–10) led to substantial quantities of **23** showing that under carefully controlled conditions either scaffold can be generated from **18**.

With conditions identified for construction of the key bicyclo[3.3.1]nonane core with the correct C-9 stereocenter, we reinvestigated the synthesis of gymnastatin G (**11**) (**Scheme 2.1**). While the epoxide found in **11** could be envisioned to arise from the chloroenone motif of gymnastatin F/Q, we had been unable to realize this process using

previously prepared isomer **19/20**. Given these observations, we proceeded to investigate a monochlorinated tyrosine derivative as a means to synthesize **11**.

Carefully controlled mono-chlorination of Boc-tyrosine methyl ester (**24**) was achieved using sulfuryl chloride under a stream of argon, by which the produced HCl could be removed thus preventing undesired removal of the Boc group under acidic conditions. The resulting ester (**25**) was then reduced with DIBAL providing aldehyde **26**, which was subsequently dearomatized with PIFA in the presence of TEMPO to provide spirolactol **27** as a mixture of four diastereomers, two of which are inconsequential. Using conditions discovered previously, treatment of **27** with allyl alcohol and KHMDS led to the bicyclo[3.3.1]nonane-containing product **28** in 35% yield as a mixture of diastereomers. Of note, the C-1 hydroxyl group, formed in the aldol step, was α-disposed in the major product. Moreover, no isomeric bicyclo[3.3.1]nonane-containing products possessing an α-chloroenone motif were formed. The carefully-chosen allyl protecting group was removed under reductive palladium-catalysis ($Pd(PPh_3)_4$,Bu_3SnH) providing triol **29**. Diastereoselective epoxidation of **29** with H_2O_2 and Triton B afforded epoxyketone **30**; notably the basic conditions employed also partially epimerized the C-1 stereocenter (presumably via a retro-aldol/aldol reaction) to now favor β-stereochemistry as found in **11**. The mixture of epoxides was then exposed to TFA, removing the Boc group, and the free amine (**31**) coupled to known acid **32** (HATU, DIPEA) thus delivering gymnastatin G (**11**) and its C1-epimer (**33**) in 60% combined yield. While gymnastatin G was reported as quite labile, we found our synthetic material was stable enough for full characterization. Nevertheless, the synthetic gymnastatin G was acylated with Ac_2O, and the NMR resonances of the resulting diacetate matched those reported by the Numata group.[113] Epimer **33** could also be converted into **11** in 50% yield by treatment with KHMDS.

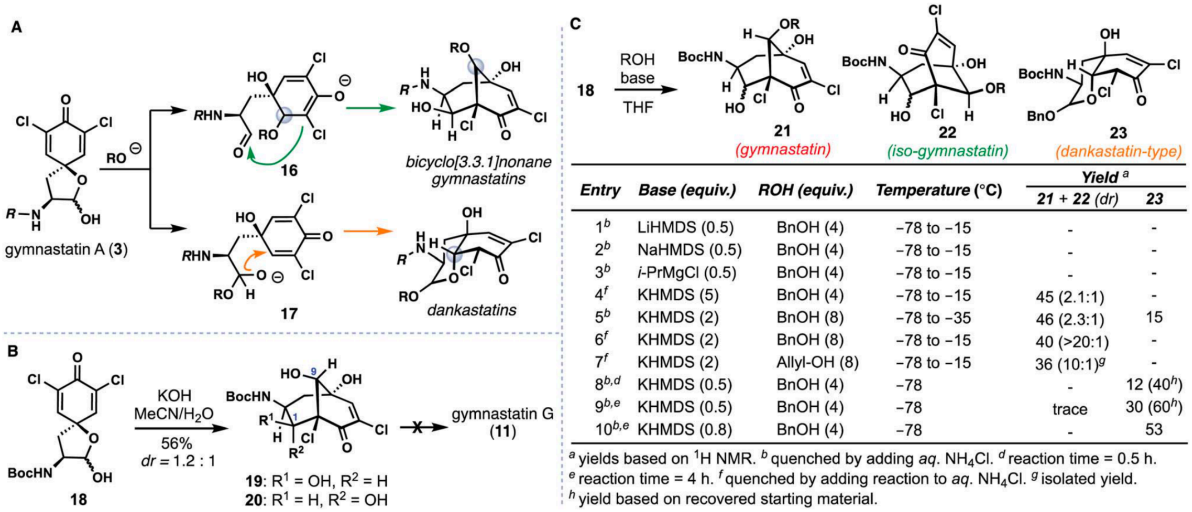

Entry	Base (equiv.)	ROH (equiv.)	Temperature (°C)	Yield [a] 21 + 22 (dr)	Yield [a] 23
1[b]	LiHMDS (0.5)	BnOH (4)	−78 to −15	-	-
2[b]	NaHMDS (0.5)	BnOH (4)	−78 to −15	-	-
3[b]	*i*-PrMgCl (0.5)	BnOH (4)	−78 to −15	-	-
4[f]	KHMDS (5)	BnOH (4)	−78 to −15	45 (2.1:1)	-
5[b]	KHMDS (2)	BnOH (8)	−78 to −35	46 (2.3:1)	15
6[f]	KHMDS (2)	BnOH (8)	−78 to −15	40 (>20:1)	-
7[f]	KHMDS (2)	Allyl-OH (8)	−78 to −15	36 (10:1)[g]	-
8[b,d]	KHMDS (0.5)	BnOH (4)	−78	-	12 (40[h])
9[b,e]	KHMDS (0.5)	BnOH (4)	−78	trace	30 (60[h])
10[b,e]	KHMDS (0.8)	BnOH (4)	−78	-	53

[a] yields based on ^{1}H NMR. [b] quenched by adding *aq*. NH_4Cl. [d] reaction time = 0.5 h. [e] reaction time = 4 h. [f] quenched by adding reaction to *aq*. NH_4Cl. [g] isolated yield. [h] yield based on recovered starting material.

Figure 2.3 Understanding ring formation in the biosynthesis of gymnastatin and dankastatin alkaloids. (A) Chemical and stereochemical possibilities. (B) Stereochemical problems encountered when employing water as an oxygen nucleophile. (C) Optimization studies.

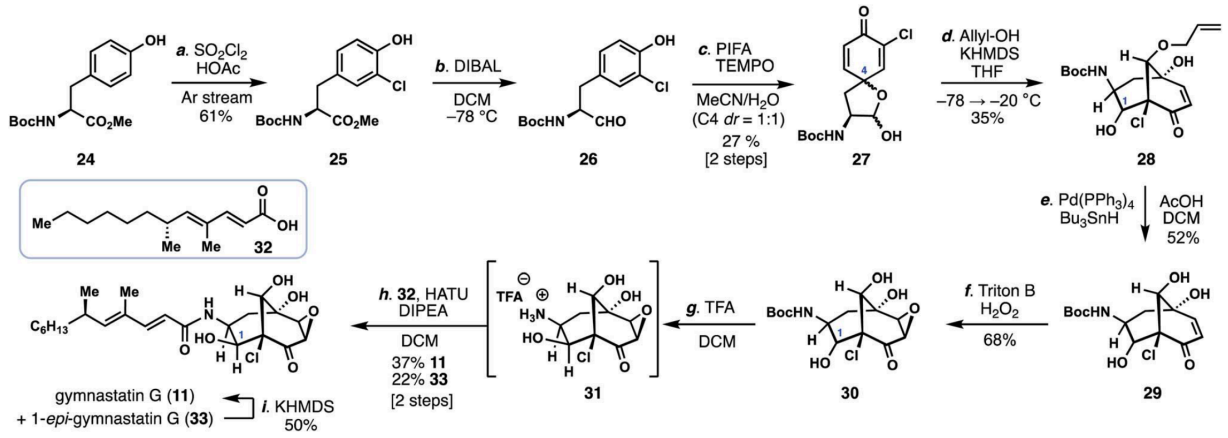

Scheme 2.1 Total synthesis of gymnastatin G.

2.2.2 Dankastatin Family Members

With access to the most complex gymnastatin member secured for biological testing, we turned our attention toward the dankastatin family given that our initial screening of cyclization conditions turned up conditions to favor this scaffold. Chlorinated dankastatin members (**12–14**), however, are produced with two different isomeric cis-decalin frameworks. Notably, in dankastatin A (**12**) the tertiary alcohol and neighboring proton (see C-4 and C-9) are on opposite faces as compared to dankastatins B (**13**) and C (**14**). In analogy to work in **Fig. 2.3C**, treating **18** with KHMDS/MeOH generated compound **37** and not the dankastatin A-type cis-fused skeleton **35** (**Fig. 2.4A**). We presume that in the cyclization of **18**, an axial configuration of the amide side chain (**see 34 vs. 36**), disfavors formation of **35**. The same result was obtained using gymnastatin A indicating this outcome is not unique to the Boc protecting group. Again, this raises the question as to how the dankastatin A-type skeleton is prepared in nature. Fortunately, isomer **37** does however, bear resemblance to dankastatins B and C, thus offering a potential pathway to these targets (**Fig. 2.4B**).

Dankastatin C, a more recently isolated member of the dankastatin family[127], possesses a structure suggestive of a hydration event on a biosynthetic intermediate akin to chloroenone **37**. To synthesize this structure, subtle adjustments were made to the conditions for the intramolecular oxa-Michael addition. Sodium methoxide was utilized as base with MeOH as solvent and the reaction mixture maintained at -20°C for a prolonged period—long enough for the double MeOH adduct (**38**) to be the major product but without significant bicyclo[3.3.1]nonane formation. If KHMDS was used as base, bicyclo[3.3.1]nonane-containing products predominated. Through this process, **38** was formed as a single diastereomer in 42% yield along with 20% of **37**. Finally, Boc deprotection of **38** with TFA, followed by coupling with side chain **32** (HATU, DIPEA) forged dankastatin C (**14**).

Unlike dankastatin C, and in fact the majority of other tyrosine-derived alkaloids from *Gymnascella*, dankastatin B (**14**) features an alcohol, rather than aldehyde, oxidation state at C-1. To access this natural product, Boc-tyrosine methyl ester (**24**) was dichlorinated ($SOCl_2$, HOAc) and reduced with DIBAL to yield **40** (**Fig. 2.5**). With **40** in

hand, we sought to find suitable oxidative dearomatization conditions that were compatible with the free hydroxy group. After some exploration, success was realized using singlet oxygen-based conditions (O_2, TPP, $h\nu$) in the presence of cesium carbonate (**Fig. 2.5**). The yields of this process were initially quite low (entries 1–3), but in the presence of PPh_3 the dankastatin core (**42**) could be formed directly, albeit in low yield (entry 4). Interestingly, in addition to **42**, we observed a minor isomer (iso-**42**) which corresponds to the dankastatin A scaffold (dr ~ 1.6:1). Through reductant and temperature optimization (entries 5–11), we found that high yields of dienone **41** (70%) could be obtained using an electron-deficient phosphine ($P(3,5\text{-}(CF_3)_2C_6H_3)_3$) at low temperature. Isolated **41** could then be converted to **42** under basic conditions (KHMDS) in 78% yield. While this sequence requires two steps, the yield (78%) and diastereoselectivity (dr = 8:1) were substantially higher than the one-pot transformation. Deprotection of **42** (TFA) and coupling with acid **32** yield dankastatin B (**13**).

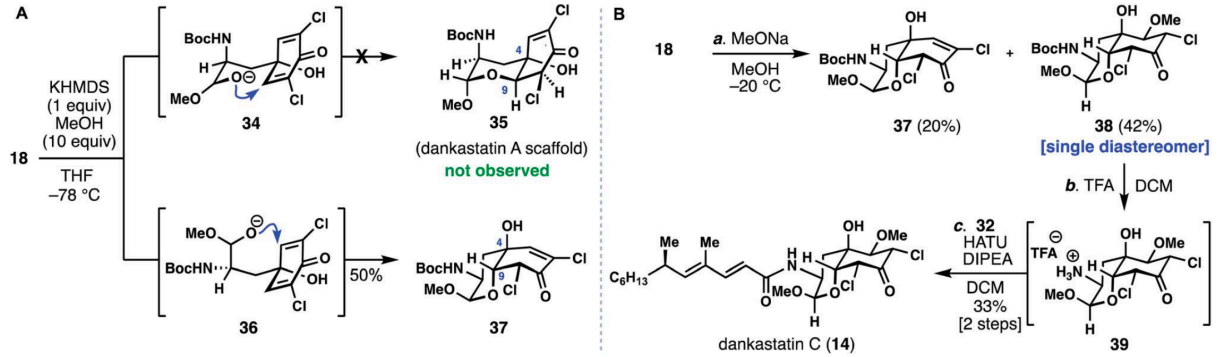

Figure 2.4 Studies toward the dankastatins. (A) Challenges in forming dankastatin A. (B) Total synthesis of dankastatin C.

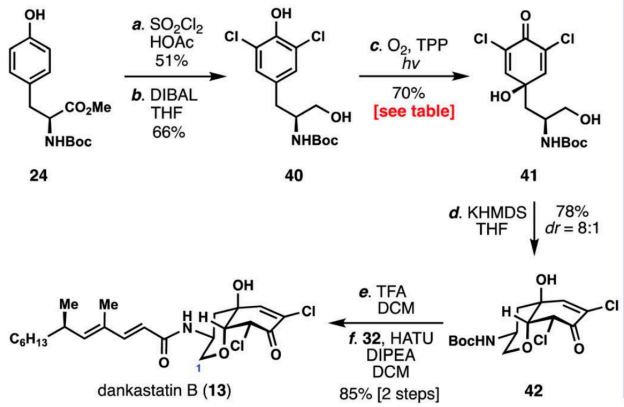

40 $\xrightarrow[\text{additive, } CHCl_3\text{/Acetone}]{O_2,\ h\nu,\ \text{TPP}}$ 41 + 42 + *iso*-42

Entry	Additives	Temp. (°C)	Yield [a]	
			41	42 + *iso*-42
1	none	25	-	-
2	Cs_2CO_3	25	<5%	-
3	Cs_2CO_3	-78 → 25	12%	-
4	Cs_2CO_3, PPh_3	25	-	25%(1.6:1)
5[b]	Cs_2CO_3, Me_2S	25	-	-
6[b]	Cs_2CO_3, $Na_2S_2O_3$	25	-	-
7	Cs_2CO_3, $P(OEt)_3$	25	15%	-
8	Cs_2CO_3, $P(o\text{-}OMeC_6H_4)_3$	-78	30%	-
9	Cs_2CO_3, $P(o\text{-}Tol)_3$	-78 → 25	35%	-
10	Cs_2CO_3, $P(3,5\text{-}(CF_3)_2C_6H_3)_3$	-78	70%	-
11	Cs_2CO_3, $P(3,5\text{-}(CF_3)_2C_6H_3)_3$	-78 → 25	-	32% (2.2:1)

[a] yields and *dr* determined by ^1H NMR. [b] complex mixture, no product detected.

Figure 2.5 Total synthesis of dankastatin B.

2.1.3 Synthesis in Nature

The successful application of proposed biomimetic strategies in the synthesis of dankastatin and gymnastatin alkaloids sheds some light on how nature might make these natural products and the challenges it faces and/or solves in doing so. Yet problems we

encountered in our pursuit of gymnastatin G and dankastatin A led us to consider alternative hypotheses for the origins of these chlorinated alkaloids derived from tyrosine. Specifically, we were drawn to the bis-epoxyketone-containing natural product aranorosin (**15**), which is not halogenated, but bears clear structural, and likely biosynthetic, similarities to **3–14**.[116] Notably, the α-chloroenone in gymnastatin A and the epoxyketone in aranorosin are of the same oxidation level and we wondered if nature might use nucleophilic, chloride-mediated chemistry and not electrophilic chloronium-induced reactions in the construction of this alkaloid family. While there is no evidence that such a transformation is related to the actual biosynthesis of these alkaloids, we note that chloroperoxidases can also carry out P450-like transformations. Given that an oxidase likely constructs aranorosin's bis epoxide motif through double epoxidation of a dienone[116], it is not inconceivable to consider that outer sphere attack by chloride on an initially oxidized product could be relevant to the biosynthesis of these metabolites. Studies by the Wipf lab on the reactivity of aranorosin with sulfur nucleophiles has shown that bicyclo[3.3.1]nonane-containing products can be formed.[131,132]

Commercially available aranorosin reacted with LiCl (1.5 equiv.) at room temperature in THF, forming a variety of chlorinated products under very mild conditions (**Fig. 2.6**). Notably, these conditions are unusually mild for chloride-induced opening/elimination of an epoxyketone, which typically require acid activation or elevated temperatures. Presumably the lithium cation is able to fulfill this role given the highly activated aranorosin bis-epoxide system. Importantly, when tetrabutyl ammonium chloride was used, no conversion occurred under the same conditions. Notably, gymnastatin G (**11**) and 1-epi-gymnastatin G (**33**) were isolated from the reaction mixture in 23% combined yield, presumably through an aldol reaction of intermediate **46**. In addition, two more natural products, namely aranochlor A (**44**) and aranochlor B (**43**), which are oxidized variants of gymnastatins D (**6**) and E (**7**) respectively, were also formed in the reaction (in 12%) and can be viewed as links between gymnastatin A and aranorosin.[133] Notably, the two diastereomeric natural products (presumably generated via E1cB reactions of **45** and **46**) were generated in nearly a 1:1 ratio — an apparent result of nonselective epoxide opening. This observation echoes back to the two diastereomeric skeletons of dankastatins found in nature. Also detected was a small amount of unsaturated aldehyde **47**, a structure reminiscent of prior C–C cleavage products. While we are unaware of **47** being a real natural product, it is interesting to consider whether *Gymnascella dankaliensis* might employ oxidized tyrosines as precursors to electrophilic small molecules containing dehydroalanine-like motifs. In any event, investigations into the enzymology surrounding gymnastatin and dankastatin alkaloid biosynthesis is appealing. **fcdx**

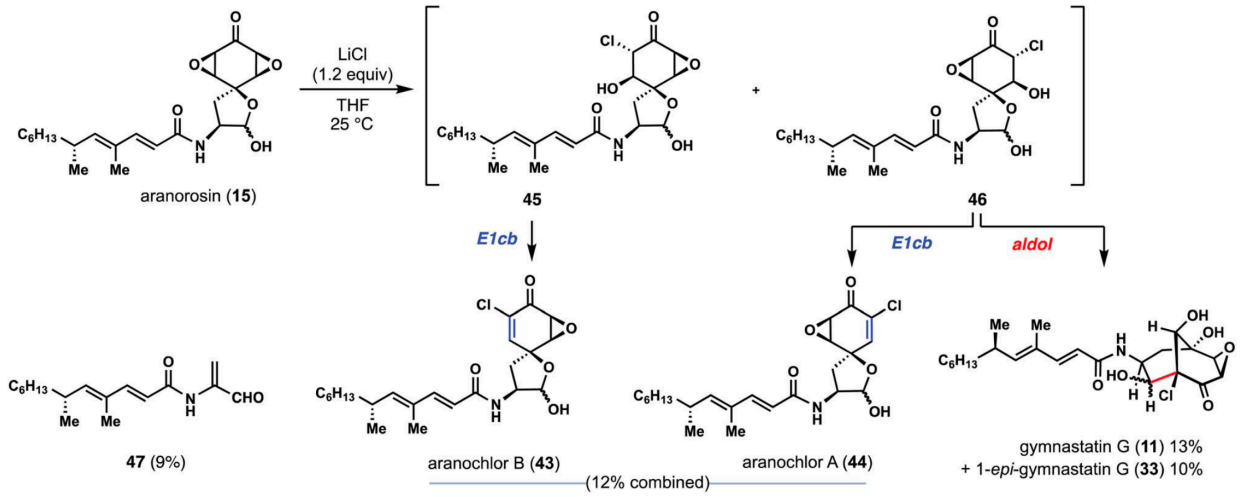

Figure 2.6 Aranorosin as a possible biosynthetic precursor to chlorinated alkaloids from *Gymnascella* sp.

2.3 Effects of Gymnastatin and Dankastatin Family Members on Breast Cancer Phenotypes

With access to five gymnastatin and dankastatin alkaloids – dankastatin B, gymnastatin A, dankastatin C, gymnastatin Q, and gymnastatin G – as well as the related natural product aranorosin, I evaluated their anti-proliferative activity against MDA-MB-231 cells, an aggressive human triple-negative breast cancer (TNBC) cell line. TNBCs that are devoid of estrogen, progesterone, and HER2 receptors are particularly malignant forms of breast cancer that show poor prognosis and have very few treatment options. Thus, identifying new agents that impair TNBC cell proliferation could potentially be therapeutically useful.[134] As noted, many chlorinated tyrosine-derived alkaloids have shown strong anticancer activity, although many of these studies have been conducted in murine tumor cell lines.[113,115,116,127–129] All of these compounds showed dose-responsive impairment of MDA-MB-231 cell proliferation with varying degrees of sensitivity. Dankastatin B exhibited the greatest potency with a 50 % effective concentration (EC_{50}) of 0.57, followed by aranorosin (EC_{50} = 1.6 μM), gymnastatin A (EC_{50} = 2.1 μM), dankastatin C (EC_{50} = 5 μM), and finally the least potent gymnastatin Q (EC_{50} = 20 μM) and gymnastatin G (EC_{50} > 10 μM) (**Fig. 2.7**). Interestingly, bicyclo[3.3.1]nonane-containing gymnastatins Q and G, which also contain only a single electrophilic site in the oxidized tyrosine core, were far less active in this cellular context.

To determine whether dankastatin B's potency was related to general cytotoxicity, we evaluated its anti-proliferative activity against healthy human breast tissue cells. Dankastatin B proved to be far less potent in MCF10a cells (EC_{50} = 3.6 μM) compared to TNBC cells, indicating that its cytotoxicity is specific to cancer phenotypes (**Fig. 2.8**).

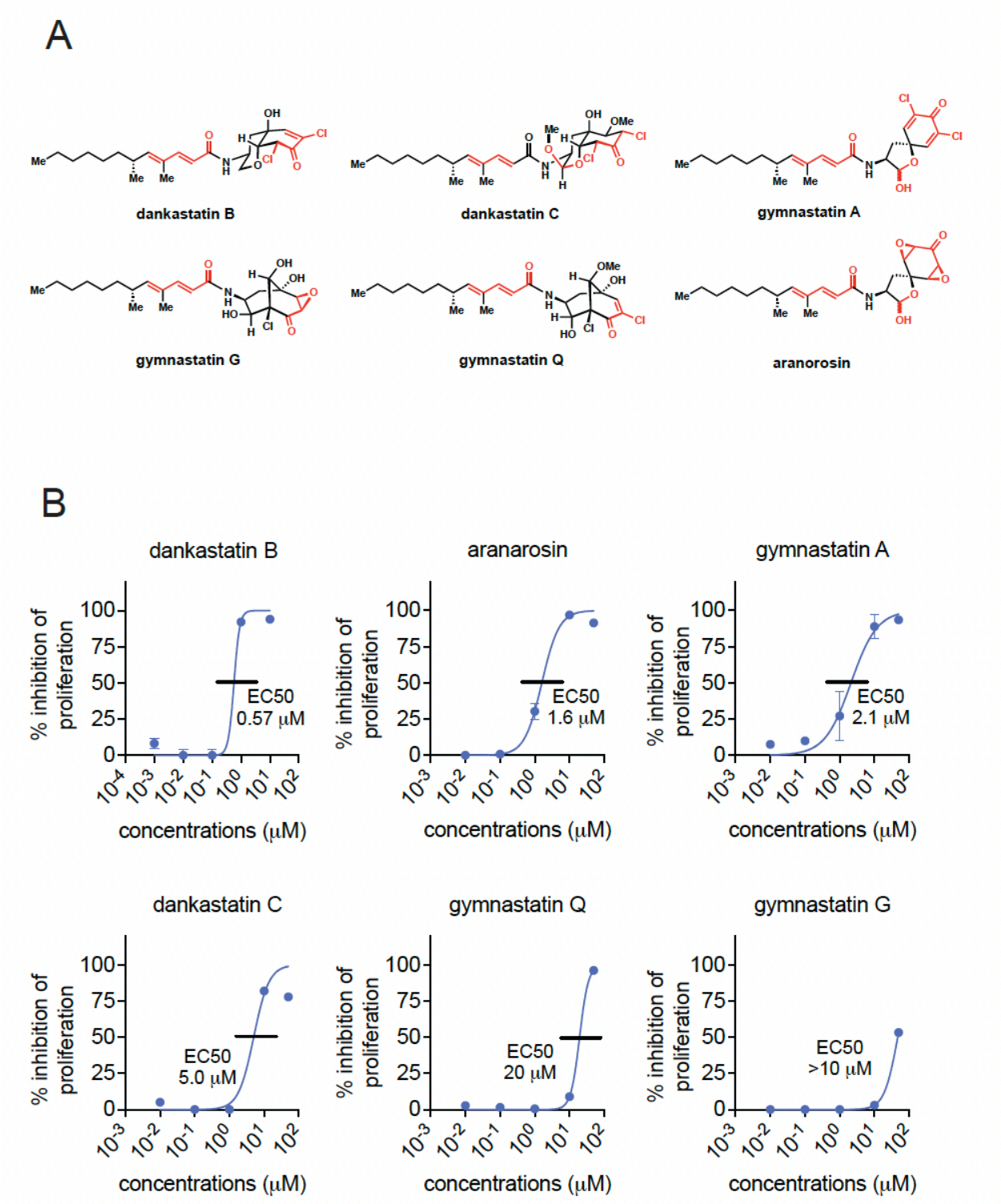

Figure 2.7 Anti-proliferative effects of gymnastatin and dankastatin alkaloids in breast cancer cells. (**A**) Structures of gymnastatin and dankastatin alkaloids tested in this study. Shown in red are potential electrophilic sites on the molecules. (**B**) Inhibition of MDA-MB-231 cell proliferation. MDA-MB-231 breast cancer cells were treated with DMSO vehicle or natural products for 24 h and cell proliferation was assessed by Hoechst

staining. 50 % effective concentration (EC_{50}) are shown. Data shown are average ± sem from n=6 biological replicates/group.

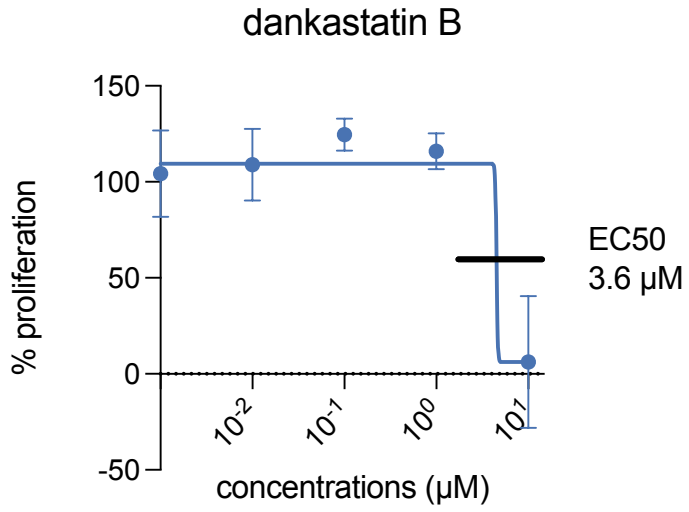

Figure 2.8 Anti-proliferative effects of dankastatin B in healthy breast cells. Inhibition of MCF10a cell proliferation. MCF10a breast cells were treated with DMSO vehicle or dankastatin B for 24 h and cell proliferation was assessed by Hoechst staining. 50 % effective concentration (EC_{50}) is shown. Data shown is average ± sem from n=6 biological replicates/group.

2.4 ABPP to Map Gymnastatin and Dankastatin Targets in Breast Cancer Cells

Given the structural similarity between these classes of natural products, we were intrigued by differences in anti-proliferative effects and the potential for differences in their potential protein target profiles. We focused on mapping the proteome-wide cysteine-reactivity of the most potent dankastatin B and the least potent gymnastatin G using activity-based protein profiling (ABPP) chemoproteomic approaches, namely isotopic tandem orthogonal proteolysis-ABPP (isoTOP-ABPP).[135–137] First performed by Weerapana and Cravatt, isoTOP-ABPP utilizes reactivity-based probes to identify reactive, functional, and ligandable hotspots in complex proteomes.[135,138] In competitive isoTOP-ABPP, covalent small molecules are competed against the binding of broadly reactive reactivity-based probes to facilitate the discovery of proteins and ligandable sites targeted by the covalent small molecule.[92,136,137]

In this study, MDA-MB-231 TNBC cells were treated *in situ* with vehicle or natural product (dankastatin B or gymnastatin G) followed by competitive labeling of the proteome with a cysteine-reactive alkyne-functionalized iodoacetamide probe (IA-alkyne). Any cysteine that was bound by dankastatin B or gymnastatin G would not be labeled by the IA-alkyne probe compared to vehicle controls. Azide-functionalized biotin enrichment handles bearing a TEV protease recognition peptide and an isotopically encoded valine were appended to probe-labeled proteins by copper-catalyzed azide-alkyne cycloaddition (CuAAC) for isoTOP-ABPP analysis. Probe-modified tryptic peptides were analyzed by liquid chromatography-mass spectrometry (LC-MS/MS) and light to heavy tryptic probe-modified peptide ratios, representing control versus treated IA-alkyne-labeled sites, were quantified. Out of >2000 cysteines profiled and quantified across each experiment, dankastatin B (treated at 10 mM) revealed only one target — cysteine 65 on the voltage-dependent anion-selective channel protein 3 (VDAC3) — with a control-to-treated ratio >4, indicating >75 % target engagement, with statistical

significance (adjusted p-value <0.05) (**Fig. 2.9A**, **Dataset S2**). We note that there were an additional 18 targets that showed a ratio >2 with adjusted p-value <0.05, indicating that there are likely additional targets beyond VDAC3 of dankastatin B in breast cancer cells that show ~50-75 % target engagement (**Dataset S2**). Interestingly, among these targets was also C76 of VDAC2, another isoform of VDAC3. VDACs are cysteine-rich, pore-forming proteins that coat the outer membrane of the mitochondria and are major regulators for metabolite exchange between the cytosol and mitochondria. Previous studies have shown that VDAC silencing lead to impaired mitochondrial function, including ATP production, calcium flux, reactive oxygen stress balance and apoptosis (**Fig. 2.10**).[139] In addition to the VDAC proteins, C8 on the RING E3 ubiquitin ligase RNF114 was identified as a target of dankastatin B with a ratio >2 and adjusted p-value <0.05. Interestingly, C8 of RNF114 was previously identified as a target of the natural product nimbolide.[64] Dankastatin B and nimbolide share an α-chloroenone motif, strengthening the findings from previous work suggesting this motif was the minimum unit required to recruit RNF114 (**Fig. 2.11**).[64–66]

In contrast, gymnastatin G did not reveal any targets with controlled-to-treated ratios >4 and only two targets with ratios >2 comparing cells treated with vehicle versus 50 mM of gymnastatin G (**Fig. S1**, **Dataset S3**). These targets with ratios >2 were C70 of RPL27A and C20 of TUB1A — both unrelated to VDAC2/3. The ratio observed for VDAC3 C65 and VDAC2 C70 with gymnastatin G treatment was 0.29 and 0.61, respectively, and not statistically significant. These data may suggest that gymnastatin G is less reactive thank dankastatin B, does not possess potency against dankastatin B targets, or may be unstable in living cells, potentially explaining why dankastatin B showed more potent anti-proliferative effects compared to gymnastatin G.

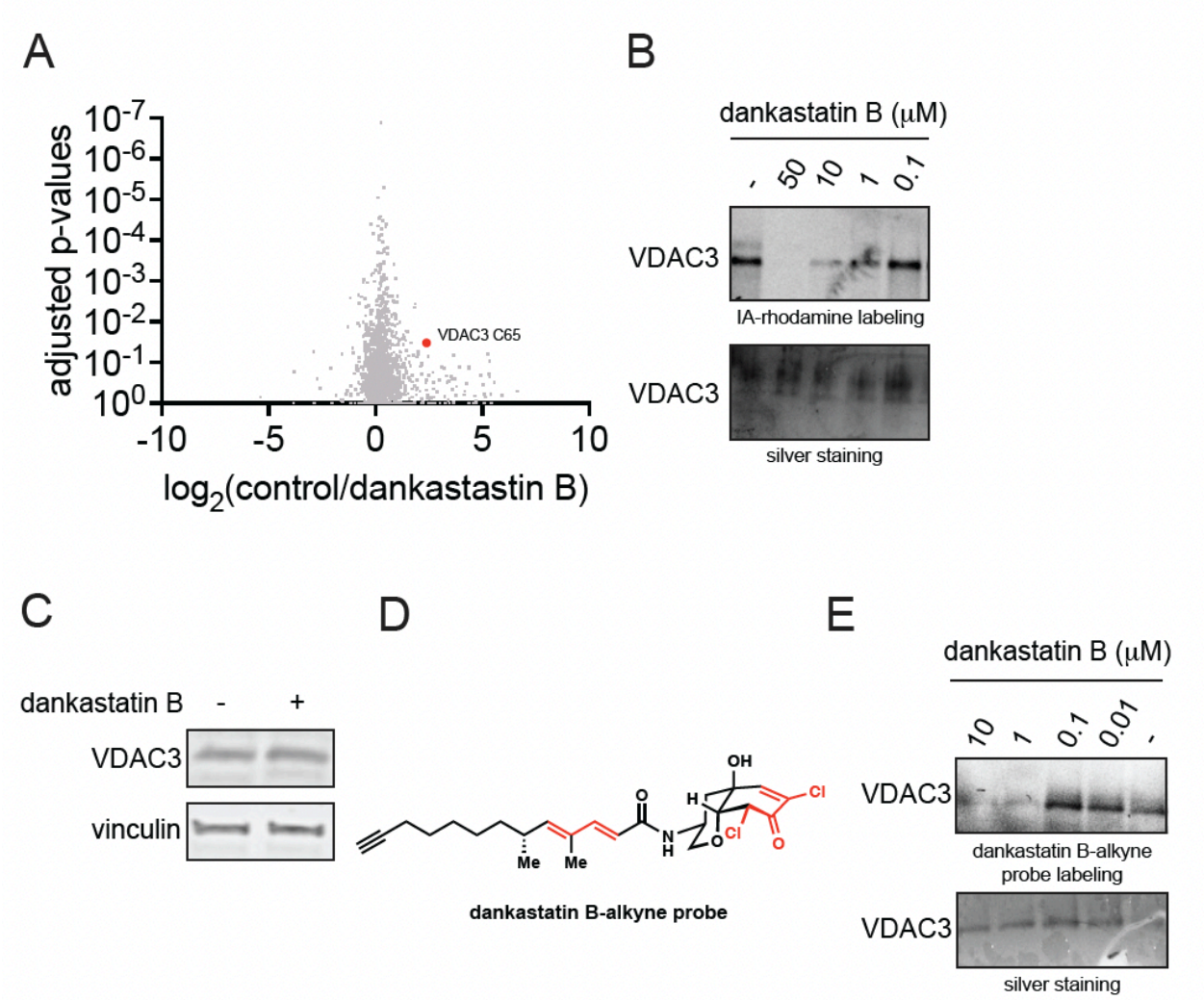

Figure 2.9 Chemoproteomic profiling reveals VDAC3 as a target of dankastatin B. (**A**) isoTOP-ABPP analysis of dankastatin B in MDA-MB-231 breast cancer cells. MDA-MB-231 breast cancer cells were treated with DMSO vehicle or dankastatin B (10 μM) for 1 h. Resulting cell lysates were treated with the cysteine-reactive alkyne-functionalized iodoacetamide probe (IA-alkyne) and subsequently taken through the isoTOP-ABPP procedure and LC-MS/MS analysis. Control (isotopically light) versus treated (isotopically heavy) probe-modified peptide ratios and adjusted p-values were calculated and shown. Shown is red are the targets that showed control/treated ratio >4 with adjusted p-values <0.05 from n=6 biological replicates/group. Only C65 of VDAC3 fit these criteria. (**B**) Gel-based ABPP analysis of dankastatin B against pure VDAC3 protein. Pure VDAC3 protein was pre-incubated with DMSO or dankastatin B for 30 min prior to labeling of protein with a rhodamine-functionalized iodoacetamide (IA-rhodamine) probe (1 μM) for 1 h. Proteins were resolved on SDS-PAGE and subsequently visualized by in-gel fluorescence and protein loading was assessed by silver staining. (**C**) MDA-MB-231 cells were treated with DMSO or dankastatin B (10 μM) for 1h and VDAC3 and loading control vinculin were read out by Western blotting. (**D**) Shown is a structure of the alkyne-functionalized dankastatin B probe, dankastatin B-alkyne. Shown in red are the potential electrophilic sites. (**E**) Dankastatin B-alkyne probe labeling of VDAC3 and competition of probe labeling by

dankastatin B. Pure VDAC3 protein was pre-incubated with DMSO or dankastatin B for 30 min prior to incubation with dankastatin B-alkyne (50 μM) for 30 min. An azide-functionalized rhodamine was subsequently appended onto probe-labeled proteins by copper-catalyzed azide-alkyne cycloaddition, proteins were resolved by SDS-PAGE, and visualized by in-gel fluorescence. Protein loading was assessed by silver staining. Shown in (B, D) are representative gels from n=3 biological replicates/group.

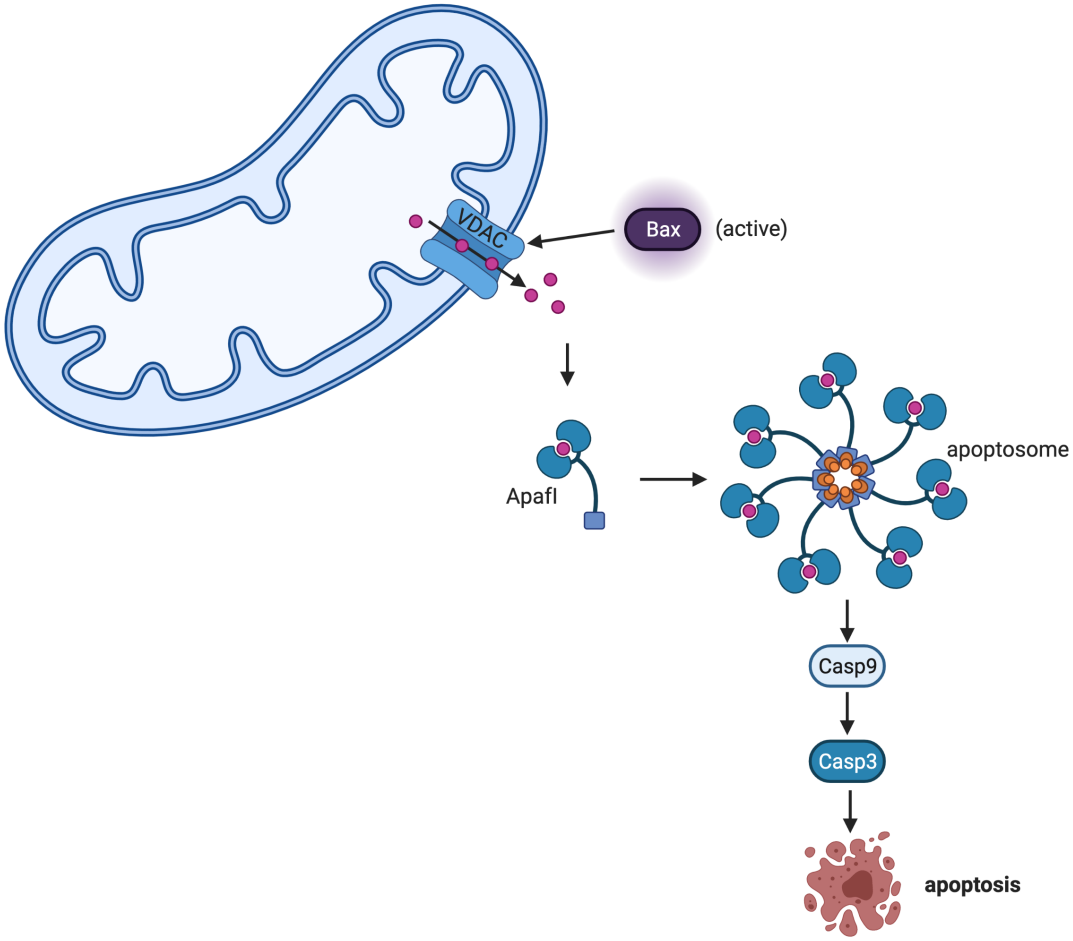

Figure 2.10 Intrinsic Apoptosis. Intrinsic apoptosis is activated by an internal cellular signaling pathway. A cellular stress signal first activates BAX, which interacts with the VDAC channels in the mitochondrial membrane. This interaction leads to the release of cytochrome *c* from the mitochondria. Cytochrome *c* binds to Apaf1, which oligomerizes to form the apoptosome, subsequently activating caspase 9 and initiating a caspase cascade that results in apoptosis.[140,141]

2.5 Characterization of Dankastatin B Interactions with VDAC Proteins

Intrigued by these results, we next biochemically confirmed the interaction of dankastatin B with VDAC3 and VDAC2. First, we showed dose-responsive competition of dankastatin B against the binding of a rhodamine-functionalized cysteine-reactive iodoacetamide probe (IA-rhodamine) to pure VDAC3 and VDAC2 by gel-based ABPP (**Fig. 2.9B**; **Fig. S2A**). We further showed that dankastatin B treatment in cells did not alter VDAC3 protein levels, indicating direct engagement of VDAC3 C65 rather than downregulation of the target in cells (**Fig 2.9C**). Next, we synthesized an alkyne-functionalized probe of dankastatin B (dankastatin B-alkyne) (**Fig. 2.9D**) and showed that this probe directly and covalently binds to pure VDAC3 and VDAC2 protein and that this labeling is also dose-responsively competed out by dankastatin B (**Fig. 2.9E**; **Fig. S2B-S2C**).

While we do not think that VDAC3 is the only target responsible for the anti-proliferative effects of dankastatin B, we nonetheless sought to determine whether VDAC3 plays at least a partial role in the anti-cancer outcomes of this natural product. We showed that VDAC3 knockdown by short-hairpin RNA interference led to hyper-sensitivity to dankastatin B effects in breast cancer cells **(Fig. 2.11A-B).** Interestingly, VDAC2 knockdown by short-hairpin RNA interference led to resistance to dankastatin B effects in TNBC cells.

We do not know currently whether dankastatin B, through targeting C65, inhibits or activates VDAC3 channel activity, its effects on pore assembly with the other VDAC proteins, or its effects on mitochondrial membrane potential or permeability. However, given the various roles of VDAC3 in modulating mitochondrial function and apoptosis[139], we conjectured that covalent targeting of VDAC3 may cause mitochondria-dependent apoptosis of breast cancer cells. Mitochondrial apoptosis occurs through the intrinsic apoptotic pathway that involves activation of caspase 9 (**Fig. 2.10**).[142] Consistent with dankastatin B causing mitochondria-dependent intrinsic apoptosis, we observed significant rescue of dankastatin B anti-proliferative effects with a caspase 9-selective inhibitor z-LEHD-FMK (**Fig. 2.11C**).

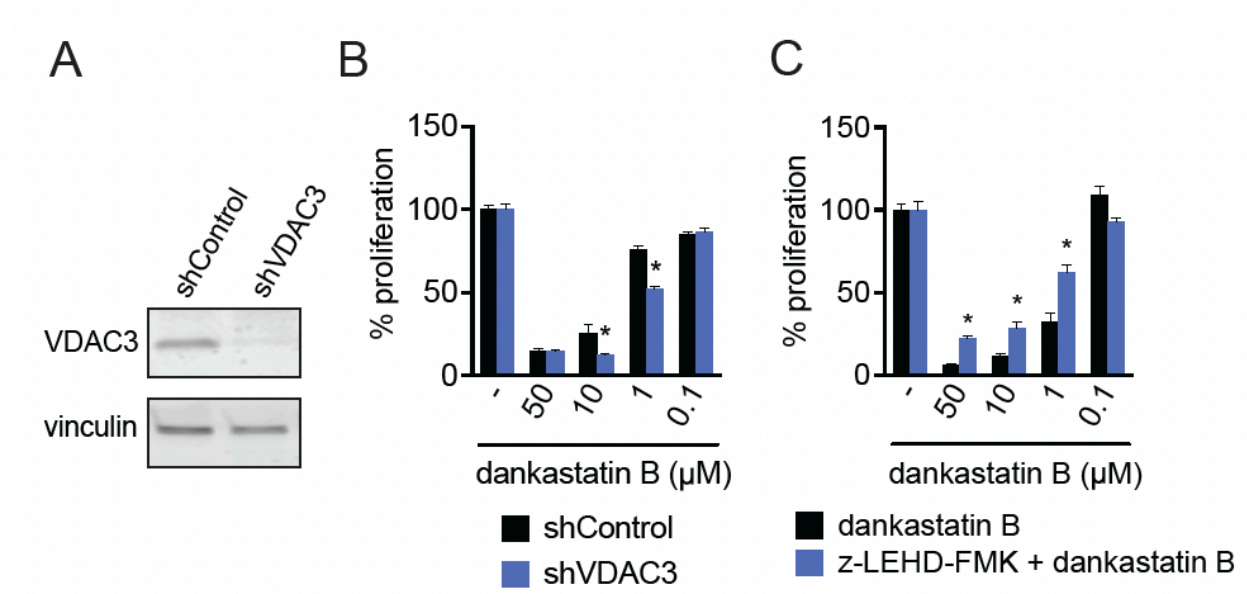

Figure 2.11 Role of VDAC3 in anti-proliferative effects. (**A**) Knockdown of VDAC3. VDAC3 was stably knocked down by short hairpin RNA (shRNA). Knockdown of VDAC3 was validated by Western blotting compared to a loading control vinculin. (**B**) MDA-MB-231 cell proliferation in shControl versus shVDAC3 cells. MDA-MB-231 shControl and shVDAC3 cells were treated with DMSO vehicle or dankastatin B for 8 h and cell proliferation was assessed by Hoechst stain. (**C**) MDA-MB-231 cell proliferation with caspase 9 inhibitor z-LEHD-FMK. MDA-MB-231 cells were pre-treated with DMSO vehicle or z-LEHD-FMK for 2 h prior to treatment with DMSO vehicle or dankastatin B for 8 h. Cell proliferation was read out by Hoechst stain. Data shown are average ± sem from n=6 biological replicates/group. Significance is shown as *p<0.05 compared to the equivalent dankastatin B concentration for shControl in (**B**) or compared to treatment with each dankastatin B concentration alone in (**C**).

2.6 Characterization of Dankastatin B Interactions with RNF114

We also biochemically confirmed the interaction of dankastatin B with RNF114. We showed does-responsive competition of dankastatin B against IA-rhodamine binding to pure RNF114 by gel-based ABPP (**Fig. S5**).

To determine whether RNF114 is at least partially responsible for the anti-proliferative effects of dankastatin B on TNBC cells, we showed that RNF114 knockdown by short-hairpin RNA interference led to resistance to dankastatin B effects in TNBC cells (**Fig. 2.12A-B**).

We do not know whether dankastatin B, through targeting C8, is inducing interactions between RNF114 and a neo-substrate, or enhancing or inhibiting the endogenous function of RNF114. To begin to elucidate this mechanism-of-action, we performed a tandem mass tagging (TMT)-based global quantitative proteomic experiment on MDA-MB-231 cells treated with dankastatin B. This experiment identified the cysteine protease legumain (LGMN) as a protein with levels decreased >50 % with statistical significance (adjusted p-value <0.05) (**Fig. 2.13A**, **Dataset S4**). LGMN plays a role in cell proliferation,

and elevated levels of LGMN correlate with tumor progression in multiple cancer types including breast cancer, indicating that decreasing the abundance of LGMN may be beneficial for anti-cancer effects.[143–146] These results were confirmed by Western blot (**Fig. 2.13B**).

To determine whether dankastatin B is inducing an RNF114-LGMN interaction leading to the subsequent degradation of LGMN, I performed a biochemical validation experiment. I performed a rescue experiment *in situ* using the proteasome inhibitor bortezomib (BTZ) to determine whether the decrease in LGMN levels upon dankastatin B treatment is proteasome-dependent. Interestingly, the decrease in LGMN levels does not appear to be proteasome-dependent. This could suggest an autophagy-based degradation pathway, and further investigation is required to draw any conclusions about the role of RNF114 in decreasing LGMN levels.

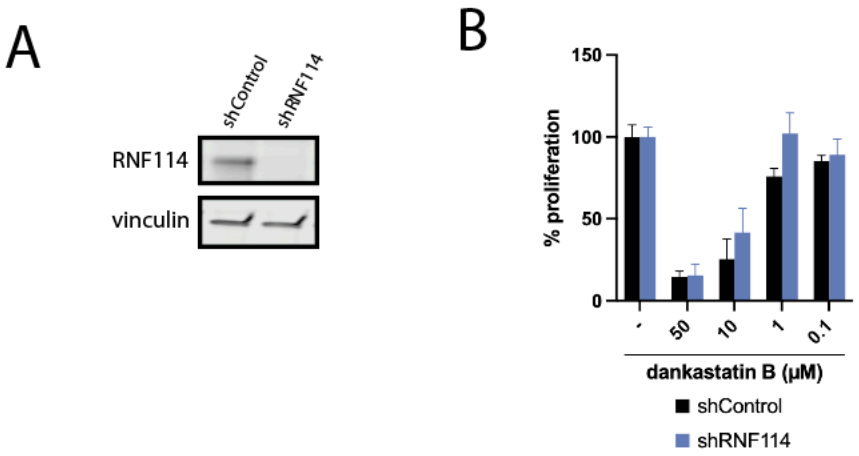

Figure 2.12 Role of RNF114 in anti-proliferative effects. (**A**) Knockdown of RNF114. RNF114 was stably knocked down by short hairpin RNA (shRNA). Knockdown of RNF114 was validated by Western blotting compared to a loading control vinculin. (**B**) MDA-MB-231 cell proliferation in shControl versus shRNF114 cells. MDA-MB-231 shControl and shRNF114 cells were treated with DMSO vehicle or dankastatin B for 8 h and cell proliferation was assessed by Hoechst stain.

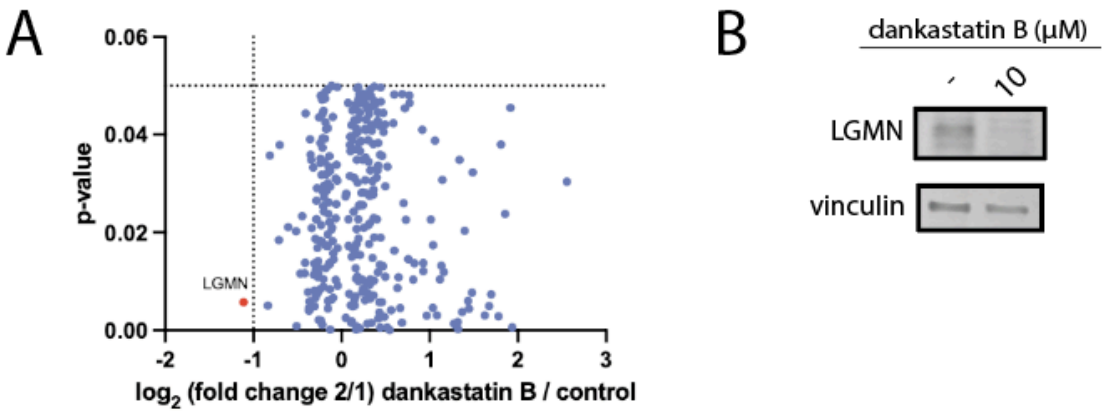

Figure 2.13 TMT Analysis of dankastatin B. (**A**) Tandem mass tag (TMT)-based quantitative proteomic profiling of dankastatin B in MDA-MB-231 breast cancer cells. MDA-MB-231 breast cancer cells were treated with DMSO vehicle or dankastatin B (10 μM) for 4 h. Shown in red are the proteins significantly enriched or reduced. Legumain (LGMN) was the only protein reduced by >50% with a p-value<0.05. Data are from n = 3 biological replicates/group. (**B**) Western blotting analysis of LGMN and loading control vinculin levels in MDA-MB-231 cells treated with DMSO vehicle or dankastatin B (10 μM) for 4 h.

2.7 Conclusions

Our studies investigated potential mode of action of the electrophilic natural product dankastatin B, a family member of an interesting class of chlorinated gymnastatin and dankastatin alkaloids. We first presented simple synthetic pathways to five of the gymnastatin and dankastatin alkaloids, spanning all three scaffold types (spirocyclic dienone, bicyclo[3.1.1]nonane, and oxo-decalin). We reported growth inhibitory activity of six gymnastatin and dankastatin family members against human triple-negative breast cancer cells. We showed relatively selective covalent targeting of C65 on the mitochondrial pore-forming VDAC3. We also demonstrate direct covalent binding to a VDAC3 isoform VDAC2 on C76. We also demonstrated that VDAC3 was at least partially involved in the anti-proliferative effects observed with dankastatin B. Interestingly, we showed that a closely related natural product gymnastatin G that demonstrated poorer anti-cancer potency, showed very little reactivity compared to dankastatin B.

Of future interest is to further investigate the structure-activity relationships of gymnastatin and dankastatin B alkaloids and their effects on VDAC2/3. Also worthy of further investigation is whether targeting key cysteines within VDAC proteins may represent a potential therapeutic strategy for cancer. Furthermore, the approaches taken here only revealed covalent cysteine targets of dankastatin B since we performed ABPP analysis with a cysteine-reactive probe. Dankastatin B may possess additional protein targets that act through covalent interactions with other amino acids or engage targets through reversible interactions. Future studies with orthogonal profiling platforms may

yield additional anti-cancer mechanisms of this interesting class of natural products. Collectively, our work further highlights the utility of chemoproteomic platforms to discover the mode of action of biologically active natural products.

2.8 Acknowledgement of Co-Author Contributions

B.P. Belcher, B. Tong, T.J. Maimone, and D.K. Nomura conceived of the project idea and wrote the papers. B.P. Belcher designed experiments, performed experiments, and analyzed and interpreted the data. B. Tong designed and performed synthetic experiments. P.A. Machicao, E. Ho, J. Friedli, B. So, H. Bui, and Y. Isobe performed experiments, analyzed and interpreted data, and provided intellectual contributions.

2.9 Methods

2.9.1 Cell Culture

MDA-MB-231 cells were obtained from the UC Berkeley Cell Culture Facility and were cultured in L15 medium (HyClone) containing 10% (v/v) fetal bovine serum (FBS) and maintained at 37°C with 0% CO_2. HEK293T cells were obtained from the UC Berkeley Cell Culture Facility and were cultured in Dulbecco's Modified Eagle Medium (DMEM) containing 10% (v/v) FBS and maintained at 37°C with 5% CO_2.

2.9.2 Proliferation Assays

Cell proliferation assays were performed using Hoechst 33342 dye (Invitrogen) according to the manufacturer's protocol and as previously described.[92] MDA-MB-231 cells were seeded into 96-well plates (20,000 cells/well) in a volume of 150 µL and allowed to adhere overnight. Cells were treated with an additional 50 µL of media containing DMSO vehicle or a 1:250 dilution of 1,000x alkaloid natural product stock. After the incubation period, the media was removed from each well and 100 µL of staining solution containing 10% formalin and Hoechst 33342 dye was added to each well. The cells were incubated for 15 min in the dark at room temperature, the staining solution was removed, and the fixed cells were washed with PBS before imaging. Fluorescence was read with a Tecan Spark plate reader (λex = 350 nm, λem = 461 nm).

2.9.3 Assessing Apoptosis in Breast Cancer Cells

MDA-MB-231 cells were seeded into 96-well plates (20,000 cells/well) in a volume of 150 µL and allowed to adhere overnight. Cells were pre-treated with caspase 9 inhibitor z-LEHD-FMK (20 µM final concentration, Abcam) for 2 h. Cells were then treated with dankastatin B (1,000x stock in DMSO) or DMSO vehicle. After an 8 h incubation, the media was removed from each well and 100 µL of staining solution containing 10% formalin and Hoechst 33342 dye was added to each well. The cells were incubated for 15 min in the dark at room temperature, the staining solution was removed, and the fixed cells were washed with PBS before imaging. Fluorescence was read with a Tecan Spark plate reader (λex = 350 nm, λem = 461 nm).

2.9.4 Preparation of Cell Lysates

Cells were washed with cold PBS, scraped, and pelleted by centrifugation (1400 g, 5 min, 4°C). Pellets were resuspended in cold PBS, lysed by sonication or using RIPA buffer, and clarified by centrifugation (12,000 g, 10 min, 4°C). Lysate was transferred to low-adhesion microcentrifuge tubes. Proteome concentrations were determined using BCA assay and lysate was diluted with PBS to appropriate working concentrations.

2.9.5 Western Blotting

Antibodies to VDAC3 (Invitrogen, PA5-51156), VDAC2 (Abcam, Ab1216120), VDAC1 (CST 4661S), RNF114 (Sigma, HPA021184), LGMN (Abcam, Ab183028), and vinculin (Bio-Rad, MCA465GA) were obtained from various commercial sources and dilutions were prepared per the manufacturers' recommendations. Proteins were resolved by SDS/PAGE and transferred to nitrocellulose membranes using the Trans-Blot Turbo transfer system (Bio-Rad). Membranes were blocked in 5% BSA in Tris-buffered saline containing Tween 20 (TBS-T) solution for 30 min at RT, washed in TBS-T, and probed with primary antibody for 1.5 h at RT. Membranes were washed again with TBS-T and incubated for 1 h at RT in the dark with IR680- and IR800-conjugated secondary antibodies at 1:10,000 dilution in 5% BSA in TBS-T. Following 3 additional TBS-T washes, bots were visualized using an Odyssey Li-Cor fluorescent scanner.

2.9.6 isoTOP-ABPP Chemoproteomics

IsoTOP-ABPP studies were performed as previously reported.[92,135,137] Cells were lysed by probe sonication in PBS and protein concentrations were measured by BCA assay. Cells were treated for 1 h with either DMSO vehicle or alkaloid natural product before cell collection and lysis. Proteomes were subsequently labeled with IA-alkyne labeling (100 μM) for 1 h at RT. CuAAC was used by sequential addition of tris(2-carboxyethyl)phosphine (1 mM, Strem), tris[(1-benzyl-1H-1,2,3-triazol-4-yl)methyl]amine (34 μM, Sigma), copper (II) sulfate (1 mM, Sigma) and biotin-linker-azide – the linker functionalized with a tobacco etch virus (TEV) protease recognition sequence as well as an isotopically light or heavy valine for treatment of control or treated proteome, respectively. After CuAAC, proteomes were precipitated by centrifugation at 6,500 g, washed in ice-cold methanol, combined in a 1:1 control/treated ratio, washed again, then denatured and resolubilized by heating in 1.2% SDS/PBS to 90°C for 5 min. Insoluble components were precipitated by centrifugation at 6,500 g and soluble proteome was diluted in 5 mL 0.2% SDS/PBS. Labeled proteins were bound to streptavidin-agarose beads (170 μL resuspended beads per sample, Thermo Fisher) while rotating overnight at 4°C. Bead-linked proteins were enriched by washing three times each in PBS and water, then resuspended in 6 M urea/PBS (Sigma), reduced in DTT (9.26 mM, Thermo Fisher), and alkylated with iodoacetamide (18 mM, Sigma) before being washed and resuspended in 2 M urea/PBS and trypsinized overnight with 0.5 μg/μL sequencing-grade trypsin (Promega). Tryptic peptides were eluted. Beads were washed three times each in PBS and water, washed in TEV buffer solution (water, TEV buffer, 100 μM dithiothreitol) and resuspended in buffer with Ac-TEV protease (Invitrogen) and incubated overnight.

Peptides were diluted in water, acidified with formic acid (1.2 M, Fisher), and prepared for analysis.

2.9.7 isoTOP-ABPP Mass Spectrometry Analysis

Peptides from all chemoproteomic experiments were pressure-loaded onto a 250 μm inner diameter fused silica capillary tubing packed with 4 cm of Aqua C18 reverse-phase resin (Phenomenex, 04A-4299), which had been previously equilibrated on an Agilent 600 series high-performance liquid chromatograph using the gradient from 100% buffer A to 100% buffer B over 10 min, followed by a 5 min wash with 100% buffer B and a 5 min wash with 100% buffer A. The samples were then attached using a MicroTee PEEK 360 μm fitting (Thermo Fisher Scientific, p-888) to a 13 cm laser-pulled column packed with 10 cm Aqua C18 reverse-phase resin and 3 cm of strong-cation exchange resin for isoTOP-ABPP studies. Samples were analyzed using an Q Exactive Plus mass spectrometer (Thermo Fisher Scientific) using a five-step Multidimensional Protein Identification Technology (MudPIT) program, using 0, 25, 50, 80 and 100% salt bumps of 500 mM aqueous ammonium acetate and using a gradient of 5–55% buffer B in buffer A (buffer A: 95:5 water/acetonitrile, 0.1% formic acid; buffer B 80:20 acetonitrile/water, 0.1% formic acid). Data were collected in data-dependent acquisition mode with dynamic exclusion enabled (60 s). One full mass spectrometry (MS1) scan (400–1,800 mass-to-charge ratio (*m/z*)) was followed by 15 MS2 scans of the *n*th most abundant ions. Heated capillary temperature was set to 200 °C and the nanospray voltage was set to 2.75 kV.

Data were extracted in the form of MS1 and MS2 files using Raw Extractor v.1.9.9.2 (Scripps Research Institute) and searched against the Uniprot human database using ProLuCID search methodology in IP2 v.3-v.5 (Integrated Proteomics Applications, Inc.).[147] Cysteine residues were searched with a static modification for carboxyaminomethylation (+57.02146) and up to two differential modifications for methionine oxidation and either the light or heavy TEV tags (+464.28596 or +470.29977, respectively). Peptides were required to be fully tryptic peptides and to contain the TEV modification. ProLUCID data were filtered through DTASelect to achieve a peptide false-positive rate below 5%. Only those probe-modified peptides that were evident across two out of three biological replicates were interpreted for their isotopic light to heavy ratios. For those probe-modified peptides that showed ratios greater than two, we only interpreted those targets that were present across all three biological replicates, were statistically significant and showed good quality MS1 peak shapes across all biological replicates. Light versus heavy isotopic probe-modified peptide ratios are calculated by taking the mean of the ratios of each replicate paired light versus heavy precursor abundance for all peptide-spectral matches associated with a peptide. The paired abundances were also used to calculate a paired sample *t*-test *P* value in an effort to estimate constancy in paired abundances and significance in change between treatment and control. *P* values were corrected using the Benjamini–Hochberg method.

2.9.8 Purification of Human RNF114

A lentiviral plasmid encoding human RNF114 with a C-terminal FLAG tag was purchased from Origene for expression in and purification from HEK293T cells. For

lentivirus production, lentiviral plasmids and packaging plasmids (pMD2.5G, Addgene catalog no. 12259 and psPAX2, Addgene catalog no. 12260) were transfected into HEK293T cells using Lipofectamine 2000 (Invitrogen). Lentivirus was collected from filtered cultured medium and used to infect the target cell line with 1:1000 dilution of polybrene. Target cells were selected over 2 d with 7.5 µg/ml of puromycin.

Cells were collected in PBS, lysed with IP lysis buffer (Pierce), and batch-bound with magnetic anti-DYKDDDDK resin (ThermoFisher) for 2 h. Bound lysate and resin were washed with PBS and protein was eluted with 1.5 mg/mL 3x FLAG peptide. Samples were desalted and concentrated. Purity and concentration were verified by PAGE, Western Blot, ultraviolet spectroscopy, and BCA assay.

2.9.9 Gel-Based ABPP

Gel-Based ABPP methods were performed as previously described.[92] Recombinant pure human VDAC2 was obtained from NOVUS (NBP1-89477PEP), recombinant pure human VDAC3 was obtained from Abnova (H00007419-P01), and recombinant pure human VDAC1 was obtained from NOVUS (H00007416-Q03). Recombinant pure human RNF114 was purified as described above. Proteins (0.1 µg) were pre-treated with either DMSO vehicle or dankastatin B for 30 min at 37°C in an incubation volume of 25 µL PBS, and subsequently treated with IA-Rhodamine (1 µM, Setareh Biotech) for 1 h in the dark at room temperature. The reactions were stopped by the addition of 4x reducing Laemmli SDS sample loading buffer (Alfa Aesar) and heated at 95°C for 5 min. The samples were separated on precast 4-20% Criterion TGX gels (Bio-Rad). Probe-labeled proteins were analyzed by in-gel fluorescence using a ChemiDoc MP (Bio-Rad). Protein loading was assessed by silver stain.

For competitive gel-based ABPP experiments, proteins (0.1 µg) were pre-treated with either DMSO vehicle or dankastatin B for 30 min at 37°C in an incubation volume of 25 µL PBS, and subsequently treated with an appropriate concentration of dankastatin B-alkyne for 30 min at 37°C. CuAAC was performed to append rhodamine-azide (1 µM final concentration) onto alkyne probe-labeled proteins. Samples were then diluted with 4x reducing Laemmli SDS sample loading buffer and heated at 95°C for 5 min. The samples were separated on precast 4-20% Criterion TGX gels (Bio-Rad). Prior to analysis, gels were fixed in a solution of 10% acetic acid and 30% ethanol for 1 h. Probe-labeled proteins were analyzed by in-gel fluorescence using a ChemiDoc MP (Bio-Rad). Protein loading was assessed by silver stain.

2.9.10 Knockdown Studies

Short-hairpin oligonucleotides were used to knock down the expression of VDAC2 and VDAC3 in MDA-MB-231 cells. For lentivirus production, lentiviral plasmids and packaging plasmids (pMD2.5G, Addgene catalog no. 12259 and psPAX2, Addgene catalog no. 12260) were transfected into HEK293T cells using Lipofectamine 2000 (Invitrogen). Lentivirus was collected from filtered cultured medium and used to infect the target cell line with 1:1000 dilution of polybrene. Target cells were selected over 2 d with 10 µg/ml of puromycin. The short-hairpin sequences which were used for generation of the knockdown lines were:

VDAC1: GCTTGGTCTAGGACTGGAATT (Sigma VDAC1 MISSION shRNA Bacterial Glycerol Stock, TRCN0000278564)
VDAC2: GCTACCCACCAATAATGAAAT (Sigma VDAC2 MISSION shRNA Bacterial Glycerol Stock, TRCN0000151244).
VDAC3: CAGGCAACCTAGAAACCAAAT (Sigma VDAC3 MISSION shRNA Bacterial Glycerol Stock, TRCN0000141213).
RNF114: CCATGGCTGCCGTAAGAATTT (Sigma RNF114 MISSION shRNA Bacterial Glycerol Stock, TRCN0000314877)
MISSION TRC1.5 pLKO.1-puro Non-Mammalian shRNA Control (Sigma) was used as a control shRNA.

2.9.11 TMT Proteomics

Cells were treated with either DMSO vehicle or dankastatin B (10 μM) for 4 h and lysate was prepared as described above. Briefly, 25-100 μg protein from each sample was reduced, alkylated, and tryptically digested overnight. Individual samples were then labeled with isobaric tags using commercially available TMTsixplex (Thermo Fisher Scientific, P/N 90061) kits, in accordance with the manufacturer's protocols. Tagged samples (20 μg per sample) were combined, dried with SpeedVac, resuspended with 300 μL 0.1% TFA in H_2O, and fractionated using high pH reversed-phase peptide fractionation kits (Thermo Scientific, P/N 84868) according to manufacturer's protocol. Fractions were dried with SpeedVac, resuspended with 50 μL 0.1% FA in H_2O, and analyzed by LC-MS/MS as described below.

Quantitative TMT-based proteomic analysis was performed as previously described using a Thermo Eclipse with FAIMS LC-MS/MS.[148] Acquired MS data was processed using ProLuCID search methodology in IP2 v.3-v.5 (Integrated Proteomics Applications, Inc.).[149] Trypsin cleavage specificity (cleavage at K, R except if followed by P) allowed for up to 2 missed cleavages. Carbamidomethylation of cysteine was set as a fixed modification. Methionine oxidation and TMT-modification of N-termini and lysine residues were set as variable modifications. Reporter ion ratio calculations were performed using summed abundances with most confident centroid selected from 20 ppm window. Only peptide-to-spectrum matches that are unique assignments to a given identified protein within the total dataset are considered for protein quantitation. High confidence protein identifications were reported with a <1% false discovery rate (FDR) cut-off. Differential abundance significance was estimated using ANOVA with Benjamini-Hochberg correction to determine p-values.

CHAPTER 3

Acyl Silanes as Photoaffinity Probes

This chapter is partially based on the *Chemical Science* publication “Photo-Brook rearrangement of acyl silanes as a strategy for photoaffinity probe design”[150] and has been adapted with permission from all co-authors.

3.1 Introduction

Identifying drivers of on- and off-target phenotypic responses to bioactive small molecules remains a significant challenge in the field of drug discovery, particularly for low-affinity or low-abundance targets.[151–154] One of the most powerful approaches to target deconvolution in a native cellular environment is photoaffinity labeling (PAL), which allows for the capture of transient, non-covalent small molecule–protein interactions in a proteome-wide fashion.[155–159] In photoaffinity labeling, a molecule of interest is conjugated to a light-reactive functional group that generates a high-energy intermediate capable of covalently capturing associated proteins when exposed to UV light. Conventional photoaffinity probes employ diazirines,[160] aryl azides,[161] and diaryl ketones,[162] which give rise to carbene, nitrene, and ketyl radical intermediates, respectively (**Fig. 3.1A**). All three have shown tremendous value as photoaffinity warheads in a variety of PAL applications,[155–159] often in a synthetically modular fashion as exemplified by the suite of "minimalist" photocrosslinking diazirines developed by the Yao group.[163,164] However, not every PAL campaign that utilizes these probes is successful, reflecting the requirements for correct positioning and distance of the photoreactive moiety as well as overall low crosslinking efficiencies typically observed. In addition, the warhead-specific labeling of non-target proteins often results in false positive hits, potentially obscuring true cellular targets of the pharmacophore.[165,166] Taken together, the dearth of photocrosslinking functionalities is an inherent limitation for applications of PAL-based workflows—a more varied set of photoreactive motifs would greatly aid target elucidation, both by providing additional tools for capture of protein targets as well as alternative synthetic approaches for a given probe of interest. However, the development of a novel PAL warhead is contingent upon fulfilling a number of rigorous requirements. Ideally, it should possess a long-wavelength UV absorbance profile to minimize cellular and protein damage during irradiation, rapidly generate a short-lived reactive intermediate capable of residue-agnostic crosslinking, and minimally perturb the native substrate–protein interactions. As a result, only a small number of motifs have been recently disclosed meeting these criteria, including aryl tetrazole[167] and thienyl ketoamide[168] probes.

Acyl silanes are an intriguing functionality with ideal properties for use as a photoaffinity warhead. Upon irradiation, acyl silanes undergo a 1,2-photo Brook rearrangement to reveal a stabilized α-siloxy carbene, which has since been shown to insert into a variety of acidic, polar, and non-polarized bonds to yield X–H insertion products in high yields (**Fig. 3.1B**).[169–175] The rearrangement occurs with high quantum yields to the α-siloxy carbene[176] at long UV wavelengths (350–420 nm) ideal for photocrosslinking. We became interested in utilizing the 1,2-photo Brook rearrangement as an orthogonal mechanism for carbene generation that could bypass deleterious competing pathways common to other carbene precursors, such as diazo formation from diazirines,[177,178] and provide complementary reactivity to known warheads (**Fig. 3.1C**). Moreover, acyl silanes allow for modular substitution on the photoactive moiety itself, offering the potential for direct tuning of desired steric and electronic properties of the probe.

Herein, we report the design, synthesis, and evaluation of several acyl silane photoaffinity probes. Upon investigation, an *i*Pr-substituted acyl silane was identified that

yielded superior labeling in cellular lysate relative to Me and Ph probe derivatives and avoided unwanted thermal background labeling. Subsequently, we synthesized (+)-JQ1- and rapamycin-derived *i*Pr acyl silanes and confirmed their labeling efficiency and selectivity on pure recombinant proteins. Furthermore, our *i*Pr-substituted acyl silane probe demonstrated similar levels of labeling to a "minimalist" diazirine probe in cellular lysate, suggesting the overall promise of acyl silanes as a novel scaffold for PAL.

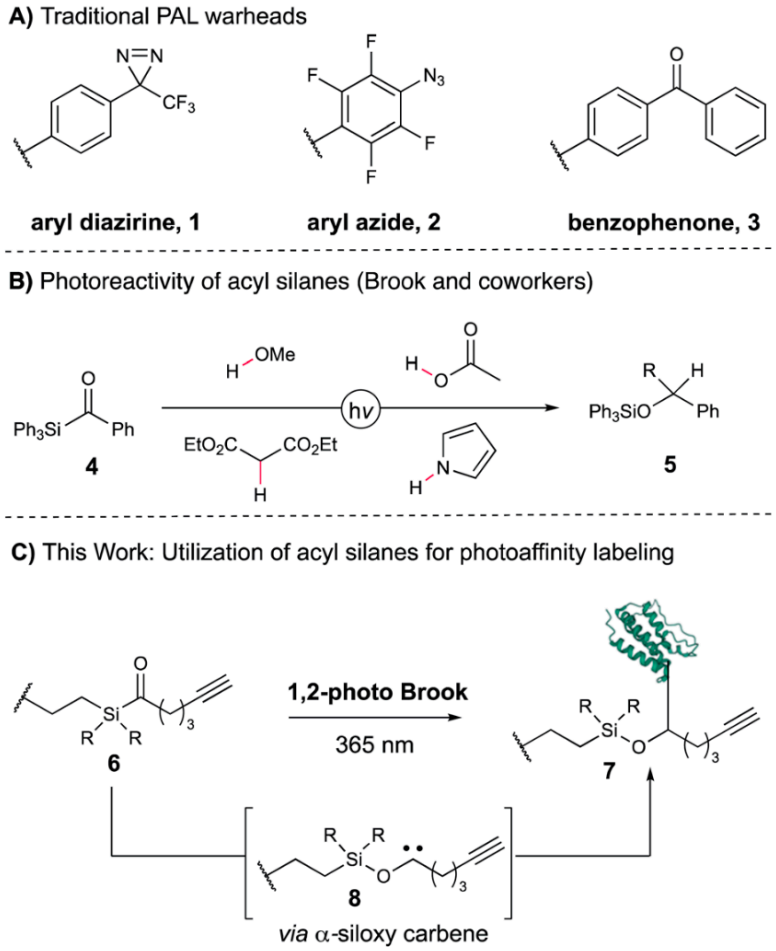

Fig. 3.1 Investigation of 1,2-photo Brook rearrangement of acyl silanes for photoaffinity labeling.

3.2 Synthesis and Evaluation of Acyl Silane Carbamate Probes

We began by synthesizing a probe that contained an alcohol as a modular site of attachment for conjugation to a small molecule of interest and an alkyne handle, which could be used for either pull-down experiments or visualization after further reaction with a suitable azide dye via Cu-catalyzed azide-alkyne click chemistry.[179] Additionally, a series of warheads with varying silane substitution were evaluated to probe the role of sterics on photolabeling. Starting from a TBS-protected allyl alcohol **9**, Me- and Ph-substituted silyl dithianes **11a and b** were obtained in 80 and 71% yields, respectively,

following a Pt-catalyzed hydrosilylation/lithiation sequence. Subsequent alkylation of the lithiated dithianes and deprotection of both the alkyne and TBS moieties yielded alcohols **13a and b** (**Scheme 3.1A**). A similar sequence was followed in the preparation of *i*Pr-substituted silane **13c** from *p*-methoxybenzyl-protected allyl alcohol (**Scheme 3.1B**). Following elaboration of the alcohol, oxidative cleavage of the dithiane with PIFA provided the desired acyl silane probes in high yields (**Scheme 3.1C**).[180] Following deprotection, we confirmed that the acyl silanes **15a–c** each possessed a long-wavelength UV λ_{max} between 364–370 nm, which was consistent with reported values and is ideally suited for utilization as a photoaffinity warhead. The reactivity of acyl silanes **15a–c** in MeOH was also evaluated. To avoid possible damage to the protein or proteins of interest, photoaffinity probes should have short irradiation times; consistent with this, all three acyl silanes showed 80% or greater conversion over a 30-minute period upon irradiation with a simple 6 W handheld UV lamp (**Fig. 3.2**). Analysis of the irradiation reaction in MeOH with acyl silane **15b** confirms the formation of an acetal consistent with α-siloxy carbene insertion into the O–H bond of MeOH, and in accordance with the adducts reported by Brook (**Fig. S3.4**).[169]

After validating the photoactivity of the acyl silane probes with long-wavelength UV irradiation, their labeling performance in cell lysate was evaluated. Following a 30-minute incubation period, lysates treated with probes **15a–c** were irradiated for 30 minutes on ice, followed by a Cu-catalyzed click reaction with rhodamine azide. Labeled proteins were subsequently visualized by in-gel fluorescence. All probes displayed light-dependent labeling of proteins as well as an increase in labeling over DMSO control (**Fig. 3.3A**). However, samples treated with *i*Pr-substituted probe **15c** showed significantly greater fluorescence over **15a** and **15b**. While the increased labeling may be the result of increased hydrophobicity of probe **15c**, we hypothesized the difference in labeling may be due to the inherent instability of the probes **15a** and **15b** in cell lysate prior to irradiation. Acyl silanes are known to undergo a slow, thermal 1,2-Brook rearrangement in the presence of primary amines (i.e. lysine), which could not only result in probe decomposition before crosslinking but could also result in uncontrolled background thermal labeling processes.[181] A more sterically hindered probe (i.e. **15c**) could minimize probe decomposition by slowing the rate of background, thermal 1,2-Brook rearrangement. Thus, to evaluate their stability, probes **15a–c** were incubated for either 0, 0.5, 2, or 24 hours in cell lysate prior to 30 minute irradiation, with labeled proteins visualized in a similar fashion as prior (**Fig. 3.3B**). Consistent with the previous results, *i*Pr-substituted acyl silane **15c** showed no increase in background signal over the course of the experiment and exhibited minimal loss of fluorescence. In contrast **15b**, and to a greater extent **15a**, showed increased thermal labeling upon extended incubation. Interestingly, all probes showed a decrease of light-dependent labeling over extended incubation, possibly due to instability of the proteome over extended time periods at ambient temperatures.

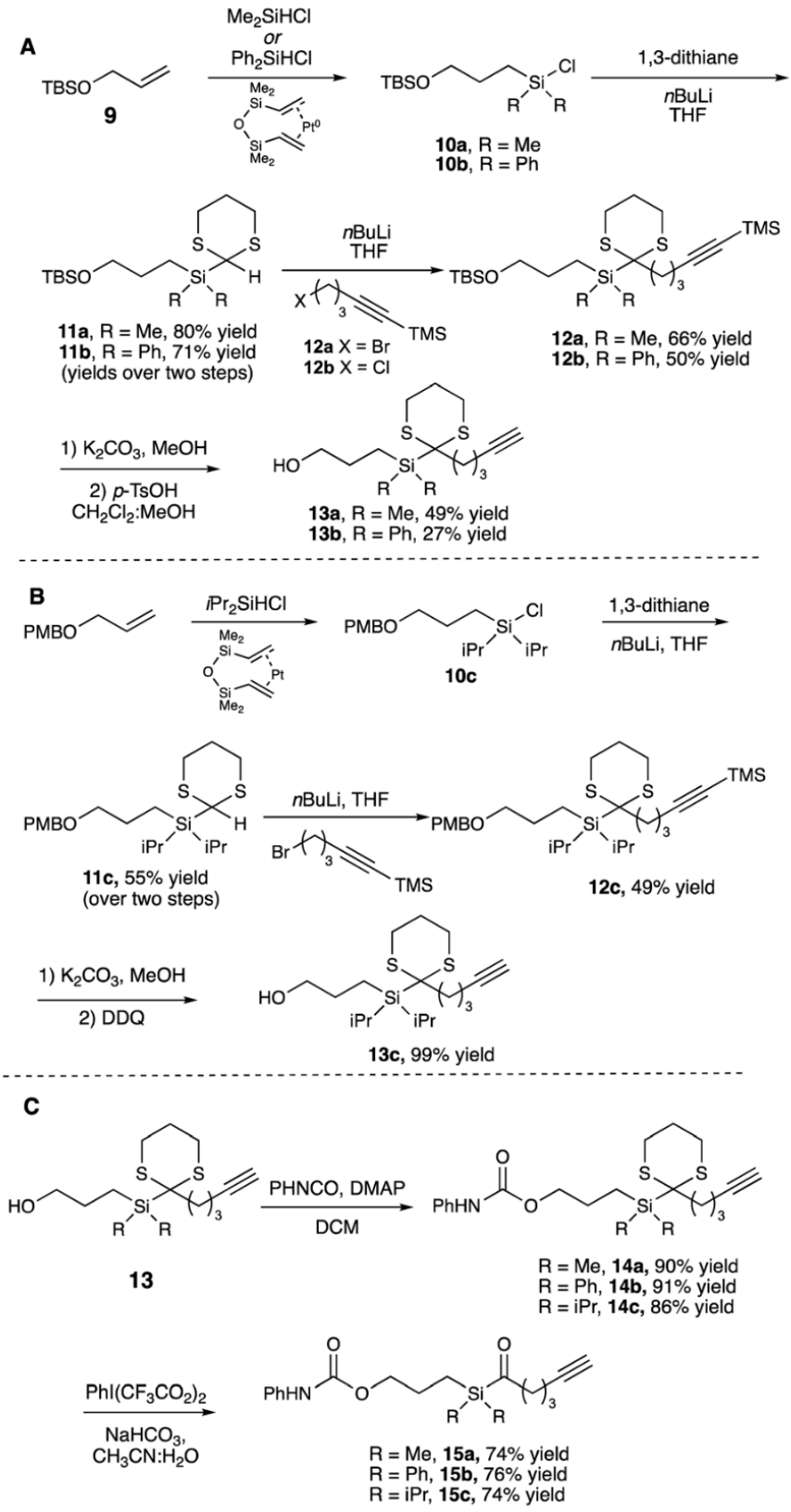

Scheme 3.1 Synthesis of acyl silanes 15a-c.

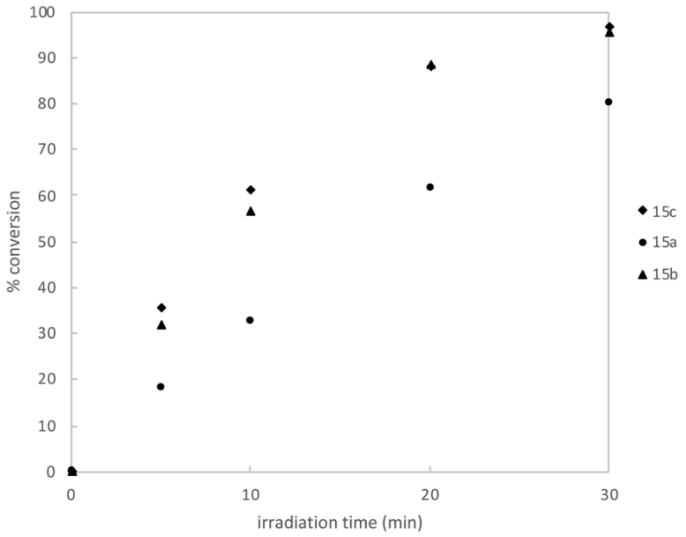

Fig. 3.2. Kinetic profile of acyl silane probes. Kinetic profile of acyl silane probes in MeOH-d_4 (n = 3, average) using a 6 W handheld UV lamp at 365 nm. Conversion was determined by ^{1}H NMR using an internal standard.

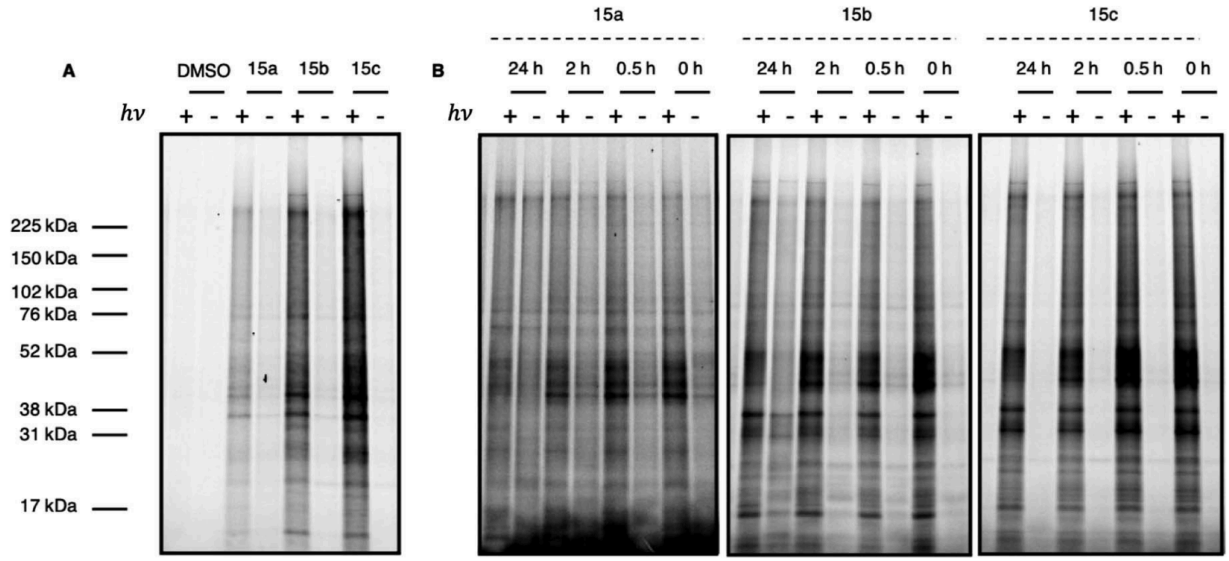

Fig. 3.3 Fluorescence labeling of acyl silane probes in cell lysate. (**A**) Full gel image of UV-dependent labeling of PAL probes **15a-c** in cell lysate. In brief, 231MFP cell lysate in pH 7.4 PBS was treated with either DMSO or 10 μM probe **15a**, **15b**, or **15c** and incubated at ambient temperature for 30 min. Samples were then irradiated for 30 min at 4ºC with a 6 W handheld UV lamp at 365 nm. Labeled proteins were visualized following Cu-catalyzed click reaction with Rh-N_3. (**B**) Evaluation of probe labeling with variable incubation time. In brief, 231MFP cell lysate in pH 7.4 PBS was treated with 10 μM probe **15a**, **15b**, or **15c** and incubated at ambient temperature for 0, 0.5, 2, or 24 h. Samples were then irradiated for 30 min at 4ºC with a 6 W handheld UV lamp at 365 nm. Labeled protein was visualized following Cu-catalyzed click reaction with Rh-N_3.

3.3 Development of Ligand-Linked Acyl Silane Probes

With these data in hand, we sought to further evaluate whether bulkier acyl silane warheads such as *i*Pr derivative **15c** could be utilized to capture targeted and specific small molecule–protein interactions; thus, we prepared two small molecule acyl silane probes utilizing the *i*Pr-substitution. The first was based on (+)-JQ1, a known inhibitor of the BET class of bromodomain proteins[182] that has seen extensive profiling[183] and has come to serve as a key benchmarking tool in the development of novel photoaffinity ligands (**Fig. 3.4**).[163,164] The second probe was based on rapamycin, a potent inhibitor of FKBP12, which, upon binding, forms a ternary complex with mTOR (**Fig. 3.4**).[184,185] Recently, Woo and coworkers elegantly demonstrated the ability to probe the formation of this ternary complex utilizing a diazirine-based rapamycin photoaffinity probe.[186] Key to both (+)-JQ1- and rapamycin-based probe designs was identification of known points of modification, such that the acyl silane would have minimal impact on protein binding. Thus, pure recombinant BRD4-BD1 and FKBP12 protein were treated with probes **16/17** and **18/19**, respectively, followed by irradiation with a 6 W handheld UV lamp at 365 nm (**Fig. 3.4**). Covalently labeled protein adducts were subsequently visualized by in-gel fluorescence after Cu-catalyzed click reaction with rhodamine azide. Photochemical labeling was observed for (+)-JQ1 probes **16** and **17** with no thermal background labeling. While more intense fluorescence was observed for the probe with the shorter linker (**16**), both probes could be inhibited by pretreatment of BRD4-BD1 with excess (+)-JQ1. These data are consistent with labeling being driven by probe-protein binding, not an artifact caused by unspecific association of the acyl silane moiety with the protein target. Interestingly, the linker length for the rapamycin probes **18** and **19** had a more profound effect, as superior labeling of FKBP12 was observed with the longer linker probe **19**. Again, minimal background labeling was observed, and for both probes, labeling was inhibited by pretreatment of FKBP12 with excess rapamycin.

To evaluate the relative labeling output of acyl silane probes against traditional photoaffinity warheads, we synthesized a “minimalist” diazirine probe modified with (+)-JQ1, **16-DA** (**Fig. 3.5**). Similar diazirine probes have been used to capture specific interactions in proteins and whole cells.[187] Acyl silane (+)-JQ1 probe **16**, the analogous dimethyl-substituted probe **16-Me**, and diazirine probe **16-DA** were incubated in cell lysate and irradiated for 30 min on ice. Following click reaction, visualization by in-gel fluorescence shows intense fluorescence for irradiated samples treated with probes **16** and **16-DA**, with minimal thermal labeling observed (**Fig. 3.5**). Consistent with previous findings, the less bulky probe **16-Me** had both lower labeling after irradiation as well as some thermal background labeling. These results support the promise of acyl silanes as novel probes for photoaffinity labeling, as the bulkier isopropyl derivative labels cell lysate on par with current photoaffinity scaffolds.

From these encouraging results, we next sought to confirm that the acyl silane probes were capable of capturing targeted and specific interactions in the proteome. Thus, (+)-JQ1-acyl silane probe **16** was incubated in 231MFP cell lysate, into which exogenous BRD4-BD1 protein was added.[188] Following irradiation and click reaction of rhodamine-azide, labeled proteins were visualized by in-gel fluorescence. Pretreatment of lysate with excess (+)-JQ1 led to inhibition of BRD4-BD1 labeling, indicating that the (+)-JQ1 acyl silane probe is able to capture the BRD4-BD1 protein in cell lysates (**Fig. 3.6**).

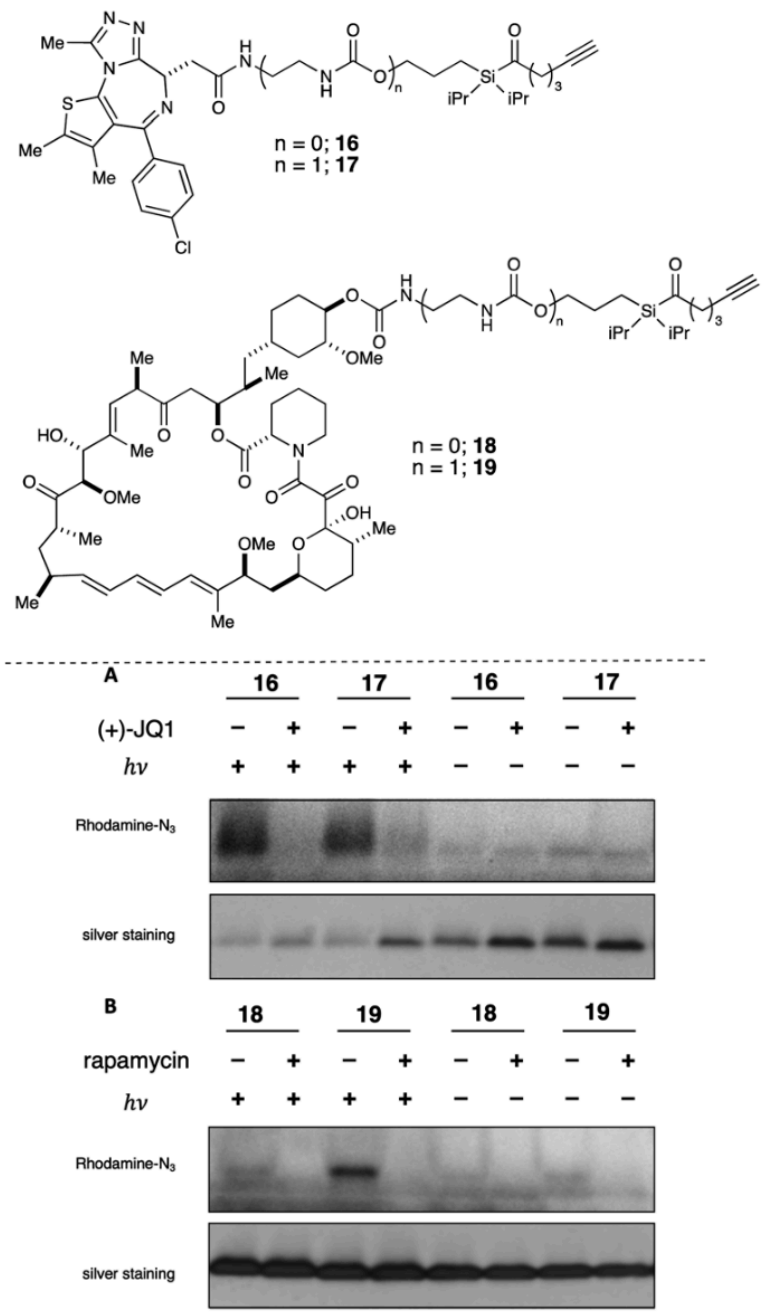

Fig. 3.4 Evaluation of labeling by (+)-JQ1 and rapamycin photoaffinity probes against pure protein. Evaluation of labeling by (+)-JQ1 (**16** and **17**) and rapamycin (**18** and **19**) photoaffinity probes with pure recombinant BRD4-BD1 and FKBP12, respectively, by in-gel fluorescence following a Cu-catalyzed click reaction with Rh-N_3 after irradiation at 365 nm. Protein loading was confirmed by silver staining. (**A**) Reactions were performed using 0.6 μg BRD4-BD1 in 50 μL PBS, with 10 μM **16** or **17** and 100 μM (+)-JQ1 for competition. (**B**) Reactions were performed with 1.0 μg FKBP12 in 50 μL PBS (0.1% Triton X-100) with 10 μM **18** or **19** and 100 μM rapamycin for competition.

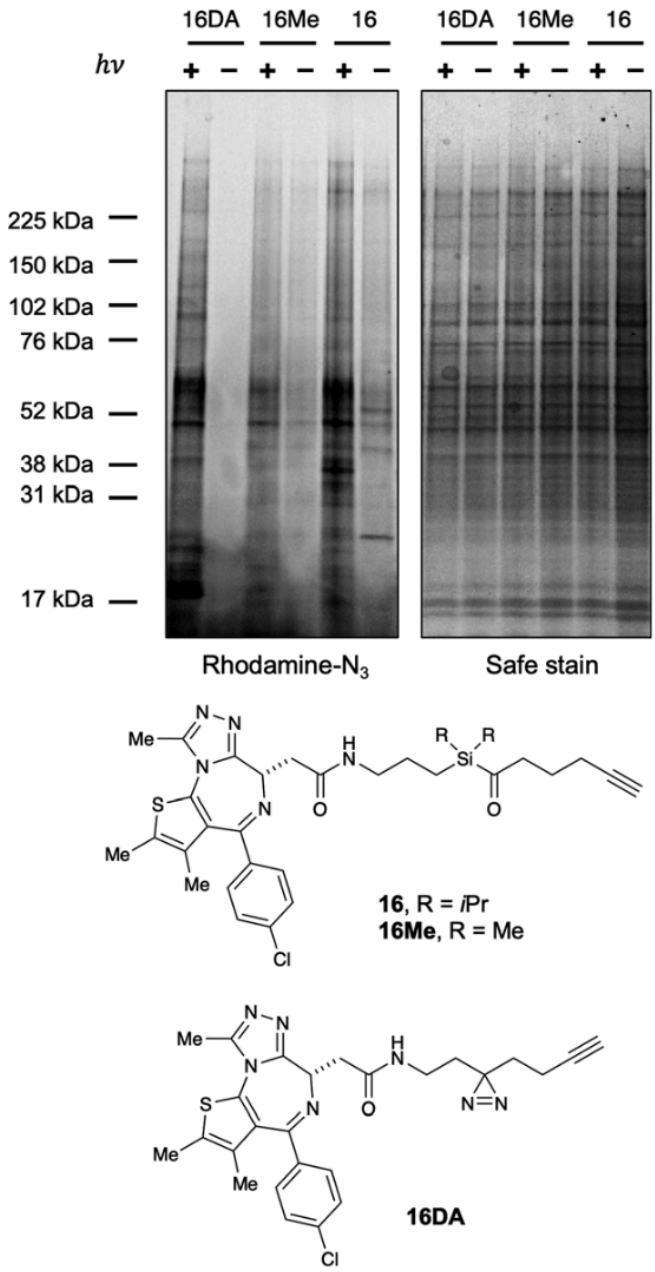

Fig. 3.5 Evaluation of labeling by (+)-JQ1 photoaffinity probes in cell lysate. Evaluation of labeling by (+)-JQ1 photoaffinity probes (**16**, **16Me**, and **16DA**) in 231MFP cell lysate by in-gel fluorescence following a Cu-catalyzed click reaction with Rh-N_3 after irradiation at 365 nm or incubation in the dark. Reactions were performed using 1 μg/μL 231MFP lysate with 10 μM probe. Protein loading was confirmed by silver stain.

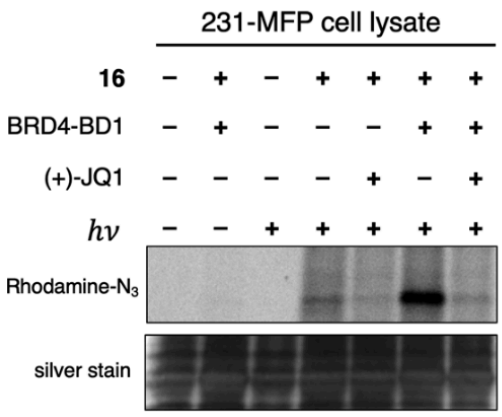

Fig. 3.6 Evaluation of (+)-JQ1 photoaffinity probe labeling in spiked cell lysate. Evaluation of labeling by (+)-JQ1 photoaffinity probe **16** in 231MFP cell lysate by in-gel fluorescence following a Cu-catalyzed click reaction with Rh-N_3 after irradiation at 365 nm or incubation in the dark. Reactions were performed in 1 µg/µL 231MFP cell lysate spiked with 0.2 µg BRD4-BD1 with 5 µM **16** and 500 µM (+)-JQ1 for competition. Protein loading was confirmed by silver stain.

3.4 Chemoproteomic Profiling of Acyl Silane Probes

Following analysis in lysate, we investigated whether the acyl silane (+)-JQ1 probe **16** would enrich BRD4 more selectively in whole-cells than the minimalist diazirine (+)-JQ1 probe **16-DA**. K562 cells were treated with either probe or DMSO vehicle for 1 h, followed by a 20 min irradiation at 365 nm. An azide-functionalized biotin enrichment handle was appended to the probes via a copper-catalyzed click reaction, and probe-modified peptides were avidin-enriched. Peptides were labeled with isobaric tags and analyzed via LC-MS/MS. We identified seven proteins that were significantly enriched by both **16** and **16-DA** (**Fig. 3.7**). At least two of these proteins (VDAC1 and VDAC2) are frequently enriched in photoaffinity labeling experiments due to their electrostatic densities and can be reasonably ruled out as true off-targets of (+)-JQ1.[177]

The acyl silane (+)-JQ1 probe **16** was much more selective than the diazirine (+)-JQ1 probe **16-DA**, significantly enriching only 15 unique proteins >2-fold compared to **16-DA**'s 84 unique proteins enriched >2-fold. Additionally, only **16** was able to enrich BRD4 >2-fold (**Fig. 3.7**). This data indicates that not only are acyl silane PAL probes suitable for PAL applications, but that they may outperform traditional diazirine PAL probes.

With multiple sources of confirmation that **16** binds to BRD4, we used bottom-up proteomics to identify the site-of-modification of **16** on BRD4. Pure human recombinant BRD4-BD1 was incubated with **16** for 30 min, followed by a 30 min irradiation at 365 nm. Protein adducts were precipitated, and peptides were analyzed by LC-MS/MS. Bottom-up proteomics identified two residues bound to **16** – D46 and C95. D46 was the only residue identified from a tryptic peptide that was bound to **16**. Because we saw 100% BRD4-BD1 sequence coverage, we can infer that these amino acid residues are the residues that form the covalent adduct with **16**. These residues do exist in the physical space occupied by (+)-JQ1 (**Fig. 3.8**), indicating that acyl silane PAL probes can be used in bottom-up proteomics to elucidate the approximate binding pocket of non-covalent drugs.

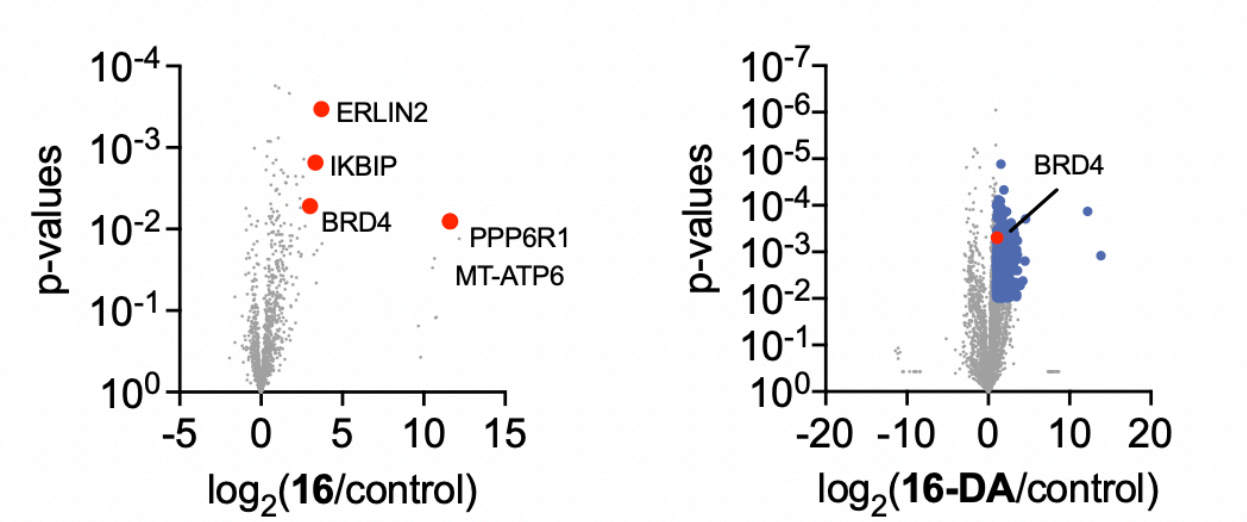

Fig. 3.7 Quantitative proteomics of (+)-JQ1 photoaffinity probes in whole cells. 16 pulldown proteomics showing significant and selective engagement of BRD4 with less significant engagement of 23 additional proteins including ERLIN2, IKBIP, MT-ATP6, and PP6R1. **16-DA** pulldown proteomics showing non-signifcant and non-selective engagement of BRD4. K562 cells were treated with DMSO vehicle or PAL probe (10 μM) for 1 h and subjected to irradiation at 365 nm for 20 min. Subsequent lysates were subjected to copper-catalyzed azide-alkyne cycloaddition (CuAAC) with an azide-functionalized biotin handle, after which probe-modified proteins were avidin-enriched, eluted, and digested, and analyzed by TMT-based quantitative proteomics. Data shown are ratio of PAL probe vs. DMSO control enriched proteins and p-values from n=3 biologically independent replicates/group.

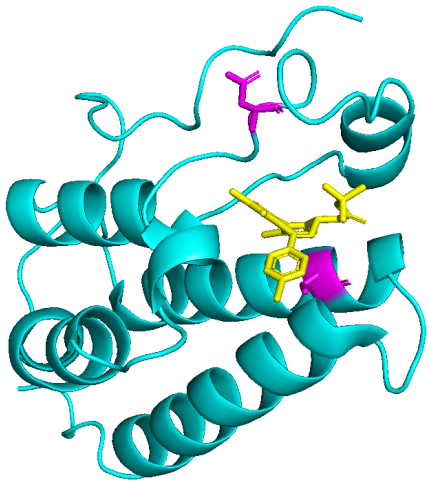

Fig. 3.8 (+)-JQ1 acyl silane photoaffinity probe site-of-modification of BRD4. BRD4-BD1 (100 μg) was incubated with **16** for 30 min at room temperature followed by irradiation at 365 nm for 30 min on ice. Protein adducts were precipitated, and peptides were analyzed by LC-MS/MS. D46 was identified as the only residue modified by **16** from a tryptic peptide and C95 was identified as the only residue modified by **16** from a non-tryptic peptide. Crystal structure of BRD4-BD1 (3MXF, cyan) in complex with (+)-JQ1 (yellow). D46 and C95 are shown in magenta.

3.5 Conclusions

In summary, we have identified a novel class of photoaffinity warheads with short irradiation times capable of generating α-siloxy carbene intermediates suitable for photoaffinity labeling applications at long UV wavelengths in both cell lysate and with pure

protein. We also demonstrated the improved selectivity of acyl silane PAL probes over traditional diazirine PAL probes. Further studies are underway to better understand residue chemoselectivity, as well as an in-depth evaluation of probe structure to allow for the broader use of acyl silanes in proteome profiling and site-of-modification studies. Further studies to examine the robustness of PAL probes against multiple protein targets are underway.

3.6 Acknowledgment of Co-Author Contributions

F.D. Toste and S.O. Scholz were responsible for the initial acyl silane probe design and experimental validation. A.C.S. Page and S.O. Scholz synthesized all compounds. B.P. Belcher designed and performed all chemoproteomic experiments. K.N. Keenan, J.N. Spradlin, and B.P. Belcher prepared material for experiments in cell lysate. A.C.S. Page, S.O. Scholz, K.N. Keenan, J.N. Spradlin, and B.P. Belcher performed experiments in cell lysate. Analysis of gels was performed by D.K. Nomura, K.N. Keenan, J.N. Spradlin, B.P. Belcher, A.C.S. Page, and S.O. Scholz. Manuscripts were prepared by S.O. Scholz, A.C.S. Page, and B.P. Belcher. S.M. Brittain, J.A. Tallarico, J.M. McKenna, M. Schirle, D.K. Nomura, and F.D. Toste contributed to overall experimental design and manuscript preparation.

3.7 Methods

3.7.1 Gel-based ABPP in cell lysate

(+)-JQ1 probes: BRD4-BD1 (Cayman Chemicals) (0.6 µg, appx. 0.7 µM) in pH 7.4 PBS (50 µL) was treated with a prepared stock solution of (+)-JQ1 acyl silane probe in DMSO and incubated in the dark for 30 min at RT. During competition, BRD4-BD1 was treated with a prepared stock solution of (+)-JQ1 (MedChemExpress, HY-13030) (10x final concentration of acyl silane) prior to acyl silane addition and incubated at RT for 30 min. Samples were irradiated for 30 min on ice using a 6 W handheld UV lamp at 365 nm. Labeled protein was visualized following Cu-catalyzed click reaction, performed by sequential addition of $CuSO_4$, (1 mM), tris(2-carboxyethyl)phosphine (1 mM), tris[(1-benzyl-1H-1,2,3-triazol-4-yl)methyl]amine (34 µM) and TAMRA azide (25 µM).[135] Following click reaction, proteins were denatured by the addition of 4X Laemmli SDS loading buffer (30 µL) and run on a 16 cm Protean II xi 10% resolving SDS-PAGE gel system (Bio-Rad) and scanned using a ChemiDoc MP (Bio-Rad).

Rapamycin probes: FKBP12 (Origene) (1.0 µg, appx. 1.5 µM) in pH 7.4 PBS (0.1% Triton X-100) (50 µL) was treated with a prepared stock solution of rapamycin acyl silane probe in DMSO and incubated in the dark for 30 min at RT. During competition, FKBP12 was treated with a prepared stock solution of rapamycin (MedChemExpress, HY-10219) (10x final concentration of acyl silane) prior to acyl silane addition and incubated at RT for 30 min. Samples were irradiated for 30 min on ice using a 6 W handheld UV lamp at 365 nm. Labeled protein was visualized following Cu-catalyzed click reaction, performed by sequential addition of $CuSO_4$, (1 mM), tris(2-carboxyethyl)phosphine (1 mM), tris[(1-benzyl-1H-1,2,3-triazol-4-yl)methyl]amine (34 µM) and TAMRA azide (25 µM). Following

click reaction, proteins were denatured by the addition of 4X Laemmli SDS loading buffer (30 µL) and run on a 16 cm Protean II xi 10% resolving SDS-PAGE gel system (Bio-Rad) and scanned using a ChemiDoc MP (Bio-Rad).

(+)-JQ1 probes in cell lysate: 231MFP cell lysate (1.0 µg/ µL) in pH 7.4 PBS (50 µL) was treated with a prepared stock solution of (+)-JQ1 probe in DMSO and incubated in the dark for 30 min at RT. Samples were irradiated for 30 min on ice using a 6 W handheld UV lamp at 365 nm. Labeled protein was visualized following Cu-catalyzed click reaction, performed by sequential addition of $CuSO_4$, (1 mM), tris(2-carboxyethyl)phosphine (1 mM), tris[(1-benzyl-1H-1,2,3-triazol-4yl)methyl]amine (34 µM) and TAMRA azide (25 µM). Following click reaction, proteins were denatured by the addition of 4X Laemmli SDS loading buffer (30 µL) and run on a 16 cm Protean II xi 10% resolving SDS-PAGE gel system (Bio-Rad) and scanned using a ChemiDoc MP (Bio-Rad).

(+)-JQ1 probes in spiked cell lysate: 231MFP cell lysate (1.0 µg/ µL) in pH 7.4 PBS (50 µL) was treated with 0.2 µg of BRD4-BD1 or DMSO control. A prepared stock solution of (+)-JQ1 probe in DMSO was added and incubated in the dark for 30 min at RT. For competition experiments, 231MFP lysate was treated with a prepared stock solution of (+)-JQ1 (100x final concentration of acyl silane) prior to acyl silane addition and incubated at RT for 30 min. Samples were irradiated for 30 min on ice using a 6 W handheld UV lamp at 365 nm. Labeled protein was visualized following Cu-catalyzed click reaction, performed by sequential addition of $CuSO_4$, (1 mM), tris(2-carboxyethyl)phosphine (1 mM), tris[(1-benzyl-1H-1,2,3-triazol4-yl)methyl]amine (34 µM) and TAMRA azide (25 µM). Following click reaction, proteins were denatured by the addition of 4X Laemmli SDS loading buffer (30 µL) and run on a 16 cm Protean II xi 10% resolving SDS-PAGE gel system (Bio-Rad) and scanned using a ChemiDoc MP (Bio-Rad).

3.7.2 Cell culture

K562 cells were obtained from the UC Berkeley Cell Culture Facility and were cultured in RPMI medium containing 10% (v/v) fetal bovine serum (FBS) and maintained at 37°C with 5% CO_2.

3.7.3 Preparation of cell lysate

Cells were pelleted by centrifugation (1400 g, 5 min, 4°C). Pellets were resuspended in RIPA buffer containing protease inhibitor and lysed on ice, and clarified by centrifugation (12,000 g, 10 min, 4°C). Lysate was transferred to low-adhesion microcentrifuge tubes. Proteome concentrations were determined using BCA assay and lysate was diluted with PBS to appropriate working concentrations.

3.7.3 Gel-based ABPP in whole cells

K562 cells were treated with either DMSO vehicle or PAL probe (10 µM) for 1 h in serum-free media and subsequently irradiated for 20 min at 365 nm. Lysate was prepared as described above. CuAAC was performed to append rhodamine-azide (1 µM final

concentration) onto alkyne probe-labeled proteins. Samples were then diluted with 4x reducing Laemmli SDS sample loading buffer and heated at 95°C for 5 min. The samples were separated on precast 4-20% Criterion TGX gels (Bio-Rad). Prior to analysis, gels were fixed in a solution of 10% acetic acid and 30% ethanol for 1 h. Probe-labeled proteins were analyzed by in-gel fluorescence using a ChemiDoc MP (Bio-Rad). Protein loading was assessed by silver stain.

3.7.4 TMT Proteomics

Cells were treated with either DMSO vehicle or PAL probe (10 μM) in serum-free media for 1 h and subsequently irradiated for 20 min at 365 nm. Lysate was prepared as described above. CuAAC was used by sequential addition of tris(2-carboxyethyl)phosphine (1 mM, Strem), tris[(1-benzyl-1H-1,2,3-triazol-4-yl)methyl]amine (34 μM, Sigma), copper (II) sulfate (1 mM, Sigma) and biotin picolyl azide (5mM). After CuAAC, proteomes were precipitated by centrifugation at 6,500 g, washed in ice-cold methanol, then denatured and resolubilized by heating in 1.2% SDS/PBS to 90°C for 5 min. Insoluble components were precipitated by centrifugation at 6,500 g and soluble proteome was diluted in 5 mL 0.2% SDS/PBS. Labeled proteins were bound to streptavidin-agarose beads (170 μL resuspended beads per sample, Thermo Fisher) while rotating overnight at 4°C. Bead-linked proteins were enriched by washing three times each in PBS and water, then resuspended in 0.1% SDS/PBS (Sigma), reduced in DTT (9.26 mM, Thermo Fisher), and alkylated with iodoacetamide (18 mM, Sigma) before being washed and resuspended in 100 mM triethylammonium bicarbonate (TEAB) and trypsinized overnight with 0.5 μg/μL sequencing-grade trypsin (Promega). Tryptic peptides were eluted. Beads were washed twice in 100 mM TEAB. Individual samples were then labeled with isobaric tags using commercially available TMTsixplex (Thermo Fisher Scientific, P/N 90061) kits, in accordance with the manufacturer's protocols. Tagged samples (20 μg per sample) were combined, dried with SpeedVac, resuspended with 300 μL 0.1% TFA in H_2O, and fractionated using high pH reversed-phase peptide fractionation kits (Thermo Scientific, P/N 84868) according to manufacturer's protocol. Fractions were dried with SpeedVac, resuspended with 50 μL 0.1% FA in H_2O, and analyzed by LC-MS/MS as described below.

Quantitative TMT-based proteomic analysis was performed as previously described using a Thermo Eclipse with FAIMS LC-MS/MS.[148] Acquired MS data was processed using ProLuCID search methodology in IP2 v.3-v.5 (Integrated Proteomics Applications, Inc.).[149] Trypsin cleavage specificity (cleavage at K, R except if followed by P) allowed for up to 2 missed cleavages. Carbamidomethylation of cysteine was set as a fixed modification. Methionine oxidation and TMT-modification of N-termini and lysine residues were set as variable modifications. Reporter ion ratio calculations were performed using summed abundances with most confident centroid selected from 20 ppm window. Only peptide-to-spectrum matches that are unique assignments to a given identified protein within the total dataset are considered for protein quantitation. High confidence protein identifications were reported with a <1% false discovery rate (FDR) cut-off. Differential abundance significance was estimated using ANOVA with Benjamini-Hochberg correction to determine p-values.

3.7.5 Shotgun Proteomics

Pure human recombinant BRD4-bd1 (100 µg) was incubated with PAL probe (10 µM) for 30 min at room temperature in PBS and subsequently irradiated for 30 min at 365 nm on ice. Trichloroacetic acid was added to a final concentration of 20% and the sample was incubated at -80ºC overnight to precipitate proteins. The precipitated proteins were pelleted and washed with 0.01 M HCl in 90% acetone and subsequently resuspended in 8 M urea/PBS. ProteaseMax (1x), ammonium bicarbonate (100 mM), and tris[(1-benzyl-1H-1,2,3-triazol-4-yl)methyl]amine (110 mM) were added to the sample and the sample was incubated for 30 min at 60ºC. Proteins were alkylated with iodoacetamide (150 mM) for 30 min at 37ºC. The sample was diluted with PBS and digested with trypsin in ProteaseMax (5x) overnight at 37ºC with agitation. The sample was acidified to a final concentration of 5% formic acid.

Proteomic analysis was performed as previously described using a Thermo Eclipse with FAIMS LC-MS/MS.[148] Acquired MS data was processed using ProLuCID search methodology in IP2 v.3-v.5 (Integrated Proteomics Applications, Inc.).[149] Peptide search tolerances were set to 10 ppm for precursors, and 0.8 Da for fragments. Trypsin cleavage specificity (cleavage at K, R except if followed by P) allowed for up to 2 missed cleavages. Carbamidomethylation of cysteine was set as a fixed modification, methionine oxidation, and probe-modification of N-termini, cysteine, methionine, lysine, and aspartic acid residues were set as variable modifications. Data validation of peptide and protein identifications was done at the level of the complete dataset consisting of combined Mascot search results for all individual samples per experiment via the Percolator validation node in Proteome Discoverer. Reporter ion ratio calculations were performed using summed abundances with most confident centroid selected from 20 ppm window. Only peptide-to-spectrum matches that are unique assignments to a given identified protein within the total dataset are considered for protein quantitation. High confidence protein identifications were reported using a Percolator estimated <1% false discovery rate (FDR) cut-off.

CONCLUDING REMARKS

The work compiled in this dissertation demonstrates the utility of chemoproteomic profiling in drug discovery and development. First, I presented a database that identifies reactive cysteines in 97% of the >600 known E3 ligases. This database compiles data from 455 isotopic tandem orthogonal proteolysis-enabled activity-based protein profiling (isoTOP-ABPP) experiments using a reactivity-based alkyne-functionalized iodoacetamide probe. These experiments encompassed target identification, target engagement, and selectivity profiling experiments, resulting in datasets including vast amounts of probe-modified peptide data from human proteomes across multiple cell lines. This database enables the facile mining of reactive cysteines as potential ligandable sites that can be pharmacologically interrogated. Historically, E3 ligase recruiters are discovered fortuitously. Chemoproteomic profiling has unlocked the potential of rational design of E3 ligase recruiters for use in targeted protein degradation.

Chemoproteomic methods can facilitate target identification of natural products. IsoTOP-ABPP was utilized to identify the protein targets of the anti-cancer natural product dankastatin B. Because I was able to identify C65 on VDAC3 as a target of dankastatin B, I could use biochemical techniques to validate VDAC3 as a target protein responsible for anti-cancer effects. Though not exploited in the presented work, a powerful advantage of chemoproteomic profiling of natural products is the ability to screen for small molecules that mimic the natural product's effects. Once the reactive site on a protein is identified, an electrophilic small molecule library can be screened against the target protein, allowing for unbiased identification of more synthetically tractable ligands that bind to the same site. If such a screen is performed against VDAC3 in the future, C65 may be exploited for the development of anti-cancer therapeutics. Facile chemoproteomic profiling of natural products that inhibit disease progression may allow for subsequent screens against target sites and result in novel protein-targeting therapeutics.

Interest in developing photoaffinity labeling (PAL) probes linked to non-covalent drugs further highlights the utility of chemoproteomic profiling for drug discovery and development. To successfully use PAL probes in chemoproteomic workflows, they must have minimal thermal background and covalently capture the target protein that is non-covalently modified by the drug of interest. I used activity-based chemoproteomic methods to evaluate the specificity of acyl silane-containing PAL probes. These probes were linked to (+)-JQ1, a non-covalent drug that targets BRD4. Using gel-based chemoproteomic profiling, I showed the low thermal background of this probe in cell lysate. Using mass-spectrometry based chemoproteomic profiling, I showed the specificity of the probe in whole human cells. This approach can be expanded to acyl-silane containing PAL probes linked to a variety of ligands.

With the continuing advances in chemoproteomic methods, the strategies used in drug discovery and development will continue to improve. As outlined in this dissertation, these strategies vastly expand the scope of drug discovery. Using chemoproteomic approaches to aid in drug discovery can eventually make the "undruggable" proteome obsolete, and will continue to expand the number of protein-targeting therapeutics.

REFERENCES

(1) Belcher, B. P.; Ward, C. C.; Nomura, D. K. Ligandability of E3 Ligases for Targeted Protein Degradation Applications. *Biochemistry* **2021**, acs.biochem.1c00464. https://doi.org/10.1021/acs.biochem.1c00464.

(2) Burslem, G. M.; Crews, C. M. Proteolysis-Targeting Chimeras as Therapeutics and Tools for Biological Discovery. *Cell* **2020**, *181* (1), 102–114. https://doi.org/10.1016/j.cell.2019.11.031.

(3) Cromm, P. M.; Crews, C. M. Targeted Protein Degradation: From Chemical Biology to Drug Discovery. *Cell Chem. Biol.* **2017**, *24* (9), 1181–1190. https://doi.org/10.1016/j.chembiol.2017.05.024.

(4) Nalawansha, D. A.; Crews, C. M. PROTACs: An Emerging Therapeutic Modality in Precision Medicine. *Cell Chem. Biol.* **2020**, *27* (8), 998–1014. https://doi.org/10.1016/j.chembiol.2020.07.020.

(5) Schreiber, S. L. The Rise of Molecular Glues. *Cell* **2021**, *184* (1), 3–9. https://doi.org/10.1016/j.cell.2020.12.020.

(6) Banik, S. M.; Pedram, K.; Wisnovsky, S.; Ahn, G.; Riley, N. M.; Bertozzi, C. R. Lysosome-Targeting Chimaeras for Degradation of Extracellular Proteins. *Nature* **2020**, *584* (7820), 291–297. https://doi.org/10.1038/s41586-020-2545-9.

(7) Takahashi, D.; Moriyama, J.; Nakamura, T.; Miki, E.; Takahashi, E.; Sato, A.; Akaike, T.; Itto-Nakama, K.; Arimoto, H. AUTACs: Cargo-Specific Degraders Using Selective Autophagy. *Mol. Cell* **2019**, *76* (5), 797-810.e10. https://doi.org/10.1016/j.molcel.2019.09.009.

(8) Samarasinghe, K. T. G.; Jaime-Figueroa, S.; Burgess, M.; Nalawansha, D. A.; Dai, K.; Hu, Z.; Bebenek, A.; Holley, S. A.; Crews, C. M. Targeted Degradation of Transcription Factors by TRAFTACs: TRAnscription Factor TArgeting Chimeras. *Cell Chem. Biol.* **2021**, *28* (5), 648-661.e5. https://doi.org/10.1016/j.chembiol.2021.03.011.

(9) Morreale, F. E.; Kleine, S.; Leodolter, J.; Junker, S.; Hoi, D. M.; Ovchinnikov, S.; Okun, A.; Kley, J.; Kurzbauer, R.; Junk, L.; Guha, S.; Podlesainski, D.; Kazmaier, U.; Boehmelt, G.; Weinstabl, H.; Rumpel, K.; Schmiedel, V. M.; Hartl, M.; Haselbach, D.; Meinhart, A.; Kaiser, M.; Clausen, T. BacPROTACs Mediate Targeted Protein Degradation in Bacteria. *Cell* **2022**, *185* (13), 2338-2353.e18. https://doi.org/10.1016/j.cell.2022.05.009.

(10) Liu, X.; Haniff, H. S.; Childs-Disney, J. L.; Shuster, A.; Aikawa, H.; Adibekian, A.; Disney, M. D. Targeted Degradation of the Oncogenic MicroRNA 17-92 Cluster by Structure-Targeting Ligands. *J. Am. Chem. Soc.* **2020**, *142* (15), 6970–6982. https://doi.org/10.1021/jacs.9b13159.

(11) Siriwardena, S. U.; Munkanatta Godage, D. N. P.; Shoba, V. M.; Lai, S.; Shi, M.; Wu, P.; Chaudhary, S. K.; Schreiber, S. L.; Choudhary, A. Phosphorylation-Inducing Chimeric Small Molecules. *J. Am. Chem. Soc.* **2020**, *142* (33), 14052–14057. https://doi.org/10.1021/jacs.0c05537.

(12) Yamazoe, S.; Tom, J.; Fu, Y.; Wu, W.; Zeng, L.; Sun, C.; Liu, Q.; Lin, J.; Lin, K.; Fairbrother, W. J.; Staben, S. T. Heterobifunctional Molecules Induce Dephosphorylation of Kinases–A Proof of Concept Study. *J. Med. Chem.* **2020**, *63* (6), 2807–2813. https://doi.org/10.1021/acs.jmedchem.9b01167.

(13) Henning, N. J.; Boike, L.; Spradlin, J. N.; Ward, C. C.; Liu, G.; Zhang, E.; Belcher, B. P.; Brittain, S. M.; Hesse, M. J.; Dovala, D.; McGregor, L. M.; Valdez Misiolek, R.; Plasschaert, L. W.; Rowlands, D. J.; Wang, F.; Frank, A. O.; Fuller, D.; Estes, A. R.; Randal, K. L.; Panidapu, A.; McKenna, J. M.; Tallarico, J. A.; Schirle, M.; Nomura, D. K. Deubiquitinase-Targeting Chimeras for Targeted Protein Stabilization. *Nat. Chem. Biol.* **2022**. https://doi.org/10.1038/s41589-022-00971-2.

(14) Komander, D.; Rape, M. The Ubiquitin Code. *Annu. Rev. Biochem.* **2012**, *81*, 203–229. https://doi.org/10.1146/annurev-biochem-060310-170328.

(15) Chen, Z. J.; Sun, L. J. Nonproteolytic Functions of Ubiquitin in Cell Signaling. *Mol. Cell* **2009**, *33* (3), 275–286. https://doi.org/10.1016/j.molcel.2009.01.014.

(16) Jevtić, P.; Haakonsen, D. L.; Rapé, M. An E3 Ligase Guide to the Galaxy of Small-Molecule-Induced Protein Degradation. *Cell Chem. Biol.* **2021**, *28* (7), 1000–1013. https://doi.org/10.1016/j.chembiol.2021.04.002.

(17) Kannt, A.; Đikić, I. Expanding the Arsenal of E3 Ubiquitin Ligases for Proximity-Induced Protein Degradation. *Cell Chem. Biol.* **2021**, *28* (7), 1014–1031. https://doi.org/10.1016/j.chembiol.2021.04.007.

(18) Bond, M. J.; Crews, C. M. Proteolysis Targeting Chimeras (PROTACs) Come of Age: Entering the Third Decade of Targeted Protein Degradation. *RSC Chem. Biol.* **2021**, *2* (3), 725–742. https://doi.org/10.1039/D1CB00011J.

(19) Bond, M. J.; Chu, L.; Nalawansha, D. A.; Li, K.; Crews, C. M. Targeted Degradation of Oncogenic KRASG12Cby VHL-Recruiting PROTACs. *ACS Cent. Sci.* **2020**. https://doi.org/10.1021/acscentsci.0c00411.

(20) Zeng, M.; Xiong, Y.; Safaee, N.; Nowak, R. P.; Donovan, K. A.; Yuan, C. J.; Nabet, B.; Gero, T. W.; Feru, F.; Li, L.; Gondi, S.; Ombelets, L. J.; Quan, C.; Jänne, P. A.; Kostic, M.; Scott, D. A.; Westover, K. D.; Fischer, E. S.; Gray, N. S. Exploring Targeted Degradation Strategy for Oncogenic KRASG12C. *Cell Chem. Biol.* **2020**, *27* (1), 19-31.e6. https://doi.org/10.1016/j.chembiol.2019.12.006.

(21) Donovan, K. A.; Ferguson, F. M.; Bushman, J. W.; Eleuteri, N. A.; Bhunia, D.; Ryu, S.; Tan, L.; Shi, K.; Yue, H.; Liu, X.; Dobrovolsky, D.; Jiang, B.; Wang, J.; Hao, M.; You, I.; Teng, M.; Liang, Y.; Hatcher, J.; Li, Z.; Manz, T. D.; Groendyke, B.; Hu, W.; Nam, Y.; Sengupta, S.; Cho, H.; Shin, I.; Agius, M. P.; Ghobrial, I. M.; Ma, M. W.; Che, J.; Buhrlage, S. J.; Sim, T.; Gray, N. S.; Fischer, E. S. Mapping the Degradable Kinome Provides a Resource for Expedited Degrader Development. *Cell* **2020**, *183* (6), 1714-1731.e10. https://doi.org/10.1016/j.cell.2020.10.038.

(22) Ciechanover, A.; Hod, Y.; Hershko, A. A Heat-Stable Polypeptide Component of an ATP-Dependent Proteolytic System from Reticulocytes. 1978. *Biochem. Biophys. Res. Commun.* **2012**, *425* (3), 565–570. https://doi.org/10.1016/j.bbrc.2012.08.025.

(23) Hershko, A.; Ciechanover, A.; Rose, I. A. Resolution of the ATP Dependent Proteolytic System from Reticulocytes: A Component That Interacts with ATP. *Proc. Natl. Acad. Sci. U. S. A.* **1979**, *76* (7), 3107–3110. https://doi.org/10.1073/pnas.76.7.3107.

(24) Bett, J. S. Proteostasis Regulation by the Ubiquitin System. *Essays Biochem.* **2016**, *60* (2), 143–151. https://doi.org/10.1042/EBC20160001.

(25) Mészáros, B.; Kumar, M.; Gibson, T. J.; Uyar, B.; Dosztányi, Z. Degrons in Cancer. *Sci. Signal.* **2017**, *10* (470). https://doi.org/10.1126/scisignal.aak9982.

(26) Sakamoto, K. M.; Kim, K. B.; Kumagai, A.; Mercurio, F.; Crews, C. M.; Deshaies, R. J. Protacs: Chimeric Molecules That Target Proteins to the Skp1-Cullin-F Box Complex for Ubiquitination and Degradation. *Proc. Natl. Acad. Sci. U. S. A.* **2001**, *98* (15), 8554–8559. https://doi.org/10.1073/pnas.141230798.
(27) Schneekloth, J. S.; Fonseca, F. N.; Koldobskiy, M.; Mandal, A.; Deshaies, R.; Sakamoto, K.; Crews, C. M. Chemical Genetic Control of Protein Levels: Selective in Vivo Targeted Degradation. *J. Am. Chem. Soc.* **2004**, *126* (12), 3748–3754. https://doi.org/10.1021/ja039025z.
(28) Schneekloth, A. R.; Pucheault, M.; Tae, H. S.; Crews, C. M. Targeted Intracellular Protein Degradation Induced by a Small Molecule: En Route to Chemical Proteomics. *Bioorg. Med. Chem. Lett.* **2008**, *18* (22), 5904–5908. https://doi.org/10.1016/j.bmcl.2008.07.114.
(29) Itoh, Y.; Ishikawa, M.; Naito, M.; Hashimoto, Y. Protein Knockdown Using Methyl Bestatin-Ligand Hybrid Molecules: Design and Synthesis of Inducers of Ubiquitination-Mediated Degradation of Cellular Retinoic Acid-Binding Proteins. *J. Am. Chem. Soc.* **2010**, *132* (16), 5820–5826. https://doi.org/10.1021/ja100691p.
(30) Ito, T.; Ando, H.; Suzuki, T.; Ogura, T.; Hotta, K.; Imamura, Y.; Yamaguchi, Y.; Handa, H. Identification of a Primary Target of Thalidomide Teratogenicity. *Science* **2010**, *327* (5971), 1345–1350. https://doi.org/10.1126/science.1177319.
(31) Epstein, A. C. R.; Gleadle, J. M.; McNeill, L. A.; Hewitson, K. S.; O'Rourke, J.; Mole, D. R.; Mukherji, M.; Metzen, E.; Wilson, M. I.; Dhanda, A.; Tian, Y. M.; Masson, N.; Hamilton, D. L.; Jaakkola, P.; Barstead, R.; Hodgkin, J.; Maxwell, P. H.; Pugh, C. W.; Schofield, C. J.; Ratcliffe, P. J. C. Elegans EGL-9 and Mammalian Homologs Define a Family of Dioxygenases That Regulate HIF by Prolyl Hydroxylation. *Cell* **2001**, *107* (1), 43–54. https://doi.org/10.1016/S0092-8674(01)00507-4.
(32) Hon, W. C.; Wilson, M. I.; Harlos, K.; Claridge, T. D. W.; Schofield, C. J.; Pugh, C. W.; Maxwell, P. H.; Ratcliffe, P. J.; Stuart, D. I.; Jones, E. Y. Structural Basis for the Recognition of Hydroxyproline in HIF-1α by PVHL. *Nature* **2002**, *417* (6892), 975–978. https://doi.org/10.1038/nature00767.
(33) Bargagna-Mohan, P.; Baek, S. H.; Lee, H.; Kim, K.; Mohan, R. Use of PROTACS as Molecular Probes of Angiogenesis. *Bioorg. Med. Chem. Lett.* **2005**, *15* (11), 2724–2727. https://doi.org/10.1016/j.bmcl.2005.04.008.
(34) Wang, X.; Feng, S.; Fan, J.; Li, X.; Wen, Q.; Luo, N. New Strategy for Renal Fibrosis: Targeting Smad3 Proteins for Ubiquitination and Degradation. *Biochem. Pharmacol.* **2016**, *116*, 200–209. https://doi.org/10.1016/j.bcp.2016.07.017.
(35) Buckley, D. L.; Van Molle, I.; Gareiss, P. C.; Tae, H. S.; Michel, J.; Noblin, D. J.; Jorgensen, W. L.; Ciulli, A.; Crews, C. M. Targeting the von Hippel-Lindau E3 Ubiquitin Ligase Using Small Molecules to Disrupt the VHL/HIF-1α Interaction. *J. Am. Chem. Soc.* **2012**, *134* (10), 4465–4468. https://doi.org/10.1021/ja209924v.
(36) Galdeano, C.; Gadd, M. S.; Soares, P.; Scaffidi, S.; Van Molle, I.; Birced, I.; Hewitt, S.; Dias, D. M.; Ciulli, A. Structure-Guided Design and Optimization of Small Molecules Targeting the Protein-Protein Interaction between the von Hippel-Lindau (VHL) E3 Ubiquitin Ligase and the Hypoxia Inducible Factor (HIF) Alpha Subunit with in Vitro Nanomolar Affinities. *J. Med. Chem.* **2014**, *57* (20), 8657–8663. https://doi.org/10.1021/jm5011258.

(37) Bondeson, D. P.; Mares, A.; Smith, I. E. D.; Ko, E.; Campos, S.; Miah, A. H.; Mulholland, K. E.; Routly, N.; Buckley, D. L.; Gustafson, J. L.; Zinn, N.; Grandi, P.; Shimamura, S.; Bergamini, G.; Faelth-Savitski, M.; Bantscheff, M.; Cox, C.; Gordon, D. A.; Willard, R. R.; Flanagan, J. J.; Casillas, L. N.; Votta, B. J.; Den Besten, W.; Famm, K.; Kruidenier, L.; Carter, P. S.; Harling, J. D.; Churcher, I.; Crews, C. M. Catalytic in Vivo Protein Knockdown by Small-Molecule PROTACs. *Nat. Chem. Biol.* **2015**, *11* (8), 611–617. https://doi.org/10.1038/nchembio.1858.

(38) Zengerle, M.; Chan, K. H.; Ciulli, A. Selective Small Molecule Induced Degradation of the BET Bromodomain Protein BRD4. *ACS Chem. Biol.* **2015**, *10* (8), 1770–1777. https://doi.org/10.1021/acschembio.5b00216.

(39) Pettersson, M.; Crews, C. M. PROteolysis TArgeting Chimeras (PROTACs) — Past, Present and Future. *Drug Discov. Today Technol.* **2019**, *31*, 15–27. https://doi.org/10.1016/j.ddtec.2019.01.002.

(40) Dale, B.; Cheng, M.; Park, K.-S.; Kaniskan, H. Ü.; Xiong, Y.; Jin, J. Advancing Targeted Protein Degradation for Cancer Therapy. *Nat. Rev. Cancer* **2021**, *21* (10), 638–654. https://doi.org/10.1038/s41568-021-00365-x.

(41) Ito, T.; Yamaguchi, Y.; Handa, H. Exploiting Ubiquitin Ligase Cereblon as a Target for Small-Molecule Compounds in Medicine and Chemical Biology. *Cell Chem. Biol.* **2021**, *28* (7), 987–999. https://doi.org/10.1016/j.chembiol.2021.04.012.

(42) Matyskiela, M. E.; Couto, S.; Zheng, X.; Lu, G.; Hui, J.; Stamp, K.; Drew, C.; Ren, Y.; Wang, M.; Carpenter, A.; Lee, C.-W.; Clayton, T.; Fang, W.; Lu, C.-C.; Riley, M.; Abdubek, P.; Blease, K.; Hartke, J.; Kumar, G.; Vessey, R.; Rolfe, M.; Hamann, L. G.; Chamberlain, P. P. SALL4 Mediates Teratogenicity as a Thalidomide-Dependent Cereblon Substrate. *Nat. Chem. Biol.* **2018**, *14* (10), 981–987. https://doi.org/10.1038/s41589-018-0129-x.

(43) Donovan, K. A.; An, J.; Nowak, R. P.; Yuan, J. C.; Fink, E. C.; Berry, B. C.; Ebert, B. L.; Fischer, E. S. Thalidomide Promotes Degradation of SALL4, a Transcription Factor Implicated in Duane Radial Ray Syndrome. *eLife* **2018**, *7*, e38430. https://doi.org/10.7554/eLife.38430.

(44) Lopez-Girona, A.; Mendy, D.; Ito, T.; Miller, K.; Gandhi, A. K.; Kang, J.; Karasawa, S.; Carmel, G.; Jackson, P.; Abbasian, M.; Mahmoudi, A.; Cathers, B.; Rychak, E.; Gaidarova, S.; Chen, R.; Schafer, P. H.; Handa, H.; Daniel, T. O.; Evans, J. F.; Chopra, R. Cereblon Is a Direct Protein Target for Immunomodulatory and Antiproliferative Activities of Lenalidomide and Pomalidomide. *Leukemia* **2012**, *26* (11), 2326–2335. https://doi.org/10.1038/leu.2012.119.

(45) Krönke, J.; Udeshi, N. D.; Narla, A.; Grauman, P.; Hurst, S. N.; McConkey, M.; Svinkina, T.; Heckl, D.; Comer, E.; Li, X.; Ciarlo, C.; Hartman, E.; Munshi, N.; Schenone, M.; Schreiber, S. L.; Carr, S. A.; Ebert, B. L. Lenalidomide Causes Selective Degradation of IKZF1 and IKZF3 in Multiple Myeloma Cells. *Science* **2014**, *343* (6168), 301–305. https://doi.org/10.1126/science.1244851.

(46) Krönke, J.; Fink, E. C.; Hollenbach, P. W.; MacBeth, K. J.; Hurst, S. N.; Udeshi, N. D.; Chamberlain, P. P.; Mani, D. R.; Man, H. W.; Gandhi, A. K.; Svinkina, T.; Schneider, R. K.; McConkey, M.; Järås, M.; Griffiths, E.; Wetzler, M.; Bullinger, L.; Cathers, B. E.; Carr, S. A.; Chopra, R.; Ebert, B. L. Lenalidomide Induces Ubiquitination and Degradation of CK1α in Del(5q) MDS. *Nature* **2015**, *523* (7559), 183–188. https://doi.org/10.1038/nature14610.

(47) Lu, G.; Middleton, R. E.; Sun, H.; Naniong, M. V.; Ott, C. J.; Mitsiades, C. S.; Wong, K. K.; Bradner, J. E.; Kaelin, W. G. The Myeloma Drug Lenalidomide Promotes the Cereblon-Dependent Destruction of Ikaros Proteins. *Science* **2014**, *343* (6168), 305–309. https://doi.org/10.1126/science.1244917.

(48) Chamberlain, P. P.; Lopez-Girona, A.; Miller, K.; Carmel, G.; Pagarigan, B.; Chie-Leon, B.; Rychak, E.; Corral, L. G.; Ren, Y. J.; Wang, M.; Riley, M.; Delker, S. L.; Ito, T.; Ando, H.; Mori, T.; Hirano, Y.; Handa, H.; Hakoshima, T.; Daniel, T. O.; Cathers, B. E. Structure of the Human Cereblon–DDB1–Lenalidomide Complex Reveals Basis for Responsiveness to Thalidomide Analogs. *Nat. Struct. Mol. Biol.* **2014**, *21* (9), 803–809. https://doi.org/10.1038/nsmb.2874.

(49) Fischer, E. S.; Böhm, K.; Lydeard, J. R.; Yang, H.; Stadler, M. B.; Cavadini, S.; Nagel, J.; Serluca, F.; Acker, V.; Lingaraju, G. M.; Tichkule, R. B.; Schebesta, M.; Forrester, W. C.; Schirle, M.; Hassiepen, U.; Ottl, J.; Hild, M.; Beckwith, R. E. J.; Harper, J. W.; Jenkins, J. L.; Thomä, N. H. Structure of the DDB1–CRBN E3 Ubiquitin Ligase in Complex with Thalidomide. *Nature* **2014**, *512* (7512), 49–53. https://doi.org/10.1038/nature13527.

(50) Matyskiela, M. E.; Lu, G.; Ito, T.; Pagarigan, B.; Lu, C.-C.; Miller, K.; Fang, W.; Wang, N.-Y.; Nguyen, D.; Houston, J.; Carmel, G.; Tran, T.; Riley, M.; Nosaka, L.; Lander, G. C.; Gaidarova, S.; Xu, S.; Ruchelman, A. L.; Handa, H.; Carmichael, J.; Daniel, T. O.; Cathers, B. E.; Lopez-Girona, A.; Chamberlain, P. P. A Novel Cereblon Modulator Recruits GSPT1 to the CRL4CRBN Ubiquitin Ligase. *Nature* **2016**, *535* (7611), 252–257. https://doi.org/10.1038/nature18611.

(51) Sievers, Q. L.; Petzold, G.; Bunker, R. D.; Renneville, A.; Słabicki, M.; Liddicoat, B. J.; Abdulrahman, W.; Mikkelsen, T.; Ebert, B. L.; Thomä, N. H. Defining the Human C2H2 Zinc Finger Degrome Targeted by Thalidomide Analogs through CRBN. *Science* **2018**, *362* (6414), eaat0572. https://doi.org/10.1126/science.aat0572.

(52) Nishiguchi, G.; Keramatnia, F.; Min, J.; Chang, Y.; Jonchere, B.; Das, S.; Actis, M.; Price, J.; Chepyala, D.; Young, B.; McGowan, K.; Slavish, P. J.; Mayasundari, A.; Jarusiewicz, J. A.; Yang, L.; Li, Y.; Fu, X.; Garrett, S. H.; Papizan, J. B.; Kodali, K.; Peng, J.; Pruett Miller, S. M.; Roussel, M. F.; Mullighan, C.; Fischer, M.; Rankovic, Z. Identification of Potent, Selective, and Orally Bioavailable Small-Molecule GSPT1/2 Degraders from a Focused Library of Cereblon Modulators. *J. Med. Chem.* **2021**, *64* (11), 7296–7311. https://doi.org/10.1021/acs.jmedchem.0c01313.

(53) Powell, C. E.; Du, G.; Che, J.; He, Z.; Donovan, K. A.; Yue, H.; Wang, E. S.; Nowak, R. P.; Zhang, T.; Fischer, E. S.; Gray, N. S. Selective Degradation of GSPT1 by Cereblon Modulators Identified via a Focused Combinatorial Library. *ACS Chem. Biol.* **2020**, *15* (10), 2722–2730. https://doi.org/10.1021/acschembio.0c00520.

(54) Winter, G. E.; Buckley, D. L.; Paulk, J.; Roberts, J. M.; Souza, A.; Dhe-Paganon, S.; Bradner, J. E. Phthalimide Conjugation as a Strategy for in Vivo Target Protein Degradation. *Science* **2015**, *348* (6241), 1376–1381. https://doi.org/10.1126/science.aab1433.

(55) Lu, J.; Qian, Y.; Altieri, M.; Dong, H.; Wang, J.; Raina, K.; Hines, J.; Winkler, J. D.; Crew, A. P.; Coleman, K.; Crews, C. M. Hijacking the E3 Ubiquitin Ligase Cereblon to Efficiently Target BRD4. *Chem. Biol.* **2015**, *22* (6), 755–763. https://doi.org/10.1016/j.chembiol.2015.05.009.

(56) Hines, J.; Lartigue, S.; Dong, H.; Qian, Y.; Crews, C. M. MDM2-Recruiting PROTAC Offers Superior, Synergistic Antiproliferative Activity via Simultaneous Degradation of BRD4 and Stabilization of P53. *Cancer Res.* **2019**, *79* (1), 251–262. https://doi.org/10.1158/0008-5472.CAN-18-2918.
(57) Sekine, K.; Takubo, K.; Kikuchi, R.; Nishimoto, M.; Kitagawa, M.; Abe, F.; Nishikawa, K.; Tsuruo, T.; Naito, M. Small Molecules Destabilize CIAP1 by Activating Auto-Ubiquitylation. *J. Biol. Chem.* **2008**, *283* (14), 8961–8968. https://doi.org/10.1074/jbc.M709525200.
(58) Itoh, Y.; Ishikawa, M.; Kitaguchi, R.; Sato, S.; Naito, M.; Hashimoto, Y. Development of Target Protein-Selective Degradation Inducer for Protein Knockdown. *Bioorg. Med. Chem.* **2011**, *19* (10), 3229–3241. https://doi.org/10.1016/j.bmc.2011.03.057.
(59) Itoh, Y.; Kitaguchi, R.; Ishikawa, M.; Naito, M.; Hashimoto, Y. Design, Synthesis and Biological Evaluation of Nuclear Receptor-Degradation Inducers. *Bioorg. Med. Chem.* **2011**, *19* (22), 6768–6778. https://doi.org/10.1016/j.bmc.2011.09.041.
(60) Ohoka, N.; Nagai, K.; Hattori, T.; Okuhira, K.; Shibata, N.; Cho, N.; Naito, M. Cancer Cell Death Induced by Novel Small Molecules Degrading the TACC3 Protein via the Ubiquitin-Proteasome Pathway. *Cell Death Dis.* **2014**, *5* (11), 1–10. https://doi.org/10.1038/cddis.2014.471.
(61) Mares, A.; Miah, A. H.; Smith, I. E. D.; Rackham, M.; Thawani, A. R.; Cryan, J.; Haile, P. A.; Votta, B. J.; Beal, A. M.; Capriotti, C.; Reilly, M. A.; Fisher, D. T.; Zinn, N.; Bantscheff, M.; MacDonald, T. T.; Vossenkamper, A.; Dace, P.; Churcher, I.; Benowitz, A. B.; Watt, G.; Denyer, J.; Scott-Stevens, P.; Harling, J. D. Extended Pharmacodynamic Responses Observed upon PROTAC-Mediated Degradation of RIPK2. *Commun. Biol.* **2020**, *3* (1), 140. https://doi.org/10.1038/s42003-020-0868-6.
(62) den Besten, W.; Verma, K.; Yamazoe, S.; Blaquiere, N.; Phung, W.; Izrael-Tomasevic, A.; Mulvihill, M. M.; Helgason, E.; Prakash, S.; Goncharov, T.; Vucic, D.; Dueber, E.; Fairbrother, W. J.; Wertz, I.; Yu, K.; Staben, S. T. Primary Amine Tethered Small Molecules Promote the Degradation of X-Linked Inhibitor of Apoptosis Protein. *J. Am. Chem. Soc.* **2021**, *143* (28), 10571–10575. https://doi.org/10.1021/jacs.1c05269.
(63) Ward, C. C.; Kleinman, J. I.; Brittain, S. M.; Lee, P. S.; Chung, C. Y. S.; Kim, K.; Petri, Y.; Thomas, J. R.; Tallarico, J. A.; McKenna, J. M.; Schirle, M.; Nomura, D. K. Covalent Ligand Screening Uncovers a RNF4 E3 Ligase Recruiter for Targeted Protein Degradation Applications. *ACS Chem. Biol.* **2019**, *14* (11), 2430–2440. https://doi.org/10.1021/acschembio.8b01083.
(64) Spradlin, J. N.; Hu, X.; Ward, C. C.; Brittain, S. M.; Jones, M. D.; Ou, L.; To, M.; Proudfoot, A.; Ornelas, E.; Woldegiorgis, M.; Olzmann, J. A.; Bussiere, D. E.; Thomas, J. R.; Tallarico, J. A.; McKenna, J. M.; Schirle, M.; Maimone, T. J.; Nomura, D. K. Harnessing the Anti-Cancer Natural Product Nimbolide for Targeted Protein Degradation. *Nat. Chem. Biol.* **2019**, *15* (7), 747–755. https://doi.org/10.1038/s41589-019-0304-8.
(65) Tong, B.; Spradlin, J. N.; Novaes, L. F. T.; Zhang, E.; Hu, X.; Moeller, M.; Brittain, S. M.; McGregor, L. M.; McKenna, J. M.; Tallarico, J. A.; Schirle, M.; Maimone, T. J.; Nomura, D. K. A Nimbolide-Based Kinase Degrader Preferentially Degrades

Oncogenic BCR-ABL. *ACS Chem. Biol.* **2020**. https://doi.org/10.1021/acschembio.0c00348.
(66) Luo, M.; Spradlin, J. N.; Boike, L.; Tong, B.; Brittain, S. M.; McKenna, J. M.; Tallarico, J. A.; Schirle, M.; Maimone, T. J.; Nomura, D. K. Chemoproteomics-Enabled Discovery of Covalent RNF114-Based Degraders That Mimic Natural Product Function. *Cell Chem. Biol.* **2021**, *28* (4), 559-566.e15. https://doi.org/10.1016/j.chembiol.2021.01.005.
(67) Zhang, X.; Crowley, V. M.; Wucherpfennig, T. G.; Dix, M. M.; Cravatt, B. F. Electrophilic PROTACs That Degrade Nuclear Proteins by Engaging DCAF16. *Nat. Chem. Biol.* **2019**, *15* (7), 737–746. https://doi.org/10.1038/s41589-019-0279-5.
(68) Baur, M.; Gneist, M.; Owa, T.; Dittrich, C. Clinical Complete Long-Term Remission of a Patient with Metastatic Malignant Melanoma under Therapy with Indisulam (E7070). *Melanoma Res.* **2007**, *17* (5), 329–331. https://doi.org/10.1097/CMR.0b013e3282ef4189.
(69) Mita, M.; Kelly, K. R.; Mita, A.; Ricart, A. D.; Romero, O.; Tolcher, A.; Hook, L.; Okereke, C.; Krivelevich, I.; Rossignol, D. P.; Giles, F. J.; Rowinsky, E. K.; Takimoto, C. Phase I Study of E7820, an Oral Inhibitor of Integrin α-2 Expression with Antiangiogenic Properties, in Patients with Advanced Malignancies. *Clin. Cancer Res.* **2011**, *17* (1), 193–200. https://doi.org/10.1158/1078-0432.CCR-10-0010.
(70) Bekaii-Saab, T. S.; Mortazavi, A.; Hicks, L. G.; Zalupski, M.; Pelley, R. J.; Chan, K. K.; Kraut, E. H. A Phase II Study of Chloroquinoxaline Sulfonamide (CQS) in Patients with Metastatic Colorectal Carcinoma (MCRC). *Invest. New Drugs* **2006**, *24* (4), 343–346. https://doi.org/10.1007/s10637-005-4827-3.
(71) Uehara, T.; Minoshima, Y.; Sagane, K.; Sugi, N. H.; Mitsuhashi, K. O.; Yamamoto, N.; Kamiyama, H.; Takahashi, K.; Kotake, Y.; Uesugi, M.; Yokoi, A.; Inoue, A.; Yoshida, T.; Mabuchi, M.; Tanaka, A.; Owa, T. Selective Degradation of Splicing Factor CAPERα By Anticancer Sulfonamides. *Nat. Chem. Biol.* **2017**, *13* (6), 675–680. https://doi.org/10.1038/nchembio.2363.
(72) Han, T.; Goralski, M.; Gaskill, N.; Capota, E.; Kim, J.; Ting, T. C.; Xie, Y.; Williams, N. S.; Nijhawan, D. Anticancer Sulfonamides Target Splicing by Inducing RBM39 Degradation via Recruitment to DCAF15. *Science* **2017**, *356* (6336). https://doi.org/10.1126/science.aal3755.
(73) Bussiere, D. E.; Xie, L.; Srinivas, H.; Shu, W.; Burke, A.; Be, C.; Zhao, J.; Godbole, A.; King, D.; Karki, R. G.; Hornak, V.; Xu, F.; Cobb, J.; Carte, N.; Frank, A. O.; Frommlet, A.; Graff, P.; Knapp, M.; Fazal, A.; Okram, B.; Jiang, S.; Michellys, P. Y.; Beckwith, R.; Voshol, H.; Wiesmann, C.; Solomon, J. M.; Paulk, J. Structural Basis of Indisulam-Mediated RBM39 Recruitment to DCAF15 E3 Ligase Complex. *Nat. Chem. Biol.* **2020**, *16* (1), 15–23. https://doi.org/10.1038/s41589-019-0411-6.
(74) Faust, T. B.; Yoon, H.; Nowak, R. P.; Donovan, K. A.; Li, Z.; Cai, Q.; Eleuteri, N. A.; Zhang, T.; Gray, N. S.; Fischer, E. S. Structural Complementarity Facilitates E7820-Mediated Degradation of RBM39 by DCAF15. *Nat. Chem. Biol.* **2020**, *16* (1), 7–14. https://doi.org/10.1038/s41589-019-0378-3.
(75) Li, L.; Mi, D.; Pei, H.; Duan, Q.; Wang, X.; Zhou, W.; Jin, J.; Li, D.; Liu, M.; Chen, Y. In Vivo Target Protein Degradation Induced by PROTACs Based on E3 Ligase

DCAF15. *Signal Transduct. Target. Ther.* **2020**, *5* (1), 4–6. https://doi.org/10.1038/s41392-020-00245-0.

(76) Tong, B.; Luo, M.; Xie, Y.; Spradlin, J. N.; Tallarico, J. A.; McKenna, J. M.; Schirle, M.; Maimone, T. J.; Nomura, D. K. Bardoxolone Conjugation Enables Targeted Protein Degradation of BRD4. *Sci. Rep.* **2020**, *10* (1), 15543. https://doi.org/10.1038/s41598-020-72491-9.

(77) Zhang, X.; Luukkonen, L. M.; Eissler, C. L.; Crowley, V. M.; Yamashita, Y.; Schafroth, M. A.; Kikuchi, S.; Weinstein, D. S.; Symons, K. T.; Nordin, B. E.; Rodriguez, J. L.; Wucherpfennig, T. G.; Bauer, L. G.; Dix, M. M.; Stamos, D.; Kinsella, T. M.; Simon, G. M.; Baltgalvis, K. A.; Cravatt, B. F. DCAF11 Supports Targeted Protein Degradation by Electrophilic Proteolysis-Targeting Chimeras. *J. Am. Chem. Soc.* **2021**, *143* (13), 5141–5149. https://doi.org/10.1021/jacs.1c00990.

(78) Henning, N. J.; Manford, A. G.; Spradlin, J. N.; Brittain, S. M.; Zhang, E.; McKenna, J. M.; Tallarico, J. A.; Schirle, M.; Rape, M.; Nomura, D. K. Discovery of a Covalent FEM1B Recruiter for Targeted Protein Degradation Applications. *J. Am. Chem. Soc.* **2022**, *144* (2), 701–708. https://doi.org/10.1021/jacs.1c03980.

(79) Manford, A. G.; Rodríguez-Pérez, F.; Shih, K. Y.; Shi, Z.; Berdan, C. A.; Choe, M.; Titov, D. V.; Nomura, D. K.; Rape, M. A Cellular Mechanism to Detect and Alleviate Reductive Stress. *Cell* **2020**, *183* (1), 46-61.e21. https://doi.org/10.1016/j.cell.2020.08.034.

(80) Nomura, D. K.; Dix, M. M.; Cravatt, B. F. Activity-Based Protein Profiling for Biochemical Pathway Discovery in Cancer. *Nat. Rev. Cancer* **2010**, *10* (9), 630–638. https://doi.org/10.1038/nrc2901.

(81) Evans, M. J.; Cravatt, B. F. Mechanism-Based Profiling of Enzyme Families. *Chem. Rev.* **2006**, *106* (8), 3279–3301. https://doi.org/10.1021/cr050288g.

(82) Moellering, R. E.; Cravatt, B. F. How Chemoproteomics Can Enable Drug Discovery and Development. *Chem. Biol.* **2012**, *19* (1), 11–22. https://doi.org/10.1016/j.chembiol.2012.01.001.

(83) Spradlin, J. N.; Zhang, E.; Nomura, D. K. Reimagining Druggability Using Chemoproteomic Platforms. *Acc. Chem. Res.* **2021**, *54* (7), 1801–1813. https://doi.org/10.1021/acs.accounts.1c00065.

(84) Weerapana, E.; Wang, C.; Simon, G. M.; Richter, F.; Khare, S.; Dillon, M. B. D.; Bachovchin, D. A.; Mowen, K.; Baker, D.; Cravatt, B. F. Quantitative Reactivity Profiling Predicts Functional Cysteines in Proteomes. *Nature* **2010**, *468* (7325), 790–795. https://doi.org/10.1038/nature09472.

(85) Wang, C.; Weerapana, E.; Blewett, M. M.; Cravatt, B. F. A Chemoproteomic Platform to Quantitatively Map Targets of Lipid-Derived Electrophiles. *Nat. Methods* **2014**, *11* (1), 79–85. https://doi.org/10.1038/nmeth.2759.

(86) Backus, K. M.; Correia, B. E.; Lum, K. M.; Forli, S.; Horning, B. D.; González-Páez, G. E.; Chatterjee, S.; Lanning, B. R.; Teijaro, J. R.; Olson, A. J.; Wolan, D. W.; Cravatt, B. F. Proteome-Wide Covalent Ligand Discovery in Native Biological Systems. *Nature* **2016**, *534* (7608), 570–574. https://doi.org/10.1038/nature18002.

(87) Hacker, S. M.; Backus, K. M.; Lazear, M. R.; Forli, S.; Correia, B. E.; Cravatt, B. F. Global Profiling of Lysine Reactivity and Ligandability in the Human Proteome. *Nat. Chem.* **2017**, *9* (12), 1181–1190. https://doi.org/10.1038/nchem.2826.

(88) Brulet, J. W.; Borne, A. L.; Yuan, K.; Libby, A. H.; Hsu, K.-L. Liganding Functional Tyrosine Sites on Proteins Using Sulfur–Triazole Exchange Chemistry. *J. Am. Chem. Soc.* **2020**, *142* (18), 8270–8280. https://doi.org/10.1021/jacs.0c00648.
(89) Kuljanin, M.; Mitchell, D. C.; Schweppe, D. K.; Gikandi, A. S.; Nusinow, D. P.; Bulloch, N. J.; Vinogradova, E. V.; Wilson, D. L.; Kool, E. T.; Mancias, J. D.; Cravatt, B. F.; Gygi, S. P. Reimagining High-Throughput Profiling of Reactive Cysteines for Cell-Based Screening of Large Electrophile Libraries. *Nat. Biotechnol.* **2021**, *39* (5), 630–641. https://doi.org/10.1038/s41587-020-00778-3.
(90) Bar-Peled, L.; Kemper, E. K.; Suciu, R. M.; Vinogradova, E. V.; Backus, K. M.; Horning, B. D.; Paul, T. A.; Ichu, T.-A.; Svensson, R. U.; Olucha, J.; Chang, M. W.; Kok, B. P.; Zhu, Z.; Ihle, N. T.; Dix, M. M.; Jiang, P.; Hayward, M. M.; Saez, E.; Shaw, R. J.; Cravatt, B. F. Chemical Proteomics Identifies Druggable Vulnerabilities in a Genetically Defined Cancer. *Cell* **2017**, *171* (3), 696-709.e23. https://doi.org/10.1016/j.cell.2017.08.051.
(91) Vinogradova, E. V.; Zhang, X.; Remillard, D.; Lazar, D. C.; Suciu, R. M.; Wang, Y.; Bianco, G.; Yamashita, Y.; Crowley, V. M.; Schafroth, M. A.; Yokoyama, M.; Konrad, D. B.; Lum, K. M.; Simon, G. M.; Kemper, E. K.; Lazear, M. R.; Yin, S.; Blewett, M. M.; Dix, M. M.; Nguyen, N.; Shokhirev, M. N.; Chin, E. N.; Lairson, L. L.; Melillo, B.; Schreiber, S. L.; Forli, S.; Teijaro, J. R.; Cravatt, B. F. An Activity-Guided Map of Electrophile-Cysteine Interactions in Primary Human T Cells. *Cell* **2020**, *182* (4), 1009-1026.e29. https://doi.org/10.1016/j.cell.2020.07.001.
(92) Grossman, E. A.; Ward, C. C.; Spradlin, J. N.; Bateman, L. A.; Huffman, T. R.; Miyamoto, D. K.; Kleinman, J. I.; Nomura, D. K. Covalent Ligand Discovery against Druggable Hotspots Targeted by Anti-Cancer Natural Products. *Cell Chem. Biol.* **2017**, *24* (11), 1368-1376.e4. https://doi.org/10.1016/j.chembiol.2017.08.013.
(93) Bateman, L. A.; Nguyen, T. B.; Roberts, A. M.; Miyamoto, D. K.; Ku, W.-M.; Huffman, T. R.; Petri, Y.; Heslin, M. J.; Contreras, C. M.; Skibola, C. F.; Olzmann, J. A.; Nomura, D. K. Chemoproteomics-Enabled Covalent Ligand Screen Reveals a Cysteine Hotspot in Reticulon 4 That Impairs ER Morphology and Cancer Pathogenicity. *Chem. Commun.* **2017**, *53* (53), 7234–7237. https://doi.org/10.1039/C7CC01480E.
(94) Ward, C. C.; Kleinman, J. I.; Nomura, D. K. NHS-Esters As Versatile Reactivity-Based Probes for Mapping Proteome-Wide Ligandable Hotspots. *ACS Chem. Biol.* **2017**, *12* (6), 1478–1483. https://doi.org/10.1021/acschembio.7b00125.
(95) Chung, C. Y.-S.; Shin, H. R.; Berdan, C. A.; Ford, B.; Ward, C. C.; Olzmann, J. A.; Zoncu, R.; Nomura, D. K. Covalent Targeting of the Vacuolar H+-ATPase Activates Autophagy via MTORC1 Inhibition. *Nat. Chem. Biol.* **2019**, *15* (8), 776–785. https://doi.org/10.1038/s41589-019-0308-4.
(96) Counihan, J. L.; Wiggenhorn, A. L.; Anderson, K. E.; Nomura, D. K. Chemoproteomics-Enabled Covalent Ligand Screening Reveals ALDH3A1 as a Lung Cancer Therapy Target. *ACS Chem. Biol.* **2018**, *13* (8), 1970–1977. https://doi.org/10.1021/acschembio.8b00381.
(97) Counihan, J. L.; Duckering, M.; Dalvie, E.; Ku, W.; Bateman, L. A.; Fisher, K. J.; Nomura, D. K. Chemoproteomic Profiling of Acetanilide Herbicides Reveals Their Role in Inhibiting Fatty Acid Oxidation. *ACS Chem. Biol.* **2017**, *12* (3), 635–642. https://doi.org/10.1021/acschembio.6b01001.

(98) Ford, B.; Bateman, L. A.; Gutierrez-Palominos, L.; Park, R.; Nomura, D. K. Mapping Proteome-Wide Targets of Glyphosate in Mice. *Cell Chem. Biol.* **2017**, *24* (2), 133–140. https://doi.org/10.1016/j.chembiol.2016.12.013.
(99) Boike, L.; Cioffi, A. G.; Majewski, F. C.; Co, J.; Henning, N. J.; Jones, M. D.; Liu, G.; McKenna, J. M.; Tallarico, J. A.; Schirle, M.; Nomura, D. K. Discovery of a Functional Covalent Ligand Targeting an Intrinsically Disordered Cysteine within MYC. *Cell Chem. Biol.* **2021**, *28* (1), 4-13.e17. https://doi.org/10.1016/j.chembiol.2020.09.001.
(100) Isobe, Y.; Okumura, M.; McGregor, L. M.; Brittain, S. M.; Jones, M. D.; Liang, X.; White, R.; Forrester, W.; McKenna, J. M.; Tallarico, J. A.; Schirle, M.; Maimone, T. J.; Nomura, D. K. Manumycin Polyketides Act as Molecular Glues between UBR7 and P53. *Nat. Chem. Biol.* **2020**, *16* (11), 1189–1198. https://doi.org/10.1038/s41589-020-0557-2.
(101) Cho, H.; Shen, Q.; Zhang, L. H.; Okumura, M.; Kawakami, A.; Ambrose, J.; Sigoillot, F.; Miller, H. R.; Gleim, S.; Cobos-Correa, A.; Wang, Y.; Piechon, P.; Roma, G.; Eggimann, F.; Moore, C.; Aspesi, P.; Mapa, F. A.; Burks, H.; Ross, N. T.; Krastel, P.; Hild, M.; Maimone, T. J.; Fisher, D. E.; Nomura, D. K.; Tallarico, J. A.; Canham, S. M.; Jenkins, J. L.; Forrester, W. C. CYP27A1-Dependent Anti-Melanoma Activity of Limonoid Natural Products Targets Mitochondrial Metabolism. *Cell Chem. Biol.* **2021**, *28* (10), 1407-1419.e6. https://doi.org/10.1016/j.chembiol.2021.03.004.
(102) Berdan, C. A.; Ho, R.; Lehtola, H. S.; To, M.; Hu, X.; Huffman, T. R.; Petri, Y.; Altobelli, C. R.; Demeulenaere, S. G.; Olzmann, J. A.; Maimone, T. J.; Nomura, D. K. Parthenolide Covalently Targets and Inhibits Focal Adhesion Kinase in Breast Cancer Cells. *Cell Chem. Biol.* **2019**, *26* (7), 1027-1035.e22. https://doi.org/10.1016/j.chembiol.2019.03.016.
(103) Roberts, A. M.; Miyamoto, D. K.; Huffman, T. R.; Bateman, L. A.; Ives, A. N.; Akopian, D.; Heslin, M. J.; Contreras, C. M.; Rape, M.; Skibola, C. F.; Nomura, D. K. Chemoproteomic Screening of Covalent Ligands Reveals UBA5 As a Novel Pancreatic Cancer Target. *ACS Chem. Biol.* **2017**, *12* (4), 899–904. https://doi.org/10.1021/acschembio.7b00020.
(104) Roberts, L. S.; Yan, P.; Bateman, L. A.; Nomura, D. K. Mapping Novel Metabolic Nodes Targeted by Anti-Cancer Drugs That Impair Triple-Negative Breast Cancer Pathogenicity. *ACS Chem. Biol.* **2017**, *12* (4), 1133–1140. https://doi.org/10.1021/acschembio.6b01159.
(105) Yau, R.; Rape, M. The Increasing Complexity of the Ubiquitin Code. *Nat. Cell Biol.* **2016**, *18* (6), 579–586. https://doi.org/10.1038/ncb3358.
(106) Smit, J. J.; Sixma, T. K. RBR E3-ligases at Work. *EMBO Rep.* **2014**, *15* (2), 142–154. https://doi.org/10.1002/embr.201338166.
(107) Tong, B.; Belcher, B. P.; Nomura, D. K.; Maimone, T. J. Chemical Investigations into the Biosynthesis of the Gymnastatin and Dankastatin Alkaloids. *Chem. Sci.* **2021**, *12* (25), 8884–8891. https://doi.org/10.1039/D1SC02613E.
(108) Belcher, B. P.; Machicao, P. A.; Tong, B.; Ho, E.; Friedli, J.; So, B.; Bui, H.; Isobe, Y.; Maimone, T. J.; Nomura, D. K. Chemoproteomic Profiling Reveals That Anti-Cancer Natural Product Dankastatin B Covalently Targets Mitochondrial VDAC3. *ChemBioChem* **2023**, e202300111. https://doi.org/10.1002/cbic.202300111.

(109) Newman, D. J.; Cragg, G. M. Natural Products as Sources of New Drugs over the Nearly Four Decades from 01/1981 to 09/2019. *J. Nat. Prod.* **2020**, *83* (3), 770–803. https://doi.org/10.1021/acs.jnatprod.9b01285.
(110) Kearney, S. E.; Zahoránszky-Kőhalmi, G.; Brimacombe, K. R.; Henderson, M. J.; Lynch, C.; Zhao, T.; Wan, K. K.; Itkin, Z.; Dillon, C.; Shen, M.; Cheff, D. M.; Lee, T. D.; Bougie, D.; Cheng, K.; Coussens, N. P.; Dorjsuren, D.; Eastman, R. T.; Huang, R.; Iannotti, M. J.; Karavadhi, S.; Klumpp-Thomas, C.; Roth, J. S.; Sakamuru, S.; Sun, W.; Titus, S. A.; Yasgar, A.; Zhang, Y.-Q.; Zhao, J.; Andrade, R. B.; Brown, M. K.; Burns, N. Z.; Cha, J. K.; Mevers, E. E.; Clardy, J.; Clement, J. A.; Crooks, P. A.; Cuny, G. D.; Ganor, J.; Moreno, J.; Morrill, L. A.; Picazo, E.; Susick, R. B.; Garg, N. K.; Goess, B. C.; Grossman, R. B.; Hughes, C. C.; Johnston, J. N.; Joullie, M. M.; Kinghorn, A. D.; Kingston, D. G. I.; Krische, M. J.; Kwon, O.; Maimone, T. J.; Majumdar, S.; Maloney, K. N.; Mohamed, E.; Murphy, B. T.; Nagorny, P.; Olson, D. E.; Overman, L. E.; Brown, L. E.; Snyder, J. K.; Porco, J. A.; Rivas, F.; Ross, S. A.; Sarpong, R.; Sharma, I.; Shaw, J. T.; Xu, Z.; Shen, B.; Shi, W.; Stephenson, C. R. J.; Verano, A. L.; Tan, D. S.; Tang, Y.; Taylor, R. E.; Thomson, R. J.; Vosburg, D. A.; Wu, J.; Wuest, W. M.; Zakarian, A.; Zhang, Y.; Ren, T.; Zuo, Z.; Inglese, J.; Michael, S.; Simeonov, A.; Zheng, W.; Shinn, P.; Jadhav, A.; Boxer, M. B.; Hall, M. D.; Xia, M.; Guha, R.; Rohde, J. M. Canvass: A Crowd-Sourced, Natural-Product Screening Library for Exploring Biological Space. *ACS Cent. Sci.* **2018**, *4* (12), 1727–1741. https://doi.org/10.1021/acscentsci.8b00747.
(111) Nomura, D. K.; Maimone, T. J. Target Identification of Bioactive Covalently Acting Natural Products. *Curr. Top. Microbiol. Immunol.* **2018**. https://doi.org/10.1007/82_2018_121.
(112) Drahl, C.; Cravatt, B. F.; Sorensen, E. J. Protein-Reactive Natural Products. *Angew. Chem. Int. Ed Engl.* **2005**, *44* (36), 5788–5809. https://doi.org/10.1002/anie.200500900.
(113) Amagata, T.; Minoura, K.; Numata, A. Gymnastatins F-H, Cytostatic Metabolites from the Sponge-Derived Fungus Gymnascella Dankaliensis. *J. Nat. Prod.* **2006**, *69* (10), 1384–1388. https://doi.org/10.1021/np0600189.
(114) Amagata, T.; Doi, M.; Ohta, T.; Minoura, K.; Numata, A. Absolute Stereostructures of Novel Cytotoxic Metabolites, Gymnastatins A–E, from a Gymnascella Species Separated from a Halichondria Sponge. *J. Chem. Soc. Perkin 1* **1998**, No. 21, 3585–3600. https://doi.org/10.1039/A804466J.
(115) Amagata, T.; Tanaka, M.; Yamada, T.; Minoura, K.; Numata, A. Gymnastatins and Dankastatins, Growth Inhibitory Metabolites of a Gymnascella Species from a Halichondria Sponge. *J. Nat. Prod.* **2008**, *71* (3), 340–345. https://doi.org/10.1021/np070529a.
(116) Hammerschmidt, L.; Aly, A. H.; Abdel-Aziz, M.; Müller, W. E. G.; Lin, W.; Daletos, G.; Proksch, P. Cytotoxic Acyl Amides from the Soil Fungus Gymnascella Dankaliensis. *Bioorg. Med. Chem.* **2015**, *23* (4), 712–719. https://doi.org/10.1016/j.bmc.2014.12.068.
(117) Gurjar, Mukund K.; Bhaket, Pushpal. Total Synthesis of a Novel Cytotoxic Metabolite Gymnastatin A. *Heterocycles* **2000**, *53* (1), 143–149. https://doi.org/10.3987/COM-99-8745.

(118) Phoon, C. W.; Somanadhan, B.; Heng, S. C. H.; Ngo, A.; Ng, S. B.; Butler, M. S.; Buss, A. D.; Sim, M. M. Isolation and Total Synthesis of Gymnastatin N, a POLO-like Kinase 1 Active Constituent from the Fungus Arachniotus Punctatus. *Tetrahedron* **2004**, *60* (50), 11619–11628. https://doi.org/10.1016/j.tet.2004.09.046.
(119) Ogamino, T.; Ohnishi, S.; Ishikawa, Y.; Sugai, T.; Obata, R.; Nishiyama, S. Synthesis and Biological Assessment of Hemiacetal Spiro Derivatives towards Development of Efficient Chemotherapeutic Agent. *Sci. Technol. Adv. Mater.* **2006**, *7* (2), 175–183. https://doi.org/10.1016/j.stam.2005.10.004.
(120) Murayama, K.; Tanabe, T.; Ishikawa, Y.; Nakamura, K.; Nishiyama, S. A Synthetic Study on Gymnastatins F and Q: The Tandem Michael and Aldol Reaction Approach. *Tetrahedron Lett.* **2009**, *50* (26), 3191–3194. https://doi.org/10.1016/j.tetlet.2009.01.156.
(121) Raffier, L.; Piva, O. Application of the Diastereoselective Photodeconjugation of α,β-Unsaturated Esters to the Synthesis of Gymnastatin H. *Beilstein J. Org. Chem.* **2011**, *7*, 151–155. https://doi.org/10.3762/bjoc.7.21.
(122) Ting, C. P.; Maimone, T. J. Total Synthesis of Hyperforin. *J. Am. Chem. Soc.* **2015**, *137* (33), 10516–10519. https://doi.org/10.1021/jacs.5b06939.
(123) Ting, C. P.; Xu, G.; Zeng, X.; Maimone, T. J. Annulative Methods Enable a Total Synthesis of the Complex Meroterpene Berkeleyone A. *J. Am. Chem. Soc.* **2016**, *138* (45), 14868–14871. https://doi.org/10.1021/jacs.6b10397.
(124) Xu, G.; Elkin, M.; Tantillo, D. J.; Newhouse, T. R.; Maimone, T. J. Traversing Biosynthetic Carbocation Landscapes in the Total Synthesis of Andrastin and Terretonin Meroterpenes. *Angew. Chem. Int. Ed.* **2017**, *56* (41), 12498–12502. https://doi.org/10.1002/anie.201705654.
(125) Shen, X.; Ting, C. P.; Xu, G.; Maimone, T. J. Programmable Meroterpene Synthesis. *Nat. Commun.* **2020**, *11* (1), 508. https://doi.org/10.1038/s41467-020-14354-5.
(126) Tong, B. Chemical Investigations into the Biosynthesis of the Gymnastatin and Dankastatin Alkaloids. *Chem Sci* **2021**, 8.
(127) Amagata, T.; Tanaka, M.; Yamada, T.; Chen, Y.-P.; Minoura, K.; Numata, A. Additional Cytotoxic Substances Isolated from the Sponge-Derived Gymnascella Dankaliensis. *Tetrahedron Lett.* **2013**, *54* (45), 5960–5962. https://doi.org/10.1016/j.tetlet.2013.08.044.
(128) Wang, H. Targeted Solid Phase Fermentation of the Soil Dwelling Fungus Gymnascella Dankaliensis Yields New Brominated Tyrosine-Derived Alkaloids. *RSC Adv.* **2016**.
(129) Xu, D.; Luo, M.; Liu, F.; Wang, D.; Pang, X.; Zhao, T.; Xu, L.; Wu, X.; Xia, M.; Yang, X. Cytochalasan and Tyrosine-Derived Alkaloids from the Marine Sediment-Derived Fungus Westerdykella Dispersa and Their Bioactivities. *Sci. Rep.* **2017**, *7* (1), 11956. https://doi.org/10.1038/s41598-017-12327-1.
(130) Gavaret, J. M.; Cahnmann, H. J.; Nunez, J. Thyroid Hormone Synthesis in Thyroglobulin. The Mechanism of the Coupling Reaction. *J. Biol. Chem.* **1981**, *256* (17), 9167–9173. https://doi.org/10.1016/S0021-9258(19)52523-6.

(131) Wipf, P.; Jeger, P.; Kim, Y. Thiophilic Ring-Opening and Rearrangement Reactions of Epoxyketone Natural Products. *Bioorg. Med. Chem. Lett.* **1998**, *8* (4), 351–356. https://doi.org/10.1016/S0960-894X(98)00026-2.
(132) Hammill, J. T.; Contreras-García, J.; Virshup, A. M.; Beratan, D. N.; Yang, W.; Wipf, P. Synthesis and Chemical Diversity Analysis of Bicyclo[3.3.1]Non-3-En-2-Ones. *Tetrahedron* **2010**, *66* (31), 5852–5862. https://doi.org/10.1016/j.tet.2010.04.112.
(133) Mukhopadhyay, T.; Bhat, R. G.; Roy, K.; Vijayakumar, E. K. S.; Ganguli, B. N. Aranochlor A and Aranochlor B, Two New Metabolites from Pseudoarachniotus Roseus: Production, Isolation, Structure Elucidation and Biological Properties. *J. Antibiot. (Tokyo)* **1998**, *51* (4), 439–441. https://doi.org/10.7164/antibiotics.51.439.
(134) Li, Y.; Zhang, H.; Merkher, Y.; Chen, L.; Liu, N.; Leonov, S.; Chen, Y. Recent Advances in Therapeutic Strategies for Triple-Negative Breast Cancer. *J. Hematol. Oncol.J Hematol Oncol* **2022**, *15* (1), 121. https://doi.org/10.1186/s13045-022-01341-0.
(135) Weerapana, E.; Wang, C.; Simon, G. M.; Richter, F.; Khare, S.; Dillon, M. B. D.; Bachovchin, D. A.; Mowen, K.; Baker, D.; Cravatt, B. F. Quantitative Reactivity Profiling Predicts Functional Cysteines in Proteomes. *Nature* **2010**, *468* (7325), 790–795. https://doi.org/10.1038/nature09472.
(136) Wang, C.; Weerapana, E.; Blewett, M. M.; Cravatt, B. F. A Chemoproteomic Platform to Quantitatively Map Targets of Lipid-Derived Electrophiles. *Nat. Methods* **2014**, *11* (1), 79–85. https://doi.org/10.1038/nmeth.2759.
(137) Backus, K. M.; Correia, B. E.; Lum, K. M.; Forli, S.; Horning, B. D.; González-Páez, G. E.; Chatterjee, S.; Lanning, B. R.; Teijaro, J. R.; Olson, A. J.; Wolan, D. W.; Cravatt, B. F. Proteome-Wide Covalent Ligand Discovery in Native Biological Systems. *Nature* **2016**, *534* (7608), 570–574. https://doi.org/10.1038/nature18002.
(138) Roberts, A. M.; Ward, C. C.; Nomura, D. K. Activity-Based Protein Profiling for Mapping and Pharmacologically Interrogating Proteome-Wide Ligandable Hotspots. *Curr. Opin. Biotechnol.* **2017**, *43*, 25–33. https://doi.org/10.1016/j.copbio.2016.08.003.
(139) Zinghirino, F.; Pappalardo, X. G.; Messina, A.; Nicosia, G.; De Pinto, V.; Guarino, F. VDAC Genes Expression and Regulation in Mammals. *Front. Physiol.* **2021**, *12*, 708695. https://doi.org/10.3389/fphys.2021.708695.
(140) Chin, H. S.; Li, M. X.; Tan, I. K. L.; Ninnis, R. L.; Reljic, B.; Scicluna, K.; Dagley, L. F.; Sandow, J. J.; Kelly, G. L.; Samson, A. L.; Chappaz, S.; Khaw, S. L.; Chang, C.; Morokoff, A.; Brinkmann, K.; Webb, A.; Hockings, C.; Hall, C. M.; Kueh, A. J.; Ryan, M. T.; Kluck, R. M.; Bouillet, P.; Herold, M. J.; Gray, D. H. D.; Huang, D. C. S.; van Delft, M. F.; Dewson, G. VDAC2 Enables BAX to Mediate Apoptosis and Limit Tumor Development. *Nat. Commun.* **2018**, *9* (1), 4976. https://doi.org/10.1038/s41467-018-07309-4.
(141) Plötz, M.; Gillissen, B.; Hossini, A. M.; Daniel, P. T.; Eberle, J. Disruption of the VDAC2–Bak Interaction by Bcl-XS Mediates Efficient Induction of Apoptosis in Melanoma Cells. *Cell Death Differ.* **2012**, *19* (12), 1928–1938. https://doi.org/10.1038/cdd.2012.71.
(142) Shakeri, R.; Kheirollahi, A.; Davoodi, J. Apaf-1: Regulation and Function in Cell Death. *Biochimie* **2017**, *135*, 111–125. https://doi.org/10.1016/j.biochi.2017.02.001.

(143) Dall, E.; Brandstetter, H. Structure and Function of Legumain in Health and Disease. *Biochimie* **2016**, *122*, 126–150. https://doi.org/10.1016/j.biochi.2015.09.022.
(144) Haugen, M. H.; Johansen, H. T.; Pettersen, S. J.; Solberg, R.; Brix, K.; Flatmark, K.; Maelandsmo, G. M. Nuclear Legumain Activity in Colorectal Cancer. *PLoS ONE* **2013**, *8* (1), e52980. https://doi.org/10.1371/journal.pone.0052980.
(145) Lewēn, S.; Zhou, H.; Hu, H.; Cheng, T.; Markowitz, D.; Reisfeld, R. A.; Xiang, R.; Luo, Y. A Legumain-Based Minigene Vaccine Targets the Tumor Stroma and Suppresses Breast Cancer Growth and Angiogenesis. *Cancer Immunol. Immunother.* **2008**, *57* (4), 507–515. https://doi.org/10.1007/s00262-007-0389-x.
(146) Gawenda, J.; Traub, F.; Lück, H. J.; Kreipe, H.; von Wasielewski, R. Legumain Expression as a Prognostic Factor in Breast Cancer Patients. *Breast Cancer Res. Treat.* **2007**, *102* (1), 1–6. https://doi.org/10.1007/s10549-006-9311-z.
(147) Xu, T.; Park, S. K.; Venable, J. D.; Wohlschlegel, J. A.; Diedrich, J. K.; Cociorva, D.; Lu, B.; Liao, L.; Hewel, J.; Han, X.; Wong, C. C. L.; Fonslow, B.; Delahunty, C.; Gao, Y.; Shah, H.; Yates, J. R. ProLuCID: An Improved SEQUEST-like Algorithm with Enhanced Sensitivity and Specificity. *J. Proteomics* **2015**, *129*, 16–24. https://doi.org/10.1016/j.jprot.2015.07.001.
(148) King, E. A.; Cho, Y.; Dovala, D.; McKenna, J. M.; Tallarico, J. A.; Schirle, M.; Nomura, D. K. Chemoproteomics-Enabled Discovery of a Covalent Molecular Glue Degrader Targeting NF-KB. bioRxiv May 18, 2022, p 2022.05.18.492542. https://doi.org/10.1101/2022.05.18.492542.
(149) Xu, T.; Park, S. K.; Venable, J. D.; Wohlschlegel, J. A.; Diedrich, J. K.; Cociorva, D.; Lu, B.; Liao, L.; Hewel, J.; Han, X.; Wong, C. C. L.; Fonslow, B.; Delahunty, C.; Gao, Y.; Shah, H.; Yates, J. R. ProLuCID: An Improved SEQUEST-like Algorithm with Enhanced Sensitivity and Specificity. *J. Proteomics* **2015**, *129*, 16–24. https://doi.org/10.1016/j.jprot.2015.07.001.
(150) Page, A. C. S.; Scholz, S. O.; Keenan, K. N.; Spradlin, J. N.; Belcher, B. P.; Brittain, S. M.; Tallarico, J. A.; McKenna, J. M.; Schirle, M.; Nomura, D. K.; Toste, F. D. Photo-Brook Rearrangement of Acyl Silanes as a Strategy for Photoaffinity Probe Design. *Chem. Sci.* **2022**, *13* (13), 3851–3856. https://doi.org/10.1039/D2SC00426G.
(151) Schenone, M.; Dančík, V.; Wagner, B. K.; Clemons, P. A. Target Identification and Mechanism of Action in Chemical Biology and Drug Discovery. *Nat. Chem. Biol.* **2013**, *9* (4), 232–240. https://doi.org/10.1038/nchembio.1199.
(152) Ziegler, S.; Pries, V.; Hedberg, C.; Waldmann, H. Target Identification for Small Bioactive Molecules: Finding the Needle in the Haystack. *Angew. Chem. Int. Ed.* **2013**, *52* (10), 2744–2792. https://doi.org/10.1002/anie.201208749.
(153) Su, Y.; Ge, J.; Zhu, B.; Zheng, Y.-G.; Zhu, Q.; Yao, S. Q. Target Identification of Biologically Active Small Molecules via in Situ Methods. *Curr. Opin. Chem. Biol.* **2013**, *17* (5), 768–775. https://doi.org/10.1016/j.cbpa.2013.06.005.
(154) Schirle, M.; Jenkins, J. L. Identifying Compound Efficacy Targets in Phenotypic Drug Discovery. *Drug Discov. Today* **2016**, *21* (1), 82–89. https://doi.org/10.1016/j.drudis.2015.08.001.

(155) Kotzyba-Hibert, F.; Kapfer, I.; Goeldner, M. Recent Trends in Photoaffinity Labeling. *Angew. Chem. Int. Ed. Engl.* **1995**, *34* (12), 1296–1312. https://doi.org/10.1002/anie.199512961.
(156) Sumranjit, J.; Chung, S. Recent Advances in Target Characterization and Identification by Photoaffinity Probes. *Molecules* **2013**, *18* (9), 10425–10451. https://doi.org/10.3390/molecules180910425.
(157) Hatanaka, Y. Development and Leading-Edge Application of Innovative Photoaffinity Labeling. *Chem. Pharm. Bull. (Tokyo)* **2015**, *63* (1), 1–12. https://doi.org/10.1248/cpb.c14-00645.
(158) Smith, E.; Collins, I. Photoaffinity Labeling in Target- and Binding-Site Identification. *Future Med. Chem.* **2015**, *7* (2), 159–183. https://doi.org/10.4155/fmc.14.152.
(159) Flaxman, H. A.; Woo, C. M. Mapping the Small Molecule Interactome by Mass Spectrometry. *Biochemistry* **2018**, *57* (2), 186–193. https://doi.org/10.1021/acs.biochem.7b01038.
(160) Smith, R. A. G.; Knowles, J. R. Aryldiazirines. Potential Reagents for Photolabeling of Biological Receptor Sites. *J. Am. Chem. Soc.* **1973**, *95* (15), 5072–5073. https://doi.org/10.1021/ja00796a062.
(161) Fleet, G. W. J.; Porter, R. R.; Knowles, J. R. Affinity Labelling of Antibodies with Aryl Nitrene as Reactive Group. *Nature* **1969**, *224* (5218), 511–512. https://doi.org/10.1038/224511a0.
(162) Galardy, R. E.; Craig, L. C.; Jamieson, J. D.; Printz, M. P. Photoaffinity Labeling of Peptide Hormone Binding Sites. *J. Biol. Chem.* **1974**, *249* (11), 3510–3518. https://doi.org/10.1016/S0021-9258(19)42601-X.
(163) Li, Z.; Wang, D.; Li, L.; Pan, S.; Na, Z.; Tan, C. Y. J.; Yao, S. Q. "Minimalist" Cyclopropene-Containing Photo-Cross-Linkers Suitable for Live-Cell Imaging and Affinity-Based Protein Labeling. *J. Am. Chem. Soc.* **2014**, *136* (28), 9990–9998. https://doi.org/10.1021/ja502780z.
(164) Pan, S.; Jang, S.-Y.; Wang, D.; Liew, S. S.; Li, Z.; Lee, J.-S.; Yao, S. Q. A Suite of "Minimalist" Photo-Crosslinkers for Live-Cell Imaging and Chemical Proteomics: Case Study with BRD4 Inhibitors. *Angew. Chem. Int. Ed.* **2017**, *56* (39), 11816–11821. https://doi.org/10.1002/anie.201706076.
(165) Park, J.; Koh, M.; Koo, J. Y.; Lee, S.; Park, S. B. Investigation of Specific Binding Proteins to Photoaffinity Linkers for Efficient Deconvolution of Target Protein. *ACS Chem. Biol.* **2016**, *11* (1), 44–52. https://doi.org/10.1021/acschembio.5b00671.
(166) Kleiner, P.; Heydenreuter, W.; Stahl, M.; Korotkov, V. S.; Sieber, S. A. A Whole Proteome Inventory of Background Photocrosslinker Binding. *Angew. Chem. Int. Ed.* **2017**, *56* (5), 1396–1401. https://doi.org/10.1002/anie.201605993.
(167) Herner, A.; Marjanovic, J.; Lewandowski, T. M.; Marin, V.; Patterson, M.; Miesbauer, L.; Ready, D.; Williams, J.; Vasudevan, A.; Lin, Q. 2-Aryl-5-Carboxytetrazole as a New Photoaffinity Label for Drug Target Identification. *J. Am. Chem. Soc.* **2016**, *138* (44), 14609–14615. https://doi.org/10.1021/jacs.6b06645.
(168) Ota, E.; Usui, K.; Oonuma, K.; Koshino, H.; Nishiyama, S.; Hirai, G.; Sodeoka, M. Thienyl-Substituted α-Ketoamide: A Less Hydrophobic Reactive Group for Photo-Affinity Labeling. *ACS Chem. Biol.* **2018**, *13* (4), 876–880. https://doi.org/10.1021/acschembio.7b00988.

(169) Duff, J. M.; Brook, A. G. Photoisomerization of Acylsilanes to Siloxycarbenes, and Their Reactions with Polar Reagents. *Can. J. Chem.* **1973**, *51* (17), 2869–2883. https://doi.org/10.1139/v73-429.
(170) Ramsey, B. G.; Brook, A.; Bassindale, A. R. (~-Vr*, A REASSIGNMENT OF THE LONG WAVELENGTH W TRANSITION IN ACYL-SILANFS AND -GERMAN-E S BY PHOTOELECTRON SPECTRO- SCOPY.
(171) Ye, J.-H.; Quach, L.; Paulisch, T.; Glorius, F. Visible-Light-Induced, Metal-Free Carbene Insertion into B–H Bonds between Acylsilanes and Pinacolborane. *J. Am. Chem. Soc.* **2019**, *141* (41), 16227–16231. https://doi.org/10.1021/jacs.9b08960.
(172) Priebbenow, D. L. Silicon-Derived Singlet Nucleophilic Carbene Reagents in Organic Synthesis. *Adv. Synth. Catal.* **2020**, *362* (10), 1927–1946. https://doi.org/10.1002/adsc.202000279.
(173) Zhang, H.-J.; Priebbenow, D. L.; Bolm, C. Acylsilanes: Valuable Organosilicon Reagents in Organic Synthesis. *Chem. Soc. Rev.* **2013**, *42* (21), 8540. https://doi.org/10.1039/c3cs60185d.
(174) Stuckhardt, C.; Wissing, M.; Studer, A. Photo Click Reaction of Acylsilanes with Indoles. *Angew. Chem. Int. Ed.* **2021**, *60* (34), 18605–18611. https://doi.org/10.1002/anie.202101689.
(175) Reimler, J.; Studer, A. Visible-Light Mediated Tryptophan Modification in Oligopeptides Employing Acylsilanes. *Chem. – Eur. J.* **2021**, *27* (62), 15392–15395. https://doi.org/10.1002/chem.202102749.
(176) Bourque, R. A.; Davis, P. D.; Dalton, J. C. Mechanistic Photochemistry of Acylsilanes. 1. Reaction with Alcohols. *J. Am. Chem. Soc.* **1981**, *103* (3), 697–699. https://doi.org/10.1021/ja00393a048.
(177) West, A. V.; Muncipinto, G.; Wu, H.-Y.; Huang, A. C.; Labenski, M. T.; Jones, L. H.; Woo, C. M. Labeling Preferences of Diazirines with Protein Biomolecules. *J. Am. Chem. Soc.* **2021**, *143* (17), 6691–6700. https://doi.org/10.1021/jacs.1c02509.
(178) O'Brien, J. G. K.; Jemas, A.; Asare-Okai, P. N.; am Ende, C. W.; Fox, J. M. Probing the Mechanism of Photoaffinity Labeling by Dialkyldiazirines through Bioorthogonal Capture of Diazoalkanes. *Org. Lett.* **2020**, *22* (24), 9415–9420. https://doi.org/10.1021/acs.orglett.0c02714.
(179) Speers, A. E.; Adam, G. C.; Cravatt, B. F. Activity-Based Protein Profiling in Vivo Using a Copper(I)-Catalyzed Azide-Alkyne [3 + 2] Cycloaddition. *J. Am. Chem. Soc.* **2003**, *125* (16), 4686–4687. https://doi.org/10.1021/ja034490h.
(180) Stork, G.; Zhao, K. A Simple Method of Dethioacetalization. *Tetrahedron Lett.* **1989**, *30* (3), 287–290. https://doi.org/10.1016/S0040-4039(00)95181-5.
(181) Brook, A. G.; Yu, Z. Reactions of Amines with Silenes and Acylsilanes. *Organometallics* **2000**, *19* (10), 1859–1863. https://doi.org/10.1021/om990997i.
(182) Filippakopoulos, P.; Qi, J.; Picaud, S.; Shen, Y.; Smith, W. B.; Fedorov, O.; Morse, E. M.; Keates, T.; Hickman, T. T.; Felletar, I.; Philpott, M.; Munro, S.; McKeown, M. R.; Wang, Y.; Christie, A. L.; West, N.; Cameron, M. J.; Schwartz, B.; Heightman, T. D.; La Thangue, N.; French, C. A.; Wiest, O.; Kung, A. L.; Knapp, S.; Bradner, J. E. Selective Inhibition of BET Bromodomains. *Nature* **2010**, *468* (7327), 1067–1073. https://doi.org/10.1038/nature09504.
(183) Anders, L.; Guenther, M. G.; Qi, J.; Fan, Z. P.; Marineau, J. J.; Rahl, P. B.; Lovén, J.; Sigova, A. A.; Smith, W. B.; Lee, T. I.; Bradner, J. E.; Young, R. A. Genome-

Wide Localization of Small Molecules. *Nat. Biotechnol.* **2014**, *32* (1), 92–96. https://doi.org/10.1038/nbt.2776.
(184) Albers, M. W.; Shin, T. B.; Ichikawa, K.; Keith, C. T.; Lane, W. S.; Schreibert, S. L. A Mammalian Protein Targeted by Gl-Arresting Rapamycin- Receptor Complex. **1994**.
(185) Sabatini, D. M.; Erdjument-Bromage, H.; Lui, M. RAFTI: A Mammalian Protein That Binds to FKBP12 in a Rapamycin-Dependent Fashion and Is Homologous to Yeast TORs.
(186) Flaxman, H. A.; Chang, C.-F.; Wu, H.-Y.; Nakamoto, C. H.; Woo, C. M. A Binding Site Hotspot Map of the FKBP12–Rapamycin–FRB Ternary Complex by Photoaffinity Labeling and Mass Spectrometry-Based Proteomics. *J. Am. Chem. Soc.* **2019**, *141* (30), 11759–11764. https://doi.org/10.1021/jacs.9b03764.
(187) Conway, L. P.; Jadhav, A. M.; Homan, R. A.; Li, W.; Rubiano, J. S.; Hawkins, R.; Lawrence, R. M.; Parker, C. G. Evaluation of Fully-Functionalized Diazirine Tags for Chemical Proteomic Applications. *Chem. Sci.* **2021**, *12* (22), 7839–7847. https://doi.org/10.1039/D1SC01360B.
(188) Wu, S.-Y.; Lee, C.-F.; Lai, H.-T.; Yu, C.-T.; Lee, J.-E.; Zuo, H.; Tsai, S. Y.; Tsai, M.-J.; Ge, K.; Wan, Y.; Chiang, C.-M. Opposing Functions of BRD4 Isoforms in Breast Cancer. *Mol. Cell* **2020**, *78* (6), 1114-1132.e10. https://doi.org/10.1016/j.molcel.2020.04.034.
(189) Käll, L.; Canterbury, J. D.; Weston, J.; Noble, W. S.; MacCoss, M. J. Semi-Supervised Learning for Peptide Identification from Shotgun Proteomics Datasets. *Nat. Methods* **2007**, *4* (11), 923–925. https://doi.org/10.1038/nmeth1113.
(190) Siow, A.; Opiyo, G.; Kavianinia, I.; Li, F. F.; Furkert, D. P.; Harris, P. W. R.; Brimble, M. A. Total Synthesis of the Highly *N*- Methylated Acetylene-Containing Anticancer Peptide Jahanyne. *Org. Lett.* **2018**, *20* (3), 788–791. https://doi.org/10.1021/acs.orglett.7b03925.
(191) Kim, S. A.; Go, A.; Jo, S.-H.; Park, S. J.; Jeon, Y. U.; Kim, J. E.; Lee, H. K.; Park, C. H.; Lee, C.-O.; Park, S. G.; Kim, P.; Park, B. C.; Cho, S. Y.; Kim, S.; Ha, J. D.; Kim, J.-H.; Hwang, J. Y. A Novel Cereblon Modulator for Targeted Protein Degradation. *Eur. J. Med. Chem.* **2019**, *166*, 65–74. https://doi.org/10.1016/j.ejmech.2019.01.023.
(192) Fukuyama, T.; Cheung, M.; Kan, T. *N* -Carboalkoxy-2-Nitrobenzenesulfonamides: A Practical Preparation of *N* -Boc-, *N* -Alloc-, and *N* -Cbz-Protected Primary Amines. *Synlett* **1999**, *1999* (8), 1301–1303. https://doi.org/10.1055/s-1999-2827.
(193) Li, Z.; Hao, P.; Li, L.; Tan, C. Y. J.; Cheng, X.; Chen, G. Y. J.; Sze, S. K.; Shen, H.-M.; Yao, S. Q. Design and Synthesis of Minimalist Terminal Alkyne-Containing Diazirine Photo-Crosslinkers and Their Incorporation into Kinase Inhibitors for Cell- and Tissue-Based Proteome Profiling. *Angew. Chem. Int. Ed.* **2013**, *52* (33), 8551–8556. https://doi.org/10.1002/anie.201300683.

APPENDICES

Chapter 2 Supplementary Information

Supplementary Figures

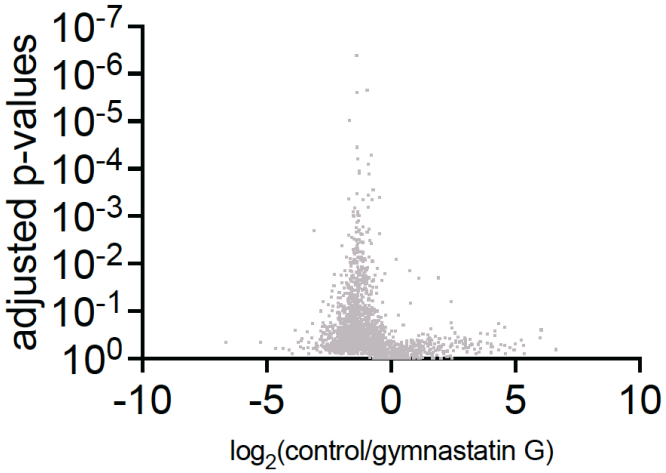

Figure S1. Chemoproteomic profiling of gymnastatin G. MDA-MB-231 breast cancer cells were treated with DMSO vehicle or gymnastatin G (50 μM) for 3 h. Resulting cell lysates were treated with the cysteine-reactive alkyne-functionalized iodoacetamide probe (IA-alkyne) and subsequently taken through the isoTOP-ABPP procedure and LC-MS/MS analysis. Data are from n=3 biological replicates. Tab 1 shows all probe-modified peptides detected and quantified. Tab 2 and Tab 3 both show probe-modified peptides that were evident in at least 2 out of 3 biological replicates. Tab 2 highlighted proteins/sites show ratio >2 with adjusted p-value <0.05. Tab 3 highlighted proteins/sites show ratio >4 with adjusted p-value <0.05.

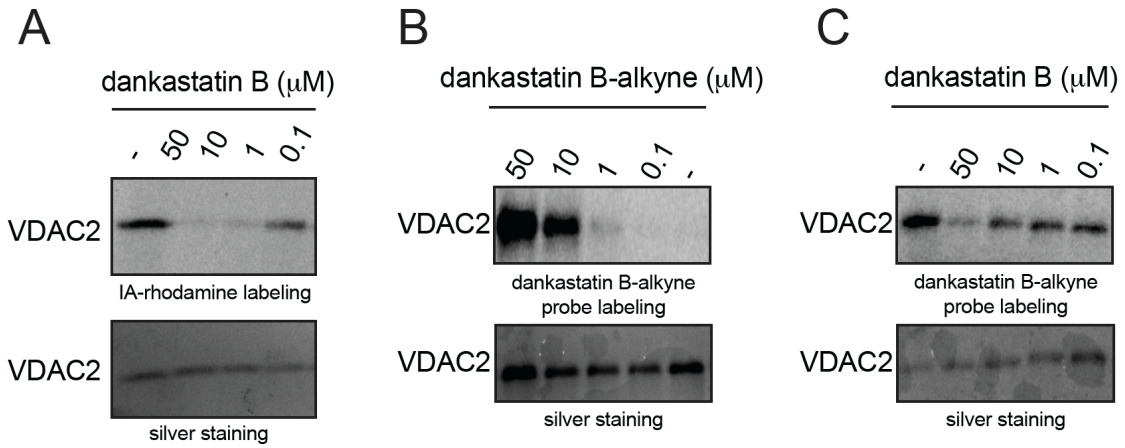

Figure S2. Dankastatin B interactions with VDAC2. (A) Gel-based ABPP analysis of dankastatin B against pure VDAC2 protein. Pure VDAC2 protein was pre-incubated with DMSO or dankastatin B for 30 min prior to labeling of protein with a rhodamine-functionalized iodoacetamide (IA-rhodamine) probe (1 μM) for 1 h. Proteins were resolved on SDS/PAGE and subsequently visualized by in-gel fluorescence and protein loading

was assessed by silver staining. (B) Dankastatin B-alkyne probe labeling of VDAC2. Pure VDAC2 protein was incubated with dankastatin B-alkyne for 30 min. An azide-functionalized rhodamine was subsequently appended onto probe-labeled proteins by copper-catalyzed azide-alkyne cycloaddition, proteins were resolved by SDS/PAGE, and visualized by in-gel fluorescence. Protein loading was assessed by silver staining. **(C)** Dankastatin B-alkyne probe labeling of VDAC2 and competition of probe labeling by dankastatin B. Pure VDAC2 protein was pre-incubated with DMSO or dankastatin B for 30 min prior to incubation with dankastatin B-alkyne for 30 min. An azide-functionalized rhodamine was subsequently appended onto probe-labeled proteins by copper-catalyzed azide-alkyne cycloaddition, proteins were resolved by SDS/PAGE, and visualized by in-gel fluorescence. Protein loading was assessed by silver staining. Shown in (B, C) are representative gels from n=3 biological replicates/group.

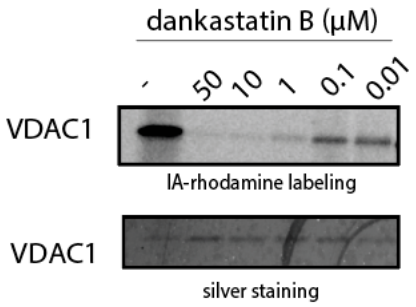

Figure S3. Dankastatin B interactions with VDAC1. A) Gel-based ABPP analysis of dankastatin B against pure VDAC1 protein. Pure VDAC1 protein was pre-incubated with DMSO or dankastatin B for 30 min prior to labeling of protein with a rhodamine-functionalized iodoacetamide (IA-rhodamine) probe (1 μM) for 1 h. Proteins were resolved on SDS/PAGE and subsequently visualized by in-gel fluorescence and protein loading was assessed by silver staining.

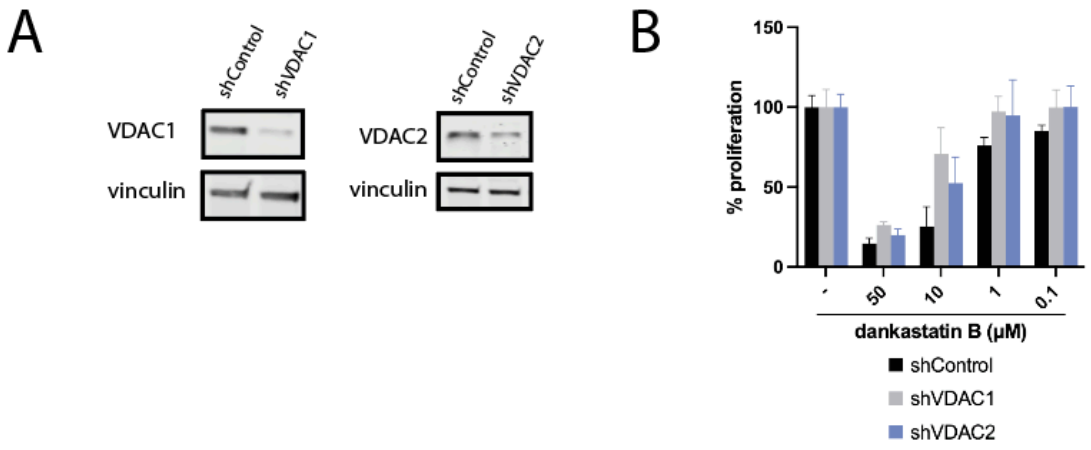

Figure S4. Role of VDAC1 and VDAC2 on proliferation effects. (**A**) Knockdown of VDAC1 and VDAC2. VDAC1 and VDAC2 were stably knocked down by short hairpin RNA (shRNA). Knockdown of VDAC1 and VDAC2 were validated by Western blotting compared to a loading control vinculin. (**B**) MDA-MB-231 cell proliferation in shControl versus shVDAC1 and shVDAC2 cells. MDA-MB-231 shControl, shVDAC1, and shVDAC2 cells were treated with DMSO vehicle or dankastatin B for 8 h and cell proliferation was assessed by Hoechst stain.

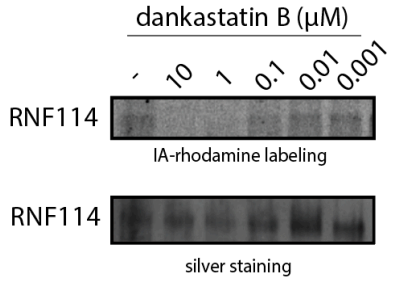

Figure S5. Dankastatin B interactions with RNF114. A) Gel-based ABPP analysis of dankastatin B against pure RNF114 protein. Pure RNF114 protein was pre-incubated with DMSO or dankastatin B for 30 min prior to labeling of protein with a rhodamine-functionalized iodoacetamide (IA-rhodamine) probe (1 μM) for 1 h. Proteins were resolved on SDS/PAGE and subsequently visualized by in-gel fluorescence and protein loading was assessed by silver staining.

Synthetic Methods and Characterization

General Procedures I

Unless otherwise noted, all reactions were performed in flame-dried glassware under positive pressure of nitrogen or argon. Air- and moisture-sensitive liquids were transferred via syringe. Dry tetrahydrofuran, dichloromethane, *N*,*N*-Dimethylformamide, toluene, acetonitrile, triethylamine and diethyl ether were obtained by passing these previously degassed solvents through activated alumina columns. Aranorosin was purchased from Cayman Chemicals. All reagents were used as received from commercial sources, unless stated otherwise. Reactions were monitored by thin layer chromatography (TLC) on TLC silica gel 60 F_{254} glass plates (EMD Millipore) and visualized by UV irradiation and staining

with *p*-anisaldehyde, phosphomolybdic acid, or Ninhydrin. Volatile solvents were removed under reduced pressure using a rotary evaporator. Flash column chromatography was performed using Silicycle F60 silica gel (60Å, 230-400 mesh, 40-63 μm). Proton nuclear magnetic resonance (^{1}H NMR) and carbon nuclear magnetic resonance (^{13}C NMR) spectra were recorded on Bruker AV-600 and AV-700 spectrometers operating at 600 and 700 MHz for ^{1}H NMR, and 151 and 176 MHz for ^{13}C NMR. Chemical shifts are reported in parts per million (ppm) with respect to the residual solvent signal $CDCl_3$ (^{1}H NMR: δ 7.26; ^{13}C NMR: δ 77.16), $(CD_3)_2CO$ (^{1}H NMR: δ 2.05; ^{13}C NMR: δ 29.84). Peak multiplicities are reported as follows: *s* = singlet, *d* = doublet, *t* = triplet, *dd* = doublet of doublets, *tt* = triplet of triplets, *m* = multiplet, *br* = broad signal. IR spectra were recorded on a Bruker Vertex 80 FTIR spectrometer. High-resolution mass spectra (HRMS) were obtained by the QB3/chemistry mass spectrometry facility at the University of California, Berkeley using a Thermo LTQ-FT mass spectrometer with electrospray ionization (ESI) technique. X-ray crystallographic analysis was performed by the X-ray crystallography facility at the University of California, Berkeley on a Bruker APEX-II diffractometer with Mo-Kα radiation (λ = 0.71073 Å) or a MicroStar-H X8 APEX-II diffractometer with Cu-Kα radiation (λ = 1.54178 Å). Optical rotations were obtained using Perkin-Elmer 241 Polarimeter.

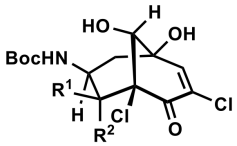

19: R^1 = OH, R^2 = H
20: R^1 = H, R^2 = OH

Triol **20** and **19**: To a 30 mL reaction tube was added compound **18** (56.5 mg, 0.107 mmol, 1.0 equiv) and MeCN (2.4 mL). The resulting solution was cooled to 0 °C and aqueous KOH (6.0 mg in 0.6 mL H_2O, 0.107 mmol, 1.0 equiv) was added. The reaction mixture was stirred at 0 °C for 30 min. The reaction was then quenched with saturated *aq.* NH_4Cl, extracted with DCM (2×2 mL) and EtOAc (2×2 mL), dried over Na_2SO_4 and concentrated *in vacuo*. The residue was purified by column chromatography (DCM/acetone = 3:1) to afford compound **19** (15.2 mg, 26% yield) and compound **20** (17.9 mg, 30% yield), both as a white solid. **19**: ^{1}H NMR (600 MHz, Acetone) δ 7.37 (s, 1H), 6.02 (d, *J* = 8.6 Hz, 1H), 5.93 (d, *J* = 7.2 Hz, 1H), 5.48 (d, *J* = 8.1 Hz, 1H), 5.15 (s, 1H), 4.07 (d, *J* = 7.4 Hz, 1H), 3.74 (d, *J* = 8.3 Hz, 1H), 3.49 (td, *J* = 8.3, 4.2 Hz, 1H), 2.30 (t, *J* = 12.7 Hz, 1H), 1.83 (dd, *J* = 13.1, 4.9 Hz, 1H), 1.37 (s, 9H). ^{13}C NMR (151 MHz, Acetone) δ 186.1, 155.7, 153.0, 130.7, 79.8, 79.4, 77.8, 75.0, 74.4, 49.3, 29.5, 28.5. IR (thin film) ν_{max} (cm^{-1}) 3398, 2955, 2923, 2851, 1709, 1518, 1460, 1369, 1293, 1249, 1164, 1084. HRMS (ESI) *calcd.* for $[C_{14}H_{19}O_6NCl_2Na]^+$ ($[M+Na]^+$): *m/z* 390.0482, found: 390.0482. **20**: ^{1}H NMR (600 MHz, Acetone) δ 7.29 (s, 1H), 6.16 (brs, 1H), 5.64 (d, *J* = 4.9 Hz, 1H), 4.98 (s, 1H), 4.50 (d, *J* = 5.0 Hz, 1H), 4.17 (dd, *J* = 10.5, 5.1 Hz, 1H), 4.04 (d, *J* = 4.6 Hz, 1H), 3.44 (m, 1H), 2.37 (t, *J* = 12.4 Hz, 1H), 1.98 (dd, *J* = 12.7, 5.4 Hz, 1H), 1.38 (s, 9H). ^{13}C NMR (151 MHz, Acetone) δ 184.0, 156.6, 151.5, 131.8, 83.5, 79.2, 79.1, 74.9, 74.5, 51.6, 35.2, 28.6. IR (thin film) ν_{max} (cm^{-1}) 3365, 2957, 2921, 2850, 1701, 1685, 1655, 1522, 1457, 1368, 1297, 1249, 1163, 1101, 946. HRMS (ESI) *calcd.* for $[C_{14}H_{19}O_6NCl_2Na]^+$ ($[M+Na]^+$): *m/z* 390.0482, found: 390.0482.

General procedure for the screening of *oxa*-Michael addition/aldol reaction conditions (Fig 2.3C):

To a 10 mL reaction tube was added compound **18**, benzyl alcohol or allyl alcohol, and THF. The resulting solution was cooled to –78 °C and base was added dropwise. The

reaction was allowed to stir at –78 °C or warm up slowly to the specified temperature over 30 – 40 min. Upon reaching the designated temperature, the reaction was quenched by either adding saturated *aq.* NH_4Cl to the reaction mixture, or adding the reaction to a stirring saturated *aq.* NH_4Cl using pipette. The layers were then separated, and the aqueous phase was extracted with Et_2O (2×1 mL) and DCM (2×1 mL). The combined organic layer was dried over Na_2SO_4 and concentrated *in vacuo*. The yields were determined by ^1H NMR using 1,3,5-trimethoxybenzene as internal standard.

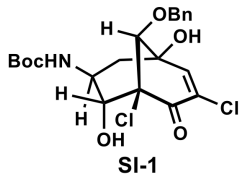

SI-1

Bicycle **SI-1**: ^1H NMR (700 MHz, Acetone) δ 7.36 – 7.33 (m, 2H), 7.32 – 7.28 (m, 2H), 7.28 – 7.24 (m, 1H), 7.06 (d, *J* = 2.5 Hz, 1H), 6.21 (s, 1H), 5.42 (d, *J* = 1.2 Hz, 1H), 5.05 (d, *J* = 4.9 Hz, 1H), 4.95 (d, *J* = 10.9 Hz, 1H), 4.89 (d, *J* = 10.9 Hz, 1H), 4.12 (dd, *J* = 10.3, 5.0 Hz, 1H), 4.04 (d, *J* = 2.5 Hz, 1H), 3.58 (dddd, *J* = 12.3, 10.3, 8.2, 5.5 Hz, 1H), 2.23 (dd, *J* = 13.2, 5.5 Hz, 1H), 2.10 (t, *J* = 13.3 Hz, 1H), 1.39 (s, 9H). ^{13}C NMR (151 MHz, Acetone) δ 182.7, 156.6, 148.8, 139.2, 131.4, 128.9, 128.7, 128.4, 91.1, 83.9, 79.3, 78.7, 76.9, 75.1, 51.8, 38.5, 28.6. IR (thin film) ν_{max} (cm^{-1}) 3383, 2922, 2852, 1709, 1516, 1454, 1368, 1311, 1294, 1253, 1164, 1098, 1060. 967, 748, 700. HRMS (ESI) *calcd.* for $[C_{21}H_{25}O_6NCl_2Na]^+$ ([M+Na]$^+$): *m/z* 480.0951, found: 480.0957.

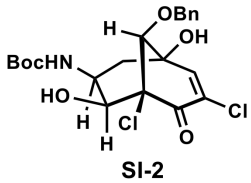

SI-2

Bicycle **SI-2**: ^1H NMR (600 MHz, Acetone) δ 7.37 – 7.33 (m, 2H), 7.33 – 7.28 (m, 2H), 7.28 – 7.23 (m, 1H), 7.11 (d, *J* = 2.4 Hz, 1H), 5.99 (d, *J* = 8.6 Hz, 1H), 5.65 (d, *J* = 5.0 Hz, 1H), 5.37 (s, 1H), 4.92 (d, *J* = 10.9 Hz, 1H), 4.83 (d, *J* = 10.9 Hz, 1H), 4.29 (d, *J* = 2.5 Hz, 1H), 3.91 (ddd, *J* = 4.7, 3.0, 1.3 Hz, 1H), 3.62 (m, 1H), 2.26 (t, *J* = 12.6 Hz, 1H), 1.97 (dd, *J* = 12.6, 3.9 Hz, 1H), 1.37 (s, 9H). ^{13}C NMR (151 MHz, Acetone) δ 185.5, 155.7, 150.1, 139.3, 130.5, 128.9, 128.6, 128.4, 87.8, 82.7, 79.4, 77.0, 75.6, 74.3, 48.8, 35.5, 28.5. IR (thin film) ν_{max} (cm^{-1}) 3394, 2955, 2923, 2852, 1709, 1509, 1456, 1392, 1368, 1310, 1295, 1251, 1164, 1095, 968, 738, 701. HRMS (ESI) *calcd.* for $[C_{21}H_{25}O_6NCl_2Na]^+$ ([M+Na]$^+$): *m/z* 480.0951, found: 480.0955.

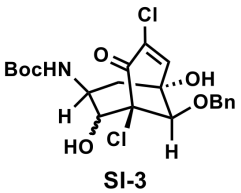

SI-3

Bicycle **SI-3**: ^1H NMR (600 MHz, Acetone) major diastereomer δ 7.35 (td, *J* = 8.3, 1.4 Hz, 2H), 7.30 (td, *J* = 7.4, 1.5 Hz, 2H), 7.28 – 7.23 (m, 1H), 7.10 (d, *J* = 2.4 Hz, 1H), 5.53 (d, *J* = 5.0 Hz, 1H), 5.28 (s, 1H), 4.92 (d, *J* = 10.9 Hz, 1H), 4.85 (d, *J* = 10.9 Hz, 1H), 4.39 (d, *J* = 2.4 Hz, 1H), 4.36 – 4.31 (m, 1H), 3.96 (dt, *J* = 6.1, 2.0 Hz, 1H), 2.53 (dd, *J* = 14.6, 6.5 Hz, 1H), 2.35 (dt, *J* = 14.6, 1.5 Hz, 1H), 1.34 (s, 9H); Minor diastereomer δ 7.35 (td, *J* = 8.3, 1.4 Hz, 2H), 7.30 (td, *J* = 7.4, 1.5 Hz, 2H), 7.28 – 7.23 (m, 1H), 6.99 (d, *J* = 2.5 Hz, 1H), 5.45 (d, *J* = 4.7 Hz, 1H), 5.28 (s, 1H), 4.95 (d, *J* = 10.9 Hz, 1H), 4.89 (d, *J* = 10.9 Hz, 1H), 4.52 (dd, *J* = 6.0, 4.7 Hz, 1H), 4.21 (tdd, *J* = 5.9, 4.0, 2.6 Hz, 1H), 4.14 (d, *J* = 2.5 Hz, 1H), 2.86 (d, *J* = 14.4 Hz, 1H), 2.22 (dd, *J* = 14.7, 5.6 Hz, 1H), 1.38 (s, 9H). ^{13}C NMR (151 MHz, Acetone) (all peaks listed) δ 185.1, 183.4, 156.5, 156.0, 150.5, 149.4, 139.4, 139.2, 131.6, 131.0, 128.94, 128.93, 128.66, 128.60, 128.40, 128.33, 90.8, 88.0, 82.8, 82.6, 79.7, 79.6, 76.95, 76.94, 76.81, 76.1, 75.7, 74.8, 53.0, 50.5, 37.0, 36.2, 28.52, 28.48. IR (thin film) ν_{max} (cm^{-1}) 3374,

2957, 2922, 2851, 1707, 1495, 1455, 1368, 1258, 1163, 1091, 1026, 968, 732, 700. HRMS (ESI) *calcd.* for $[C21H25O6NCl_2Na]^+$ ($[M+Na]^+$): *m/z* 480.0951, found: 480.0954.

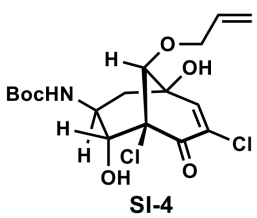

SI-4

Bicycle **SI-4**: ^{1}H NMR (600 MHz, Acetone) δ 7.03 (d, *J* = 2.5 Hz, 1H), 6.16 (s, 1H), 5.93 (dddd, *J* = 16.7, 9.7, 6.2, 5.3 Hz, 1H), 5.28 (s, 1H), 5.20 (d, *J* = 17.4 Hz, 1H), 5.08 (d, *J* = 10.4 Hz, 1H), 4.98 (d, *J* = 4.9 Hz, 1H), 4.40 (dd, *J* = 12.4, 5.9 Hz, 1H), 4.33 (dd, *J* = 12.0, 5.4 Hz, 1H), 4.07 (dd, *J* = 10.4, 4.7 Hz, 1H), 3.87 (d, *J* = 2.5 Hz, 1H), 3.55 (dddd, *J* = 12.9, 10.3, 8.1, 5.5 Hz, 1H), 2.20 (dd, *J* = 13.2, 5.5 Hz, 1H), 2.02 (t, *J* = 12.8 Hz, 1H), 1.38 (s, 9H). ^{13}C NMR (151 MHz, Acetone) δ 182.6, 156.5, 148.9, 135.8, 131.3, 117.2, 90.7, 83.7, 79.3, 78.7, 76.0, 74.8, 51.8, 38.3, 28.6. IR (thin film) ν_{max} (cm^{-1}) 3387, 2956, 2925, 2854, 1709, 1520, 1456, 1393, 1386, 1311, 1294, 1252, 1164, 1095, 1061, 777, 754. HRMS (ESI) *calcd.* for $[C_{17}H_{23}O_6NCl_2Na]^+$ ($[M+Na]^+$): *m/z* 430.0795, found: 430.080. Other minor diastereomers were assigned based on the similarity of the ^{1}H-NMR compared with Bn analogues.

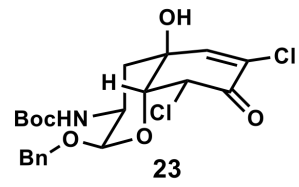

23

Acetal **23**: ^{1}H NMR (600 MHz, Acetone) δ 7.41 (d, *J* = 7.0 Hz, 2H), 7.37 (t, *J* = 7.6 Hz, 2H), 7.31 (t, *J* = 7.2 Hz, 1H), 7.10 (d, *J* = 2.3 Hz, 1H), 5.99 (d, *J* = 8.5 Hz, 1H), 5.57 (d, *J* = 2.4 Hz, 1H), 5.42 (s, 1H), 4.91 (d, *J* = 3.4 Hz, 1H), 4.83 (d, *J* = 11.9 Hz, 1H), 4.59 (d, *J* = 11.9 Hz, 1H), 4.35 (t, *J* = 2.4 Hz, 1H), 3.66 (tt, *J* = 8.7, 4.1 Hz, 1H), 2.25 – 2.17 (m, 2H), 1.38 (s, 9H). ^{13}C NMR (151 MHz, Acetone) δ 183.7, 155.9, 144.9, 138.4, 132.9, 129.3, 128.8, 128.6, 96.1, 79.3, 76.9, 70.3, 69.6, 62.3, 48.7, 38.4, 28.6. IR (thin film) ν_{max} (cm^{-1}) 3373, 2957, 2921, 2851, 1691, 1506, 1457, 1368, 1259, 1163, 1095, 1022, 798, 738, 701. HRMS (ESI) *calcd.* for $[C_{21}H_{25}O_6NCl_2Na]^+$ ($[M+Na]^+$): *m/z* 480.0951, found: 480.0954.

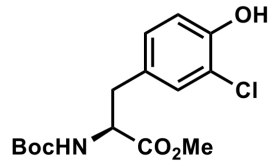

25

3'-Chloro-*N*-Boc-L-tyrosine methyl ester (**25**): To a 25 mL round-bottom flask was added *L*-Boc-Tyr-OMe (**24**) (500 mg, 1.69 mmol, 1.0 equiv) and acetic acid (13 mL). A stream of argon was gently bubbled through the solution and to the solution was added dropwise SO_2Cl_2 (0.21 mL, 2.54 mmol, 1.5 equiv). After stirring for 30 minutes, another portion of SO_2Cl_2 (0.21 mL, 2.54 mmol, 1.5 equiv) was added and the reaction was continued for another 30 minutes. The reaction was then poured into a mixture of Et_2O (50 mL) and saturated *aq.* $NaHCO_3$ (50 mL) with vigorous stirring. The layers were separated, and the aqueous phase was extracted with Et_2O (3×30 mL). The combined organic layer was concentrated *in vacuo*, redissolved in DCM (50 mL) and washed with saturated *aq.* $NaHCO_3$ (50 mL). The organic layer was then dried over Na_2SO_4 and concentrated *in vacuo*. The residue was purified by column chromatography (hexanes/EtOAc = 3:1) to afford ester **25** (342 mg, 61% yield) as a yellow oil. $[\alpha]_D^{20}$ +49.9 (*c* 1.0, $CHCl_3$). ^{1}H NMR (600 MHz, $CDCl_3$) δ 7.08 (s, 1H), 6.92 (m, 2H), 5.64 (s, 1H), 5.01 (d, *J* = 8.2 Hz, 1H), 4.59 – 4.47 (m, 1H), 3.72 (s, 3H), 3.04 (dd, *J* = 13.8, 6.0 Hz, 1H), 2.95 (dd, *J* = 14.1, 6.3 Hz, 1H), 1.42 (s, 9H). ^{13}C NMR (151 MHz, $CDCl_3$) δ 172.3, 155.2, 150.6, 130.6, 129.8, 129.4, 119.9, 116.4, 80.3, 54.6, 52.4, 37.5, 28.4. IR (thin film) ν_{max} (cm^{-1}) 3365, 2978, 2955, 2928, 1739, 1691, 1505,

1439, 1367, 1293, 1254, 1221, 1165, 1057, 1020. HRMS (ESI) *calcd.* for $[C_{15}H_{20}O_5NClNa]^+$ ($[M+Na]^+$): *m/z* 352.0922, found: 352.0923.

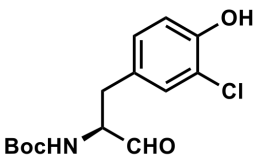

26

Aldehyde **26**: To a 100 mL round-bottom flask was added ester **25** (685 mg, 2.08 mmol, 1.0 equiv) and DCM (30 mL). The reaction was cooled to –78 °C and DIBAL (1.0 M in hexanes, 6.2 mL, 6.2 mmol. 3.0 equiv) was added very slowly. The reaction was allowed to stir at –78 °C for 1 h, after which it was quenched by the addition of MeOH (1 mL) at –78 °C followed by saturated *aq.* potassium sodium tartrate (20 mL). The reaction mixture was warmed to room temperature and stirred for another 2 h. The layers were then separated, and the aqueous phase was extracted with DCM (3×30 mL). The combined organic layer was dried over Na_2SO_4 and concentrated *in vacuo*. The resulting yellow oil was further dried under high vacuum for 3 h to provide a foam-like solid. Hexanes (5 mL) was added to the solid, stirred for 10 min, and carefully removed with pipette. This process was repeated for two more times. The resulting solid was dried in vacuo to afford crude aldehyde **26** (520 mg, 83%) which was used for next step without further purification. Pure aldehyde **26** can be obtained by column chromatography (hexanes/EtOAc = 2:1) but partial racemization may occur during the process. $[\alpha]_D^{20}$ +11.2 (*c* 0.42, $CHCl_3$). ^{1}H NMR (600 MHz, $CDCl_3$) δ 9.63 (s, 1H), 7.14 (d, *J* = 1.9 Hz, 1H), 6.98 (dd, *J* = 8.3, 2.0 Hz, 1H), 6.95 (d, *J* = 8.3 Hz, 1H), 5.48 (s, 1H), 5.04 (brs, 1H), 4.37 (m, 1H), 3.08 (dd, *J* = 14.3, 6.5 Hz, 1H), 3.02 (dd, *J* = 14.4, 6.5 Hz, 1H), 1.44 (s, 9H). ^{13}C NMR (151 MHz, $CDCl_3$) δ 199.1, 155.5, 150.6, 129.9, 129.5, 129.1, 120.1, 116.6, 80.6, 60.9, 34.4, 28.4. IR (thin film) ν_{max} (cm^{-1}) 3361, 2954, 2922, 2851, 1687, 1504, 1457, 1369, 1292, 1255, 1165, 822. HRMS (ESI) *calcd.* for $[C_{14}H_{17}O_4NCl]^-$ ($[M–H]^-$): *m/z* 298.0852, found: 298.0857.

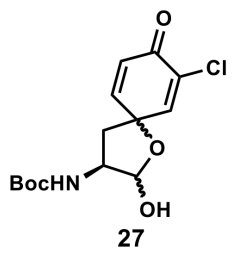

27

Lactol **27**: A 100 mL round-bottom flask was charged with aldehyde **26** (520 mg, 1.73 mmol, 1.0 equiv), TEMPO (136 mg, 0.867 mmol, 0.5 equiv) and MeCN/H_2O (5:1, 30 mL). The solution was cooled to 0 °C and PIFA (709 mg, 1.65 mmol, 0.95 equiv) was added in one portion. After stirring at 0 °C for 10 min, H_2O (10 mL) and DCM (30 mL) was added to the reaction. The layers were separated, and the aqueous phase was extracted with DCM (3×30 mL). The combined organic layer was dried over Na_2SO_4 and concentrated *in vacuo*. The residue was purified by column chromatography (hexanes/EtOAc = 2:1) to afford lactol **27** (182 mg, 33%, mixture of 4 diastereomers) as a pale-yellow foam. $[\alpha]_D^{20}$ –8.3 (*c* 0.24, $CHCl_3$). One of the two diastereomers at C-4: ^{1}H NMR (700 MHz, $CDCl_3$) δ 7.17 (d, *J* = 2.8 Hz, 0.36H), 7.08 (d, *J* = 2.8 Hz, 0.64H), 6.82 (dd, *J* = 9.8, 2.8 Hz, 0.36H), 6.79 (dd, *J* = 9.8, 2.8 Hz, 0.64H), 6.25 (d, *J* = 9.8 Hz, 0.36H), 6.22 (d, *J* = 9.8 Hz, 0.64H), 5.57 (brs, 0.36H), 5.50 (brs, 0.64H), 5.02 (brs, 0.64 H), 4.65 (brs, 0.36H), 4.45 (brs, 0.64H), 4.29 (brs, 0.36H), 3.22 (d, *J* = 16.1 Hz, 0.64H), 3.10 (d, *J* = 19.6 Hz, 0.36H), 2.72 (dd, *J* = 14.7, 7.0 Hz, 0.36H), 2.47 (m, 0.64H), 2.17 (dd, *J* = 14.7, 9.8 Hz, 0.64H), 2.11 (t, *J* = 14.7 Hz, 0.36H), 1.46 (s, 9H). The other diastereomer at C-4: ^{1}H NMR (700 MHz, $CDCl_3$) δ 7.00 (m, 0.36H), 6.97 (d, *J* = 2.8 Hz, 0.36H), 6.96 (d, *J* = 2.8 Hz, 0.64H), 6.90 (dd, *J* = 9.8, 2.8 Hz, 0.64H), 6.24 (m, 1H), 5.57 (brs, 0.36H), 5.50 (brs, 0.64H), 5.02 (brs, 0.64 H), 4.65 (brs, 0.36H), 4.45 (brs, 0.64H), 4.29 (brs, 0.36H), 2.69 (dd, *J* = 14.7, 7.0 Hz, 0.36H), 2.47

(m, 0.64H), 2.17 (dd, *J* = 14.7, 9.8 Hz, 0.64H), 2.11 (t, *J* = 14.7 Hz, 0.36H), 1.46 (s, 9H). ^{13}C NMR (151 MHz, $CDCl_3$) (peaks for all the diastereomers are listed) δ 178.40, 178.38, 155.36, 155.25, 152.0, 151.3, 149.4, 148.6, 147.6, 146.9, 145.1, 144.3, 132.0, 131.8, 131.4, 126.6, 126.4, 126.1, 103.53, 103.48, 96.42, 96.36, 80.54, 80.50, 78.93, 78.86, 53.8, 38.5, 28.5. IR (thin film) ν_{max} (cm^{-1}) 3374, 2977, 2926, 2853, 1684, 1507, 1455, 1393, 1368, 1291, 1252, 1165, 1051, 1019, 863, 822, 777, 737. HRMS (ESI) *calcd.* for $[C_{14}H_{18}O_5NClNa]^+$ ($[M+Na]^+$): *m/z* 338.0766, found: 338.0768.

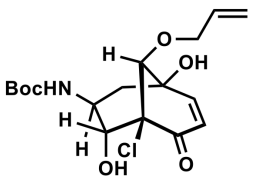

28a

Diol **28**: To a 50 mL reaction tube was added compound **27** (50.0 mg, 0.158 mmol, 1.0 equiv), THF (10 mL) and allyl alcohol (42 µL, 0.62 mmol, 4.0 equiv). The resulting solution was cooled to –78°C and KHMDS (0.5M in toluene, 1.6 mL, 0.79 mmol, 5.0 equiv) was added dropwise. The reaction was allowed to warm up slowly to –15°C over 40 min. The reaction was quenched by adding the reaction mixture to a stirring saturated *aq.* NH_4Cl using pipette. The layers were separated, and the aqueous phase was extracted with DCM (3×10 mL). The combined organic layer was dried over Na_2SO_4 and concentrated *in vacuo*. The residue was purified by column chromatography (45% EtOAc/hexanes) to afford diol **28a** along with a small amount of other diastereomers (**28b** and **28c**) as a pale-yellow foam (20.5 mg, 35%). $[\alpha]_D^{20}$ +7.2 (*c* 0.25, acetone). ^{1}H NMR (600 MHz, Acetone) δ 6.76 (dd, *J* = 10.2, 2.6 Hz, 1H), 6.14 (d, *J* = 10.2 Hz, 1H), 6.10 (brs, 1H), 5.92 (ddt, *J* = 17.3, 10.4, 5.7 Hz, 1H), 5.19 (dq, *J* = 17.3, 1.7 Hz, 1H), 5.07 (dq, *J* = 10.5, 1.5 Hz, 1H), 4.97 (s, 1H), 4.64 (d, *J* = 4.7 Hz, 1H), 4.38 (ddt, *J* = 12.5, 5.7, 1.5 Hz, 1H), 4.32 (ddt, *J* = 12.6, 5.4, 1.5 Hz, 1H), 3.99 (dd, *J* = 10.3, 4.8 Hz, 1H), 3.79 (d, *J* = 2.6 Hz, 1H), 3.64 – 3.53 (m, 1H), 2.09 (dd, *J* = 13.1, 5.5 Hz, 1H), 1.96 (t, *J* = 13.2 Hz, 1H), 1.38 (s, 9H). ^{13}C NMR (151 MHz, Acetone) δ 188.8, 156.6, 152.5, 136.1, 129.3, 116.8, 91.2, 83.9, 79.1, 78.8, 75.8, 74.6, 51.9, 38.3, 28.6. IR (thin film) ν_{max} (cm^{-1}) 3380, 2957, 2925, 2854, 1688, 1524, 1456, 1368, 1297, 1251, 1164, 1086, 1060, 926, 806, 761. HRMS (ESI) *calcd.* for $[C_{17}H_{24}O_6NClNa]^+$ ($[M+Na]^+$): *m/z* 396.1184, found: 396.1183.

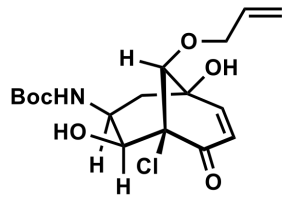

28b

28b: ^{1}H NMR (600 MHz, Acetone) δ 6.83 (dd, *J* = 10.1, 2.6 Hz, 1H), 6.16 (d, *J* = 10.1 Hz, 1H), 5.92 (ddt, *J* = 17.3, 10.4, 5.6 Hz, 1H), 5.87 (d, *J* = 8.6 Hz, 1H), 5.38 (d, *J* = 4.7 Hz, 1H), 5.19 (dt, *J* = 17.3, 1.8 Hz, 1H), 5.06 (dq, *J* = 10.4, 1.5 Hz, 1H), 4.97 (s, 1H), 4.34 (ddt, *J* = 12.5, 5.7, 1.5 Hz, 1H), 4.26 (ddt, *J* = 12.5, 5.6, 1.6 Hz, 1H), 4.11 (d, *J* = 2.6 Hz, 1H), 3.83 – 3.77 (m, 1H), 3.66 (td, *J* = 8.0, 3.9 Hz, 1H), 2.15 (t, *J* = 12.6 Hz, 1H), 1.82 (dd, *J* = 12.8, 4.9 Hz, 1H), 1.37 (s, 9H). ^{13}C NMR (151 MHz, Acetone) δ 191.6, 155.7, 153.7, 136.3, 128.5, 116.6, 87.8, 82.7, 79.2, 75.8, 75.0, 74.4, 48.8, 35.3, 28.5. IR (thin film) ν_{max} (cm^{-1}) 3390, 2956, 2922, 2851, 1692, 1498, 1458, 1369, 1298, 1258, 1163, 1085, 1043, 804, 700. HRMS (ESI) *calcd.* for $[C_{17}H_{24}O_6NClNa]^+$ ($[M+Na]^+$): *m/z* 396.1184, found: 396.1187.

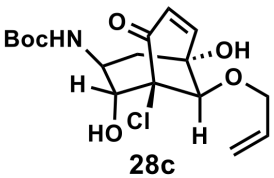

28c

28c: ^{1}H NMR (600 MHz, Acetone) δ 6.96 (dd, *J* = 10.1, 2.5 Hz, 1H), 6.08 (d, *J* = 10.1 Hz, 1H), 5.93 (ddt, *J* = 17.3, 10.5, 5.6 Hz, 1H), 5.35 (br s, 1H), 5.25 (d, *J* = 4.7 Hz, 1H), 5.19 (dq, *J* = 17.3, 1.8 Hz, 1H), 5.06 (dp, *J* = 10.4, 1.6 Hz, 1H), 4.90 (s, 1H), 4.34 (ddt, *J* = 12.5, 5.7, 1.5 Hz, 1H), 4.28 (ddt, *J* = 12.5, 5.5, 1.6 Hz, 1H), 4.20 (d, *J* = 2.5 Hz, 1H), 4.08 (dt, *J* = 4.2, 1.8 Hz, 1H), 4.02 – 3.97 (m, 1H), 2.46 (dd, *J* = 14.6, 6.9 Hz, 1H), 2.15 (dt, *J* = 14.6, 1.5 Hz, 1H), 1.33 (s, 9H). ^{13}C NMR (151 MHz, Acetone) δ 191.5, 155.6, 155.1, 136.3, 129.7, 116.5, 87.9, 82.7, 79.5, 76.4, 75.8, 75.4, 52.7, 36.5, 28.5. IR (thin film) ν_{max} (cm^{-1}) 3398, 2955, 2922, 2851, 1692, 1494, 1455, 1369, 1281, 1252, 1165, 1093, 1045, 1019, 794, 699. HRMS (ESI) *calcd.* for $[C_{17}H_{24}O_6NClNa]^+$ ($[M+Na]^+$): *m/z* 396.1184, found: 396.1188.

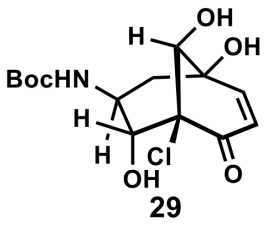

29

Triol **29**: To a 30 mL reaction tube was added diol **28** (64.4 mg, 0.172 mmol, 1.0 equiv), $Pd(PPh_3)_4$ (39.8 mg, 0.0345 mmol, 0.2 equiv) and DCM (5 mL). The reaction was cooled to 0 °C and AcOH (30 µL, 0.52 mmol, 3.0 equiv) was added, followed by dropwise addition of Bu_3SnH (55.6 µL, 0.21 mmol, 1.2 equiv). After stirring at 0 °C for 1 h, the reaction was quenched with saturated *aq.* KF (3 mL) and stirred vigorously for 2 h. The layers were then separated, and the aqueous phase was extracted with DCM (2×5 mL) and EtOAc (2×5 mL). The combined organic layer was dried over Na_2SO_4 and concentrated *in vacuo*. The residue was purified by column chromatography (5% MeOH/DCM) to afford triol **29** (30.1 mg, 52%) as a pale-yellow oil. $[\alpha]_D^{20}$ –3.3 (*c* 0.090, acetone). ^{1}H NMR (600 MHz, Acetone) δ 6.73 (dd, *J* = 10.2, 2.6 Hz, 1H), 6.15 (d, *J* = 10.2 Hz, 1H), 6.10 (brs, 1H), 5.10 (d, *J* = 4.8 Hz, 1H), 4.81 (s, 1H), 4.58 (d, *J* = 4.7 Hz, 1H), 3.99 – 3.94 (m, 2H), 3.63 (m, 1H), 2.11 (dd, *J* = 13.2, 5.4 Hz, 1H), 1.90 (t, *J* = 12.7 Hz, 1H), 1.38 (s, 9H). ^{13}C NMR (151 MHz, Acetone) δ 189.2, 156.6, 152.2, 129.4, 84.5, 83.2, 79.1, 78.7, 73.8, 52.0, 38.0, 28.6. IR (thin film) ν_{max} (cm^{-1}) 3368, 2956, 2922, 2852, 1688, 1532,1460, 1370, 1298, 1251, 1165, 1085, 1046, 803. HRMS (ESI) *calcd.* for $[C_{14}H_{20}O_6NClNa]^+$ ($[M+Na]^+$): *m/z* 356.0871, found: 356.0872.

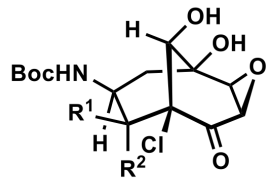

30a: R^1 = OH, R^2 = H
30b: R^1 = H, R^2 = OH

Epoxide **30**: To a 20 mL reaction tube was added triol **29** (40.2 mg, 0.121 mmol, 1.0 equiv) and THF (2 mL). The solution was cooled to 0 °C and Triton B (40%w/w, 14 µL, 0.036 mmol, 0.3 equiv) was added, followed by H_2O_2 (50% w/w, 136 µL, 2.4 mmol, 20 equiv). The reaction was stirred at 0 °C for 2 h before being quenched with saturated *aq.* $NaHSO_3$ (2 mL). The layers were then separated, and the aqueous phase was extracted with DCM (2×2 mL) and EtOAc (2×2 mL). The combined organic layer was dried over Na_2SO_4 and concentrated *in vacuo*. The residue was purified by column chromatography (5% MeOH/DCM) to afford epoxide **30a** and **30b** (28.4 mg, 68% combined) as a pale-yellow foam. **30b**: $[\alpha]_D^{20}$ –2.4 (*c* 0.17, acetone). ^{1}H NMR (600 MHz, Acetone) δ 5.94 (d, *J* = 8.3 Hz, 1H), 5.64 (d, *J* = 5.2 Hz, 1H), 5.13 (s, 1H), 4.12 (dd, *J* = 10.8, 2.3 Hz, 1H), 3.85 (d, *J* = 3.9 Hz, 1H), 3.82 (m, 1H), 3.80 (dd, *J* = 4.0, 2.3 Hz, 1H), 3.72 – 3.67 (m, 1H), 3.65 (d, *J* = 10.7 Hz, 1H), 2.14 (dd, *J* = 12.9, 4.5 Hz, 1H), 2.05 (1H,

under solvent residue peak), 1.38 (s, 9H). ^{13}C NMR (151 MHz, Acetone) δ 199.2, 155.6, 80.9, 79.4, 76.4, 75.5, 70.6, 61.2, 56.0, 48.9, 36.5, 28.5. IR (thin film) ν_{max} (cm^{-1}) 3369, 2957, 2922, 2851, 1731, 1690, 1520, 1458, 1393, 1368,1304, 1248, 1164, 1102, 1055, 926, 898, 869, 793. HRMS (ESI) *calcd.* for $[C_{14}H_{20}O_7NClNa]^+$ ([M+Na]$^+$): *m/z* 372.0821, found: 372.0821. **30a**: $[\alpha]_D^{20}$ +3.6 (*c* 0.14, acetone). ^{1}H NMR (600 MHz, Acetone) δ 6.13 (s, 1H), 5.07 (s, 1H), 4.97 (d, *J* = 4.9 Hz, 1H), 3.97 – 3.89 (m, 2H), 3.79 (dd, *J* = 9.0, 1.8 Hz, 1H), 3.78 – 3.73 (m, 1H), 3.73 – 3.70 (m, 2H), 2.39 (dd, *J* = 13.3, 5.5 Hz, 1H), 1.88 (t, *J* = 13.1 Hz, 1H), 1.40 (s, 9H). ^{13}C NMR (151 MHz, Acetone) δ 194.0, 156.5, 83.2, 80.1, 79.45, 79.34, 70.7, 61.0, 54.5, 52.0, 39.2, 28.6. IR (thin film) ν_{max} (cm^{-1}) 3381, 2955, 2923, 2851, 1717, 1688, 1517, 1459, 1369, 1304, 1249, 1164, 1102, 1055, 1007, 870, 795. HRMS (ESI) *calcd.* for $[C_{14}H_{20}O_7NClNa]^+$ ([M+Na]$^+$): *m/z* 372.0821, found: 372.0821.

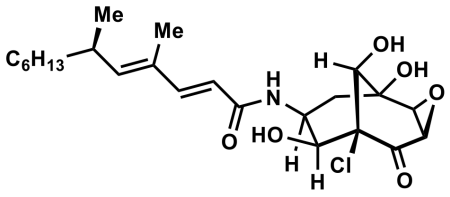

gymnastatin G (**11**)

Gymnastatin G (**11**) *i.* To a 10 mL reaction tube was added a mixture of epoxide **30** (18.9 mg, 0.0542 mmol, 1.0 equiv) and DCM (0.8 mL). Trifluoroacetic acid (0.16 mL) was added slowly at 0 °C. The reaction mixture was warmed up to room temperature and stirred for 3 hours. After completion of the reaction, the mixture was concentrated by rotatory evaporation. The residue was dried under high vacuum for 3 hours to provide crude primary amine TFA salt as a yellow oil, which was used directly in the next step without further purification.

ii. To a 10 mL reaction tube was added acid **32** (12.2 mg, 0.054 mmol, 1.0 equiv), HATU (20.6 mg, 0.054 mmol, 1.0 equiv), DIPEA (19 µL, 0.11 mmol, 2.0 equiv) and DCM (0.5 mL). After stirring at room temperature for 4 h, the reaction was quenched with saturated *aq.* NH_4Cl and extracted with DCM (3 × 1 mL). The combined organic layer was dried over Na_2SO_4 and concentrated *in vacuo*. The resulting activated ester was then transferred into another 10 mL reaction tube containing the crude primary amine TFA salt prepared above. DCM (0.5 mL) and DIPEA (28 µL, 0.16 mmol, 3.0 equiv) was added and the reaction mixture was stirred at room temperature for 12 hours before quenching with saturated aq. NH_4Cl. The layers were separated, and the aqueous phase was extracted with DCM (3×1 mL). The combined organic layer was dried over Na_2SO_4 and concentrated *in vacuo*. The residue was purified by preparative TLC (DCM/acetone = 4:1) to afford gymnastatin G (**11**) (9.1 mg, 37% yield, 2 steps) and 1-*epi*- gymnastatin G (**33**) (5.5 mg, 22% yield, 2 steps), both as a colorless oil which slowly solidifies. Gymnastatin G (**11**): $[\alpha]_D^{20}$ –32.1 (*c* 0.48, acetone). ^{1}H NMR (600 MHz, Acetone) δ 7.25 (d, *J* = 8.1 Hz, 1H), 7.14 (d, *J* = 15.4 Hz, 1H), 6.04 (d, *J* = 15.4 Hz, 1H), 5.67 (d, *J* = 4.8 Hz, 1H), 5.62 (d, *J* = 9.8 Hz, 1H), 5.18 (s, 1H), 4.18 – 4.08 (m, 2H), 3.87 (d, *J* = 3.9 Hz, 1H), 3.85 – 3.79 (m, 2H), 3.67 (d, *J* = 10.8 Hz, 1H), 2.62 – 2.51 (m, 1H), 2.16 (dd, *J* = 13.0, 5.4 Hz, 1H), 2.06 (t, *J* = 13.0 Hz, 1H), 1.76 (s, 3H), 1.42 – 1.35 (m, 1H), 1.34 – 1.22 (m, 9H), 0.97 (d, *J* = 6.6 Hz, 3H), 0.86 (t, *J* = 6.8 Hz, 3H). ^{13}C NMR (151 MHz, Acetone) δ 199.1, 165.9, 146.9, 146.0, 132.2, 119.8, 80.9, 76.5, 75.6, 70.7, 61.2, 56.0, 47.2, 38.1, 36.5, 33.8, 32.6, 30.1, 28.2, 23.3, 20.9, 14.3, 12.7. IR (thin film) ν_{max} (cm^{-1}) 3318, 2957, 2925, 2853, 1732,

1651, 1610, 1542, 1462, 1276, 1262, 1096, 844, 764, 751. HRMS (ESI) *calcd.* for $[C_{23}H_{34}O_6NClNa]^+$ ($[M+Na]^+$): *m/z* 478.1967, found: 478.1960.

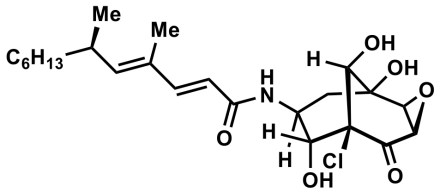

1-*epi*-gymnastatin G (**33**)

1-*epi*-gymnastatin G (**33**): $[\alpha]_D^{20}$ –50.0 (*c* 0.55, acetone). ^{1}H NMR (600 MHz, Acetone) δ 7.38 (d, *J* = 7.3 Hz, 1H), 7.17 (dd, *J* = 15.4, 0.8 Hz, 1H), 5.94 (d, *J* = 15.4 Hz, 1H), 5.65 (d, *J* = 9.6 Hz, 1H), 5.24 (d, *J* = 4.3 Hz, 1H), 5.11 (s, 1H), 4.16 (dddd, *J* = 12.8, 10.5, 7.3, 5.5 Hz, 1H), 3.98 (dd, *J* = 10.5, 4.4 Hz, 1H), 3.94 (d, *J* = 8.8 Hz, 1H), 3.84 (dd, *J* = 8.9, 1.5 Hz, 1H), 3.74 – 3.72 (m, 2H), 2.57 (m, 1H), 2.45 (dd, *J* = 13.3, 5.5 Hz, 1H), 1.93 (t, *J* = 13.0 Hz, 1H), 1.77 (d, *J* = 1.3 Hz, 3H), 1.42 – 1.36 (m, 1H), 1.33 – 1.22 (m, 9H), 0.98 (d, *J* = 6.6 Hz, 3H), 0.87 (t, *J* = 7.0 Hz, 3H). ^{13}C NMR (151 MHz, Acetone) δ 194.0, 167.6, 147.4, 146.4, 132.2, 119.5, 83.2, 80.7, 79.4, 70.7, 61.0, 54.5, 51.2, 38.6, 38.0, 33.8, 32.6, 30.1, 28.2, 23.3, 20.9, 14.3, 12.7. IR (thin film) ν_{max} (cm^{-1}) 3342, 2956, 2924, 2853, 1733, 1651, 1611, 1544, 1459, 1377, 1293, 1080, 980, 845. HRMS (ESI) *calcd.* for $[C_{23}H_{34}O_6NClNa]^+$ ($[M+Na]^+$): *m/z* 478.1967, found: 478.1960.

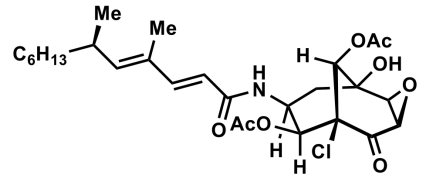

gymnastatin G diacetate (**SI-5**)

Gymnastatin G diacetate (**SI-5**): To a 10 mL reaction tube was added subsequently gymnastatin G (2.4 mg, 0.0053 mmol, 1.0 equiv), DMAP (trace, ~ 0.1 mg), DCM (0.3 mL), Et_3N (11 µL, 0.079 mmol, 15 equiv) and Ac_2O (2.5 µL, 0.026 mmol, 5 equiv). The reaction was stirred for 6 h before being quenched with saturated aq. NH_4Cl. The layers were separated, and the aqueous phase was extracted with DCM (3×1 mL). The combined organic layer was dried over Na_2SO_4 and concentrated *in vacuo*. The residue was purified by preparative TLC (hexanes/acetone = 2:1) to afford gymnastatin G diacetate (**1.67**) (1.0 mg, 35% yield) as a colorless oil. $[\alpha]_D^{20}$ –31.0 (*c* 0.10, $CHCl_3$). ^{1}H NMR (600 MHz, $CDCl_3$) δ 7.20 (d, *J* = 15.2 Hz, 1H), 5.66 (d, *J* = 9.9 Hz, 1H), 5.64 (d, *J* = 2.1 Hz, 1H), 5.61 (d, *J* = 15.2 Hz, 1H), 5.40 (d, *J* = 8.1 Hz, 1H), 5.33 (dd, *J* = 3.2, 1.2 Hz, 1H), 4.45 – 4.37 (m, 1H), 3.78 (d, *J* = 3.6 Hz, 1H), 3.59 (dd, *J* = 3.7, 2.0 Hz, 1H), 3.02 (s, 1H), 2.54 – 2.47 (m, 1H), 2.44 (ddd, *J* = 13.2, 5.1, 1.3 Hz, 1H), 2.26 (s, 3H), 2.18 (s, 3H), 2.05 (t, *J* = 13.1 Hz, 1H), 1.74 (d, *J* = 1.3 Hz, 3H), 1.38 – 1.31 (m, 1H), 1.31 – 1.18 (m, 9H), 0.97 (d, *J* = 6.6 Hz, 3H), 0.87 (t, *J* = 7.0 Hz, 3H). ^{13}C NMR (151 MHz, $CDCl_3$) δ 194.6, 171.7, 169.6, 166.0, 149.1, 148.4, 130.9, 116.2, 74.5, 74.1, 73.8, 71.1, 58.2, 53.9, 45.5, 37.4, 37.2, 33.4, 32.0, 29.5, 27.6, 22.8, 20.99, 20.97, 20.6, 14.2, 12.7. IR (thin film) ν_{max} (cm^{-1}) 3361, 2957, 2924, 2852, 1737, 1653, 1614, 1533, 1459, 1375, 1218, 1087, 1060, 1017, 896, 799. HRMS (ESI) *calcd.* for $[C_{27}H_{38}O_8NClNa]^+$ ($[M+Na]^+$): *m/z* 562.2178, found: 562.2184.

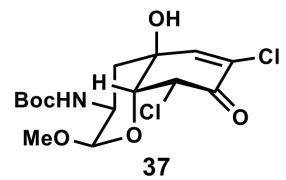

37

Acetal **37**: To a 10 mL reaction tube was added compound **18** (1.6 mg, 0.0046 mmol, 1.0 equiv), THF (0.3 mL) and MeOH (1.8 µL, 0.046 mmol, 10 equiv). The resulting solution was cooled to –78 °C and KHMDS (0.5 M in toluene, 9.1 µL, 0.0046 mmol, 1.0 equiv) was added. The reaction was stirred at –78 °C for 3 h before being

quenched with saturated *aq.* NH_4Cl. The layers were separated, and the aqueous phase was extracted with Et_2O (3×1 mL). The combined organic layer was dried over Na_2SO_4 and concentrated *in vacuo*. The yield was determined by ^{1}H-NMR of the crude mixture with 1,3,5-trimethoxybenzene as the internal standard. The crude mixture was purified by preparative TLC (hexanes/EtOAc = 2:1) to afford pure compound **37** as a colorless oil (50%). ^{1}H NMR (600 MHz, $CDCl_3$) δ 6.79 (s, 1H), 5.25 (d, *J* = 2.3 Hz, 1H), 4.77 (d, *J* = 9.4 Hz, 1H), 4.64 (d, *J* = 3.5 Hz, 1H), 4.22 (t, *J* = 2.5 Hz, 1H), 3.80 – 3.70 (m, 1H), 3.46 (s, 3H), 2.24 (s, 1H), 2.21 (dd, *J* = 12.3, 4.5 Hz, 1H), 1.96 (t, *J* = 12.4 Hz, 1H), 1.44 (s, 9H). ^{13}C NMR (151 MHz, $CDCl_3$) δ 183.0, 155.1, 141.7, 134.2, 97.2, 80.5, 75.4, 69.8, 60.7, 55.4, 47.6, 39.4, 28.5. IR (thin film) ν_{max} (cm^{-1}) 3362, 2958, 2923, 2850, 1723, 1689, 1611, 1511, 1454, 1392, 1369, 1290, 1253, 1165, 1098, 1040, 1002, 749. HRMS (ESI) *calcd.* for $[C_{15}H_{21}O_6NCl_3]^-$ ($[M+Cl]^-$): *m/z* 416.0440, found: 416.0447.

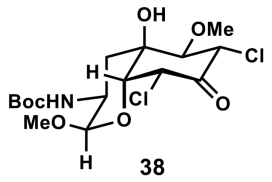

38

Acetal **38**: To a 10 mL reaction tube was added lactol **18** (3.8 mg, 0.011 mmol, 1.0 equiv) and MeOH (0.3 mL). The resulting solution was cooled to –20°C and NaOMe (0.7 mg, 0.013 mmol, 1.2 equiv, dissolved in MeOH) was added. The reaction mixture was stirred at –20°C for 2 hours before being quenched with saturated *aq.* NH_4Cl. The layers were separated, and the aqueous phase was extracted with DCM (3×1 mL). The combined organic layer was dried over Na_2SO_4 and concentrated *in vacuo*. The residue was purified by preparative TLC (Et_2O/hexanes = 3:2) to afford acetal **38** (1.9 mg, 42% yield) as a colorless oil, together with **37** (0.9 mg, 20% yield). $[\alpha]_D^{20}$ –43.2 (*c* 0.19, $CHCl_3$). ^{1}H NMR (600 MHz, $CDCl_3$) δ 5.09 (dd, *J* = 3.6, 1.1 Hz, 1H), 4.79 (d, *J* = 5.2 Hz, 1H), 4.78 (d, *J* = 9.6 Hz, H), 4.67 (d, *J* = 3.9 Hz, 1H), 4.27 (d, *J* = 3.6 Hz, 1H), 3.92 (ddt, *J* = 13.0, 8.9, 4.7 Hz, 1H), 3.83 (s, 3H), 3.69 (d, *J* = 10.0 Hz, 1H), 3.45 (s, 3H), 2.79 (s, 1H), 2.35 (dd, *J* = 12.6, 5.2 Hz, 1H), 1.75 (t, *J* = 12.6 Hz, 1H), 1.44 (s, 9H). ^{13}C NMR (151 MHz, $CDCl_3$) δ 190.2, 155.0, 97.8, 83.7, 80.2, 73.7, 72.7, 66.3, 63.4, 61.1, 55.5, 47.7, 35.6, 28.5. IR (thin film) ν_{max} (cm^{-1}) 2957, 2921, 2851, 1721, 1695, 1461, 1377, 1261, 1050, 800, 764, 751. HRMS (ESI) *calcd.* for $[C_{16}H_{25}O_7NCl_2Na]^+$ ($[M+Na]^+$): *m/z* 436.0900, found: 436.0905.

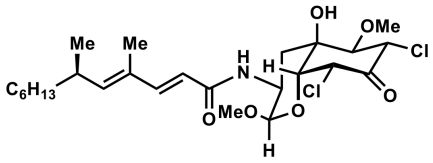

dankastatin C (**14**)

Dankastatin C (**14**): *i.* To a 10 mL reaction tube was added acetal **38** (3.0 mg, 0.0073 mmol, 1.0 equiv) and DCM (0.3 mL). Trifluoroacetic acid (0.06 mL) was added and the reaction mixture was stirred for 1 hour. After completion of the reaction, the mixture was concentrated by rotatory evaporation. The residue was dried under high vacuum for 3 hours to provide crude primary amine TFA salt as a yellow oil, which was used directly in the next step without further purification.

ii. To a 10 mL reaction tube was added acid **32** (2.0 mg, 0.0087 mmol, 1.2 equiv), HATU (3.6 mg, 0.0094 mmol, 1.3 equiv), DIPEA (6.3 µL, 0.036 mmol, 5.0 equiv) and DCM (0.3 mL). After stirring at room temperature for 4 h, the reaction was quenched with saturated *aq.* NH_4Cl and extracted with DCM (3 × 1 mL). The combined organic layer was dried over Na_2SO_4 and concentrated *in vacuo*. The resulting activated ester was then

transferred into another 10 mL reaction tube containing the crude primary amine TFA salt prepared above. DMAP (~0.1 mg, catalytic amount), DCM (0.3 mL) and DIPEA (6.3 µL, 0.036 mmol, 5.0 equiv) was added and the reaction mixture was stirred at room temperature for 1 h before quenching with saturated aq. NH_4Cl. (Note: longer reaction time will result in the E1cb elimination of the methoxy group). The layers were separated, and the aqueous phase was extracted with DCM (3×1 mL). The combined organic layer was dried over Na_2SO_4 and concentrated *in vacuo*. The residue was purified by preparative TLC (hexane/EtOAc = 2:1) to afford dankastatin C (**14**) as a colorless oil (2.3 mg, 61% yield over 2 steps, yield includes the diastereomer formed from *ent*-**38**). $[\alpha]_D^{20}$ – 72.9 (*c* 0.07, $CHCl_3$). ^1H NMR (600 MHz, $CDCl_3$) δ 7.25 (d, 1H), 5.72 (d, *J* = 15.6 Hz, 1H), 5.71 (d, *J* = 8.4 Hz, 1H), 5.65 (d, *J* = 9.8 Hz, 1H), 5.10 (d, *J* = 3.0 Hz, 1H), 4.79 (dd, *J* = 9.9, 0.9 Hz, 1H), 4.69 (d, *J* = 3.9 Hz, 1H), 4.41 – 4.34 (m, 1H), 4.30 (d, *J* = 3.6 Hz, 1H), 3.87 (s, 3H), 3.76 (d, *J* = 10.0 Hz, 1H), 3.48 (s, 3H), 2.81 (s, 1H), 2.55 – 2.46 (m, 1H), 2.40 (dd, *J* = 12.7, 5.1 Hz, 1H), 1.77 (d, *J* = 1.2 Hz, 3H), 1.76 (t, *J* = 12.6 Hz, 1H), 1.40 – 1.12 (m, 10H), 0.97 (d, *J* = 6.7 Hz, 3H), 0.87 (t, *J* = 7.1 Hz, 3H). ^{13}C NMR (151 MHz, $CDCl_3$) δ 190.1, 166.3, 148.6, 147.5, 130.9, 117.0, 97.7, 83.6, 73.8, 72.6, 66.3, 63.4, 61.1, 55.5, 46.3, 37.4, 35.2, 33.4, 32.0, 29.5, 27.6, 22.8, 20.7, 14.2, 12.7. IR (thin film) ν_{max} (cm^{-1}) 2956, 2923, 2852, 1725, 1648, 1612, 1530, 1462, 1378, 1033, 982, 846. HRMS (ESI) *calcd.* for $[C_{25}H_{39}O_6NCl_2Na]^+$ ($[M+Na]^+$): *m/z* 542.2048, found: 542.2050.

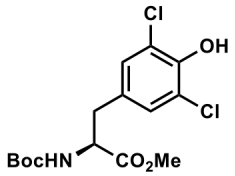

SI-6

3’5’-Dichloro-*N*-Boc-L-tyrosine methyl ester (**SI-6**): To a 25 mL round- bottom flask was added *L*-Boc-Tyr-OMe (**24**) (500 mg, 1.69 mmol, 1.0 equiv) and acetic acid (13 mL). A stream of argon was gently bubbled through the solution and to the solution was added dropwise SO_2Cl_2 (0.41 mL, 5.1 mmol, 3.0 equiv). After stirring for 30 minutes, another portion of SO_2Cl_2 (0.41 mL, 5.1 mmol, 3.0 equiv) was added and the reaction was continued for another 30 minutes. The reaction was then poured into a mixture of Et_2O (50 mL) and saturated *aq.* $NaHCO_3$ (50 mL) with vigorous stirring. The layers were separated, and the aqueous phase was extracted with Et_2O (3×30 mL). The combined organic layer was concentrated *in vacuo*, redissolved in DCM (50 mL) and washed with saturated *aq.* $NaHCO_3$ (50 mL). The organic layer was then dried over Na_2SO_4 and concentrated *in vacuo*. The residue was purified by column chromatography (hexanes/EtOAc = 4:1) to afford ester **SI-6** (312 mg, 51% yield) as a yellow oil. ^1H NMR (600 MHz, $CDCl_3$) δ 7.03 (s, 2H), 5.79 (brs, 1H), 5.03 (brs, 1H), 4.51 (m, 1H), 3.74 (s, 3H), 3.08 – 3.01 (m, 1H), 2.96 – 2.89 (m, 1H), 1.44 (s, 9H). The ^1H NMR matches that reported in literature.[2]

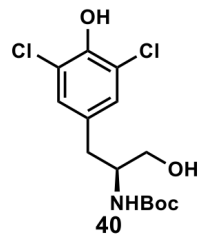

40

Alcohol **40**: To a 100 mL round-bottom flask was added ester **SI-6** (390 mg, 1.07 mmol, 1.0 equiv) and THF (16 mL). The reaction was cooled to –78 °C and DIBAL (1.0 M in hexanes, 6.4 mL, 6.4 mmol. 6.0 equiv) was added dropwise. After stirring at –78 °C for 30 min, the reaction mixture was moved to an ice-water bath and then quenched with saturated *aq.* potassium sodium tartrate (20 mL). The reaction mixture was stirred at room temperature for another 10 h. The layers were then separated, and the aqueous phase was extracted with Et_2O (3×30 mL). The combined organic layer was dried over Na_2SO_4 and concentrated *in vacuo*. The

residue was purified by column chromatography (hexanes/EtOAc = 2:1) to afford alcohol **40** (237 mg, 66% yield) as a pale-yellow foam. $[\alpha]_D^{20}$ – 53.0 (*c* 0.20, $CHCl_3$). ^1H NMR (600 MHz, $CDCl_3$) δ 7.13 (s, 2H), 5.87 (brs, 1H), 4.77 (d, *J* = 8.3 Hz, 1H), 3.77 (m, 1H), 3.66 (dd, *J* = 11.2, 3.8 Hz, 1H), 3.56 (dd, *J* = 11.0, 4.9 Hz, 1H), 2.75 (d, *J* = 7.3 Hz, 2H), 2.24 (brs, 1H), 1.42 (s, 9H). ^{13}C NMR (151 MHz, $CDCl_3$) δ 156.1, 146.6, 131.6, 129.1, 121.1, 80.1, 64.0, 53.7, 36.2, 28.5. IR (thin film) ν_{max} (cm^{-1}) 3372, 2965, 2925, 2852, 1688, 1488, 1413, 1368, 1168, 1019, 797. HRMS (ESI) *calcd.* for $[C_{14}H_{19}O_4NCl_2Na]^+$ ($[M+Na]^+$): *m/z* 358.0583, found: 358.0585.

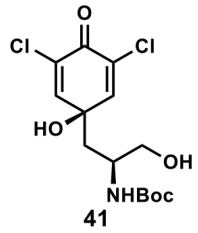

41

Diol **41**: To a 30 mL reaction tube was added alcohol **40** (28.5 mg, 0.0848, 1.0 equiv), tris[3,5-bis(trifluoromethyl)phenyl]phosphine (114 mg, 0.170 mmol, 2.0 equiv) and Cs_2CO_3 (30.4 mg, 0.0932, 1.1 equiv). The reaction tube was evacuated and then backfilled with O_2 using a balloon. Acetone (1.4 mL) was added, and the reaction tube was placed in a dry ice-acetone bath. The solvent level inside the reaction tube was kept ~1 cm below the cooling bath level. A solution of TPP (0.0020M in $CHCl_3$, 1.4 mL) was added at –78 °C, and the resulting mixture was irradiated with a fluorescent lamp for 24 h (the time required for the completion of the reaction varies depending on the scale of the reaction and TLC should be used to monitor the progress of the reaction). Upon completion of the reaction, saturated *aq*. NH_4Cl (2 mL) was added at –78 °C and the resulting mixture was allowed to warm to room temperature. The layers were separated, and the aqueous phase was extracted with DCM (3×5 mL). The combined organic layer was dried over Na_2SO_4 and concentrated *in vacuo*. The residue was purified by column chromatography (DCM/acetone = 4:1 to 3:1) to afford compound **41** (21.1 mg, 70% yield) as a colorless oil. $[\alpha]_D^{20}$ +29.0 (*c* 0.20, $CHCl_3$). ^1H NMR (600 MHz, $CDCl_3$) δ 7.12 (d, *J* = 2.8 Hz, 1H), 7.11 (d, *J* = 2.8 Hz, 1H), 5.07 (brs, 1H), 4.26 (s, 1H), 3.93 (brs, 1H), 3.75 – 3.62 (m, 2H), 2.06 (dd, *J* = 8.4, 3.6 Hz, 1H), 2.05 (brs, 1H), 1.98 (dd, *J* = 14.6, 8.7 Hz, 1H), 1.46 (s, 9H). ^{13}C NMR (151 MHz, $CDCl_3$) δ 172.7, 156.7, 147.3, 146.9, 131.05, 130.96, 81.3, 71.2, 65.9, 48.6, 43.9, 28.5. IR (thin film) ν_{max} (cm^{-1}) 3368, 2954, 2925, 2852, 1685, 1520, 1457, 1394, 1368, 1250, 1166, 1108, 978, 748. HRMS (ESI) *calcd.* for $[C_{14}H_{19}O_5NCl_2Na]^+$ ($[M+Na]^+$): *m/z* 374.0532, found: 374.0533.

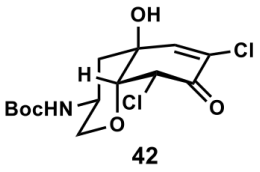

42

Oxa-decalin **42**: To a 10 mL reaction tube was added compound **41** (7.3 mg, 0.021 mmol, 1.0 equiv) and THF (0.6 mL). The solution was cooled to – 78 °C and KHMDS (0.5 M in toluene, 8.3 μL, 0.0042 mmol, 0.2 equiv) was added. After that, the reaction mixture was warmed up slowly to –15 °C over a period of 40 min, before being quenched with saturated *aq*. NH_4Cl (1 mL). The layers were separated, and the aqueous phase was extracted with DCM (3×1 mL). The combined organic layer was dried over Na_2SO_4 and concentrated *in vacuo*. The residue was purified by column chromatography (DCM/acetone = 10:1) to afford compound **42** and *iso*-**42** (5.7 mg, 78% yield, dr = 10:1) as a colorless oil. **42** and *iso*-**42** can be separated by preparative TLC (7% MeOH/$CHCl_3$). Major diastereomer **42**: $[\alpha]_D^{20}$ –10.3 (*c* 0.36, $CHCl_3$). ^1H NMR (700 MHz, $CDCl_3$) δ 6.75 (brs, 1H), 5.26 (d, *J* = 2.3 Hz,

1H), 4.34 (brs, 1H), 4.11 (d, *J* = 10.0 Hz, 1H), 3.90 (t, *J* = 2.4 Hz, 1H), 3.70 (brs, 1H), 3.13 (t, *J* = 11.0 Hz, 1H), 2.49 (s, 1H), 2.45 (d, *J* = 12.0 Hz, 1H), 1.66 (t, *J* = 12.4 Hz, 1H), 1.43 (s, 9H). ^{13}C NMR (151 MHz, $CDCl_3$) δ 182.8, 155.0, 142.0, 134.1, 83.7, 80.6, 70.5, 70.0, 61.3, 45.0, 44.6, 28.4. IR (thin film) ν_{max} (cm^{-1}) 3379, 2952, 2924, 2850, 1723, 1690, 1525, 1461, 1394. 1369, 1250, 1166, 1106, 1011, 748. HRMS (ESI) *calcd.* for $[C_{14}H_{19}O_5NCl_2Na]^+$ ([M+Na]$^+$): *m/z* 374.0532, found: 374.0533.

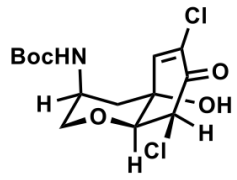

iso-**42**

Minor diastereomer *iso*-**42**: $[\alpha]_D^{20}$ +46.1 (*c* 0.23, $CHCl_3$). ^{1}H NMR (600 MHz, $CDCl_3$) δ 6.67 (d, *J* = 2.4 Hz, 1H), 5.29 (d, *J* = 2.4 Hz, 1H), 4.74 (d, *J* = 6.4 Hz, 1H), 3.99 (t, *J* = 2.4 Hz, 1H), 3.93 (dt, *J* = 12.3, 2.0 Hz, 1H), 3.87 – 3.82 (m, 1H), 3.70 (dd, *J* = 12.3, 2.1 Hz, 1H), 2.70 (d, *J* = 13.6 Hz, 1H), 2.21 (s, 1H), 1.87 (dd, *J* = 13.6, 3.4 Hz, 1H), 1.46 (s, 9H). ^{13}C NMR (151 MHz, $CDCl_3$) δ 182.8, 155.1, 143.6, 131.6, 84.6, 80.3, 71.1, 68.3, 61.2, 46.3, 41.8, 28.5. IR (thin film) ν_{max} (cm^{-1}) 3371, 2957, 2920, 2852, 1678, 1458, 1397, 1369, 1251, 1168, 1041, 978, 747. HRMS (ESI) *calcd.* for $[C_{14}H_{19}O_5NCl_2Na]^+$ ([M+Na]$^+$): *m/z* 374.0532, found: 374.0534.

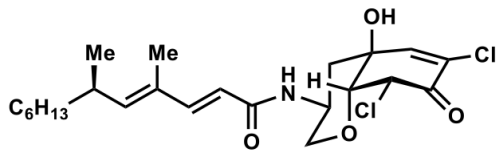

dankastatin B (**13**)

Dankastatin B (**13**): *i.* To a 10 mL reaction tube was added compound **42** (3.8 mg, 0.011 mmol, 1.0 equiv) and DCM (0.4 mL). Trifluoroacetic acid (0.08 mL) was added and the reaction mixture was stirred for 2 hours. After completion of the reaction, the mixture was concentrated by rotatory evaporation. The residue was dried under high vacuum for 3 hours to provide crude primary amine TFA salt as a yellow oil, which was used directly in the next step without further purification. *ii.* To a 10 mL reaction tube was added acid **32** (2.4 mg, 0.011 mmol, 1.0 equiv), HATU (4.1 mg, 0.011 mmol, 1.0 equiv), DIPEA (5.7 µL, 0.032 mmol, 3.0 equiv) and DCM (0.5 mL). After stirring at room temperature for 4 h, the reaction was quenched with saturated *aq.* NH_4Cl and extracted with DCM (3 ×1 mL). The combined organic layer was dried over Na_2SO_4 and concentrated *in vacuo*. The resulting activated ester was then transferred into another 10 mL reaction tube containing the crude primary amine TFA salt prepared above. DCM (0.4 mL) and DIPEA (5.7 µL, 0.032 mmol, 3.0 equiv) was added and the reaction mixture was stirred at room temperature for 12 hours before quenching with saturated aq. NH_4Cl. The layers were separated, and the aqueous phase was extracted with DCM (3×1 mL). The combined organic layer was dried over Na_2SO_4 and concentrated *in vacuo*. The residue was purified by preparative TLC (DCM/acetone = 10:1) to afford dankastatin B (**13**) (4.2 mg, 85% yield, 2 steps) as a colorless oil which slowly solidifies. $[\alpha]_D^{20}$ –36.3 (*c* 0.30, $CHCl_3$). ^{1}H NMR (700 MHz, $CDCl_3$) δ 7.18 (d, *J* = 15.3 Hz, 1H), 6.84 (d, *J* = 2.4 Hz, 1H), 5.73 (d, *J* = 15.4 Hz, 1H), 5.67 (d, *J* = 9.8 Hz, 1H), 5.59 (d, *J* = 8.1 Hz, 1H), 5.39 (d, *J* = 2.3 Hz, 1H), 4.36 (brs, 1H), 4.12 (ddd, *J* = 11.0, 4.8, 2.0 Hz, 1H), 4.07 – 4.00 (m, 1H), 3.96 (t, *J* = 2.3 Hz, 1H), 3.20 (t, *J* = 10.9 Hz, 1H), 2.53 – 2.47 (m, 1H), 2.44 (ddd, *J* = 12.3, 4.1, 2.0 Hz, 1H), 1.76 (t, *J* = 11.9 Hz, 1H), 1.74 (d, *J* = 1.2 Hz, 3H), 1.38 – 1.32 (m, 1H), 1.31 – 1.17 (m, 9H), 0.96 (d, *J* = 7.0 Hz, 3H), 0.86 (t, *J* = 7.1 Hz, 3H). ^{13}C NMR (151 MHz, $CDCl_3$) δ 184.1, 167.2, 149.2, 148.1, 143.6, 133.1,

130.9, 116.7, 84.0, 70.0, 69.7, 61.7, 44.1, 43.6, 37.3, 33.4, 32.0, 29.5, 27.6, 22.8, 20.6, 14.2, 12.6. IR (thin film) ν_{max} (cm^{-1}) 3359, 3194, 2956, 2922, 2852, 1722, 1658, 1633, 1539, 1467, 1423, 1107, 1055, 1031, 974, 806. HRMS (ESI) *calcd.* for $[C_{23}H_{32}O_4NCl_2]^-$ ($[M–H]^-$): *m/z* 456.1714, found: 456.1723.

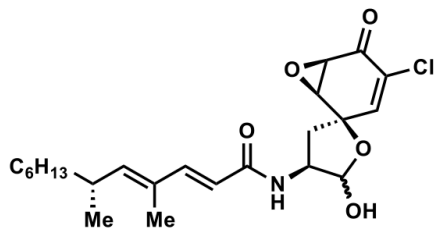

aranochloro A (**44**)

Aranochloro A (**44**) and Aranochloro B (**43**): To a 10 mL reaction tube was added aranorosin (5.0 mg, 0.012 mmol, 1.0 equiv), LiCl (0.61 mg, 0.014 mmol, 1.2 equiv, dissolved in THF) and THF (0.8 mL). The reaction was stirred at 22°C for 15 hours. The reaction was then quenched with saturated aq. NH_4Cl and extracted with DCM (3×1 mL). The combined organic layer was dried over Na_2SO_4 and concentrated *in vacuo*. ^1H NMR yields were obtained using 1,2,4,5-tetrachloro-3-nitrobenzene as internal standard. The crude mixture was then purified by preparative TLC (8% MeOH/DCM) to afford aranchloro A and B, gymnastatin G, and 1-*epi*-gymnastatin G. Aranochloro A and B was separated by a second preparative TLC (15% acetone/DCM). Aranochloro A (**44**): (only peaks from the major diastereomer at C-1 is listed) ^1H NMR (600 MHz, $CDCl_3$) δ 7.24 (under solvent peak), 6.67 (d, *J* = 2.7 Hz, 1H), 5.97 (d, *J* = 8.5 Hz, 1H), 5.75 (d, *J* = 15.3 Hz, 1H), 5.68 (d, *J* = 9.7 Hz, 1H), 5.56 (d, *J* = 4.5 Hz, 1H), 4.85–4.77 (m, 1H), 3.78 (dd, *J* = 3.9, 2.7 Hz, 1H), 3.63 (d, *J* = 3.7 Hz, 1H), 3.50 (brs, 1H), 2.55 (dd, *J* = 12.9, 8.5 Hz, 1H), 2.57 – 2.47 (m, 1H), 2.17 (ddd, *J* = 13.1, 11.0, 2.4 Hz, 1H), 1.77 (s, 3H), 1.40 – 1.20 (m, 10H), 0.97 (d, *J* = 6.6 Hz, 3H), 0.87 (t, *J* = 6.6 Hz, 3H). ^{13}C NMR (151 MHz, $CDCl_3$) δ 186.3, 166.7, 148.7, 147.7, 143.1, 130.9, 128.3, 117.0, 96.6, 80.7, 58.3, 53.0, 52.1, 39.2, 37.4, 33.4, 32.0, 29.5, 27.6, 22.8, 20.7, 14.2, 12.6. IR (thin film) ν_{max} (cm^{-1}) 3307, 2957, 2924, 2852, 1708, 1651, 1611, 1535, 1456, 1377, 1033, 984, 700. HRMS (ESI) *calcd.* for $[C_{23}H_{32}O_5NClNa]^+$ ($[M+Na]^+$): *m/z* 460.1861, found: 460.1863.

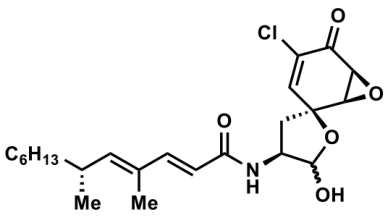

aranochloro B (**43**)

Aranochloro B (**43**): (only peaks from the major diastereomer at C1 is listed) ^1H NMR (600 MHz, $CDCl_3$) δ 7.24 (under solvent peak), 6.76 (d, *J* = 2.6 Hz, 1H), 5.93 (d, *J* = 8.4 Hz, 1H), 5.75 (d, *J* = 15.3 Hz, 1H), 5.68 (d, *J* = 9.7 Hz, 1H), 5.57 (d, *J* = 4.6 Hz, 1H), 4.89 – 4.82 (m, 1H), 3.67 (dd, *J* = 3.8, 2.6 Hz, 1H), 3.62 (d, *J* = 3.6 Hz, 1H), 3.37 (brs, 1H), 2.62 (dd, *J* = 13.1, 8.3 Hz, 1H), 2.54 – 2.47 (m, 1H), 2.13 (dd, *J* = 13.2, 10.8 Hz, 1H), 1.77 (s, 3H), 1.40 – 1.20 (m, 10H), 0.98 (d, *J* = 6.6 Hz, 3H), 0.87 (t, *J* = 6.9 Hz, 3H). ^{13}C NMR (151 MHz, $CDCl_3$) δ 186.2, 166.7, 148.7, 147.7, 144.5, 130.9, 128.0, 116.9, 96.7, 80.4, 57.0, 52.6, 51.7, 38.3, 37.4, 33.4, 32.0, 29.5, 27.6, 22.8, 20.7, 14.2, 12.7. IR (thin film) ν_{max} (cm^{-1}) 3358, 2956, 2923, 2851, 1707, 1651, 1611, 1531, 1461, 1377, 1022, 806, 699. HRMS (ESI) *calcd.* for $[C_{23}H_{32}O_5NClNa]^+$ ($[M+Na]^+$): *m/z* 460.1861, found: 460.1864.

General Procedures II

Unless otherwise stated, all reactions were performed in oven-dried or flame-dried Fisherbrand® borosilicate glass tubes or round bottom flasks under an atmosphere of dry

nitrogen. Anhydrous tetrahydrofuran, dichloromethane, *N,N*-Dimethylformamide, toluene, acetonitrile, triethylamine, and diethyl ether were obtained by passing these previously degassed solvents through activated alumina columns. All other solvents were used directly from Sigma-Aldrich Sure/Seal^{TM} bottles. 2-Methyloct-7-yn-1-ol and SI-7 were prepared according to literature proceedures.[107,190] Reactions were monitored by thin layer chromatography (TLC) on TLC silica gel 60 F_{254} glass plates (EMD Millipore) and visualized by UV irradiation and staining with *p*-anisaldehyde, phosphomolybdic acid, or potassium permanganate. Volatile solvents were removed under reduced pressure using a rotary evaporator. Flash column chromatography was performed using Silicycle F60 silica gel (60Å, 230-400 mesh, 40-63 μm). Ethyl acetate and hexanes were purchased from Fisher Chemical and used for chromatography without further purification. Proton nuclear magnetic resonance (^{1}H NMR) and carbon nuclear magnetic resonance (^{13}C NMR) spectra were recorded on a Bruker AV-600 spectrometer operating at 600 MHz for ^{1}H, and 150 MHz for ^{13}C. Chemical shifts are reported in parts per million (ppm) with respect to the residual solvent signal $CDCl_3$ (^{1}H NMR: δ = 7.26; ^{13}C NMR: δ = 77.16). High-resolution mass spectra (HRMS) were obtained by the QB3/chemistry mass spectrometry facility at the University of California, Berkeley.

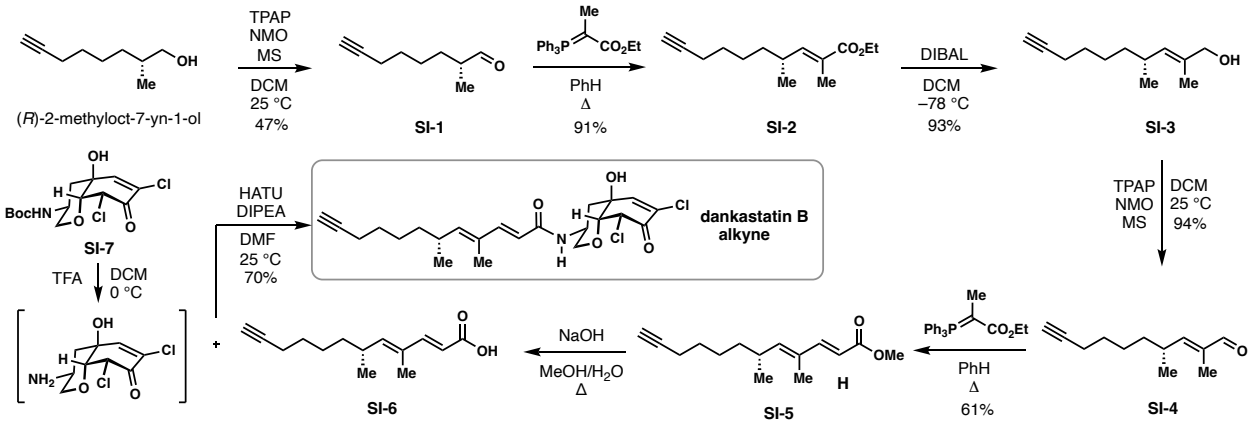

Figure S6. Synthetic scheme for dankastatin B alkyne probe.

Compound SI-1. *(R)*-2-methyloct-7-yn-1-ol (250 mg, 1.78 mmol) was dissolved in 15 mL of anhydrous DCM and to this solution was added Tetrapropylammonium perruthenate (7.3 mg, 18 μmol), 4-methylmorpholine 4-oxide (632 mg, 5.35 mmol), and powdered molecular sieves (500 mg). The reaction mixture was stirred at room temperature for 8 hours under an atmosphere of argon. Upon reaction completion as indicated by TLC, the reaction mixture was filtered through a pad of SiO_2 and the resulting solution concentrated *in vacuo*. The residue was purified by column chromatography (0 to 60% Et_2O/hexanes) to afford aldehyde **SI-1** as a pale-yellow oil (115 mg, 47%): R_f = 0.72 (30% EtOAc/hexanes); IR (thin film) ν_{max} = 3294, 2936, 2862, 2714, 1724, 1461, 1115, 1078, 634 cm^{-1}; ^{1}H NMR (600 MHz, $CDCl_3$) δ 9.63 (d, *J* = 1.9 Hz, 1H), 2.35 (hd, *J* = 6.9, 2.0 Hz, 1H), 2.21 (td, *J* = 7.0, 2.7 Hz, 2H), 1.94 (t, *J* = 2.7 Hz, 1H), 1.79 – 1.66 (m, 1H), 1.61 – 1.34 (m, 5H), 1.11 (d, *J* = 7.0 Hz, 3H); ^{13}C NMR (151 MHz, $CDCl_3$) δ 205.0, 84.1, 77.2,

77.0, 76.7, 68.4, 46.1, 29.9, 28.3, 25.9, 18.2, 13.3; HRMS (*m/z*): (ESI) calcd. for $C_9H_{13}O$ $[M–H]^+$: 137.0966, found 137.0965.

Compound SI-2. Aldehyde **SI-1** (102 mg, 0.74 mmol) was dissolved in 6 mL of anhydrous benzene and (Carbethoxyethylidene)triphenylphosphorane (802 mg, 2.21 mmol) was added in one portion. The reaction mixture was heated to reflux and maintained at this temperature for 15 hours. Upon completion, as indicated by TLC, the reaction mixture was cooled to room temperature and directly purified by silica gel column chromatography (0 to 40% Et_2O/hexanes) to afford ester **SI-2** (150 mg, 91%): R_f = 0.75 (15% Et_2O/hexanes); IR (thin film) ν_{max} = 2934, 2862, 1700, 1649, 1458, 1243, 1209, 1176, 751, 632 cm^{-1}; ^1H NMR (600 MHz, $CDCl_3$) δ 6.53 (dd, *J* = 10.1, 1.6 Hz, 1H), 4.19 (q, *J* = 7.1 Hz, 2H), 2.54 – 2.44 (m, 1H), 2.18 (td, *J* = 7.1, 2.6 Hz, 2H), 1.93 (t, *J* = 2.6 Hz, 1H), 1.84 (s, 3H), 1.55 – 1.47 (m, 2H), 1.44 – 1.25 (m, 7H), 1.00 (d, *J* = 6.6 Hz, 3H); ^{13}C NMR (151 MHz, $CDCl_3$) δ 168.8, 148.1, 126.9, 84.8, 77.6, 77.4, 77.2, 68.6, 60.8, 36.6, 33.5, 28.9, 27.0, 20.4, 18.7, 14.7, 12.9; HRMS (*m/z*): (ESI) calcd. for $C_{14}H_{23}O_2$ $[M+H]^+$: 223.1693, found 223.1693.

Compound SI-3. Ester **SI-2** (150 mg, 0.68 mmol) was dissolved in anhydrous DCM and cooled to –78 °C under argon. A solution of DIBAL (1M in hexane, 1.48 mL, 1.48 mmol) was added dropwise and the reaction mixture stirred at –78 °C. Upon completion, as indicated by TLC, the reaction mixture was quenched with saturated aqueous Rochelle's salt solution, warmed to room temperature, and vigorously stirred for 2 hours at room temperature. The aqueous layer was extracted with Et_2O (3 x 50 mL) and the combined organic layers dried over Na_2SO_4 and concentrated *in vacuo*. The residue was purified by column chromatography (0 to 30% EtOAc/hexanes) to afford alcohol **SI-3** as an oil (120 mg, 98%): R_f = 0.25 (15% EtOAc/hexanes); IR (thin film) ν_{max} = 3307, 2929, 2861, 1455, 1376, 1068 cm^{-1}; ^1H NMR (600 MHz, $CDCl_3$) δ 5.17 (dp, *J* = 9.5, 1.4 Hz, 1H), 3.99 (dd, *J* = 6.0, 1.2 Hz, 2H), 2.38 (dtdd, *J* = 13.4, 6.7, 3.0, 1.3 Hz, 1H), 2.21 – 2.13 (m, 2H), 1.93 (t, *J* = 2.7 Hz, 1H), 1.67 (d, *J* = 1.4 Hz, 3H), 1.55 – 1.45 (m, 2H), 1.41 – 1.17 (m, 5H), 0.94 (dd, *J* = 6.7, 2.8 Hz, 3H); ^{13}C NMR (151 MHz, $CDCl_3$) δ 133.3, 132.6, 84.6, 69.0, 68.0, 36.9, 31.9, 28.6, 26.5, 20.9, 18.3, 13.8; HRMS (*m/z*): (ESI) calcd. for $C_{12}H_{18}$ $[M–H_2O]^+$: 162.1409, found 162.1406.

Compound SI-4. Alcohol **SI-3** (110 mg, 0.61 mmol) was dissolved in 6 mL of anhydrous dichloromethane followed by the addition of Tetrapropylammonium perruthenate (2.4 mg, 6.1 µmol), 4-methylmorpholine 4-oxide (216 mg, 1.83 mmol) and powdered molecular sieves (500 mg). The reaction mixture was stirred at room temperature until starting material was consumed, as indicated by TLC. The reaction mixture was filtered through a pad of celite and the filtrate rinsed with DCM. The solvent was removed *in vacuo* and the residue purified by column chromatography (0 to 20% EtOAc/hexanes) to give aldehyde **SI-4** as an oil (102 mg, 94%): R_f = 0.72 (40% EtOAc/hexanes); IR (thin film) ν_{max} = 2929, 2858, 1730, 1688, 1642, 1459, 1324, 1017, 632 cm^{-1}; ^1H NMR (600 MHz, $CDCl_3$) δ 9.39 (s, 1H), 6.25 (dq, *J* = 9.9, 1.4 Hz, 1H), 2.75 – 2.65 (m, 1H), 2.18 (td, *J* = 7.0, 2.6 Hz, 2H), 1.93 (t, *J* = 2.6 Hz, 1H), 1.75 (d, *J* = 1.4 Hz, 3H), 1.55 – 1.33 (m, 6H), 1.07 (d, *J* = 6.7 Hz, 3H); ^{13}C NMR (151 MHz, $CDCl_3$) δ 195.5, 160.1, 138.1, 84.2, 77.2, 77.0, 76.8,

68.4, 36.1, 33.4, 28.4, 26.4, 19.8, 18.2, 9.4; HRMS (*m/z*): (ESI) calcd. for $C_{12}H_{17}O$ $[M–H]^+$: 177.1276, found 177.1277.

Compound SI-5. Aldehyde **SI-4** (97 mg, 0.54 mmol) was dissolved in 6 mL of anhydrous toluene. To this solution was added Methyl (triphenylphosphoranylidene)acetate (565 mg, 1.63 mmol) and the resulting solution was heated at 90 °C. Upon completion, as indicated by TLC, the reaction mixture was cooled to room temperature and directly purified by silica gel chromatography (20% Et_2O/hexanes) to afford ester **SI-5** as an oil (76 mg, 60%): R_f = 0.51 (15% Et_2O/hexanes); IR (thin film) ν_{max} = 2932, 2861,1717, 1623, 1455, 1434, 1394, 1270, 1169, 847 cm^{-1}; ^1H NMR (600 MHz, $CDCl_3$) δ 7.31 (d, *J* = 15.7 Hz, 1H), 5.79 (d, *J* = 15.7 Hz, 1H), 5.67 (d, *J* = 9.8 Hz, 1H), 3.75 (s, 3H), 2.58 – 2.48 (m, 1H), 2.17 (tdd, *J* = 7.1, 2.7, 1.1 Hz, 2H), 1.93 (q, *J* = 2.8 Hz, 1H), 1.78 (s, 3H), 1.57 – 1.22 (m, 6H), 0.99 (d, *J* = 6.6 Hz, 3H); ^{13}C NMR (151 MHz, $CDCl_3$) δ 168.2, 150.3, 148.5, 131.6, 115.4, 84.6, 77.4, 77.2, 77.0, 68.4, 51.6, 36.8, 33.3, 28.7, 26.7, 20.6, 18.5, 12.5; HRMS (*m/z*): (ESI) calcd. for $C_{15}H_{23}O$ $[M+H]^+$: 235.1693, found 235.1694.

Compound SI-6. To ester **SI-5** (75.0 mg, 0.32 mmol) was added 4.8 mL of MeOH and 1.0 mL of H_2O. To this suspension was added NaOH (64.0 mg, 1.60 mmol) and the reaction mixture stirred at 35 °C. Upon reaction completion, as indicated by TLC, the reaction mixture was cooled to 0 °C and 1N HCl (10 mL) and EtOAc (10 ml) were added. The aqueous layer was extracted with ethyl acetate (3 x 25 mL) and the combined organic layers were combined, dried over Na_2SO_4 and concentrated *in vacuo*. The resulting residue was purified by column chromatography (30% to 100% EtOAc/hexanes) to afford acid **SI-6** as a pale-yellow oil (65 mg, 92%): R_f = 0.56 (3.5% MeOH/Dichloromethane); IR (thin film) ν_{max} = 3305, 2935, 2861, 2684, 2593, 1685, 1617, 1208, 851 cm^{-1}; ^1H NMR (600 MHz, $CDCl_3$) δ 7.39 (d, *J* = 15.6 Hz, 1H), 5.79 (d, *J* = 15.6 Hz, 1H), 5.72 (d, *J* = 9.8 Hz, 1H), 2.60 – 2.50 (m, 1H), 2.17 (tdd, *J* = 7.1, 2.7, 1.1 Hz, 2H), 1.93 (t, *J* = 2.6 Hz, 1H), 1.80 (d, *J* = 1.2 Hz, 3H), 1.51 (dq, *J* = 8.7, 6.3 Hz, 2H), 1.44 – 1.24 (m, 4H), 1.00 (d, *J* = 6.7 Hz, 3H); ^{13}C NMR (151 MHz, $CDCl_3$) δ 172.9, 152.4, 149.8, 131.7, 114.9, 84.6, 68.4, 36.7, 33.4, 28.7, 26.7, 20.5, 18.5, 12.5; HRMS (*m/z*): (ESI) calcd. for $C_{14}H_{21}O_2$ $[M+H]^+$: 221.1536, found 221.1536.

Dankastatin B alkyne. Alcohol **SI-7** (3 mg, 8.5 µmol) was dissolved in anhydrous DCM (0.5 mL) and the resulting solution was cooled to 0 °C wherein 50 µL of trifluoracetic acid was added. The reaction mixture was stirred at 0 °C for an hour at which point additional TFA (50 µL) was added and the reaction warmed to room temperature and stirred for 30 additional minutes. The volatiles were removed *in vacuo* to afford a yellow oil which was redissolved in 0.7 mL of anhydrous DMF. To this solution was added acid **8** (2.1 mg, 9.3 µmmol), DIPEA (5.9 µL, 35.7 µmol), HATU (3.6 mg, 9.4 µmol) and the reaction mixture was stirred at room temperature. Upon completion, as indicated by TLC, the reaction mixture was diluted with 5 mL of Et_2O and quenched with saturated ammonium chloride solution (10 mL). The aqueous layer was extracted with Et_2O (3 x 10 mL) and the combined organic layers were dried over Na_2SO_4 and concentrated *in vacuo*. The resulting residue was purified by preparative thin layer chromatography (35% Acetone/hexanes) to afford **Dankastatin B alkyne** as a film (2.7 mg, 70%): R_f = 0.46 (35% Acetone/hexanes); IR (thin film) ν_{max} = 3379, 3295, 2932, 2856, 1721, 1649, 1609,

1528, 1107, 748 cm^{-1}; ^{1}H NMR (700 MHz, $CDCl_3$) δ 7.24 (d, *J* = 15.3 Hz, 1H), 6.82 (d, *J* = 2.5 Hz, 1H), 5.79 – 5.66 (m, 2H), 5.32 (d, *J* = 2.2 Hz, 1H), 5.25 (d, *J* = 8.0 Hz, 1H), 4.20 – 4.10 (m, 2H), 3.97 (t, *J* = 2.4 Hz, 1H), 3.24 (t, *J* = 10.8 Hz, 1H), 2.88 (s, 1H), 2.57 – 2.50 (m, 2H), 2.19 (tt, *J* = 7.1, 2.4 Hz, 2H), 1.96 (t, *J* = 2.6 Hz, 1H), 1.82 – 1.74 (m, 4H), 1.56 – 1.49 (m, 2H), 1.45 – 1.33 (m, 2H), 1.35 – 1.26 (m, 2H), 1.01 (dd, *J* = 6.7, 2.1 Hz, 3H); ^{13}C NMR (151 MHz, $CDCl_3$) δ 182.9, 166.6, 148.5, 147.8, 142.4, 133.9, 131.1, 116.9, 84.6, 83.9, 70.1, 69.9, 68.4, 61.4, 44.2, 44.1, 36.8, 33.3, 28.7, 26.8, 20.6, 18.5, 12.7; HRMS (*m/z*): (ESI) calcd. for $C_{23}H_{30}O_4NCl_2$ $[M+H]^+$: 454.1546, found 454.1542.

Chapter 3 Supplementary Information

Supplementary Figures

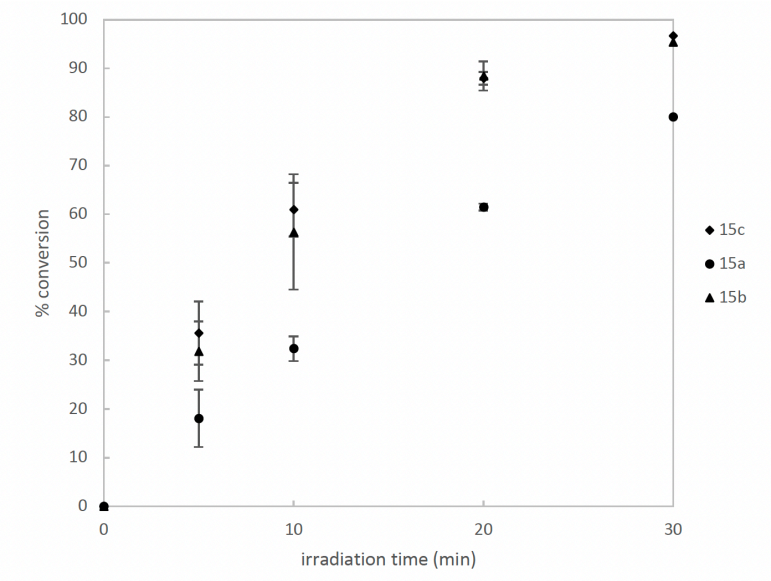

Fig. S3.1 Irradiation time course of acyl silanes 15a-c. Irradiation time course of acyl silanes **15a-c** in CD_3OD at 365 nm using a 6 W hand-held UV lamp at 25ºC. Acyl silane prepared as a stock solution in CD_3OD was added to an NMR tube with dimethylsulfone as an internal standard for a total volume of 50 µL (24 mM). Reactions were run in triplicate and analyzed by ^1H NMR (d1 = 10 s).

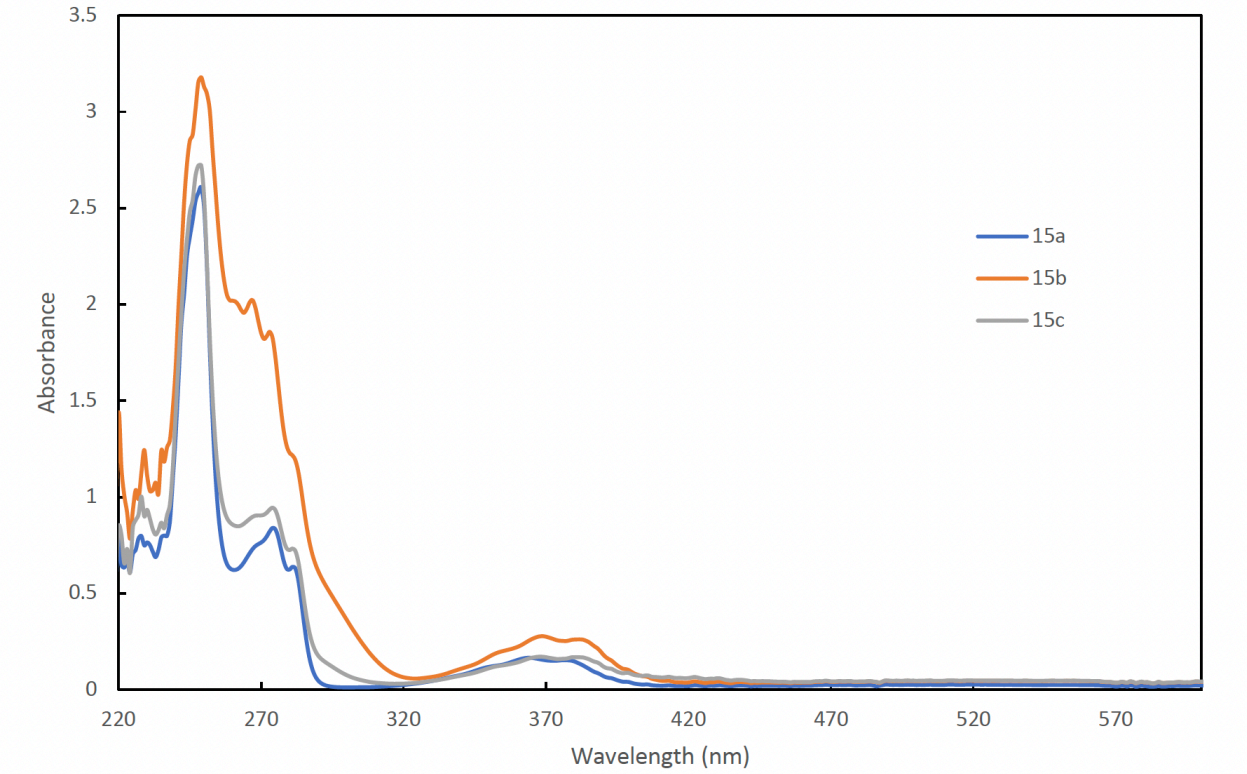

Fig. S3.2 UV-Visible spectra of acyl silanes 15a-c in MeOH. Acyl silanes **15a**, **15b**, and **15c** show a λ_{max} = 364 nm, 370 nm, and 368 nm, respectively, and an ε = 115.7 M^{-1} cm^{-1}, 236.5 M^{-1} cm^{-1}, and 111.0 M^{-1} cm^{-1}, respectively, at 5 mM concentration.

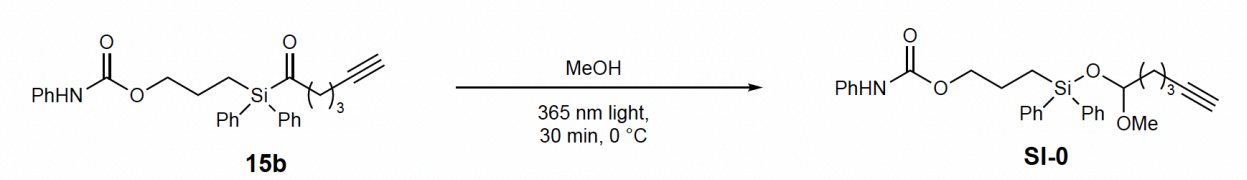

15b **SI-0**

Fig. S3.3 Irradiation of probe 15b in MeOH. Product was characterized from the crude reaction mixture. **^{1}H NMR** (600.1 MHz, DMSO-d_6): Aromatic region contains multiple overlapped species. 9.54 (br. s), 7.60 – 7.54 (m), 7.50 – 7.40 (m), 7.29-7.24 (m), 7.00 – 6.95 (m), 4.77 (dd, *J* = 4.5, 5.6 Hz, 1H, $CHOCH_3$), 4.06 (t, *J* = 6.9 Hz, 2H), 3.12 (s, 3H, OCH_3), 2.72 (t, *J* = 2.6 Hz, 1H, spC–H), 2.08 (dt, *J* = 7.1, 2.7 Hz, 2H), 1.70 – 1.60 (m, 2 or 4 H), overlap with 1.63 (dt, *J* = 4.5, 7.6 Hz, 2H) 1.45 (dt, *J* = 14.7, 7.3 Hz, 2H), 1.29 – 1.26 (m, 2H). **HRMS** (ESI_+): calculated for $[C_{29}H_{33}NO_4Si + Na]^+$ required m/z 510.2071, found m/z 510.2065.

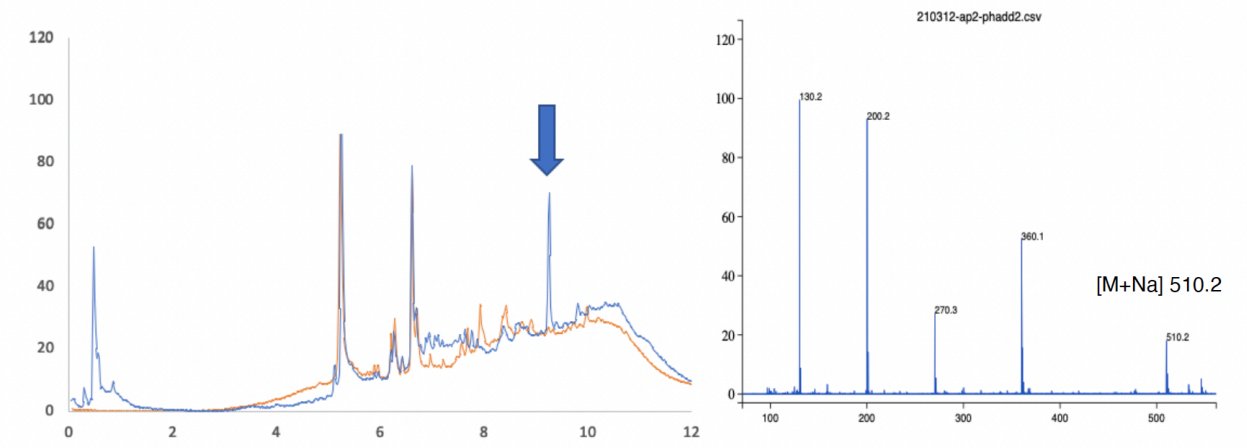

Fig. S3.4. (**A**) LCMS trace (MeCN : H_2O 5-95% with 0.1% formic acid over 12 minutes) of MeOH insertion adduct of 1**5b**. Background profile after injection of blank sample is shown in orange. Trace following irradiation of **15b** in MeOH for 30 min at 0ºC shown in blue,with acetal adduct indicated by arrow. (**B**) Expansion of mass spectrum of acetal. LCMS (ESI^+) calculated for $[C_{29}H_{33}NNaO_4Si]^+$ requires m/z 510.2, found m/z 510.2.

Photochemical 1,2-Brook Rearrangement:

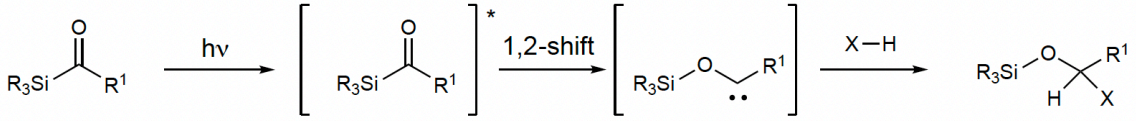

Thermal 1,2-Brook Rearrangement:

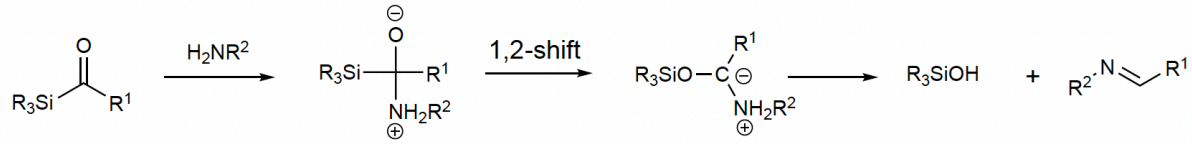

Scheme S3.1. Mechanism of photochemical and thermal 1,2-Brook rearrangements.[171,181]

Synthetic Methods and Characterization

General Procedures

Unless otherwise noted, all reagents were purchased from commercial suppliers and used without further purification. Tetrahydrofuran, dichloromethane, diethyl ether, toluene, trimethylamine, and N,N-dimethylformamide were purified by passage through an activated alumina column under argon. Thin-layer chromatography (TLC) analysis of reaction mixtures was performed using Merck silica gel 60 F_{254} TLC plates and visualized under UV or by staining with $KMnO_4$ or *p*-anisaldehyde. Column chromatography was performed on Merck Silica Gel 60 Å, 230 X 400 mesh. Nuclear magnetic resonance (NMR) spectra were recorded using Bruker AV-600, AV-500, DRX-500, Neo-500, AVB-400, AVQ-400, and AV-300 spectrometers. These CoC-NMR instruments at UC Berkeley are funded in part by the NIH (S10OD024998). ^{1}H and ^{13}C chemical shifts are reported in ppm downfield of tetramethylsilane and referenced to residual solvent peak ($CHCl_3$; δH = 7.268 ppm and δC = 77.16 ppm). Multiplicities are reported using the following abbreviations: s = singlet, d = doublet, t = triplet, q = quartet, p = pentet, hept = heptet/septet, m = multiplet, br = broad, dt = doublet of triplet resonance. Mass spectral data for EMM were obtained from the QB3 mass spectral facility at the University of California, Berkeley on a Thermo LTQ-FTICR (7T, ESI) and in the Center of Catalysis at the University of California, Berkeley. Solvent abbreviations are reported as follows: EtOAc = ethyl acetate, hex = hexanes, DCM = dichloromethane, Et_2O = diethyl ether, MeOH = methanol, THF = tetrahydrofuran, DMSO = dimethylsulfoxide, Et_3N = trimethylamine, MeCN = acetonitrile. (+)-JQ1-OH was prepared from commercial (+)-JQ1 according to literature precedent without modification.[191] N-boc-2-nitrobenzenesulfonamide (**SI-1**) was prepared according to literature precedent without modification.[192] 2-(3-(but-3-yn-1-yl)-3H-diazirin-3-yl)ethan-1-amine (**SI-12**) was prepared according to literature precedent.[193]

Synthesis of acyl silane 15a

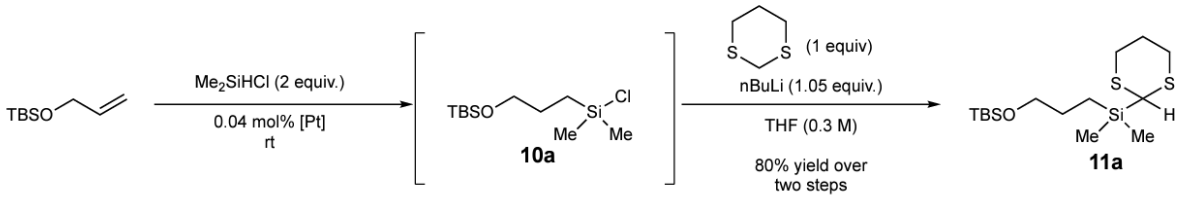

(3-((1,3-dithian-2-yl)dimethylsilyl)propoxy)(tert-butyl)dimethylsilane (11a): To an oven-dried Schlenk flask fitted with a rubber septum and cooled under N_2 was added platinum(0)-1,3-divinyl 1,1,1,3,3-tetramethyldisiloxane complex solution (Karstedt's catalyst) [0.1 M in vinyl terminated poly(dimethylsiloxane), ca 19 µL, 0.04 mol%] and Me_2SiHCl (9.3 mmol, 1.03 mL, 2.0 equiv.) by syringe drop-wise. After stirring at room temperature for 10 min, (allyloxy)(tert-butyl)dimethylsilane (4.65 mmol, 800 mg, 1.0 equiv.) was added dropwise over 15 min. After an additional 15 min stirring, the solution was cooled to 0 °C and evacuated under vacuum for 15 min to remove excess $ClSiMe_2H$. After purging with N_2 for an additional 15 min, silyl chloride **10a** was obtained (4.14 mmol, 1.09 g, 89% yield) and used immediately without further purification. **^{1}H NMR** (400.0 MHz, $CDCl_3$): δ 3.60 (t, J = 6.6 Hz, 2H), 1.67 – 1.58 (m, 2H), 0.90 (s, 9H), 0.86 – 0.79 (m, 2H), 0.42 (s, 6H), 0.06 (s, 6H). A flame dried 50 mL round bottom flask cooled under vacuum was charged with 1,3-dithiane (0.411 g, 3.42 mmol, 1.0 equiv.) and THF (9 mL, 0.3 M). The reaction vessel was cooled to –30 ˚C and a solution of *n*BuLi (2.2 M in hexanes, 1.64 mL, 3.59 mmol, 1.05 equiv.) was added dropwise. The solution was allowed to warm to room temperature and stir for 1 h before cooling to –78 ˚C and adding 1**0a** (1.2 equiv.) dropwise. The reaction mixture was allowed to warm to room temperature overnight and the resulting orange solution was quenched by addition of sat. aqueous NH_4Cl solution and extracted with Et_2O three times. The combined organic layers were washed with saturated brine, dried over MgSO4, and concentrated in vacuo. The residual 1,3-dithiane was removed by Kugelrohr distillation under full vacuum at 70–100 °C to give **11a** (1.04 g, 3.08 mmol, 90% yield) as a pale oil. **^{1}H NMR** (400.0 MHz, $CDCl_3$): δ 3.73 (s, 1H), 3.56 (t, J = 6.9 Hz, 2H), 2.91 – 2.83 (m, 2H), 2.74 – 2.68 (m, 2H), 2.15 – 2.08 (m, 1H), 2.05 – 1.95 (m, 1H), 1.61 – 1.52 (m, 2H), 0.89 (s, 9H) (overlap with m, 2H), 0.67 – 0.61 (m, 2H), 0.14 (s, 6H), 0.05 (s, 6H). **^{13}C NMR** (125 MHz, $CDCl_3$): δ 68.1, 66.1, 33.7, 31.3, 27.1, 26.4, 26.2, 18.5, 9.3, –4.8, –5.1. **HRMS** (ESI): calculated for $[C_{15}H_{34}OS_2Si_2+H]^+$ required m/z 351.1662, found m/z 351.1664.

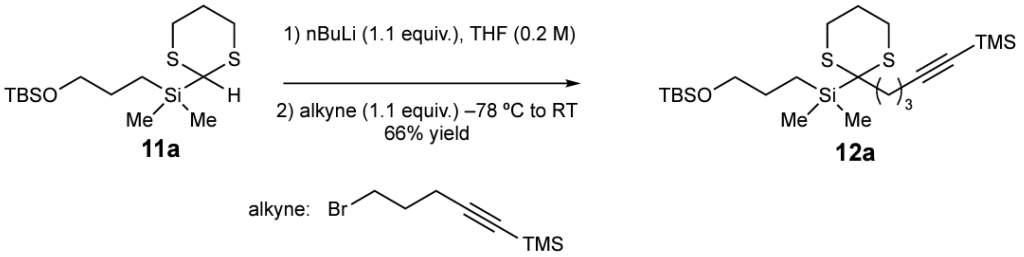

***tert*-butyl(3-(dimethyl(2-(5-(trimethylsilyl)pent-4-yn-1-yl)-1,3-dithian-2-yl)silyl)propoxy)dimethylsilane (12a)**: A flame dried 50 mL round bottom flask cooled under vacuum was charged with **11a** (840 mg, 2.5 mmol, 1.0 equiv.) and THF (5 mL, 0.2 M) and cooled to –30 ˚C, followed by the dropwise addition of *n*BuLi (2.2 M, 1.2 mL, 1.1 equiv.). After stirring for 45 min at –30 ˚C, a solution of (5-bromopent-1-yn-1-

yl)trimethylsilane (539 mg, 2.63 mmol, 1.1 equiv.) in THF (5 mL) was added dropwise. The reaction was then allowed to warm to room temperature and stir overnight. After 16 h, the reaction was quenched by the addition of sat. aqueous NH_4Cl and extracted with a 1:1 mixture of Et_2O/hexanes. The combined organics were washed with saturated brine, dried over $MgSO_4$, and concentrated to an oil. Purification of the crude material by flash column chromatography on silica gel in 95:5 hex/EtOAc yielded the desired product **12a** as a clear, colorless oil (817 mg, 66% yield). **^{1}H NMR** (500.0 MHz, $CDCl_3$): δ 3.57 (t, J = 7.0 Hz, 2H), 3.12 – 3.05 (m, 2H), 3.42 (dt, J = 14.3, 4.1 Hz, 2H), 2.39 – 2.33 (m, 2H), 2.30 (t, J = 6.7 Hz, 2H), 2.09–2.01 (m, 1H), 1.96 – 1.85 (m, 1H), 1.74 – 1.65 (m, 2H), 1.61 – 1.52 (m, 2H), 0.89 (s, 9H), 0.74 – 0.68 (m, 2H), 0.18 (s, 6H), 0.15 (s, 9H), 0.05 (s, 6H). **^{13}C NMR** (125.7 MHz, $CDCl_3$): δ 107.3, 85.2, 66.2, 38.9, 36.1, 27.5, 26.7, 26.1, 25.3, 23.3, 20.2, 18.5, 14.2, 9.3, 0.3, –4.4, –5.1. **HRMS** (ESI^+): calculated for $[C_{12}H_{48}OS_2Si_3+H]^+$ required m/z 489.2527, found m/z 489.2524.

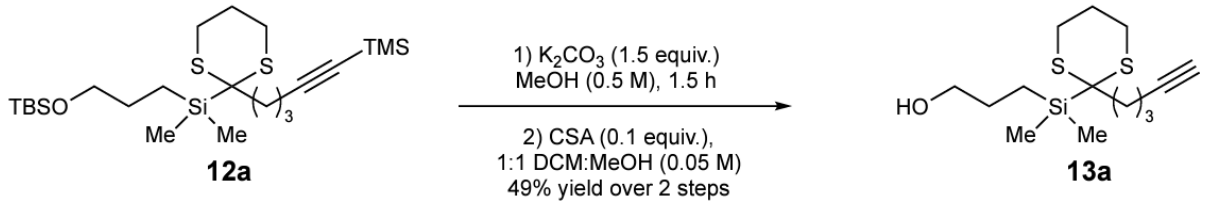

3-(dimethyl(2-(pent-4-yn-1-yl)-1,3-dithian-2-yl)silyl)propyl benzoate (13a): To a solution of **12a** (331 mg, 0.697 mmol, 1.0 equiv.) in MeOH (1.5 mL, 0.5 M) was added potassium carbonate (140 mg, 1.02 mmol, 1.5 equiv.). The reaction was monitored by TLC and after 4 h quenched by addition of sat. aqueous NH_4Cl, diluted with sat. aqueous brine, and extracted with Et_2O three times. The combined organic layers were dried over $MgSO_4$, filtered, and concentrated *in vacuo* to give a residue that was subsequently added to a solution of camphorsulfonic acid (15 mg, 0.068 mmol, 0.1 equiv.) in a 1:1 mixture of DCM:MeOH (0.05 M) and stirred at room temperature. After 3 h, the solution was diluted with 1:1 hex:EtOAc, washed with sat. aqueous $NaHCO_3$ and sat. aqueous brine, dried, filtered, and concentrated to an oil. Purification of the crude material by gradient elution of 10–30% EtOAc in hex by flash column chromatography gave **13a** (130 mg, 49% over two steps) as a clear oil. **^{1}H NMR** (600.1 MHz, CDCl3): δ 3.56 (t, J = 6.7 Hz, 2H), 3.05 – 2.97 (m, 2H), 2.38 (dt, J = 14.4, 3.7 Hz, 2H), 2.32 – 2.28 (m, 2H), 2.21 (td, J = 6.8, 2.7 Hz, 2H), 2.04 – 1.93 (m, 3H), 1.84 (ddq, J = 3.2, 3.2, 12.6 Hz, 1H), 1.70 – 1.63 (m, 2H), 1.61 – 1.54 (m, 2H), 0.75 – 0.68 (m, 2H), 0.14 (s, 6H). **^{13}C NMR** (150.9 MHz, $CDCl_3$): δ 84.13, 68.80, 65.42, 38.50, 36.20, 27.16, 26.47, 25.00, 23.21, 18.69, 9.25, –4.47. **HRMS** (ESI^+): calculated for $[C_{14}H_{26}OS_2Si+Na]^+$ required m/z 325.1087, found m/z 325.1089.

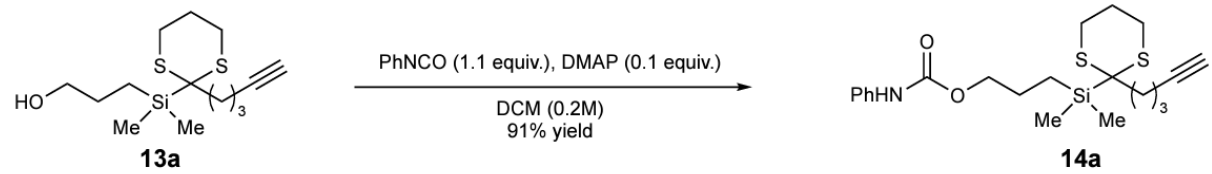

3-(dimethyl(2-(pent-4-yn-1-yl)-1,3-dithian-2-yl)silyl)propyl benzoate (14a): A flame-dried screw-capped culture tube cooled under vacuum was charged with **13a** (161 mg, 0.532 mmol, 1.0 equiv.) and DCM (2.66 mL, 0.2 M). Phenylisocyanate (64 mL, 0.585

mmol, 1.1 equiv.) and DMAP (6.5 mg, 0.053 mmol, 0.1 equiv.) were quickly added and the resulting mixture was stirred under N_2 at room temperature overnight. After 16 h, the resulting cloudy mixture was diluted with DCM, washed sequentially with sat. aqueous NH_4Cl, H_2O, and brine, dried over $MgSO_4$, filtered, and concentrated in vacuo to give **14a** (204 mg, 0.483 mmol, 91% yield) as a pale yellow oil which was used in the next step without further purification. **^{1}H NMR** (500.0 MHz, $CDCl_3$): δ 7.41 – 7.36 (m, 2H), 7.3 (t, *J* = 7.5 Hz, 2H), 7.05 (tt, *J* = 1.2, 7.5 Hz, 1H), 4.14 (t, *J* = 6.8 Hz, 2H), 3.07 (ddd, *J* = 2.7, 12.5, 14.7 Hz, 2H), 2.44 (ddd, J = 2.7 2.7, 14.3 Hz, 2H), 2.38 – 2.34 (m J = 3.7, 5.0, 7.9 Hz, 2H), 2.27 (ddd, *J* = 2.7, 6.7, 6.7 Hz, 2H), 2.09 – 2.02 (m, 1H), 2.00 (t, *J* = 2.5 Hz, 1H), 1.90 (ddq, *J* = 3.3, 3.3, 12.7 Hz, 1H), 1.80 – 1.69 (m, 4H), 0.85 – 0.80 (m, 2H), 0.21 (s, 6H).

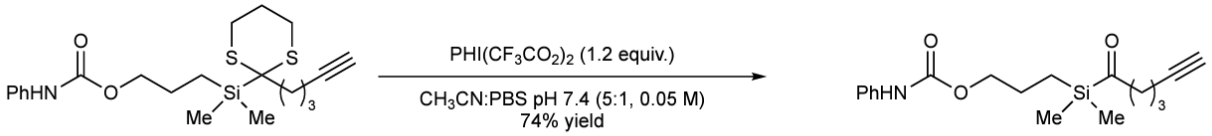

14a **15a**

3-(hex-5-ynoyldimethylsilyl)propyl phenylcarbamate (15a) A flame-dried scintillation vial was charged with 14a (138 mg, 0.328 mmol 1.0 equiv.) and a 5:1 solution of MeCN:PBS 7.4 buffer (0.05 M, 6 mL). To the rapidly stirred mixture was added PIFA (169 mg, 0.393 mmol, 1.2 equiv.), and the resulting solution was allowed to stir at room temperature. After 2 h, the mixture was diluted with Et_2O, washed sequentially with sat. aqueous NH_4Cl, H_2O, and brine, dried over $MgSO_4$, filtered, and concentrated *in vacuo*. The crude material was purified using flash column chromatography (hex:EtOAc 90:10) to give acyl silane **15a** (80 mg, 74% yield) as a colorless clear oil. **^{1}H NMR** (600.1 MHz, $CDCl_3$): δ 7.48 – 7.36 (m, 2H), 7.30 (t, *J* = 7.6 Hz, 2H), 7.06 (t, *J* = 7.2 Hz, 1H), 6.68 (br. s, 1H), 4.12 (t, *J* = 6.6 Hz, 2H), 2.77 (t, *J* = 7.1 Hz, 2H), 2.20 (dt, *J* = 2.6, 6.8 Hz, 2H), 1.93 (t, *J* = 2.6 Hz, 1H), 1.75 (ddd, *J* = 7.0, 7.0, 13.9 Hz, 2H), 1.73 – 1.68 (m, 2H), 0.82 – 0.77 (m, 2H), 0.23 (s, 6H). **^{13}C NMR** (150.9 MHz, $CDCl_3$): δ 247.3, 153.6, 138.1, 129.2, 123.5, 118.8, 83.9, 69.1, 67.3, 47.2, 23.4, 20.8, 17.9, 10.0, –4.6. **HRMS** (ESI^+): calculated for $[C_{18}H_{25}NO_3Si+Na]^+$ required m/z 354.1496, found m/z 354.1499.

Synthesis of acyl silane 15b

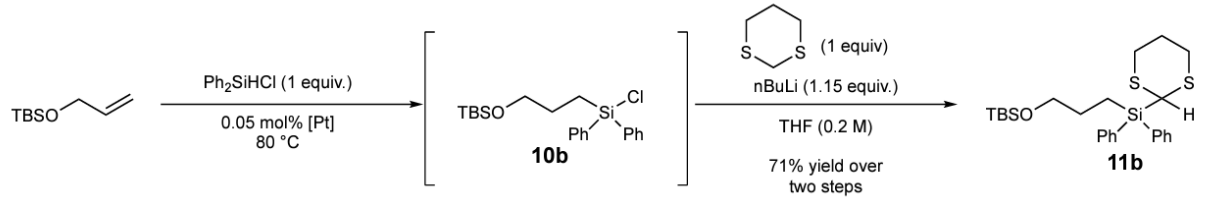

(3-((1,3-dithian-2-yl)diphenylsilyl)propoxy)(tert-butyl)dimethylsilane (11b): To an oven-dried Schlenk flask fitted with a rubber septum and cooled under N_2 was added platinum(0)-1,3-divinyl 1,1,1,3,3-tetramethyldisiloxane complex solution (Karstedt's catalyst) [0.1 M in vinyl terminated poly(dimethylsiloxane), ca 15 µL, 0.05 mol%] and Ph_2SiHCl (0.6 mL, 3.09 mmol, 1 equiv.) by syringe drop-wise. The resulting solution was stirred for 10 min at room temperature, then (allyloxy)(tertbutyl)dimethylsilane (0.531 g, 3.09 mmol, 1 equiv.) was added as a neat liquid by syringe and the solution was heated in an 80 °C oil bath for 25 min. After cooling to room temperature, the reaction mixture

(10b) was used immediately in the next step without further purification. **^{1}H NMR** (400 MHz, $CDCl_3$): δ 7.66 – 7.60 (m, 4H), 7.47 – 7.39 (m, 6H), 3.61 (t, *J* = 6.4 Hz, 2H), 1.76 – 1.66 (m, 2H), 1.42 – 1.35 (m, 2H), 0.89 (s, 9H), 0.03 (s, 6H). A flame dried 50 mL round bottom flask cooled under vacuum was charged with 1,3-dithiane (0.312 g, 2.6 mmol, 1.0 equiv.) and THF (13 mL, 0.2 M). The reaction vessel was cooled to –30 ˚C and a solution of *n*BuLi (2.99 mmol, 1.15 equiv.) was added dropwise. The solution was allowed to warm to room temperature and stir for 1 h before cooling to –78 ˚C and adding **10b** (1.2 equiv.) dropwise. The reaction mixture was allowed to warm to room temperature overnight and the resulting orange solution was quenched by addition of sat. aqueous NH_4Cl solution and extracted with EtOAc three times. The combined organic layers were washed with saturated brine, dried over MgSO4, and concentrated in vacuo. The resulting oil was purified using flash column chromatography (hex:EtOAc 95:5) to give **11b** (0.894 g, 1.84 mmol, 71% over two steps) as an oil. **^{1}H NMR** (300.1 MHz, $CDCl_3$): δ 7.70 – 7.63 (m, 4H), 7.46 – 7.34 (m, 6H), 4.25 (s, 1H), 3.60 (t, *J* = 6.6 Hz, 2H), 2.92 (ddd, *J* = 3.3, 11.6, 14.3 Hz, 2H), 2.71 (dt, J = 14.1, 3.7 Hz, 2H), 2.16 – 1.99 (m, 2H), 1.74 – 1.61 (m, 2H), 1.32 – 1.23 (m, 2H), 0.89 (s, 9H), 0.03 (s, 6H). **^{13}C NMR** (125.7 MHz, $CDCl_3$): δ 135.8, 132.5, 130.0, 127.9, 65.8, 32.6, 31.8, 27.1, 26.15, 26.10, 22.15, 18.5, 7.5, –5.1 **HRMS** (ESI^+): calculated for $[C_{25}H_{38}OS_2Si_2+Na]^+$ required m/z 497.1795, found m/z 497.1792.

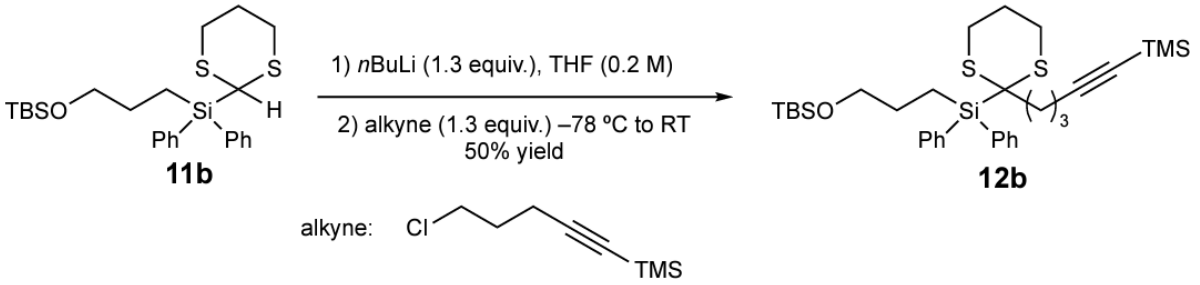

tert-butyl(3-(diphenyl(2-(5-(trimethylsilyl)pent-4-yn-1-yl)-1,3-dithian-2-yl)silyl)propoxy)dimethylsilane (12b): A flame dried 50 mL round bottomed flask cooled under vacuum was charged with **11b** (0.500 g, 1.05 mmol, 1.0 equiv.) and THF (5.27 mL, 0.2 M) and cooled to –78 ˚C, followed by the dropwise addition of *n*BuLi (2.4 M, 0.57 mL, 1.3 equiv.). After stirring for 5 min at –78 ˚C, the reaction was allowed to warm to room temperature over an hour, then returned to –78 ˚C prior to the dropwise addition of (5-chloropent-1-yn-1-yl) trimethylsilane (0.239 g, 1.37 mmol, 1.3 equiv.). The reaction was then allowed to warm to room temperature and stir overnight. After 16 h, the reaction was quenched by the addition of sat. aqueous NH_4Cl and extracted with a 1:1 mixture of Et_2O/hexanes. The combined organics were washed with saturated brine, dried over $MgSO_4$, and concentrated to an oil. Purification of the crude material by flash column chromatography on silica gel in 95:5 hex/EtOAc yielded the desired product **12b** as a clear, colorless oil (0.333 g, 50% yield). **^{1}H NMR** (500.0 MHz, $CDCl_3$): δ 7.81 (br.d *J* = 7 Hz, 4H), 7.46 – 7.31 (m, 6H), 3.53 (t, *J* = 6.0 Hz, 2H), 3.14 – 3.05 (m, 2H), 2.47 – 2.40 (m, 2H), 2.30 – 2.25 (m, 2H), 2.09 (t, *J* = 6.6 Hz, 2H), 1.60 – 1.53 (m, 2H), 1.48 – 1.42 (m, 2H), 1.41 – 1.35 (m, 2H), 1.34 – 1.24 (m, 2H), 0.87 (s, 9H), 0.12 (s, 9H), 0.0 (s, 6H). **^{13}C NMR** (125.7 MHz, $CDCl_3$): δ 136.57, 132.52, 129.81, 127.68, 107.27, 84.89, 65.71, 39.69, 36.44, 27.57, 26.42, 26.09, 25.38, 24.98, 23.93, 18.44, 7.66, 0.27, –5.14. **HRMS** (ESI^+): calculated for $[C_{33}H_{52}OS_2Si_3+H]^+$ required m/z 613.2840, found m/z 613.2838.

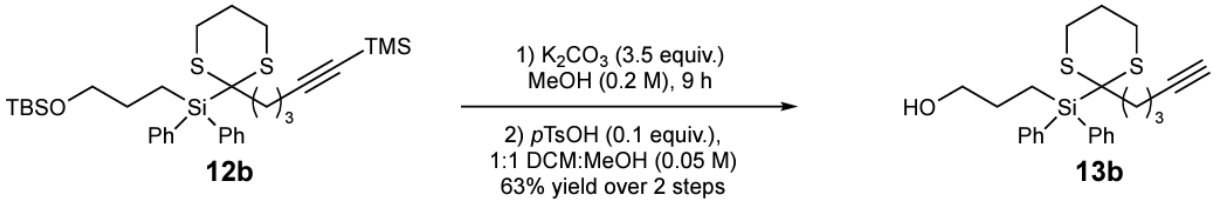

3-((2-(pent-4-yn-1-yl)-1,3-dithian-2-yl)diphenylsilyl)propan-1-ol (13b): A flame dried scintillation vial was charged with **12b** (0.436 g, 0.711 mmol, 1 equiv.), K_2CO_3 (146 mg, 1.06 mmol, 1.5 equiv.) and MeOH (1.5 mL, 0.5 M) and stirred rapidly. Partial conversion was observed by TLC after workup following 6 h of stirring, at which point the material was charged with an additional batch of K_2CO_3 (278 mg, 2.0 equiv) and MeOH (3mL), until full consumption of **12b** was observed by TLC, approximately 3 h. The reaction was transferred to a separatory funnel with Et_2O and hexanes, washed with water, dried over $MgSO_4$, and concentrated. The crude material was then transferred to a scintillation vial charged with *p*-toluenesulfonic acid (13 mg, 0.075 mmol, 0.1 equiv.) and a 1:1 solution of DCM:MeOH (0.05 M, 14 mL). After stirring for 4 h, the solution was diluted with EtOAc, washed sequentially with sat. aqueous NH_4Cl, H_2O, and brine, dried over $MgSO_4$, filtered, and concentrated in vacuo to give **13b** (191 mg, 0.448 mmol, 63% yield over two steps) as a viscous oil. **^{1}H NMR** (500.0 MHz, $CDCl_3$): δ 7.80 (app d, J = 7.5 Hz, 4H), 7.45 – 7.35 (m, 6H), 3.57 (t, J = 6.4 Hz, 2H), 3.07 (ddd, J = 3.1, 12.0, 14.7 Hz, 2H), 2.45 (dt, J = 14.4, 3.8 Hz, 2H), 2.30 – 2.26 (m, 2H), 2.08 – 2.01 (m, 2H), 2.07 – 1.93 (m, 2H), 1.88 (t, J = 2.5 Hz, 1H), 1.64 – 1.56 (m, 2H), 1.55 – 1.47 (m, 2H), 1.46 – 1.40 (m, 2H). **^{13}C NMR** (125.7 MHz, $CDCl_3$): δ 136.48, 132.22, 129.84, 127.68, 84.12, 68.63, 65.51, 39.49, 36.64, 27.56, 26.42, 24.80, 23.94, 18.56, 7.72. **HRMS** (ESI^+): calculated for $[C_{24}H_{30}OS_2Si+Na]^+$ required m/z 449.1400, found m/z 449.1396.

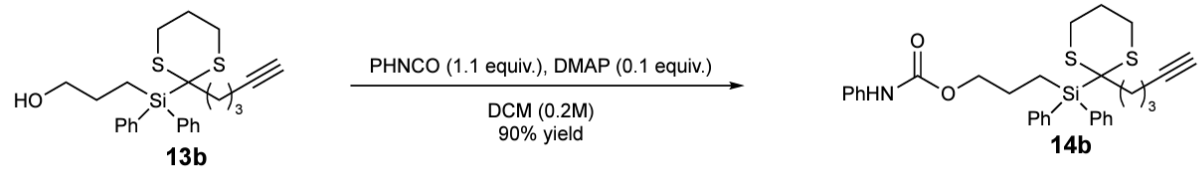

3-((2-(pent-4-yn-1-yl)-1,3-dithian-2-yl)diphenylsilyl)propyl benzoate (14b): A flame-dried screw-capped culture tube cooled under vacuum was charged with **13b** (156.4 mg, 0.36 mmol, 1.0 equiv.) and DCM (0.91 mL, 0.2 M). Phenylisocyanate (43 mL, 0.40 mmol, 1.1 equiv.) and DMAP (4.4 mg, 0.036 mmol, 0.1 equiv.) were quickly added and the resulting mixture was stirred under N_2 at room temperature overnight. After 16 h, the resulting cloudy mixture was diluted with DCM, washed sequentially with sat. aqueous NH_4Cl, H_2O, and brine, dried over $MgSO_4$, filtered, and concentrated in vacuo to give **14b** (178.6 mg, 0.327 mmol, 90% yield) as a crude white solid which was used in the next step without further purification. **^{1}H NMR** (400.1 MHz, $CDCl_3$): δ 7.80 (d, J = 7.0 Hz, 4H), 7.48 – 7.28 (m, 10H), 7.09 – 7.02 (m, 1H), 6.55 (br. s, 1H), 4.10 (t, J = 6.5 Hz, 2H), 3.14 – 3.02 (m, 2H), 2.48 (dt, J = 14.1, 2.6 Hz, 2H), 2.34 – 2.26 (m, 2H), 2.08 – 2.03 (m, 2H), 1.88 (t, J = 2.7 Hz, 1H), 1.70 – 1.54 (m, 6H), 1.50 – 1.44 (m, 2H).

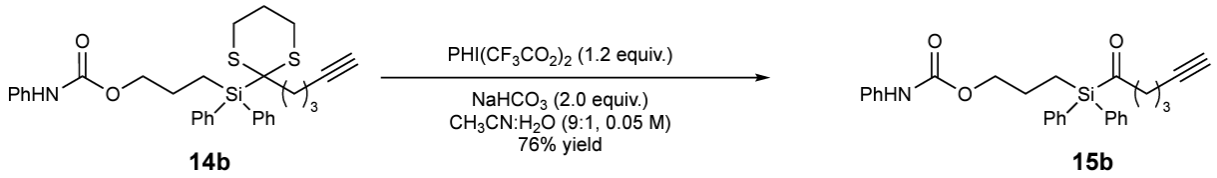

14b **15b**

3-(hex-5-ynoyldiphenylsilyl)propyl phenylcarbamate (15b): A flame-dried scintillation vial was charged with **14b** (17 mg, 0.037 mmol 1.0 equiv.), $NaHCO_3$ (6.2 mg, 0.075 mmol, 2.0 equiv.), and 9:1 solution of $MeCN:H_2O$ (700:75 uL, 0.05 M). To the rapidly stirred mixture was added PIFA (19 mg, 0.045 mmol, 1.2 equiv.), and the resulting orange solution was allowed to stir at room temperature. After 2 h, the mixture was diluted with Et_2O, washed sequentially with sat. aqueous NH_4Cl, H_2O, and brine, dried over $MgSO_4$, filtered, and concentrated in vacuo. The crude material was purified using flash column chromatography (hex:EtOAc 95:5) to give **15b** (13 mg, 76% yield) as a pale yellow oil. **^{1}H NMR** (600.1 MHz, $CDCl_3$): δ 7.58 (br. d, J = 7.0 Hz, 4H), 7.46 (tt, J = 6.4, 1.4 Hz, 2H), 7.40 (app. t, J = 7.5 Hz, 4H), 7.35 (br. d, J = 7.5 Hz, 2H), 7.30 (tt, J = 7.3, 2.0 Hz, 2H), 7.05 (t, J = 7.2 Hz, 1H), 6.54 (br. s, 1H), 4.14 (dd, J = 6.5 Hz, 2H), 2.78 (t, J = 7.0 Hz, 2H), 2.12 (td, J = 7.0, 2.6 Hz, 2H), 1.87 (t, J = 2.6 Hz, 1H), 1.82 – 1.76 (m, 2H), 1.71 (ddd, J = 13.9, 7.0, 7.0 Hz, 2H), and 1.38 – 1.33 (m, 2H). **^{13}C NMR** (150.9 MHz, $CDCl_3$): δ 243.76, 187.88, 137.58, 135.38, 131.35, 130.34, 129.04, 128.37, 123.38, 83.67, 68.94, 48.23, 29.72, 23.12, 20.81, 17.70, and 7.83. **HRMS** (ESI^+): calculated for $[C_{28}H_{29}NO_3Si+Na]^+$ required m/z 478.1809, found m/z 478.1819.

Synthesis of acyl silane 15c

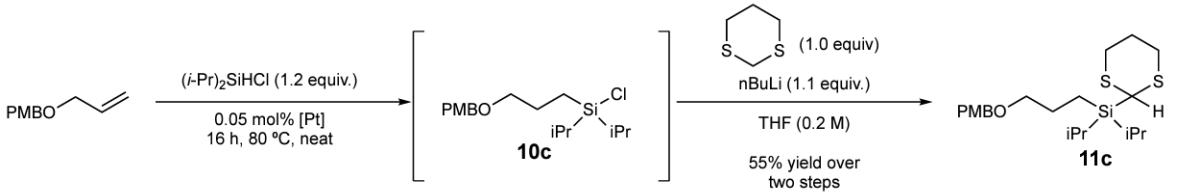

(1,3-dithian-2-yl)diisopropyl(3-((4-methoxybenzyl)oxy)propyl)silane (11c): To an oven-dried Schlenk flask fitted with a rubber septum and cooled under N_2 was added platinum(0)-1,3-divinyl 1,1,1,3,3-tetramethyldisiloxane complex solution (Karstedt's catalyst) [0.1 M in vinyl terminated poly(dimethylsiloxane), ca 150 µL, 0.05 mol%] and *i*Pr_2SiHCl (4.5 g, 30 mmol, 1.0 equiv.) by syringe dropwise. The resulting yellow solution was stirred for 10 min at room temperature, then 1((allyloxy)methyl)-4-methoxybenzene (9c, 4.92 g, 30 mmol, 1.0 equiv.) was added as a neat liquid by syringe. The vessel was heated to 80 ˚C in an oil bath for 16 h. After cooling to room temperature, the reaction mixture (**10c**) was used immediately in the next step without further purification. **^{1}H NMR**: (300.1 MHz, $CDCl_3$) δ 7.27 (d, 2H, J = 8.7 Hz), 6.90 (d, 2H, J = 8.7 Hz), 4.45 (s, 2H), 3.82 (s, 3H), 3.44 (t, 2H, J = 6.7 Hz), 1.79–1.69 (m, 2H), 1.11 – 1.06 (m, 14H), 0.89 – 0.83 (m, 2H). A flame dried 250 mL round bottom flask cooled under vacuum was charged with 1,3-dithiane (2.57 g, 21.4 mmol, 1.0 equiv.) and THF (70 mL, 0.3 M). The reaction vessel was cooled to –30 ˚C and a solution of *n*BuLi (2.4 M in hexanes, 9.83 mL, 23.6 mmol, 1.1 equiv.) was added dropwise resulting in a persistent, but faint yellow color. The solution was maintained at –30 ˚C for 1 h before cooling to –78 ˚C and adding 10c (1.2 equiv.) as a solution in THF (10 mL) dropwise. The reaction mixture was allowed to warm to room

temperature overnight and then quenched by addition of 200 mL sat. aqueous NH_4Cl solution and extracted with a 1:1 mixture of Et_2O/hex (3x, 100 mL). The combined organic layers were washed with saturated brine, dried over MgSO4, and concentrated in vacuo. The resulting residue was purified by flash column chromatography on silica gel in 95:5 hex/EtOAc to yield a clear, colorless oil (4.84 g, 55% yield). **^{1}H NMR**: (500.0 MHz, $CDCl_3$) δ 7.29 (d, *J* = 8.5 Hz 2H), 6.89 (d, *J* = 8.6 Hz,2H), 4.47 (s, 2H), 3.91 (s, 1H) 3.81 (s, 3H), 3.44 (t, *J* = 7.0 Hz, 2H), 2.90 (ddd, *J* = 14.7, 12.2, 2.8, 2H), 2.71 (dt, *J* = 13.8, 3.9 Hz, 2H), 2.16 – 2.00 (m, 2H), 1.83 – 1.76 (m, 2H), 1.26 – 1.17 (m, 2H), 1.14 (d, *J* = 7.4 Hz, 6H), 1.13 (d, *J* = 7.0 Hz, 6H), 0.77 – 0.72 (m, 2H). **^{13}C NMR** (125.7 MHz) δ 159.1, 130.8, 129.3, 113.8, 73.3, 72.5, 55.3, 32.1, 31.9, 26.6, 24.2, 18.59, 18.56, 11.0, 5.1. **HRMS** (ESI^+): calculated for $[C_{21}H_{36}O_2S_2Si+Na]^+$ required m/z 435.1823, found m/z 435.1829.

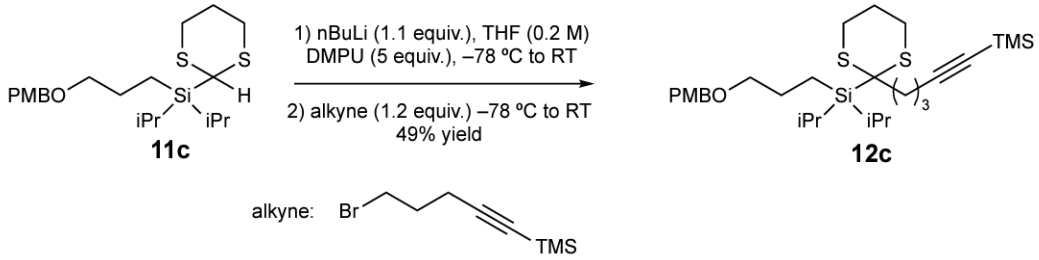

(5-(2-(diisopropyl(3-((4-methoxybenzyl)oxy)propyl)silyl)-1,3-dithian-2-yl)pent-1-yn-1-yl)trimethylsilane (12c): A flame dried 100 mL round bottom flask cooled under vacuum was charged with **11c** (1.95 g, 4.73 mmol, 1.0 equiv.) and THF (24 mL, 0.2 M) and cooled to –78 ˚C, followed by the dropwise addition of *n*BuLi (2.4 M, 2.27 mL, 1.1 equiv.). After stirring for 5 min at –78 ˚C, the reaction was allowed to warm to room temperature over an hour, resulting in an orange solution that was then returned to –78 ˚C prior to the addition of anhydrous DMPU (2.7 mL, 23.7 mmol, 5 equiv.) and (5-bromopent-1-yn-1-yl) trimethylsilane (1.24 g, 5.66 mmol, 1.2 equiv.). The reaction was then allowed to warm to room temperature and stir overnight. After 16 h, the reaction was quenched by the addition of 100 mL sat. NH_4Cl and extracted with a 1:1 mixture of Et_2O/hexanes (3x50 mL). The combined organics were washed with saturated brine, dried over $MgSO_4$, filtered, and concentrated to an oil. Purification of the crude material by flash column chromatography on silica gel in 95:5 hex/EtOAc yielded the desired product as a clear, colorless oil (1.29 g, 49% yield). **^{1}H NMR** (500.0 MHz, $CDCl_3$) δ 7.28 (d, *J* = 9.2 Hz, 1H), 6.88 (d, *J* = 8.8 Hz, 1H), 4.45 (s, 2H), 3.81 (s, 3H), 3.42 (t, *J* = 6.9 Hz, 2H), 3.14 (ddd, *J* = 14.3, 11.8, 2.7 Hz, 2H), 2.49 – 2.44 (m, 2H), 2.38 (dt, *J* = 14.1, 3.5 Hz, 2H), 2.33 (t, *J* = 6.5 Hz, 2H), 2.07 – 2.00 (m, 1H), 1.99 – 1.89 (m, 1H), 1.87 – 1.80 (m, 1H), 1.80 – 1.73 (m, 2H), 1.37 (hept, *J* = 7.5 Hz, 2H), 1.19 (d, *J* = 7.2, 6H), 1.18 (d, *J* = 7.5, 6H), 0.16 (s, 9H). **^{13}C NMR** (125.7 MHz, $CDCl_3$) δ 159.2, 131.0, 129.4, 113.9, 107.3, 85.2, 73.5, 72.5, 55.4, 40.5, 36.9, 26.9, 25.2, 25.0, 23.8, 20.2, 19.8, 19.8, 12.3, 6.4, 0.3. **HRMS** (ESI^+) calculated for $[C_{29}H_{50}O_2S_2Si_2+Na]^+$ required m/z 573.2683, found m/z 573.2686.

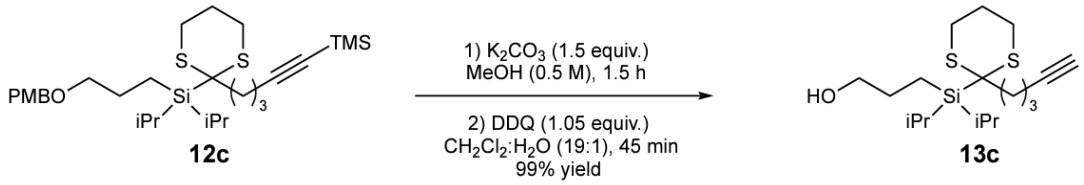

3-(diisopropyl(2-(pent-4-yn-1-yl)-1,3-dithian-2-yl)silyl)propan-1-ol (13c): A flame dried 25 mL round bottom flask was charged with **5** (1.29 g, 2.24 mmol, 1 equiv.), K_2CO_3 (464 mg, 3.36 mmol, 1.5 equiv.) and MeOH (5 mL, 0.5 M) and stirred rapidly until full consumption of **5c** was observed by TLC, approximately 1.5 h. The reaction was transferred to a separatory funnel with Et_2O, washed with water, dried over $MgSO_4$, and concentrated. The crude product was transferred to a 25 mL round bottom flask and dissolved in a mixture of CH_2Cl_2:H_2O (19:1, 12 mL). To the stirred solution was added DDQ (497 mg, 2.19 mmol, 1.05 equiv.) resulting in a dark purple color. After stirring for 45 min, the reaction was quenched by the addition of sat. $NaHCO_3$ sol. and filtered through a short pad of Celite washing with CH_2Cl_2. The filtrate was washed with water, brine, dried over $MgSO_4$, and concentrated to a colored oil. The crude material was purified by a gradient column (9:1 to 8:2 hex:EtOAc) to yield the desired product as a clear, colorless oil (735 mg, 99% yield). **^{1}H NMR** (300.1 MHz, $CDCl_3$): δ 3.60 (t, J = 6.7 Hz, 2H), 3.09 (ddd, 14.9, 12.7, 3.0 Hz, 2H), 2.45 – 2.42 (m, 2H), 2.38 (dt, J = 14.3, 3.9 Hz, 2H), 2.28 (td, J = 6.74, 2.70, 2H), 2.05 – 2.02 (m, 1H), 1.99 (t, J = 2.63 Hz, 1H), 1.96 – 1.88 (m, 1H), 1.821.75 (m, 4H), 1.67 (br. s, 1H) 1.39 – 1.33 (m, 2H), 1.18 – 1.16 (m, 12H), 0.85 – 0.82 (m, 2H). **^{13}C NMR** (125.7 MHz, $CDCl_3$): δ 84.3, 69.0, 66.1, 40.4, 37.2, 28.0, 27.0, 25.1, 23.9, 19.8, 19.7, 18.8, 12.3, 6.1. HRMS (ESI+) calculated for $[C_{18}H_{34}OS_2Si+Na]^+$ required m/z 381.1740 , found m/z 381.1712.

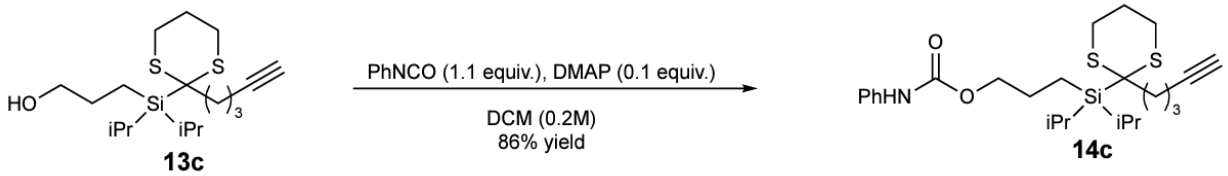

3-(diisopropyl(2-(pent-4-yn-1-yl)-1,3-dithian-2-yl)silyl)propyl phenylcarbamate (14c): A flame-dried culture tube cooled under vacuum was charged with **13c** (65 mg, 0.18 mmol, 1.0 equiv.) and DCM (0.91 mL, 0.2 M). Phenylisocyanate (22 mL, 0.20 mmol, 1.1 equiv.) and DMAP (2.2 mg, 0.018 mmol, 0.1 equiv.) were quickly added and the resulting mixture was stirred under N_2 at room temperature overnight. After 16 h, the resulting cloudy mixture was diluted with DCM, washed sequentially with sat. aqueous NH_4Cl, H_2O, and brine, dried over $MgSO_4$, filtered, and concentrated in vacuo to give **14c** (74.2 mg, 0.155 mmol, 86% yield) as a crude white solid which was used in the next step without further purification. **^{1}H NMR** (400.0 MHz, $CDCl_3$): 7.41 – 7.36 (m, 2H), 7.33 – 7.28 (m, 2H), 7.09 – 7.03 (m, 1H), 6.61 (br. s, 1H), 4.14 (t, J = 6.7 Hz, 2H), 3.15 – 3.05 (m, 2H), 2.49 – 2.35 (m, 4H), 2.29 (dt, J = 2.7, 6.7 Hz, 2H), 2.08 – 2.00 (m, 2H), 1.97 – 1.88 (m, 2H), 1.84 – 1.75 (m, 2H), 1.43 – 1.33 (m, 2H), 1.21 – 1.16 (m, 12 H), 0.92 – 0.85 (m, 2H).

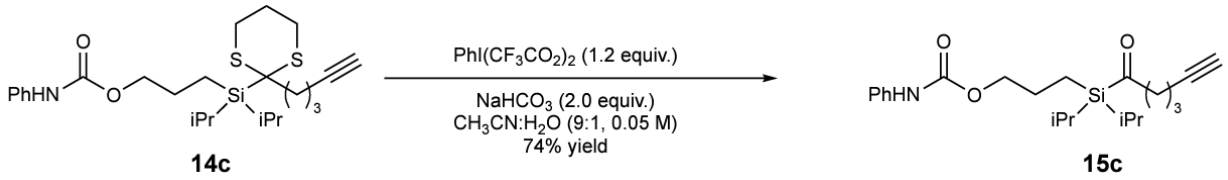

14c **15c**

3-(hex-5-ynoyldiisopropylsilyl)propyl phenylcarbamate (15c): A flame-dried scintillation vial was charged with **14c** (9 mg, 0.023 mmol, 1.0 equiv.), $NaHCO_3$ (3.9 mg, 0.047 mmol, 2.0 equiv.), and a solution of MeCN:H_2O (9:1, 0.05 M, 0.5 mL). To the rapidly stirred mixture was added PIFA (12 mg, 0.028 mmol, 1.2 equiv.), and the resulting yellow solution was allowed to stir at room temperature. After 30 min, the mixture was diluted with Et_2O, washed sequentially with sat. aqueous NH_4Cl, H_2O, and brine, dried over $MgSO_4$, filtered, and concentrated in vacuo. The crude material was purified using flash column chromatography (hex:EtOAc 95:5) to give acylsilane **15c** (6.7 mg, 0.017 mmol, 74% yield) as a clear solid. **^{1}H NMR** (500.0 MHz, $CDCl_3$): 7.42 – 7.34 (m, 2H), 7.33-7.28 (m, 2H), 7.06 (t, *J* = 7.3 Hz, 1H), 6.62 (br. s, 1H), 4.14 (t, *J* = 6.7 Hz, 2H), 2.73 (t, *J* = 7.0 Hz, 2H), 2.20 (dt, *J* = 6.9, 2.7 Hz, 2H), 1.95 (t, *J* = 2.7 Hz, 1H), 1.80 – 1.72 (m, 4H), 1.28 – 1.17 (m, 2H (overlap with EtOAc)), 1.09 – 1.04 (m, 12H), 0.88 – 0.83 (m, 2H). **^{13}C NMR** (125.7 MHz, $CDCl_3$): 137.9, 135.4, 129.1, 128.4, 123.4, 83.7, 69.0, 67.6, 49.3, 23.5, 20.4, 18.2, 18.1, 17.8, 10.6, 4.7. **HRMS** (ESI^+): calculated for $[C_{22}H_{33}NO_3Si+Na]^+$ required m/z 410.2122, found m/z 410.2126.

Synthesis of acyl silane (+)-JQ1 probes

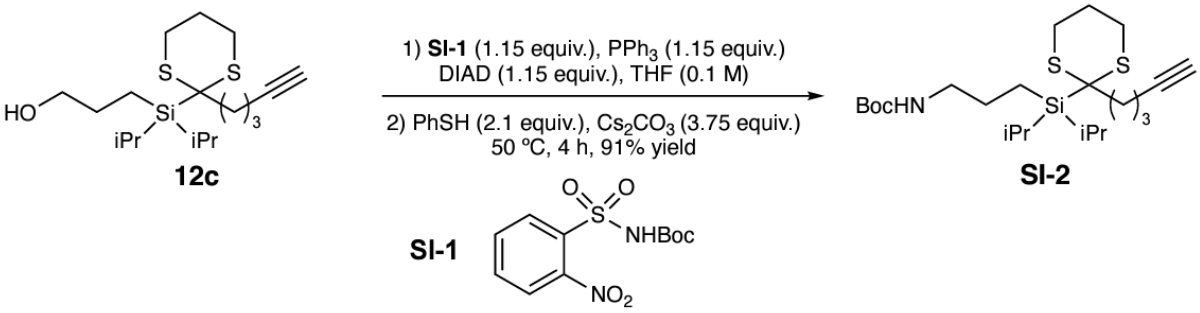

12c **SI-2**

SI-1

***tert*-butyl (3-(diisopropyl(2-(pent-4-yn-1-yl)-1,3-dithian-2-yl)silyl)propyl)carbamate (SI-2):** A 10 mL flame dried round bottom flask cooled under vacuum was charged with **13c** (100 mg, 0.280 mmol, 1 equiv.), N-boc-2-nitrobenzenesulfonamide (**SI-1**, 100 mg, 0.32 mmol, 1.15 equiv., prepared according to literature[192], triphenyl phosphine (84 mg, 0.32 mmol, 1.15 equiv.), and DIAD (63 µL, 0.32 mmol, 1.15 equiv.) in THF (0.1 M). The mixture was stirred for 16 h before the addition of thiophenol (60 µL, 0.588 mmol, 2.1 equiv.) and Cs_2CO_3 (340 mg, 1.05 mmol, 3.75 equiv.). The reaction was heated to 50 ˚C and vigorously stirred for 4 h before cooling to room temperature. The reaction was quenched by the addition of 5 mL 0.5 M NaOH (5 mL) and extracted with Et_2O (3 x 10 mL). The combined organic layers were washed with brine, dried over $MgSO_4$ before concentrating to an oil. Purification of the crude product by flash chromatography by gradient elution of 9:1 to 8:2 hex:EtOAc yield the N-Boc protected amine (115 mg, 91% yield). The product appears faintly on TLC under UV, but presents as a significant dark band upon heating in *p*-anisaldehyde stain. **^{1}H NMR:** (500.0 MHz, $CDCl_3$) δ 4.64 (bs, 1H), 3.10 (apparent t, *J* = 13.2 Hz, 2H) 2.45 – 2.41 (m, 2H), 2.38 (dt, *J* = 14.3, 3.74 Hz, 2H,),

2.28 (td, *J* = 6.7, 2.6 Hz, 2H), 2.06 – 2.02 (m, 1H), 2.34 (t, *J* = 2.34 Hz, 1H), 1.96–1.88 (m, 1H), 1.81 – 1.75 (m, 2H), 1.74 – 1.67 (m, 2H), 1.44 (s, 9H), 1.34 (hept, *J* = 7.4 Hz, 1H) 1.17 (d, *J* = 7.4 Hz, 6H), 1.16 (d, *J* = 7.6 Hz, 6H), 0.83 – 0.79 (m, 2H). **^{13}C NMR** (125.7 MHz, $CDCl_3$) δ 156.1, 84.3, 79.0, 69.1, 44.1, 40.3, 37.3, 28.6, 27.0, 25.1, 23.9, 19.8, 19.7, 18.9, 12.3, 7.5. **HRMS** (ESI$^+$) calculated for $[C_{23}H_{43}NO_2S_2Si+H]^+$ required m/z 458.2577, found m/z 458.2609.

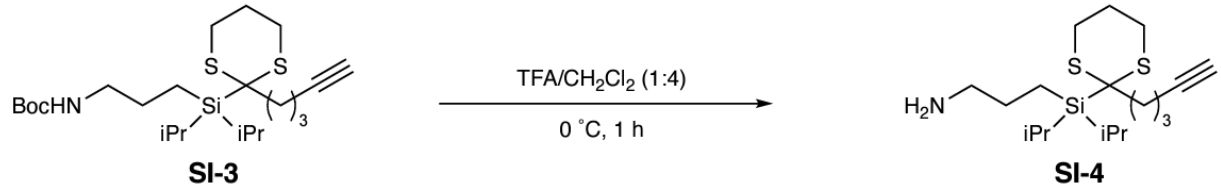

SI-3 **SI-4**

Amine linker SI-4: N-Boc protected amine **SI-3** (91 mg, 0.200 mmol, 1 equiv.) was dissolved in DCM (1 mL, 0.2 M) and cooled to 4 °C before adding TFA (0.25 mL). After 1 h, the reaction was complete by TLC and concentrated, diluted with Et_2O and washed with 1 N NaOH. The organic layer was concentrated to a yellow oil and immediately used in the next reaction without further purification (crude mass 70 mg, crude yield 98%).

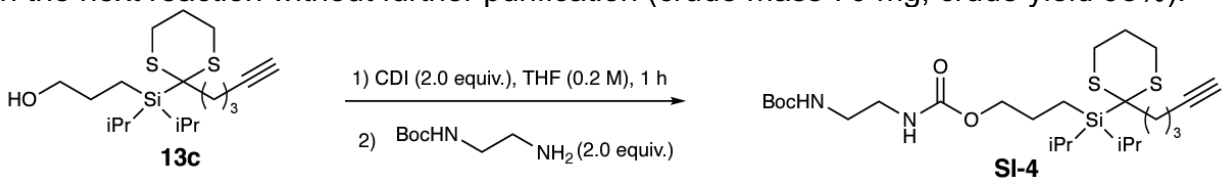

13c **SI-4**

N-Boc protected amine linker SI-4: A 1 dram vial was charged with **13c** (50 mg, 0.140 mmol, 1.0 equiv.), THF (0.7 mL, 0.2 M), and CDI (45 mg, 0.280 mmol, 2.0 equiv) and stirred at ambient temperature for 1 h. Subsequently, N-boc-ethylenediamine (67 mg, 0.420 mmol, 3.0 equiv.) and DMAP (51 mg, 0.420 mmol, 3.0 equiv.) were added. The reaction was stirred overnight before diluting with water and extracting the mixture with EtOAc. The organic extract was washed with brine, dried over $MgSO_4$, filtered, and concentrated in vacuo. The crude residue was purified by flash chromatography of EtOAc in hexanes to yield **SI-4** (67 mg, 88% yield). **^{1}H NMR** (500.0 MHz, $CDCl_3$) δ 5.11 (s, 1H), 4.93 (s, 1H), 4.00 (t, *J* = 6.1 Hz, 2H) 3.26 – 3.24 (m, 4H), 3.09 (td, *J* = 14.9, 12.8, 2.7 Hz, 2H), 2.45 – 2.40 (m, 2H) 2.38 (dt, *J* = 14.2, 3.7 Hz, 2H), 2.28 (td, *J* = 6.7, 2.7 Hz, 2H), 2.05 – 2.00 (m, 2H), 1.951.76 (m, 5H), 1.42 (s, 9H), 1.35 (hept, *J* = 7.4 Hz, 2H), 1.17 (d, J = 7.5 Hz, 6H), 1.16 (d, *J* = 7.6 Hz, 6H), 0.88 – 0.77 (m, 2H). **^{13}C NMR** (125.7 MHz, $CDCl_3$) δ 157.2, 156.5, 84.3, 79.6, 69.1, 67.9, 41.4, 40.8, 40.3, 37.3, 28.5, 27.0, 25.0, 24.4, 23.9, 19.8, 19.7, 18.9, 12.3, 6.3. **HRMS** (ESI$^+$) calculated for $[C_{26}H_{48}O_4S_2Si+Na]^+$ required m/z 567.2717, found m/z 567.2718.

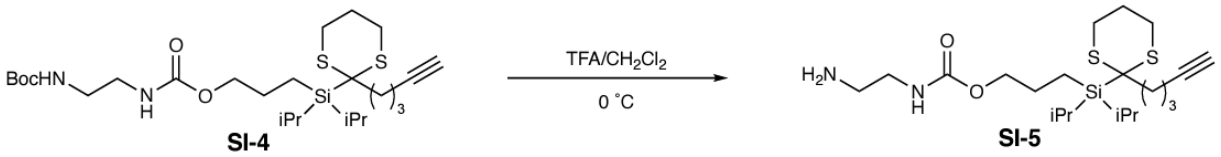

SI-4 **SI-5**

Amine linker SI-5: A 1 dram vial was charged with **SI-4** (67 mg, 0.123 mmol) and DCM (1.4 mL, 0.09 M) and cooled in an ice bath. Subsequently, TFA (0.11 mL, 1.4 mmol, 11.3 equiv.) was added and stirred until complete by TLC. The reaction was concentrated,

diluted with Et_2O and washed with 1 N NaOH. The organic layer was concentrated to 84 mg of a yellow oil and immediately used in the next reaction without further purification.

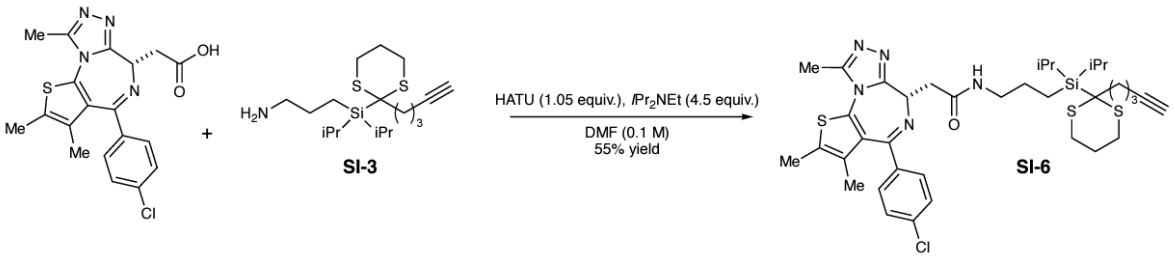

Acyl silane dithiane precursor to 16 (SI-6): To a solution of (+)-JQ1-OH (50 mg, 0.125 mmol, 1.0 equiv.) in a 2 dram vial was added DMF (1.25 mL, 0.1 M), HATU (50 mg, 0.131 mmol, 1.05 equiv.), and *i*-PrNEt$_2$ (65 µL, 0.575 mmol, 4.5 equiv.). After 10 min, freshly prepared **SI-3** was added (46 mg, 0.138 mmol, 1.05 equiv.) and the reaction was allowed to stir for 16 h before removing the DMF in vacuo and purifying by silica gel chromatography using a gradient elution of 99.5:0.05-96:4 DCM/MeOH. The product was isolated as a white solid (50 mg, 55% yield). **^{1}H NMR** (500.0 MHz, $CDCl_3$) δ 7.39 (d, J = 8.5 Hz, 2H), 7.31 (d, J = 8.7 Hz, 2H), 6.70 (t, J = 5.7 Hz, 1H), 4.61 (t, J = 6.8 Hz, 1H), 3.71 (hept, J = 6.7 Hz, 1H), 3.51 (dd, J = 14.4, 6.9 Hz, 1H), 3.37 – 3.29 (m, 2H), 3.25 – 3.14 (m, 2H), 3.08 (ddd, J = 15.2, 12.8, 2.7 Hz, 2H), 2.65 (s, 3H), 2.45 – 2.40 (m, 2H), 2.38 (s, 4H), 2.35 (dt, J = 14.0, 3.8 Hz, 2H), 2.27 (td, J = 6.7, 2.7 Hz, 2H), 2.03 – 1.99 (m, 1H), 2.01 (s, J = 2.6 Hz, 1 H), 1.98 – 1.86 (m, 1H), 1.82 – 1.72 (m, 4H), 1.36 – 1.29 (m, 1H), 1.18 – 1.10 (m, 12H), 0.84 – 0.78 (m, 2H). **^{13}C NMR** (125.7 MHz, $CDCl_3$) δ 170.4, 164.0, 155.8, 150.0, 136.8, 136.7, 132.2, 131.0, 130.5, 129.9, 128.8, 84.3, 69.1, 54.5, 43.7, 43.3, 40.3, 39.4, 37.2, 26.9, 25.0, 24.8, 23.9, 19.8, 19.8, 19.7, 18.8, 14.4, 13.2, 12.22, 12.21, 11.9, 7.7. **HRMS** (ESI$^+$) calculated for $[C_{37}H_{51}N_5OClS_3Si+H]^+$ required m/z 740.2714, found m/z 740.2708.

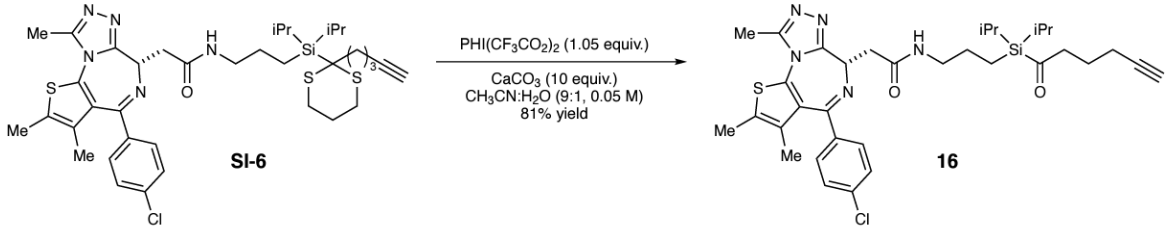

Acyl silane 16: To a solution of **SI-6** (48 mg, 0.0649 mmol, 1 equiv.) and $CaCO_3$ (64.9 mg, 0.649 mmol, 10 equiv.) in CH_3CN:H_2O (9:1, 0.05 M, 1.4 mL) cooled in an ice bath to 4 °C was added PIFA (29.3 mg, 0.0681 mmol, 1.05 equiv.) dropwise in CH_3CN (0.1 mL). The solution was stirred for 30 min in the ice bath before dilution with EtOAc. The resulting mixture was washed with sat. aqueous $NaHCO_3$, brine, and dried over $MgSO_4$ before concentrating in vacuo. The crude material was purified by flash column chromatography using a gradient elution of 99.5:0.05–96:4 DCM/MeOH to give **16** as a white solid (34 mg, 81% yield). **^{1}H NMR** (500.0 MHz, $CDCl_3$) δ 7.34 (d, J = 8.3 Hz, 2H), 7.26 (d, J = 8.6 Hz, 2H), 6.76 (t, J = 6.0 Hz, 1H), 4.57 (t, J = 6.9 Hz, 1H), 3.50 (dd, J = 14.3, 7.5 Hz, 1H), 3.29 (dd, J = 14.4, 6.3 Hz, 1H), 3.24 (p, J = 6.6 Hz, 1H), 3.19 (p, J = 6.6 Hz, 1H), 2.64 (t, J = 7.0 Hz, 2H), 2.60 (s, 3H), 2.33 (s, 3H), 2.12 (td, J = 6.9, 2.6 Hz, 2H), 1.90 (t, J = 2.6 Hz, 1H), 1.67 (p, J = 6.9 Hz, 2H), 1.60 (s, 3H), 1.59–1.49 (m, 2H), 1.11 (hept, J = 7.3 Hz, 2H), 1.00 – 0.92 (m, 12H), 0.74 – 0.68 (m, 2H). **^{13}C NMR** (125.7 MHz, $CDCl_3$) δ 246.6, 170.2,

164.7, 155.4, 150.2, 137.5, 135.9, 132.2, 131.7, 131.3, 130.5, 130.2, 128.9, 84.0, 69.1, 54.3, 49.5, 43.0, 38.8, 24.1, 20.6, 18.3, 18.2, 17.9, 14.5, 13.3, 11.8, 10.7, 5.9. **HRMS** (ESI^+) calculated for $[C_{34}H_{45}N_5O_2ClSSi+H]^+$ required m/z 650.2752, found m/z 650.2744.

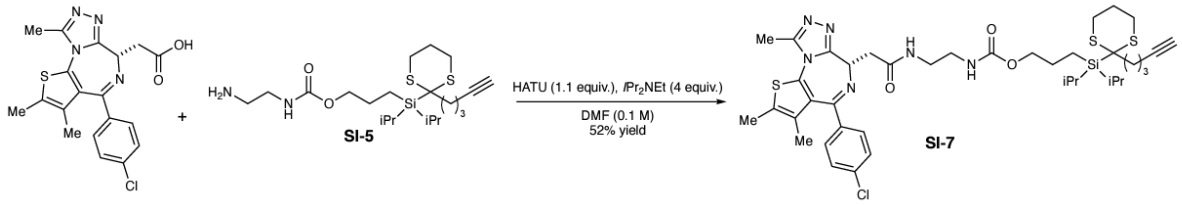

Acyl silane dithiane precursor to 17 SI-7: To a solution of (+)-JQ1-OH (30 mg, 0.075 mmol, 1.0 equiv.) in a 2 dram vial was added DMF (0.75 mL, 0.1 M), HATU (31 mg, 0.0825 mmol, 1.1 equiv.), and *i*-$PrNEt_2$ (52 µL, 0.30 mmol, 4.0 equiv.). After 10 min, freshly prepared **SI-5** was added (36 mg, 0.0825 mmol, 1.1 equiv.) and the reaction was allowed to stir for 16 h before removing the DMF in vacuo and purifying by silica gel chromatography using a gradient elution of 99.5:0.05 – 96:4 DCM/MeOH. The product was isolated as a white solid (32 mg, 52% yield). **^{1}H NMR** (500 MHz, $CDCl_3$) δ 7.72 (br. s, 1H), 7.38 (d, *J* = 8.4 Hz, 2H), 7.30 (d, *J* = 8.6 Hz, 2H), 6.03 (m, 1H), 4.69 (t, *J* = 7.0 Hz, 1H), 4.00 – 3.93 (m, 1H), 3.58 (dd, *J* = 14.7, 7.7 Hz, 1H), 3.54 – 3.46 (m, 1H), 3.43 (dd, *J* = 14.6, 5.9, Hz, 1H), 3.403.25 (m, 3H), 3.08 (d, J = 13.1 Hz, 2H), 2.69 (s, 3H), 2.44 – 2.36 (m, 2H), 2.40 (s, 3H), 2.30 – 2.22 (m, 2H), 2.06 – 1.99 (m, 2H), 1.97 – 1.89 (m, 1H), 1.88 – 1.73 (m, 4H), 1.67 (s, 3H), 1.35 (hept, *J* = 7.3 Hz, 2H), 1.20 – 1.14 (m, 12H), 0.85 – 0.78 (m, 2H). **^{13}C NMR** (125.7 MHz, $CDCl_3$) δ 171.2, 164.1, 157.2, 155.9, 150.1, 136.9, 136.6, 132.1, 131.1, 131.0, 130.7, 130.0, 128.9, 84.3, 69.1, 67.9, 54.4, 53.6, 41.2, 40.3, 39.9, 39.0, 37.3, 26.9, 25.1, 24.5, 23.9, 19.8, 19.7, 18.9, 14.5, 13.2, 12.3, 11.9, 6.2. **HRMS** (ESI^+) calculated for $[C_{40}H_{44}N_6O_3ClS_3Si+H]^+$ required m/z 827.3034, found m/z 827.3034.

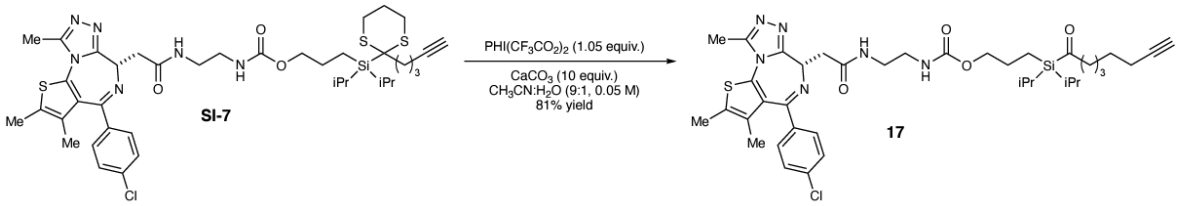

Acyl silane 17: To a solution of **SI-7** (32 mg, 0.0387 mmol, 1 equiv.) and $CaCO_3$ (38.7 mg, 0.387 mmol, 10 equiv.) in CH_3CN:H_2O (9:1, 0.05 M, 0.8 mL) cooled in an ice bath to 4 °C was added PIFA (17.5 mg, 0.0407 mmol, 1.05 equiv.) dropwise in CH_3CN (0.1 mL). The solution was stirred for 30 min in the ice bath before dilution with EtOAc. The resulting mixture was washed with sat. aqueous $NaHCO_3$, brine, and dried over $MgSO_4$ before concentrating in vacuo. The crude material was purified by flash column chromatography using a gradient elution of 99.5:0.05–96:4 DCM/MeOH to give **17** as a white solid (23 mg, 81% yield). **^{1}H NMR** (500.0 MHz, $CDCl_3$) δ 7.59 (t, *J* = 5.6 Hz, 1H), 7.39 (d, *J* = 8.3 Hz, 2H), 7.31 (d, *J* = 8.4 Hz, 2H), 5.91 (t, *J* = 5.5 Hz, 1H), 4.70 (t, *J* = 7.1 Hz, 1H), 4.03 – 3.97 (m, 2H), 3.59 (dd, *J* = 14.7, 7.7 Hz, 1H), 3.52 – 3.46 (m, 1H), 3.43 (dd, *J* = 14.7, 6.5 Hz, 1H), 3.40 – 3.25 (m, 3H), 2.71 (t, *J* = 7.0 Hz, 2H), 2.69 (s, 3H), 2.41 (s, 3H), 2.19 (td, *J* = 6.9, 2.6 Hz, 2H), 1.96 (t, *J* = 2.6 Hz, 1H), 1.73 (p, *J* = 6.9 Hz, 2H), 1.67 (s, 3H), 1.20 (m, 1H), 1.05 (d, *J* = 4.8 Hz, 7H), 1.03 (d, *J* = 4.9 Hz, 6H), 0.82 – 0.75 (m, 2H). **^{13}C NMR** (125.7 MHz, $CDCl_3$) δ 246.6, 170.8, 165.1, 157.1, 155.3, 150.3, 137.7, 135.5, 132.5, 131.8, 130.4, 128.9, 84.0, 69.1, 67.4, 54.1, 49.5, 41.1, 40.0, 38.4, 23.7, 20.6, 18.3, 18.2,

17.9, 14.6, 13.3, 11.9, 10.7, 4.6. **HRMS** (ESI$^+$) calculated for $[C_{37}H_{49}N_6O_4ClSSi+H]^+$ required m/z 737.3072, found m/z 737.3075.

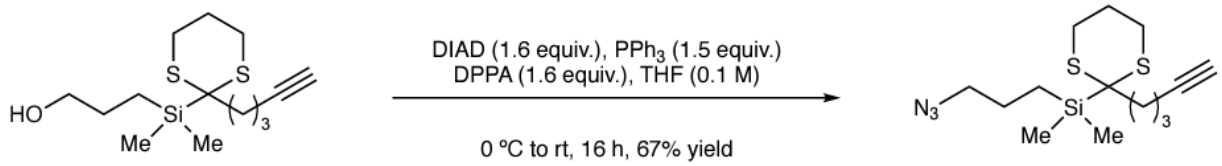

13a **20**

(3-azidopropyl)dimethyl(2-(pent-4-yn-1-yl)-1,3-dithian-2-yl)silane (20): To a solution of triphenylphosphine (0.393 g, 1.5 mmol, 1.5 equiv.) in THF (6 mL) at 0 °C was added DIAD (0.316 mL, 1.6 mmol, 1.6 equiv.). After stirring for 10 minutes, alcohol **13a** (0.302 g, 1.00 mmol, 1.0 equiv.) was added to the cloudy white suspension and allowed to stir at 0 °C for 30 minutes, at which point diphenylphosphoylazide (0.346 mL, 1.6 mmol, 1.6 equiv.) was added dropwise and the reaction was allowed to stir overnight. After 16h, the reaction was quenched by addition of H_2O, extracted thrice with EtOAc, and concentrated to an oil. The crude residue was purified by flash column chromatography (hex:EtOAc = 93:7) to give **20** (220 mg, 67% yield) as a clear oil which contained 92% product by mass. **^{1}H NMR** (500 MHz, $CDCl_3$) δ 3.26 (td, J = 7.0, 1.4 Hz, 2H), 3.11 – 3.01 (m, 2H), 2.48 – 2.39 (m, 2H), 2.38 – 2.29 (m, 2H), 2.05 (dddt, J = 12.9, 4.5, 3.0, 1.5 Hz, 1H), 1.99 (td, J = 2.6, 1.1 Hz, 1H), 1.96 – 1.83 (m, 1H), 1.76 – 1.64 (m, 4H), 0.85 – 0.76 (m, 2H), 0.19 (d, J = 1.4 Hz, 6H). **^{13}C NMR** (125.7 MHz, $CDCl_3$): δ 84.17, 68.85, 54.43, 38.46, 36.38, 26.59, 25.06, 23.89, 23.35, 18.79, 11.07, -4.37. **HRMS** (EI$^+$) calculated for $[C_{37}H_{49}N_6O_4ClSSi+H]^+$ required m/z 327.1259, found m/z 327.1259.

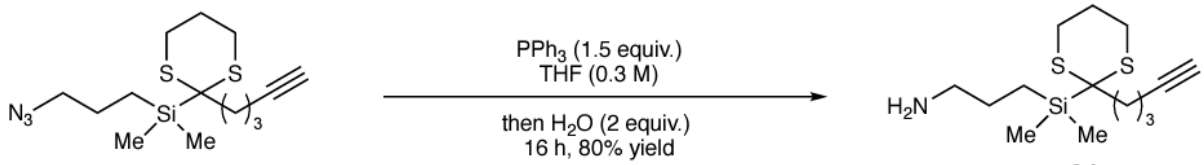

20 **21**

3-(dimethyl(2-(pent-4-yn-1-yl)-1,3-dithian-2-yl)silyl)propan-1-amine (21) To a solution of **20** (110 mg, 0.336 mmol, 1.0 equiv.) in THF (1 mL) cooled to 0 °C was added triphenylphosphine (132 mg, 0.505 mmol, 1.5 equiv.) and the mixture was allowed to stir for 1 h at room temperature before adding H_2O (10 uL, 0.672 mmol, 2.0 equiv.) and the reaction was allowed to stir for 16 h. The mixture was concentrated and purified by flash column chromatography using a gradient elution of 98:2 to 8:2 DCM/MeOH to give **21** (88 mg, 80% yield) as a clear oil. **^{1}H NMR** (500 MHz, $CDCl_3$) δ 3.06 (ddd, J = 14.8, 12.6, 2.7 Hz, 2H), 2.76 – 2.70 (m, 2H), 2.43 (dt, J = 14.2, 3.8 Hz, 2H), 2.38 – 2.32 (m, 2H), 2.26 (td, J = 6.7, 2.7 Hz, 5H), 2.10 – 2.01 (m, 1H), 1.99 (t, J = 2.6 Hz, 1H), 1.90 (qt, J = 13.0, 3.4 Hz, 1H), 1.71 (dq, J = 11.8, 6.9 Hz, 2H), 1.54 (ddd, J = 16.6, 11.1, 5.9 Hz, 2H), 0.80 – 0.73 (m, 2H), 0.18 (s, 6H). **^{13}C NMR** (125.7 MHz, $CDCl_3$) : δ 84.24, 68.83, 45.09, 38.60, 36.34, 27.49, 26.59, 25.10, 23.33, 18.80, 10.68, -4.37. **HRMS** (ESI$^+$) calculated for $[C_{14}H_{27}NS_2Si+H]^+$ required m/z 302.1247, found m/z 302.1243.

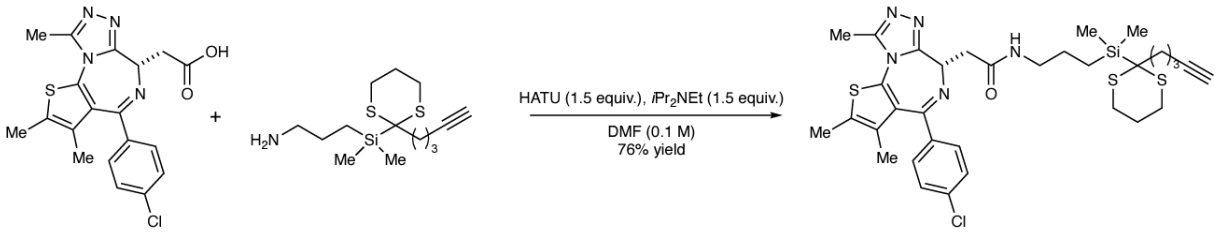

Dithiane precursor to acyl silane 16Me SI-8. To a solution of (+)-JQ1-OH (26 mg, 0.0625 mmol, 1.0 equiv.) in a 2 dram vial was added DMF (0.625 mL, 0.1 M), HATU (35.6 mg, 0.0938 mmol, 1.5 equiv.), and *i*-PrNEt$_2$ (16 µL, 0.0938 mmol, 1.5 equiv.). After 10 min, **21** was added (19.7 mg, 0.0656 mmol, 1.05 equiv.) and the reaction was allowed to stir for 16 h before removing the DMF in vacuo and purifying by silica gel chromatography using a gradient elution of 99:1 – 96:4 DCM/MeOH. The product was isolated as a white solid (33 mg, 76% yield). **^{1}H NMR** (600 MHz, $CDCl_3$) δ 7.40 (dd, *J* = 8.7, 3.6 Hz, 2H), 7.32 (d, *J* = 8.6 Hz, 2H), 6.57 (t, *J* = 5.8 Hz, 1H), 4.62 (t, *J* = 6.9 Hz, 1H), 3.71 (pd, *J* = 6.7, 4.1 Hz, 1H), 3.56 – 3.49 (m, 1H), 3.33 (dt, *J* = 13.1, 6.5 Hz, 2H), 3.22 (dt, *J* = 12.7, 6.3 Hz, 1H), 3.17 (qd, *J* = 7.4, 4.2 Hz, 1H), 3.09 – 3.01 (m, 2H), 2.66 (s, 3H), 2.45 – 2.40 (m, 2H), 2.39 (s, 3H), 2.37 – 2.30 (m, 2H), 2.26 (td, *J* = 6.7, 2.7 Hz, 2H), 2.08 – 2.04 (m, 1H), 2.01 (t, *J* = 2.6 Hz, 1H), 1.90 (qt, *J* = 12.7, 3.3 Hz, 1H), 1.74 – 1.67 (m, 2H), 1.66 (s, 3H), 1.65 – 1.57 (m, 2H), 1.44 (d, *J* = 6.6 Hz, 2H), 1.41 (d, *J* = 6.6 Hz, 2H), 0.80 – 0.72 (m, 2H), 0.17 (d, *J* = 1.6 Hz, 6H). **^{13}C NMR** (151 MHz, $CDCl_3$) δ 170.48, 164.06, 155.80, 150.02, 136.94, 136.73, 132.25, 131.07, 131.01, 130.61, 129.96, 128.87, 84.35, 69.02, 55.63, 54.60, 43.62, 42.91, 39.52, 38.70, 36.47, 28.29, 26.70, 25.20, 24.44, 23.46, 18.90, 18.72, 17.33, S2514.50, 13.21, 12.63, 11.94, 11.16, -4.21 (2 extraneous peaks). **HRMS** (ESI$^+$): calculated for $[C_{33}H_{42}ClN_5OS_3Si+H]^+$ required m/z 684.2082, found m/z 684.2094.

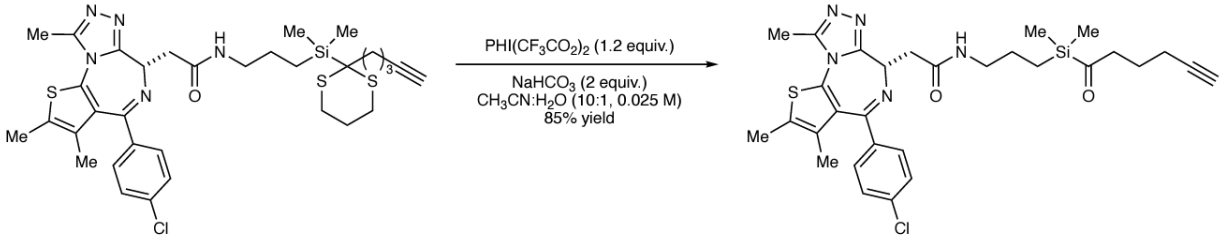

Acyl silane 16Me. To a solution of **SI-8** (5 mg, 0.00714 mmol, 1.0 equiv.) and $NaHCO_3$ (1.2 mg, 0.0413 mmol, 2.0 equiv.) in a solution of MeCN:H_2O (0.025 M, 270 µL:30 µL) was added PIFA (3.7 mg, 0.00857 mmol, 1.2 equiv.) and the resulting yellow solution was allowed to stir for 30 minutes, at which point the solvent was removed in vacuo and the residue was purified by flash column chromatography using a gradient elution of 99:1 to 97:3 DCM:MeOH to give **16Me** (3.7 mg, 85% yield) as a white powder. **^{1}H NMR** (600 MHz, $CDCl_3$) δ 7.40 (d, *J* = 8.5 Hz, 2H), 7.33 (d, *J* = 8.7 Hz, 2H), 6.62 (t, *J* = 6.0 Hz, 1H), 4.60 (dd, *J* = 7.9, 6.1 Hz, 1H), 3.57 (dd, *J* = 14.1, 8.0 Hz, 1H), 3.36 – 3.19 (m, 3H), 2.74 (t, *J* = 7.1 Hz, 2H), 2.67 (s, 3H), 2.40 (s, 3H), 2.19 (td, *J* = 6.9, 2.7 Hz, 2H), 1.97 (t, *J* = 2.6 Hz, 1H), 1.74 (p, *J* = 7.0 Hz, 2H), 1.57 – 1.48 (m, 2H), 0.72 – 0.65 (m, 2H), 0.19 (d, *J* = 4.6 Hz, 6H). **^{13}C NMR** (151 MHz, $CDCl_3$) δ 247.08, 170.54, 164.04, 155.75, 150.02, 136.94, 136.71, 132.23, 131.03, 130.97, 130.61, 129.92, 128.86, 83.90, 69.13, 54.68, 47.27, 42.50, 39.66, 29.80, 23.84, 22.79?, 20.75, 17.89, 14.47, 13.19, 11.91, 10.71, -4.74. **HRMS** (ESI$^+$) calculated for $[C_{30}H_{36}ClN_5O_2SSi+H]^+$ required m/z 594.2121, found m/z 594.2127.

Synthesis of diazirine (+)-JQ1 probe

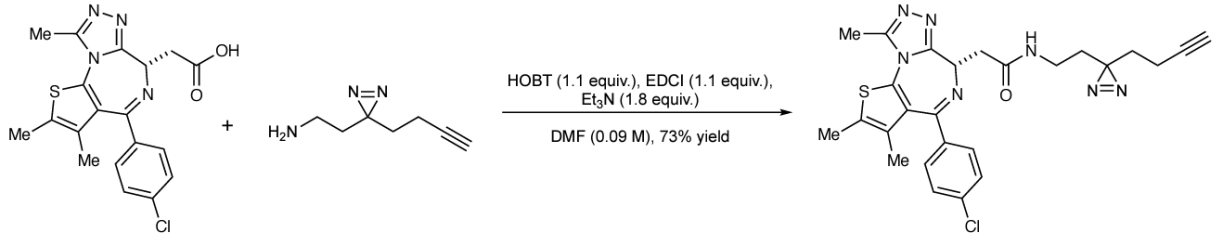

Diazirine 16-DA. To a solution of (+)-JQ1-OH (14.6 mg, 0.0365 mmol, 1.0 equiv.) in a 2 dram vial was added DMF (0.2 mL), HOBT (5.4 mg, 0.0402 mmol, 1.1 equiv.), EDCI (6.2 mg, 0.0402 mmol, 1.1 equiv.), and NEt_3 (9.1 mg, 0.0657 mmol, 1.8 equiv.). After 10 min, 2-(3-(but-3-yn-1-yl)-3H-diazirin-3-yl)ethan-1-amine (**SI-12**) was added (5.0 mg, 0.0365 mmol, 1.0 equiv.) in DMF (0.6 mL) and the reaction was allowed to stir for 12 h at which point the solution was diluted with H_2O extracted 5 times with EtOAc, and the combined organic layers were passed through a short silica plug with EtOAc and concentrated. The material was purified by silica gel chromatography using a gradient elution of 99:1-95:5 DCM:MeOH. The product was isolated as a white solid (13.7 mg, 73% yield). **^{1}H NMR** (500 MHz, $CDCl_3$) δ 7.41 (d, J = 8.2 Hz, 2H), 7.34 (d, J = 8.4 Hz, 2H), 6.89 (t, J = 6.0 Hz, 1H), 4.63 (dd, J = 7.8, 6.0 Hz, 1H), 3.61 (dd, J = 14.3, 7.8 Hz, 1H), 3.37 (dd, J = 14.3, 6.1 Hz, 1H), 3.17 (ddt, J = 16.8, 13.9, 7.0 Hz, 2H), 2.68 (s, 3H), 2.41 (s, 3H), 2.05 – 1.95 (m, 3H), 1.68 (s, 3H), 1.72 – 1.58 (m, 4H). **^{13}C NMR** (126 MHz, $CDCl_3$) δ 170.62, 164.15, 137.05, 136.55, 131.11, 131.09, 130.62, 130.00, 128.87, 82.86, 69.51, 54.58, 39.43, 34.57, 32.77, 32.14, 31.71, 26.89, 22.78, 14.52, 14.25, 13.36, 13.23, 11.93, 1.14. **HRMS** (ESI^+): calculated for $[C_{26}H_{26}ClN_7OS+Na]^+$: required m/z 542.1500, found m/z 542.1502.

Synthesis of rapamycin acyl silane probes

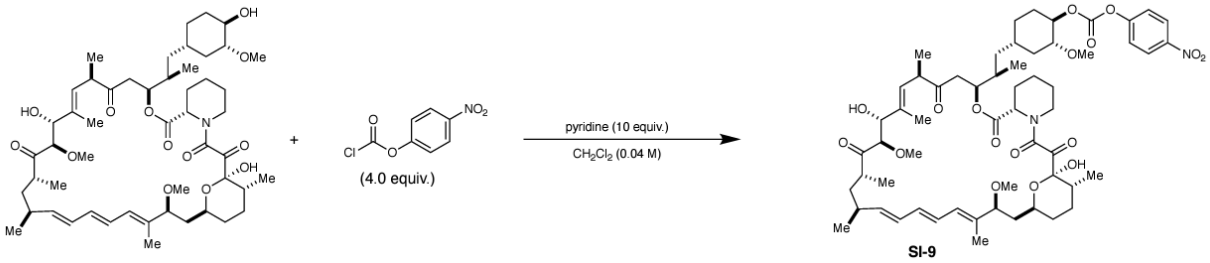

Rapamycin p-nitrophenyl carbonate (SI-9): A two-dram vial was charged with rapamycin (35 mg, 0.0385 mmol, 1.0 equiv.) and CH_2Cl_2 (1 mL) followed by pyridine (31 µL, 0.385 mmol, 10 equiv.). A solution of *p*-nitrophenylchloroformate (31 mg, 0.155 mmol, 4.0 equiv.) in CH_2Cl_2 (0.4 mL) was added dropwise. After complete addition, the reaction was stirred for 30 min before diluting with EtOAc and washing with 0.5 M HCl cooled in an ice bath. The organic layer was concentrated and the crude material was purified by flash column chromatography using a gradient of 99:1 to 96:4 DCM/MeOH. The product was isolated as a white crystalline solid (37 mg, 89% yield). **HRMS** (ESI^+) calculated for $[C_{58}H_{82}N_2O_{17}+Na]^+$ required m/z 1101.5511, found m/z 1101.5491.

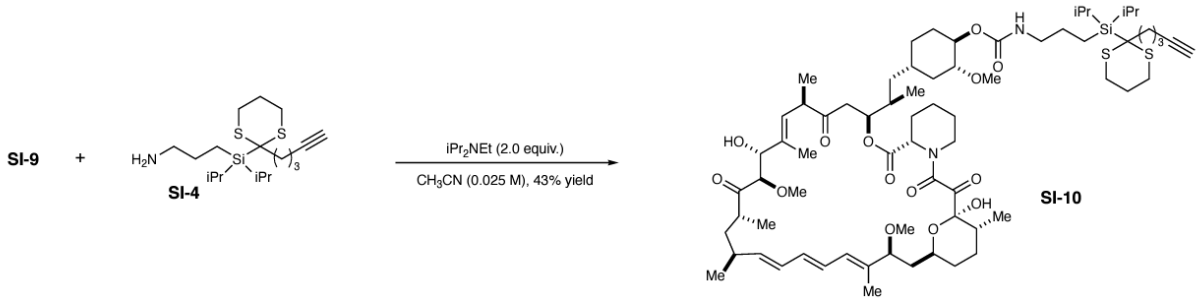

Dithiane rapamycin precursor (SI-10): A two-dram vial was charged with **SI-9** (32 mg, 0.0300 mmol, 1 equiv.), freshly prepared **SI-4** (14 mg, 0.0306 mmol, 1.3 equiv.), *i*-Pr_2NEt (10.4 µL, 0.0600 mmol, 2.0 equiv.) and CH_3CN (0.6 mL, 0.05 M). The reaction was stirred for 16 h before diluted with EtOAc. The solution was washed with 0.5 M HCl cooled in an ice bath and brine, before drying over $NaSO_4$ and concentrating in vacuo. The crude material was purified by flash column chromatography using a gradient of 99:1 to 96:4 CH_2Cl_2:MeOH. The product was isolated as a white solid (20 mg, 53% yield). **HRMS** (ESI^+) calculated for $[C_{70}H_{112}N_2O_{14}S_2Si+Na]^+$ required m/z 1319.7222, found m/z 1319.7217.

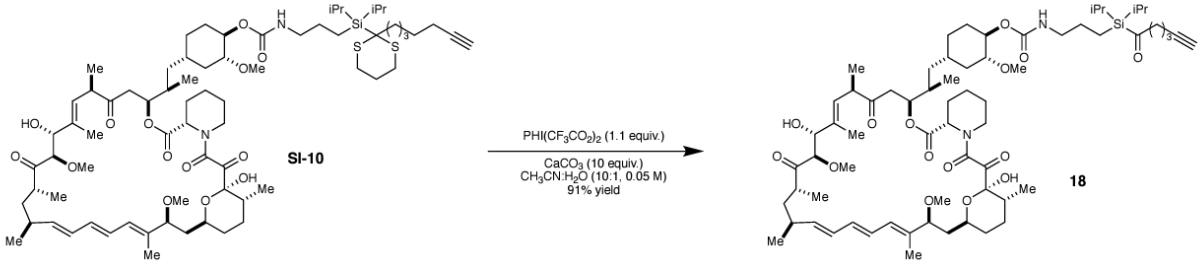

Rapamycin acyl silane (18): To a solution of **SI-10** (20 mg, 0.0154 mmol, 1 equiv.) and $CaCO_3$ (16 mg, 0.154 mmol, 10 equiv.) in CH_3CN:H_2O (9:1, 0.025 M, 0.62 mL) cooled in an ice bath to 4 °C was added PIFA (7.0 mg, 0.0163 mmol, 1.06 equiv.) dropwise in CH_3CN (0.1 mL). The solution was stirred for 30 min in the ice bath before dilution with EtOAc. The resulting mixture was washed with sat. aqueous $NaHCO_3$, brine, and dried over $MgSO_4$ before concentrating in vacuo. The crude material was purified by flash column chromatography using a gradient elution of 99:1-96:4 DCM/MeOH to give **18** as a white solid (17 mg, 91% yield). **HRMS** (ESI^+) calculated for $[C_{67}H_{106}N_2O_{15}Si+Na]^+$ required m/z 1229.7260, found m/z 1229.7241.

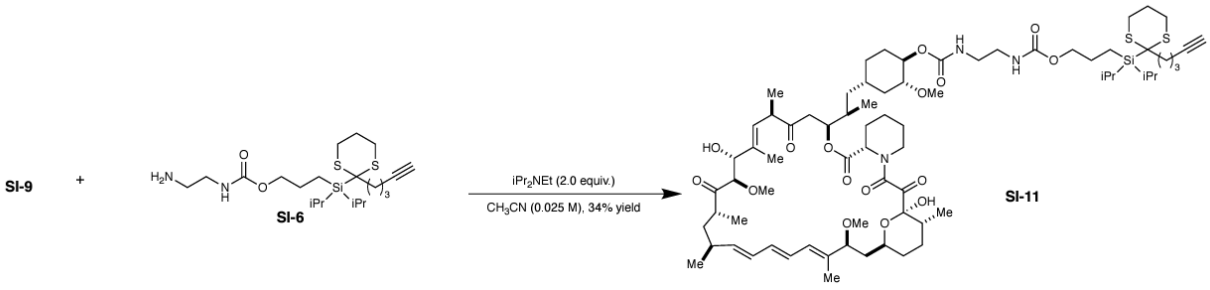

Dithiane rapamycin precursor (SI-11): A two-dram vial was charged with **SI-9** (50 mg, 0.0463 mmol, 1 equiv), freshly prepared **SI-6** (22.2 mg, 0.0510 mmol, 1.1 equiv.), *i*-Pr_2NEt (16.2 µL, 0.0930 mmol, 2.0 equiv.) and CH_3CN (1.85 mL, 0.025 M). The reaction was stirred for 16 h before diluted with EtOAc. The solution was washed with 0.5 M HCl cooled

in an ice bath and brine, before drying over $NaSO_4$ and concentrating in vacuo. The crude material was purified by flash column chromatography using a gradient of 99:1 to 96:4 CH_2Cl_2:MeOH. The product was isolated as a white solid (22 mg, 34% yield). **HRMS** (ESI^+) calculated for $[C_{73}H_{117}N_3O_{16}S_2Si+Na]^+$ required m/z 1406.7542, found m/z 1406.7537.

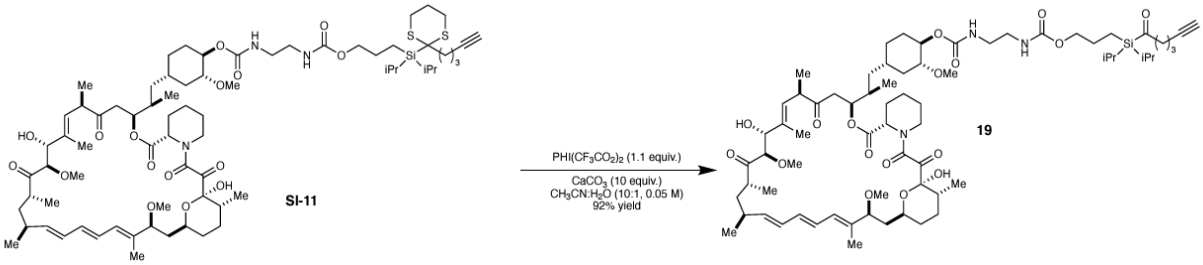

Rapamycin acyl silane (19): To a solution of **SI-11** (22 mg, 0.0152 mmol, 1 equiv.) and $CaCO_3$ (15.2 mg, 0.152 mmol, 10 equiv.) in CH_3CN:H_2O (9:1, 0.05 M, 0.3 mL) cooled in an ice bath to 4 °C was added PIFA (6.8 mg, 0.0159 mmol, 1.05 equiv.) dropwise in CH_3CN (0.1 mL). The solution was stirred for 30 min in the ice bath before dilution with EtOAc. The resulting mixture was washed with sat. aqueous NaHCO3, brine, and dried over $MgSO_4$ before concentrating in vacuo. The crude material was purified by flash column chromatography using a gradient elution of 99:1-96:4 DCM/MeOH to give **19** as a white solid (17 mg, 92% yield). **HRMS** (ESI^+) calculated for $[C_{71}H_{114}N_3O_{17}Si+Na]^+$ required m/z 1316.7580, found m/z 1316.7569.

Supplementary Datasets
The following supplementary datasets have been deposited online with the submission of this dissertation.

Supplementary Dataset 1. Aggregate quantified chemoproteomic data of probe-modified peptides for E3 ligases and other components of the ubiquitin proteasome machinery. We have aggregated all of our chemoproteomic data from 455 distinct experiments using the alkyne-functionalized iodoacetamide probe and the isoTOP-ABPP method first reported by Weerapana and Cravatt *et al.* [1] across various human cell line proteomes. We have quantified the total number of spectral counts for each tryptic peptide identified within each E3 ligase family member across all experiments. These include data from our research group's published papers as well as our currently unpublished studies all using the same methods described in these studies[2–17]. We have consolidated redundant probe-modified peptides as much as we can and have added the total number of spectral counts and aggregate numbers of experiments where each probe-modified peptide was identified across the 455 distinct chemoproteomic experiments.
Tab 1 shows a summary of E3 ligases and other components of the ubiquitin proteasome machinery that we searched against our ligandability database with total probe-modified peptide spectral counts and experiments for each protein, separated out by the various classes of E3 ligases.
Tabs 2-10 list the individual E3 ligases, the Uniprot ID for each E3 ligase, the probe-modified peptide sequence with the modified cysteine annotated by a "*" next to the cysteine, the cysteine number, the probe used (which is all cases is the alkyne-functionalized iodoacetamide probe abbreviated as IAyne), aggregate spectral counts for each probe-modified site, and aggregate number of experiments in which the probe-modified peptide was found.

Supplementary Dataset 2. IsoTOP-ABPP analysis of dankastatin B. MDA-MB-231 breast cancer cells were treated with DMSO vehicle or dankastatin B (10 μM) for 2 h. Resulting cell lysates were treated with the cysteine-reactive alkyne-functionalized iodoacetamide probe (IA-alkyne) and subsequently taken through the isoTOP-ABPP procedure and LC-MS/MS analysis. Data are from n=6 biological replicates.
Tab 1 shows all probe-modified peptides detected and quantified.
Tab 2 and Tab 3 both show probe-modified peptides that were evident in at least 3 out of 6 biological replicates.
Tab 2 highlighted proteins/sites show ratio >2 with adjusted p-value <0.05.
Tab 3 highlighted proteins/sites show ratio >4 with adjusted p-value <0.05.

Supplementary Dataset 3. IsoTOP-ABPP analysis of gymnastatin G. MDA-MB-231 breast cancer cells were treated with DMSO vehicle or gymnastatin G (50 mM) for 3 h. Resulting cell lysates were treated with the cysteine-reactive alkyne-functionalized iodoacetamide probe (IA-alkyne) and subsequently taken through the isoTOP-ABPP procedure and LC-MS/MS analysis. Data are from n=3 biological replicates.
Tab 1 shows all probe-modified peptides detected and quantified.

Tab 2 and Tab 3 both show probe-modified peptides that were evident in at least 2 out of 3 biological replicates.
Tab 2 highlighted proteins/sites show ratio >2 with adjusted p-value <0.05.
Tab 3 highlighted proteins/sites show ratio >4 with adjusted p-value <0.05.

Supplementary Dataset 4. TMT-based quantitative proteomic analysis of dankastatin B treatment in MDA-MB-231 cells. MDA-MB-231 breast cancer cells were treated with DMSO vehicle or dankastatin B (10 μM) for 1 h. Resulting cell lysates were treated with isobaric tags. Proteomes were analyzed by TMT-based quantitative proteomics. Data are from n=3 biological replicates.
Tab 1 shows all proteins detected and quantified.
Tab 2 shows only proteins enriched or depleted with adjusted p-value <0.05.

Supplementary Dataset 5. TMT-based quantitative proteomic analysis of proteins enriched by iPr-JQ1-alkyne probe treatment in K562 cells. K562 leukemia cells were treated with DMSO vehicle or acyl silane (+)-JQ1 **16** (10 μM) for 1 h and irradiated for 20 min at 265 nm. Resulting cell lysates were subjected to CuAAC to append an azide-functionalized biotin enrichment handle to probe-labeled proteins. Labeled proteins were then avidin-enriched, digested with trypsin, and resulting tryptic peptides were treated with isobaric tags. Proteomes were analyzed by TMT-based quantitative proteomics. Data are from n=3 biological replicates.
Tab 1 shows all proteins detected and quantified.
Tab 2 shows all proteins with adjusted p-values <0.05.

Supplementary Dataset 6. TMT-based quantitative proteomic analysis of proteins enriched by Diazarine-JQ1-alkyne probe treatment in K562 cells. K562 leukemia cells were treated with DMSO vehicle or diazirine (+)-JQ1 **16-DA** (10 μM) for 1 h and irradiated for 20 min at 265 nm. Resulting cell lysates were subjected to CuAAC to append an azide-functionalized biotin enrichment handle to probe-labeled proteins. Labeled proteins were then avidin-enriched, digested with trypsin, and resulting tryptic peptides were treated with isobaric tags. Proteomes were analyzed by TMT-based quantitative proteomics. Data are from n=3 biological replicates.
Tab 1 shows all proteins detected and quantified.
Tab 2 shows all proteins with adjusted p-values <0.05.